Inflammatory Cancer Associated Fibroblasts Decisive Role in Therapy Resistance Among Rectal Cancer Patients

Dissertation

zur Erlangung des Doktorgrades
der Naturwissenschaften

vorgelegt beim Fachbereich Biochemie, Chemie und Pharmazie
der Johann Wolfgang Goethe -Universität
in Frankfurt am Main

von Adele Mikheal Nicolas
aus Kafaraaka, Libanon

Frankfurt, Januar 2022
(D 30)

vom Fachbereich Biochemie, Chemie und Pahrmazie (FB14) der Johann Wolfgang Goethe - Universität als Dissertation angenommen.

Dekan: Prof. Dr. Clemens Glaubitz

Gutachter: Prof. Dr. Robert Fürst
Prof. Dr. Rolf Marschalek
Prof. Dr. Florian Greten
Prof. Stefan Knapp

Datum der Disputation: 12 April 2022

Teile dieser Arbeit wurden zur Veröffentlichung angenommen (Angaben für Autoren und Titel):

Inflammatory fibroblasts mediate resistance to neoadjuvant therapy in rectal cancer

Adele M. Nicolas, Marina Pesic, Esther Engel, Paul K. Ziegler, Markus Diefenhardt, Kilian B. Kennel, Florian Buettner, Claire Conche, Valentina Petrocelli, Eiman Elwakeel, Andreas Weigert, Anna Zinoveva, Maximilian Fleischmann, Björn Häupl, Cem Karakütük, Hanibal Bohnenberger, Mohammed H. Mosa, Lars Kaderali, Jochen Gaedcke, Michael Ghadimi, Franz Rödel, Melek C. Arkan, Thomas Oellerich, Claus Rödel, Emmanouil Fokas and Florian R. Greten. **Cancer Cell.**

Table of Contents

List of Figures

List of Tables

Abbreviations

ACTA2	actin alpha 2
APC	adenomatous polyposis coli
APTRA	o-Aminophenol-N,N,N-triacetate
BAFF	B-cell activating factor
CAFs	cancer associated fibroblasts
CCL2	chemokine ligand 2
CCL20	chemokine ligand 20
CIMPhi	CpG island methylation phenotype
CIN	chromosomal instability
CMS	consensus molecular subtype
CRC	colorectal cancer
CRT	chemoradiotherapy
CXCL12	stromal cell derived factor 12
CXCR4	C-X-C Chemokine receptor 4
DCN	Decorin
DDR	DNA damage response
DFS	disease free survival
Dpt	dermatopontin
ECAR	extracellular acidification rate
ECM	extracellular matrix
EGFR	epidermal growth factor receptor
EMT	epithelial mesenchymal transition
FGF7	fibroblast growth factor 7
FOXP3	forkhead box P3
GPR77C5a	anaphylatoxin chemotactic receptor C5a2
HA	hyaluronic Acid
HGF	hepatocyte growth factor
HIF	hypoxia-inducible factor
iCAFs	inflammatory cancer associated fibroblasts
IL1R	interleukin 1 receptor
IL1RA	interleukin 1 receptor antagonist

IL-1α	interleukin 1 alpha
IL6	interleukin 6
iNOS	inducible nitric oxide synthase
JAK	Janus kinase
Ki67	antigen KI-67
KRAS	Kirsten rat sarcoma viral oncogene homolog
LCCRT	long course chemoradiotherapy
LOX	lysyl oxidase
MET	mesenchymal epithelial transition tyrosine kinase
MMP	matrix metalloproteinase
MPO	myeloperoxidase
MSI	microsatellite instability
MTC1/4	Monocarboxylate transporter 1 and 4
mTOR	mammalian target of rapamycin
myCAFs	myofibroblasts
NFkB	Nuclear factor 'kappa-light-chain-enhancer' of activated B-cells
NOS	Nitrogen oxygen species
NSCLC	Non-small cell lung carcinoma
OCR	oxygen consumption rate
OS	overall survival
p38 MAPK	p38 mitogen-activated protein kinase
PCA	principal component analysis
pCR	pathological complete response
PD1	programmed cell death protein 1
PDAC	pancreatic ductal adenocarcinoma
PDGFRα/ß	platelet derived growth factor receptor α/β
PDL1	programmed death-ligand 1
PDOs	patients derived organoids
PIK3CA	PI3K catalytic subunit alpha
PSCs	pancreatic stellate cells
RCA	rectal cancer
SARRP	small animal radiation research platform
SASP	senescence associated secretory phenotype
SCRT	short course radiotherapy

SLC6A14	solute carrier family 6 member 14
SMAD4	SMAD family member 4
SMO	smoothed homolog precursor
SNP	single nucleotide polymorphism
SRF	serum response factor
STAT 3	signal transducer and activator of transcription 3
TCA	tricarboxylic acid cycle
TGFβ	transforming growth factor beta
TIS	therapy induced senescence
TME	tumor microenvironment
TNBC	triple negative breast cancer
TN-C	tenascin C
TNFα	tumor necrosis factor alpha
Tp53	tumor protein p53
TRG	tumor regression grade
VEGF	vascular endothelial growth factor
YAP1	yes associated protein 1
ypTNM	pathological tumor node metastasis classification

Aim

Neoadjuvant chemoradiotherapy (CRT) followed by surgical resection is the standard of care in the therapeutic management of patients with locally advanced rectal cancer (RCA) (Goodman et al., 2016; Rodel et al., 2015; Rodel et al., 2012). Despite technological advances in conventional CRT, rectal cancer patients of matching tumor stages respond heterogeneously to therapy. In fact, post preoperative CRT, it was demonstrated that only around 20% of patients show an excellent prognosis or the complete pathological tumor regression (pCR) which positively correlates with better prognostic outcomes such disease-free survival (DFS) and overall survival (OS) (Fokas et al., 2014; Maas et al., 2010). Hence the urgent need to unravel the molecular pathways underlying therapy resistance among RCA patients and thus bringing forward new targeted therapies, increasing the number of pCR and patients selected for organ preservation. To address this research question, the project aimed: 1) performing an in-depth characterization of the bulk and single-cell transcriptomic, proteomic and histologic profiles of responders and non-responders RCA patients' biopsies before CRT; 2) establishing and characterizing a novel preclinical mouse model that mimic the clinical scenario and 3) employing patient-derived organoids (PDOs) as well as the preclinical mouse model to provide thorough assessments of novel therapeutic agents that can be used in conjunction with conventional CRT. Collectively, the study intended to yield novel insights in the field of radiobiology and neoadjuvant personalized therapy with the purpose of driving promising clinical trials among rectal cancer and potentially other solid malignancies.

Summary

Standard cancer therapy research targets tumor cells while not considering the damage on the tumor microenvironment (TME) and its associated implications in impairing therapy response. Employing patients-derived organoids (PDOs) and matched stroma cells or a novel murine preclinical rectal cancer model of local radiotherapy, it was demonstrated that tumor cells-derived IL-1α polarizes cancer-associated fibroblasts towards an inflammatory (iCAFs) phenotype. While numerous studies in different tumor entities highlighted the molecular heterogeneity of CAFs, so far there are no clear findings on their functional heterogeneity and relevance in therapy resistance and response. The present study molecularly characterized iCAFs subpopulation among RCA patients as well as the preclinical mouse model and importantly unraveled the detailed molecular mechanism underlying their contribution to impair therapy response. Mechanistically, iCAFs were demonstrated to be characterized by an upregulation of nitric oxide synthase (iNOS) which triggered accumulation of reactive nitrogen species (RNS) and subsequently an oxidative DNA damage response (DDR). Such a baseline IL-1α-driven DNA damage further sensitized iCAFs to a p53-mediated therapy induced senescence (TIS) causing extensive extracellular matrix (ECM) changes and induction of senescence associated secretory phenotype (SASP) that favored tumor progression and hindered tumor cell death. Moreover, iCAFs reversibility and repolarization into more quiescent like phenotype was demonstrated upon IL-1 signaling inhibition by anakinra, a recombinant IL-1 receptor antagonist (IL1RA). Accordingly, treating mice with anakinra or specific deletion of *Il1r1* in CAFs sensitized stroma-rich resistant tumors to chemoradiotherapy (CRT). Similarly, targeting CAFs senescence by senotherapy (venetoclax chemical) or employing *Trp53* deficient mice reverted therapy resistance among non-responsive tumors *in vivo* by reducing ECM deposition and consequently favoring $CD8^+$ T cells intratumoral infiltration posttherapy. Importantly, rectal cancer patients that do not completely respond to neoadjuvant therapy displayed an iCAFs senescence program post-CRT. Moreover, these patients presented a baseline increased CAFs content, a dominant iCAFs signature that correlated with poorer disease-free survival (DFS) and a significantly reduced circulating IL1RA serum levels. While reduced pretherapeutic *IL1RN* gene expression predicted poor prognosis among RCA patients, IL1RA serum levels were associated with rs4251961 (T/C) single nucleotide polymorphism (SNP) in the *IL1RN* gene. Finally, functional validation assays

revealed that conditioned media of PDOs drove inflammatory polarization of fibroblasts and consequently rendered them sensitive to RNS-mediated DNA damage and TIS. Collectively, the study highlighted a crucial and novel role of a CAFs subset, iCAFs, in therapy resistance among RCA patients, shedding light on their functional relevance by identifying IL-1 signaling as an appealing target for their repolarization and successful targeting. Therefore, it makes sense to combine the newly demonstrated and thoroughly proven therapeutic approach of targeting IL-1 signaling in combination with conventional CRT and possibly immunotherapy. This might have a major impact on RCA therapy and be of immense relevance for other stroma-rich tumors.

Deutsche Zusammenfassung

Das Tumor *Mikroenvironment* (TME) spielt eine Schlüsselrolle in der Tumorgenese und der Antwort auf Krebstherapien (Greten and Grivennikov, 2019). Therapie gegen rektalen Krebs (*rectal cancer*, RCA) ist ein Beispiel für eine erfolgreiche Anwendung einer multimodalen Krebsbehandlung (Rodel et al., 2016). Die neoadjuvante Chemoradiotherapie (CRT) vor der chirurgischen Resektion war ein Wendepunkt in der RCA-Therapie, die teilweise zu verbessertem Überleben führte (Sauer et al., 2012; van Gijn et al., 2011). Trotz übereinstimmender Tumorhistologie und –stadien variieren die Reaktionen der Patienten auf CRT deutlich (Fokas et al., 2020). Diese Variabilität wird durch die Klassifizierung von ypTNM (d.h. Tumorstadium nach neoadjuvanter Behandlung) bewertet, wobei die pCR-Reaktion (pCR, *pathological complete response*, d.h. vollständige Tumorregression und Fehlen verbleibender Lymphknotenmetastasen: ypT0N0M0) nach CRT signifikant mit einem besseren krankheitsfreien Überleben (DFS) und Gesamtüberleben (OS) korreliert im Vergleich zu Patienten ohne pCR (Nicht-pCR) (Fokas et al., 2018; Fokas *et al.*, 2020; Fokas et al., 2017). Es fehlt jedoch eine geeignete Identifizierung der molekularen Grundlagen, die das individuelle Ansprechen auf die Therapie vorhersagt. Die kürzlich etablierte Klassifizierung der molekularen Subtypen (*consensus molecular subtype*, CMS) für Darmkrebs (CRC) basierend auf transkriptomischen Profilen ganzer Tumoren zeigte, dass die Tumorsubtypisierung eine Prognosevorhersage ermöglicht und dass eine mesenchymale Signatur (CMS4) im Vergleich zu den anderen Subtypen mit einem schlechteren Überleben korreliert. (Eide et al., 2017; Guinney et al., 2015), was die Bedeutung von krebsassoziierten Fibroblasten (CAFs) für das Überleben von CRC-Patienten unterstreicht. Aufgrund ihrer relativen Nähe zu Krebszellen sowie ihrer Reaktion auf die Aktivierung von IL-1R oder TGF-βR polarisieren CAFs entweder in einen entzündlichen (iCAFs) oder einen myofibroblastenähnlichen Zustand (myCAFs) (Biffi et al., 2019; Ohlund et al., 2017) die durch unterschiedliche immunmodulierende Sekretome oder matrixproduzierende, kontraktile Phänotypen gekennzeichnet sind. Bisher ist nicht bekannt, ob und wie diese unterschiedlichen CAF-Phänotypen zur Krebstherapie beitragen.

Fibroblasten prognostizieren das Überleben von Rektumkrebspatienten

Um zu untersuchen, ob CMS-Klassifikatoren auch eine Prognosevorhersage bei RCA-Patienten ermöglichen würden, wurde ein Vergleich des Überlebens von 212 Patienten, behandelt mit neoadjuvanter CRT und Operation, durchgeführt. Ein vergleichbares Ergebnis wurde für die verschiedenen CMS-Untergruppen festgestellt (Abbildung 10), was darauf hinwies, dass die Einteilung von RCA-Patienten nach ihrem CMS keine DFS-Vorhersage zulässt (Eide *et al.*, 2017; Guinney *et al.*, 2015). Um prognostische Marker für das Ansprechen auf die Therapie zu identifizieren, wurde eine umfassende proteomische Analyse an *laser capture* mikrodissezierten Tumorzellen durchgeführt, die aus prätherapeutischen Biopsien von pCR-Patienten (d.h. ausgezeichnete Prognose) und nicht-pCR-Patienten (d.h. restliche Lymphknotenmetastasen mit schlechter Prognose) nach CRT stammen. Proteomprofile zeigten keine eindeutige Differenzierung der beiden Patientenkohorten (Abb. 10), was darauf hindeutete, dass das TME anstelle der Tumorzellen die CRT-Reaktion bestimmen könnte. In der Tat zeigte eine detaillierte fluoro-immunhistochemische Multiplex-Analyse von prä-therapeutischen Biopsieproben von pCR- oder Nicht-pCR-Patienten eine signifikante Anreicherung von Vimentin^{+} mesenchymalen Zellen bei Nicht-pCR-Patienten, ohne einen Unterschied in Bezug auf T-Zellen, Makrophagen oder Epithelzellen (Abb. 10). Darüber hinaus gab es eine Anreicherung der Signaturen krebsassoziierter Fibroblasten, epithelialer-mesenchymaler Transition (EMT) und von Entzündung in Transkriptomen von Nicht-pCR-Patienten (Abb. 11), was die Relevanz von Fibroblasten bei vermindertem Therapieansprechen der RCA-Patienten hervorhebt (Isella et al., 2015). In einem Versuch, die Relevanz eines CAF-Subtyps für die Therapieresistenz bei Rektumkarzinompatienten zu bewerten, wurde eine Analyse von öffentlich verfügbaren Einzelzell-RNA-Sequenzierungsdaten von 23 CRC-Patienten durchgeführt und ermöglichte die Identifizierung von 18 CAF-Clustern, von denen vier als inflammatorische CAFs identifiziert wurden (Cluster 3, Cluster 6, Cluster 7 und Cluster 17 (Abbildung 12 und Tabelle S2) (Lee et al., 2020). Der dominanteste iCAFs-Cluster C3 präsentierte IL-1, TNFα und NFκB als *upstream*-Regulatoren und seine Signatur war bei Nicht-pCR-Patienten vor der CRT signifikant angereichert (Abbildung 12). Wichtig ist, dass Patienten, die vor CRT einen hohem Tumorgehalt von Decorin (DCN), einem extrazellulären Marker für iCAFs, besaßen eine signifikant schlechtere DFS im Vergleich zu Patienten mit geringer Expression aufwiesen (Abb. 12). Insgesamt deuteten die Daten darauf hin, dass eine

bestimmte CAF-Polarisation, insbesondere iCAFs, Resistenz gegenüber CRT verleihen könnte (Sahai et al., 2020).

Orthotopes Mausmodell für Rektumkrebs

Um die funktionelle Bedeutung von iCAFs in der RCA-Therapie zu bestimmen, wurde ein neues präklinisches Modell etabliert, bei dem Tumororganoide orthotop in das distale Lumen von C57BL/6-Mäusen transplantiert wurden. Das Wachstum einzelner Tumore wurde durch Kolonoskopie bestätigt, und die lokale Bestrahlung des Tumors erfolgte daraufhin unter Verwendung einer speziellen Kleintierbestrahlungsanlage (*small animal radiation research platform,* SARRP) (Abb. 13). Die orthotope Transplantation von Organoiden, die Mutationen in *Apc*, *Trp53*, *Tgfbr2* und *K-ras*^{G12D} (APTK) aufwiesen, induzierte einzelne invasive Tumoren im distalen Rektum, von denen 10% Lebermetastasen ausbildeten (Varga et al., 2020). Die Transplantation von APTK-Organoiden, die zusätzlich myristoyliertes AKT (APTKA) exprimierten, förderte zudem eine ausgeprägte Malignität, die durch eine gesteigerte Häufigkeit von Lebermetastasen gekennzeichnet war (~60%) (Varga *et al.*, 2020). Interessanterweise zeigten APTKA-Tumoren eine Anreicherung von CAF-assoziierten Genen (Abb. 14), ähnlich den prätherapeutischen Biopsien von Nicht-pCR-Patienten. Darüber hinaus zeigte die molekulare Charakterisierung der CAF-Heterogenität bei APTKA-Tumoren das Vorhandensein von fünf verschiedenen CAF-Subtypen: IL-1β C0_Cluster, TGF-β C1_Cluster, IFNγ C2_Cluster, DNMT/EPO/FST C3_Cluster und RICTOR C4_Cluster (Abbildung 14). In Übereinstimmung mit den Befunden der CRC-Patienten war der prominenteste CAF-Cluster iCAFs C0_IL-1β-Cluster mit DCN als differentiell exprimiertem Marker. Wichtig ist, dass erhöhte DCN-Spiegel bei APTKA-Tumoren im Vergleich zu APTK-Tumoren durch IHC bestätigt wurden (Abbildung 14). Daher lieferten APTKA-Tumoren ein geeignetes präklinisches Modell, da sie den mit entzündlichem Stroma angereicherten Tumoren von Nicht-pCR-Rektumkarzinompatienten ähnelten. *In vivo* sprachen APTK-stämmige Tumoren auf eine Strahlentherapie (5×2Gy) an und zeigten 21 Tage nach Therapiebeginn eine Verringerung der Tumorgröße und Invasion (Abb. 15). Im Gegensatz dazu waren APTKA-induzierte Tumoren vollständig bestrahlungsresistent und wiesen nach Bestrahlung eine höhere Invasivität und Häufigkeit von Lebermetastasen auf (Abb. 15). Darüber hinaus zeigten bestrahlte APTKA-Tumoren histologisch gleichgerichtete morphologische Muster von CAFs, was auf Änderungen der Bestandteile der extrazellulären Matrix (ECM) hindeutete, die durch die Zunahme von Kollagenablagerungen und DCN und einer ausgeprägten Infiltration

zytotoxischer T-Zellen bestätigt wurde (Abb. 16) (Gaggioli et al., 2007). Wichtig ist, dass APTK- und APTKA-Organoide *ex vivo* gleichermaßen empfindlich gegenüber Bestrahlung waren und das Tumorwachstum in beiden Fällen deutlich verzögert war, wenn Organoide nach 5x2Gy *ex-vivo*-Bestrahlung subkutan injiziert wurden (Abb. 17), was die Annahme stark untermauerte, dass APTKA-Organoide nicht intrinsisch resistent gegen Bestrahlung waren, sondern dies eher durch das TME *in vivo* vermittelt wurde.

Resistente Tumoren induzieren Polarisierung inflammatorischer CAFs abhängig von IL-1α

Um zu untersuchen, wie APTK- und APTKA-Tumororganoide Fibroblasten auf parakrine Weise beeinflussen, wurden Überstände von beiden Linien gesammelt und Darmfibroblasten von unbehandelten Wildtyp-Mäusen 24 Stunden *ex vivo* behandelt (Abb. 3A). Die RNAseq-Analyse bestätigte unterschiedliche transkriptomische Profile in Fibroblasten, die den beiden Organoidüberständen ausgesetzt waren (Abb. 3B). *Gene set enrichment* Analysen (GSEA) ergaben eine starke inflammatorische Polarisation in Fibroblasten, die APTKA-konditioniertem Überstand ausgesetzt waren und eine deutliche Anreicherung von iCAFs oder Cluster 0_IL1β CAFs, aber keine der anderen CAF-Clustern assoziierten Genen (Abb. 18), ähnlich dem Phänotyp, der in ganzen Tumoren *in vivo* beobachtet wurde (Ohlund *et al.*, 2017). Laut *Ingenuity-pathway* Analyse (IPA) waren NF-κB und p38 als *upstream* Komplexe für das inflammatorische Profil verantwortlich (Abb. 19). Tatsächlich konnte die Induktion eines iCAF-Phänotyps in Wildtyp-Fibroblasten durch APTKA-konditioniertes Medium durch die Anwesenheit spezifischer IKKß- oder p38-Inhibitoren signifikant inhibiert werden (Abb. 19). Um die von APTKA-Organoiden sekretierten Faktoren zu identifizieren, die für die Aktivierung von NF-κB und p38 in Fibroblasten verantwortlich waren, wurde eine RNAseq-Analyse von APTK- und APTKA-Tumororganoiden durchgeführt, die die Identifizierung mehrerer differentiell exprimierter Gene ermöglichte, die für Zytokine kodieren (Abb. 20). Neutralisierende Antikörper gegen ausgewählte Zytokine wurden zusammen mit APTKA-Überständen verwendet und die Expression inflammatorischer Gene in Fibroblasten untersucht. Nur die Inhibierung von IL-1α verhinderte die Hochregulation pro-inflammatorischer Gene in Fibroblasten, die mit APTKA-konditioniertem Medium behandelt wurden (Abb. 20). Um die Stabilität der iCAF-Polarisierung und die mögliche Reversibilität des Phänotyps nach IL-1α-Blockade zu untersuchen, wurden Fibroblasten 24 Stunden lang mit APTKA-konditioniertem Medium

stimuliert, bevor der IL-1R-Antogonist Anakinra oder frisches APTKA-Medium zugegeben wurde oder reguläres Medium ersetzt wurde. Interessanterweise reduzierte das einfache Ersetzen von APTKA-Medium durch reguläres Medium die Expression entzündlicher Gene in Fibroblasten (Abb. 20). Ebenso hob die Zugabe von Anakinra zu APTKA-Medium die Expression dieser Gene vollständig auf, was darauf hinwies, dass von Organoiden abgegebenes IL-1α erforderlich war, um die CAF-Polarisierung aufrechtzuerhalten.

IL-1 ist für die Therapieresistenz von orthotopen Tumoren verantwortlich

Um zu untersuchen, ob eine IL-1α-Blockade die Reaktion von APTKA-Tumoren auf eine Strahlentherapie *in vivo* verbessern würde, wurden Mäuse mit Anakinra behandelt, sobald sich Tumore gebildet hatten (Abb. 21). Die Verabreichung führte zu einer deutlichen Reduktion der Tumorgrößen und -invasivität und blockierte die Formation von Metastasen nach Bestrahlung (Abb. 21). Dies ging mit einer signifikanten Verringerung der Kollagenablagerung, DCN Positivität und myeloider Inflitration einher während eine ausgeprägte zytotoxische T-Zell-Infiltration auftrat (Abb. 21), was bedeutet, dass Anakinra einen ausgeprägten Effekt auf die CAF-Aktivierung hatte und dass von Tumorzellen stammendes IL-1α einen Schlüsselfaktor für die Therapieresistenz *in vivo* darstellt. Ähnliche Verbesserungen im Therapieerfolg wurden bei der Verwendung des genetischen präklinischen Mausmodells *Col1a2CreERT2 Il1rF/F* der eingeschränkten *Il1r1*-Ablation in CAFs festgestellt (Abbildung 22), was auf die zentrale Rolle von IL-1-polarisierten CAFs bei der Förderung der Therapieresistenz und der Entgegenwirkung zytotoxischer Strahlentherapieeffekte hinweist. Um dies weiter zu bestätigen, wurde die *Il1a*-Transkription in Strahlungs-sensitiven APTK-Organoiden durch CRISPRa/Cas9 aktiviert (Abb. 23). Fibroblasten, die konditioniertem Medium von APTK-sg*Il1a*-Organoiden ausgesetzt wurden, zeigten ein inflammatorisches Profil, das mit dem APTKA-induzierten vergleichbar war (Abb. 23). Darüber hinaus machte eine erhöhte IL-1α Freisetzung durch APTK-Organoide die entsprechenden Tumoren *in vivo* resistent gegen Strahlentherapie (Abb. 23). APTK-sg*Il1a*-Tumore nahmen nach Bestrahlung nicht an Größe ab und wurden invasiver (Abb. 23). Ähnlich den APTKA-Tumoren, wiesen APTK-sg*Il1a*-Tumore eine verstärkte Stroma-Reaktion nach Bestrahlung auf (Abb. 23). Zusammengenommen bestätigten diese Daten die Schlussfolgerung, dass von Tumorzellen stammendes IL-1α CAFs in Richtung eines inflammatorischen Phänotyps polarisiert, der die Resistenz gegen Strahlentherapie antreibt.

Chemotherapie inflammatorischer Fibroblasten induziert Seneszenz

Um zu untersuchen, wie deutlich polarisierte Fibroblasten auf eine Strahlentherapie ansprechen, wurden primäre Fibroblasten mit APTK- oder APTKA-konditioniertem Medium behandelt oder unbehandelt gelassen und dann einer Bestrahlung *ex vivo* unterzogen (3×2Gy; Abb. 24). Dies führte zu deutlichen morphologischen Unterschieden zwischen den unterschiedlich behandelten Fibroblasten und im Vergleich zu unbehandelten oder APTK-polarisierten Fibroblasten entwickelten APTKA-inkubierte Fibroblasten eine länglichere Form (Abb. 24), die dem *in vivo*-Phänotyp ähnelte. Die Morphologie der ausgerichteten Fibroblasten ist mit ECM-Veränderungen verbunden (Gaggioli *et al.*, 2007). Daher wurde das Matrisom von bestrahlten und nicht bestrahlten APTKA-polarisierten Fibroblasten durch Massenspektrometrie analysiert (Naba et al., 2015; Naba et al., 2017). In Übereinstimmung mit den morphologischen Veränderungen führte die Bestrahlung zu einem signifikanten Anstieg verschiedener ECM-Proteine (Abb. 24), von denen viele die Tumorprogression unterstützen (Naba et al., 2014; Tian et al., 2019). Darüber hinaus ergab die RNAseq-Analyse von bestrahlten und nicht bestrahlten APTKA-polarisierten Fibroblasten eine Herunterregulierung von Zellzyklus- und Zellzyklus-Checkpoint-assozierten Genen, sowie die Induktion von Seneszenz-regulierenden Genen (Abb. 25). Darüber hinaus zeigte IPA, dass viele der induzierten Gene, einschließlich derjenigen, die verschiedene sekretierte Faktoren kodieren (extrazelluläre Proteine: Kollagene, Proteoglycane, Wachstumsfaktoren, ECM-Regulatoren, ECM-assoziierte Proteine), die in der Matrisomanalyse identifiziert wurden, sowie der Zellzyklusinhibitor *Cdkn1a* in p53-abhängiger Weise reguliert waren, was auf die Induktion einer p53-abhängigen Seneszenz in APTKA-polarisierten Fibroblasten bei Bestrahlung hinwies, was durch Immunblot-Analyse und SA-βgal-positive Färbung weiter bestätigt wurde (Abb. 25). Die Seneszenzinduktion war abhängig von IL-1 und ging mit einer deutlich erhöhten DNA-Schädigung einher (Abb. 25). In Übereinstimmung mit diesen Ergebnissen wurde ein signifikanter Anstieg des nuklearen p21 in Stromazellen und β-Gal-Positivität bei orthotopen APTKA-Tumoren bei Bestrahlung nachgewiesen, was auf die Induktion eines Seneszenzprogramms *in vivo* hinweist (Abb. 25). Darüber hinaus wurde Seneszenz auch bei mit APTKA-Überstand konditionierten Fibroblasten oder IL-1α-stimulierten menschlichen Fibroblasten, die einer 5-Fluorouracil (5-FU) -Chemotherapie unterzogen wurden, beobachtet. Um die funktionelle Relevanz der CAF-Seneszenz in der Therapieresistenz zu bestätigen, wurden orthotope APTKA-Tumortransplantationen in *Trp53*$^{-/-}$ durchgeführt, die *in vivo* auf die Strahlentherapie ansprachen während die Seneszenzinduktion verhindert wurde (Abb. 27). In

ähnlicher Weise sensibilisierte die Behandlung von APTKA-tumortragenden Mäusen mit der senolytischen Verbindung Venetoclax (100 mg/kg/Tag) zusätzlich zu RT APTKA-Tumore für Bestrahlung und führte zu einer signifikanten Abnahme von Tumorlast, Invasion und Lebermetastasen, begleitet von einer verminderten CAF-Aktivierung, was sich in einer reduzierten DCN- und Kollagenablagerung widerspiegelte (Abb. 28). Insgesamt unterstreichten diese Ergebnisse die Rolle von IL-1α bei der Steuerung eines p53-vermittelten Seneszenzprogramms von iCAFs nach genotoxischer Therapie.

Es wurde angenommen, dass IL-1α Fibroblasten für die bestrahlungsinduzierte Seneszenz durch reaktive Sauerstoff- und Stickstoffspezies (ROS und RNS) sensibilisiert, was wiederum oxidative DNA-Schäden auslöst. Es wurden jedoch keine Unterschiede in den ROS-Spiegeln zwischen unbehandelten, APTKA- oder APTK-konditionierten Fibroblasten festgestellt (Abb. 30). Darüber hinaus zeigten iCAFs eine geringere mitochondriale Aktivität und Glykolyserate, eine verminderte Proliferation und einen verstärkt ruhenden Phänotyp (Abb. 29).

Demgemäß waren 72 Stunden nach Exposition gegenüber APTKA-konditioniertem Medium oder rekombinantem IL-1α, die Nitritspiegel in Fibroblastenüberständen signifikant erhöht, was mit einer Zunahme der durch 8-OHdG-Immunfluoreszenz bestimmten oxidativen DNA-Schädigung einherging (Abb. 30) Die Verabreichung des NOS2-Inhibitors W1400 blockierte die Nitritproduktion und verhinderte eine oxidative DNA-Schädigung sowie eine Seneszenzinduktion in Fibroblasten, die mit APTKA-konditioniertem Medium behandelt worden waren (Abb. 30). Zusammengenommen bestätigten diese Ergebnisse, dass die IL-1α–abhängige Polarisierung von iCAFs die Nitritproduktion und die oxidative DNA-Schädigung in diesen Zellen erhöhte. Die anschließende Bestrahlung verstärkte die DNA-Schädigung weiter und löste ein p53-abhängiges Seneszenzprogramm aus, das durch ein ausgeprägtes ECM-Profil gekennzeichnet war, das die Tumorprogression unterstützte.

Niedrige IL-1RA-Spiegel erhöhen die IL-1-Signalübertragung bei Rektumkrebspatienten und sensibilisieren CAFs für therapieinduzierte Seneszenz

Um zu untersuchen, ob die beobachteten IL-1α–induzierten Veränderungen im TME im Mausmodell mit einem schlechten Therapieansprechen verbunden sind, wurden Serumproben von Nicht-pCR- und pCR-Patienten unter Verwendung des *Luminex Bio-Plex-Assays* analysiert. Während die IL-1α–Spiegel bei allen untersuchten Patienten unter der

Nachweisgrenze lagen, waren die IL-1RA-Spiegel im Serum bei Nicht-pCR-Patienten mit verbleibenden Lymphknotenmetastasen und schlechter Prognose nach CRT deutlich reduziert (Abb. 32). Dies deutete darauf hin, dass diese Patienten aufgrund der geringeren Expression des Antagonisten tatsächlich eine verstärkte IL-1-Signalübertragung zeigten. Es wurde gezeigt, dass IL-1RA-Spiegel *in vivo* häufig mit zwei *single nucleotide polymorphisms* (SNPs) in *IL-1RA* (rs4251961 T/C und rs579543 G/A) assoziiert sind, wobei homozygote Träger der Genotypen rs4251961 T/T und rs579543 G/G höhere IL-RA-Spiegel aufweisen (Rafiq et al., 2007). Erhöhte IL-1RA-Serumspiegel wurden nur bei homozygoten rs4251961 T/T-Patienten bestätigt (Abb. 31). Wichtig ist, dass eine niedrigere *IL1RN*-Genexpression in prä-therapeutischen Tumorbiopsien mit einem signifikant schlechteren DFS assoziiert war (Abb. 31), was die Relevanz einer verstärkten IL-1-Signalübertragung für das Ansprechen auf die Therapie unterstützte. RNA-Expressionsprofile von 12 Nicht-pCR-Patienten vor und nach CRT wurden verglichen (Abb. 32). Die Analyse ergab, dass die CRT bei diesen Patienten eine EMT-, ECM- und Kollagenbildungssignatur induzierte, sowie eine ausgeprägte Stromareaktion, die durch Sirius-Rot-Färbung, DCN-Positivität und ein p21-Seneszenzprofil nachgewiesen wurde (Abb. 32), was einen Zusammenhang zwischen der IL-1-Signalkaskade und der therapieinduzierten stromalen Seneszenz bei RCA-Patienten stark andeutete. Um dies weiter zu validieren, wurden von Patienten stammende Organoide (PDO) aus Biopsien hergestellt, die vor Beginn der CRT von Nicht-pCR-Patienten entnommen wurden, und die Organoide, die durch unterschiedliche IL-1RA-Werte, aber vergleichbare IL-1α–Werte gekennzeichnet waren wurden bewertet (Abb. 33). Die Inkubation von menschlichen Darmfibroblasten mit konditionierten Überständen von Organoiden mit niedrigem IL-1RA-Gehalt induzierte ein stärkeres proinflammatorisches Profil als Überstände von Organoiden mit hohem IL-1RA-Gehalt und führte zu einer höheren Nitritproduktion durch Fibroblasten. Dies wurde auch bestätigt, wenn Fibroblasten nur mit IL-1α stimuliert wurden (Abb. 33). Die SA-β-gal-Färbung zeigte, dass eine stärkere Seneszenzinduktion nach Bestrahlung auftrat, wenn Fibroblasten mit niedrigem IL-1RA-Gehalt vorkonditioniert wurden. Dies konnte durch Anakinra blockiert werden, was die IL-1-Abhängigkeit der therapieinduzierten Seneszenz in CAFs bestätigte (Abb. 33).

Zusammengefasst zeigt diese Studie die Bedeutung von CAFs in der Therapieresistenz von RCA-Patienten und das gegenseitige Wechselspiel zwischen Tumorzellen und CAFs, welches das CRT-Ergebnis stark beeinflusst. Interessanterweise scheinen die IL-1RA-Serumspiegel, die die allgemeine IL-1-Signalübertragung beeinflussen, anstelle eines

eindeutigen Mutationsprofils in Tumorzellen, das Ausmaß der CAF-Polarisierung und der iNOS-abhängigen Nitritproduktion zu bestimmen, welche eine oxidative DNA-Schädigung auslöst und so CAFs für die therapieinduzierte Seneszenz sensibilisiert. Die seneszenzassoziierte Produktion einer Vielzahl von ECM-Faktoren wirkt dem therapieinduzierten Tumorzelltod entgegen und fördert die Resistenz und Tumorprogression (Abb. 1). Wichtig ist, dass die Reversibilität des CAF-Phänotyps aufgrund ihrer Plastizität eine therapeutische Intervention mit Anakinra auch bei etablierten Tumoren ermöglicht und eine Seneszenz verhindert. Daher können die Ergebnisse zu einem Paradigmenwechsel in der RCA-Therapie führen und auch für andere stromareiche Tumoren von großer Relevanz sein.

Graphical abstract

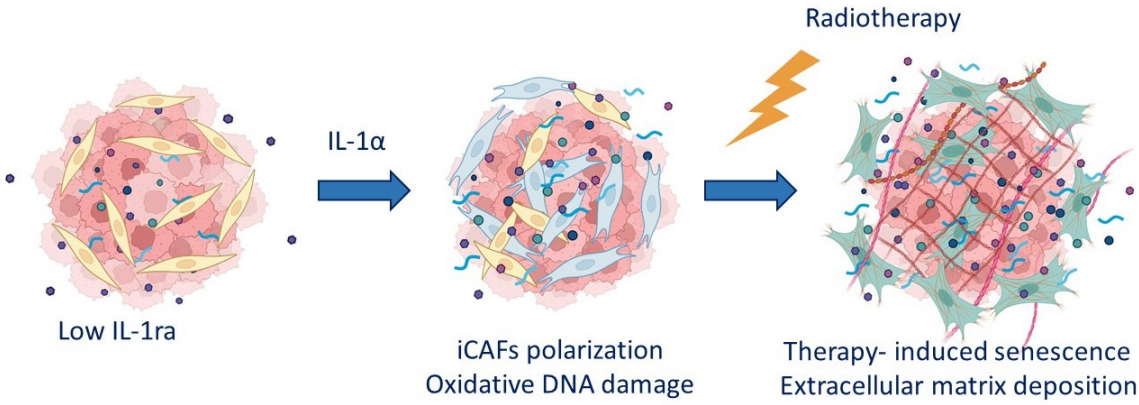

Figure 1: Graphical abstract. Among rectal cancer patients with reduced circulating levels of IL-1ra, tumor cells-derived IL-1α drives inflammatory polarization of CAFs and consequently an upregulation of iNOS, which elevates nitrite production in iCAFs resulting in an enhanced oxidative DNA damage. Radiotherapy induced genotoxic stress further triggers senescence among iCAFs. Senescent iCAFs display pronounced secretome and enhanced ECM deposition which counteracts irradiation-induced cell death, hence promoting tumor progression and therapy resistance. Scheme generated by BioRender (publication license has been obtained).

1. Introduction

1.1 Rectal cancer

The rectum is the distal part of the large intestine located between the sigmoid colon and the anal canal. It starts from the rectosigmoid junction and terminates at the anorectal ring (Fazeli and Keramati, 2015). The rectum length is approximately 12 to 15 cm and near its end it forms a dilated rectal ampulla. The rectal wall presents five distinct layers: mucosa, submucosa, inner circular muscle, outer longitudinal muscle and serosa (Fazeli and Keramati, 2015; Paschke et al., 2018). Diverse pathologies within the rectum are common and include abscesses, hemorrhoids, incontinence and rectal cancer (RCA) (Keller et al., 2020).

1.1.1 Epidemiology and risk factors

After colon cancers, RCA constitutes the second most common cancer of large intestine (28%) (Hervas Moron et al., 2010). In epidemiologic studies, RCA have always been considered a part of colorectal cancer (CRC). Cancers of the rectum and rectosigmoid junction represent 30% of all CRC diagnosed (Paschke *et al.*, 2018). Within the European union, the yearly incidence of RCA is around 125 000, accounting yearly for 15-25 cases/100 000 population and predicted of further presenting increasing incidence among both genders (Glynne-Jones et al., 2017). The median age for RCA diagnosis is younger than CRC with 63 years in men and 65 years in women (Siegel et al., 2014). The 5-years overall survival rate for RCA patients is modestly better than CRC patients with a rate of 66.5% compared to 64.2%. The mortality rates are gender affected with a 30-40% higher incidence in men compared to woman (Siegel *et al.*, 2014) . Accumulating scientific evidence over the last years allowed approaching RCA as a distinct entity with characterized diagnosis, therapeutic approaches and outcomes. Considering their different embryonic origins, cancers arising from the colon and rectum parts of the large bowel present distinct features as well as etiologies and risk factors (Keller *et al.*, 2020; Paschke *et al.*, 2018; Wei et al., 2004). For instance, the rectum positioning within the pelvic cavity, its connection with genitourinary organs, rectal tumors confinement to distinct blood supply, lymphatic drainage and nervous innervation compared to colon tumors account for clear existing differences in molecular carcinogenesis, surgical topography and multimodal treatments plans.

There is a highly recognized hereditary component for colon cancer compared to RCA with findings revealing that a familial history of hereditary syndromes such as hereditary non-polyposis colorectal cancer (HNPCC), familial adenomatous polyposis (FAP) and MUTYH-associated polyposis (MAP) more strongly affects colon cancer risks compared than RCA (Lynch and Smyrk, 1998). Environmental factors such as healthy lifestyle and exercise reduce the risk of RCA. High intake of calcium, milk and dietary fibers are considered as protective dietary components against RCA development (Murphy et al., 2012). Excessive consumption of red or processed meat, tobacco and alcohol is reported to increase RCA incidence (Wei *et al.*, 2004). Type II diabetes mellitus is an additional risk factor with a 20% higher incidence of RCA compared to non-diabetic patients (Yuhara et al., 2011).

1.1.2 Diagnosis and histopathology

Rectal bleeding is the prominent clinical manifestation of rectal cancer. Additional symptoms comprise tenesmus, incomplete stool evacuation, obstruction, pelvic or rectal pain. Additional yet rare reported symptoms include bladder fistula, fever, bacteremia or sepsis and abscesses. RCA screening includes a digital rectal examination (DRE) and endoscopic-based biopsies for histological evaluation and assessment (Fokas *et al.*, 2020; Glynne-Jones *et al.*, 2017; Roeder et al., 2020). Distal tumors with a margin of ≤15 cm from the anus as assessed by rigid sigmoidoscopy are classified as rectal cancer and further categorized a low (≤5 cm), middle ranging from 5 – 10 cm and high between 10 to 15 cm (Glynne-Jones *et al.*, 2017). Pelvic magnetic resonance imaging (MRI) is considered a highly accurate diagnostic test for RCA patients enabling detection of extramural vascular invasion (EMVI), tumor stage determination as well as distance to the circumferential resection margin (CRM) and prediction of potential distant lungs or liver metastasis which are further confirmed by computed tomography (CT) scan of abdomen and thorax, liver MRI and positron emission tomography (PET) (Roeder *et al.*, 2020). Further classification of locally advanced T3-stages tumors, of a 6-15 mm depth invasion beyond the muscularis propria, is allowed by high-quality MRI which is crucial for guiding further therapeutic plans and presents a sensitivity of 87% and 77% in the assessment of tumor size and nodal infiltration (Edge and Compton, 2010; Hunter et al., 2012; Taylor et al., 2014).

1.1.3 Local and locoregional management

A convenient treatment modality for the management of early stage, low grade local rectal tumors (cT1N0) is transanal endoscopic microsurgery (TEM) allowing on site full-thickness excision of rectal lesions without affecting anorectal function. An alternative approach to surgery might be local radiotherapy (RT) alone or in conjunction with chemotherapy (Bach et al., 2009; Gerard et al., 2008; Junginger et al., 2016). For treating patients with locally advanced rectal cancer including lymph nodes positivity, neoadjuvant therapy is recommended followed by total mesorectal excision surgery (TME) (Figure 2) (Bujko et al., 2006; Fokas *et al.*, 2020; Fokas *et al.*, 2014; Ngan et al., 2012). Short course radiotherapy (SCRT) and long-course chemoradiotherapy (LCCRT) are the employed neoadjuvant therapeutic approaches. The SCRT plan is performed by daily delivery of 5 Gy irradiation over 5 days followed by an immediate surgery within 10 days post first fraction irradiation (Erlandsson et al., 2017). On the other hand, LCCRT is delivered by fractions of low dose irradiation of 1.8-2 Gy over 5 to 6 weeks treatment plan leading to a cumulative dose of 45-50.4 Gy (Braendengen et al., 2008) in combination with cytotoxic chemotherapy including infusion of 5-fluorouracil or oral fluoropyrimidines, oxaliplatin, irinotecan and cetuximab (Deng et al., 2016b; Hofheinz et al., 2012; Rodel *et al.*, 2015). Several phase III randomized trials reported no statistically significant differences between SCRT and LCCRT with respect to prognostic parameters of overall survival, disease free survival and relapse-free survival rates (Bujko *et al.*, 2006; Cisel et al., 2019). Therefore, there are real evidence for recommending one regimen over the other. Neoadjuvant chemo-radiotherapy followed by TME resulted in a reduction in local recurrence rates specially for tumors localized at 5-10 cm depth from the anal verge with a 6% five-year cumulative incidence of local relapse for patients assigned to pre-surgical CRT compared to a 13% rate among patients subjected to postoperative-CRT (Fokas *et al.*, 2014; Sauer et al., 2004). Compared to surgical resection alone, the multimodal treatment plan of neoadjuvant SCRT and surgical excision, proved to be an efficient approach in promoting higher 5-years survival rates among patients (Roeder *et al.*, 2020). The prognostic outcomes of RCA patients treated with neoadjuvant CRT followed by surgical resection are assessed by tumor regression grade (TRG) parameter for grading post-therapeutic fibrosis, primary tumor regression, local invasion to nearby lymph nodes and distant metastasis which are collectively assessed by digital rectal examination, proctoscopy and reimaging by MRI (Fokas *et al.*, 2020; Keller *et al.*, 2020; Roeder *et al.*, 2020). Clinical or pathological complete response (cCR or pCR respectively) corresponding to excellent

prognosis, is a clinical outcome reported in 10%-40% of rectal cancer patients after 12 weeks of therapy initiation (Glynne-Jones *et al.*, 2017). It is defined as the complete absence of a residual tumor at the primary site, negative malignant histological outcomes for examined pos-therapeutic scar and lack of residual tumor cells in the draining lymph nodes as revealed by MRI (Glynne-Jones and Hughes, 2012). The likelihood of pCR occurrence among RCA patients relatively depends on the pretherapeutic TNM stage and a set of undefined nor fully uncovered molecular factors.

The therapeutic management of RCA patients with distant metastasis takes into consideration the tumor characteristic and the diagnostic features as well as the treatment plan potentially associated adverse effects and side toxicity. Alleviation of RCA local symptoms is achieved by RT with the recommended SCRT along a systemic chemotherapy applied within 2 weeks from therapy initiation, promoting palliation of symptoms in 80% of patients (Tyc-Szczepaniak et al., 2013). In the case of a curable oligometastatic disease, a prompt and effective treatment plan includes a safe combination of SCRT with triplet chemotherapy of capecitabine, oxaliplatin and bevacizumab for a facilitated liver mastectomy (van Dijk et al., 2013). The lack of molecular markers in rectal cancer for an effective evaluation of therapeutic outcomes and optimization of pCR rates among RCA patients sparring surgical intervention and associated unfavorable adverse effects hinders implementation of personalized treatment plans.

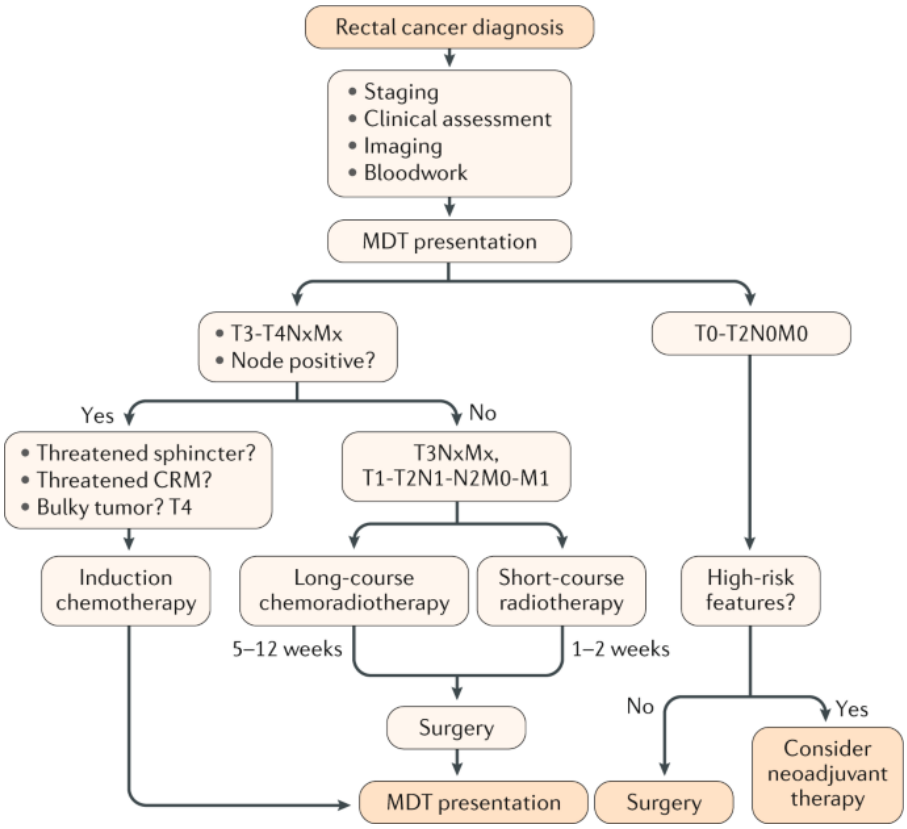

Figure 2: Multidisciplinary treatment plan for rectal cancer. Scheme summarizing the multimodal treatment plan for rectal cancer therapy based on tumor initial stage (TNM classification). MDT: multidisciplinary team. Nx: undetermined residual lymph node metastases. Mx: undetermined secondary site metastases. CRM: circumferential resection margin. Copied from (Keller *et al.*, 2020). Copyright permission has been obtained.

1.1.4 Molecular characterization of colon and rectal cancer

Among solid malignancies, CRC was the first to be molecularly characterized with a detailed identification of implicated altered signaling pathways (Fearon, 2011). An earlier model described sequential accumulation of "leading" genetic and epigenetic alterations driving malignant evolution of an adenoma into an aggressive carcinoma (Vogelstein et al., 2013) . A deregulation of critical genetic pathways that control cellular differentiation, cell death and proliferation such as adenomatous polyposis coli (*APC*), tumor protein p53 (*Tp53*), SMAD family member 4 (*SMAD4*), Kirsten rat sarcoma viral oncogene homolog (*KRAS*), and PI3K catalytic subunit alpha (*PIK3CA*), underlines a non-random progression of colorectal carcinogenesis (Vogelstein et al., 1988; Vogelstein *et al.*, 2013). The joint efforts of the Cancer Genome Atlas Network, conveyed a fully integrated view of the genetic and epigenetic landscape of human colon and rectal cancer (Network, 2012). Hence enabling, through analysis of exosome sequencing, transcriptomic profiles, methylation patterns, microRNAs expression and DNA copy number among 276 samples, thorough insights on CRC pathogenesis and potential therapeutic targets (Network, 2012). Findings demonstrated no genomic differences among non-hypermutated adenocarcinomas of the colon and rectum. However, chromosomal instability (CIN), aneuploidy and loss of heterozygosity governed 85% of malignant CRC tumors (Network, 2012). Alternatively, hypermethylated tumors were majorly encountered in the right colon, predominantly presenting high CpG island methylation phenotype ($CIMP^{hi}$) and consequently exhibiting microsatellite instability (MSI) driven by inactivation of DNA mismatch repair genes (mutL homologue 1 "*MLH1*", mutS homologue 2 "*MSH2*", "*MSH3*", *MSH6* and PMS1 homologue 2 "PMS2") (Dienstmann et al., 2017; Network, 2012; Schmitt and Greten, 2021). Genomic studies further recognized nearly ubiquitous events in CRC such as WNT signaling inactivation, TGF-β pathway deregulation as well as EGFR pathway alterations (Network, 2012; Seshagiri et al., 2012; Sjoblom et al., 2006).

As the genomic characterization of tumor cells seemed of limited prediction power on patients' therapy response and prognosis (Grasso et al., 2018; Network, 2012), further international

efforts emerged, integrating large scale transcriptomic data from whole CRC tumors and aimed to convey a broadly accepted molecular stratification of CRC by comparing six independent transcriptomic-based classifiers (Budinska et al., 2013; De Sousa et al., 2013; Marisa et al., 2013; Perez-Villamil et al., 2012; Roepman et al., 2014; Sadanandam et al., 2013). The international consortium pioneering work enabled subcategorization of CRC tumors into four robust subtypes, each of well-defined genomic, epigenetic, histological and clinical features (Figure 3) (Guinney *et al.*, 2015). The consensus molecular subtype (CMS) system identified 14% of CRC tumors as CMS1 group or the "immune subtype" which is characterized by MSI, hypermethylation patterns, pronounced BRAFV600F mutational profile and a marked intra-tumoral infiltration of T lymphocytes. Hence, CMS1 tumors seem mostly encountered in the right colon and exhibiting good prognosis and DFS rates (Guinney *et al.*, 2015). In contrast, tumors of CIS belong to one of the following subtypes: canonical- CMS2, metabolic- CMS3 or mesenchymal- CMS4 subtype representing respectively 37%, 13% and 23% of all CRC tumors (Guinney *et al.*, 2015). Firstly, CMS2 subgroup, additionally known as the "canonical subtype", display low gene hypermethylation and pronounced activation of WNT/MYC signaling pathways. Secondly, tumors belonging to the CMS3 group, or "metabolic subcluster", garner, in contrast to CMS2, MSI, intermediate level of hypermethylation and prominent epithelial cells glutaminolysis or lipogenesis metabolic programs (Dienstmann *et al.*, 2017; Guinney *et al.*, 2015). Moreover, CMS3 tumors display pronounced KRAS-gain of function mutation which has been previously linked to glucose metabolism among CRC tumor cells (Guinney *et al.*, 2015; Yun et al., 2009). Finally, worst DFS and OS rates were reported among CMS4 tumors, or the mesenchymal subtype, exhibiting significant enrichment of epithelial mesenchymal transition (EMT) and extracellular matrix (ECM) pathways with a distinguished pronounced content of stromal cells, precisely cancer associated fibroblasts (CAFs) and TGF-β signaling activation. Importantly, the global gene expression profiles of mesenchymal CRC tumors and their significantly poor clinical outcomes seemed to be majorly governed by the TME CAFs. Immunohistochemical and bioinformatic analysis employing patients-derived organoids and xenografts identified a CAFs-specific signature and a stroma-TGFβ-mediated gene program that recapitulate the clinical features of the mesenchymal subtype of CRC with higher aggressiveness, poor survival and therapy resistance (Calon et al., 2012; Isella *et al.*, 2015). Interestingly TGFβ blockade in CAFs in conjunction with checkpoint inhibition halts CRC progression while favoring cytotoxic T cells intra-tumoral infiltration (Tauriello et al., 2018).

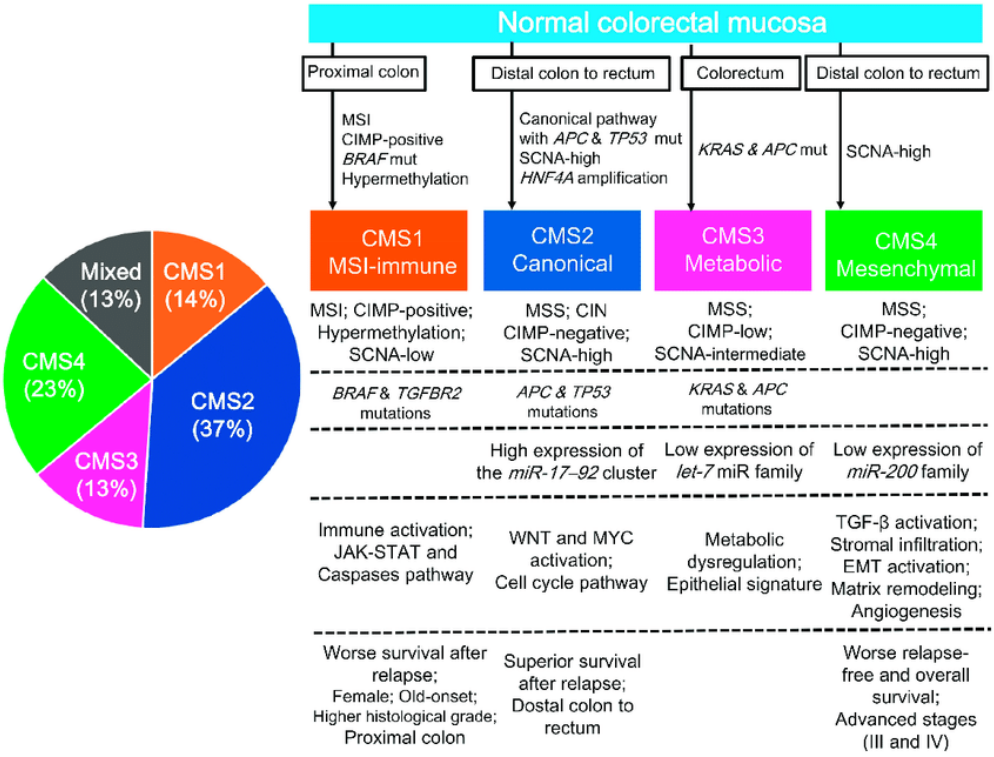

Figure 3: The consensus molecular subtype classifier of colorectal cancer and its four identified subtypes. Bulk transcriptomic data of whole CRC tumors is employed to classify the tumors according to one of the following subgroups: MSI-immune (CMS1), canonical (CMS2), metabolic (CMS3) and mesenchymal (CMS4) subtype. CIN: chromosomal instability; CMS: consensus molecular subtype; MSS: microsatellite stable; SCNA: somatic copy number alteration; CIMP: CpG island methylator phenotype; MSI: microsatellite instability; EMT: epithelial-mesenchymal transition. Copied from (Inamura, 2018). Open access article.

The findings summarized above emphasizes CRC evolution and progression as a complex process that cannot be merely confined to the mutational profile of epithelial cells but rather their dynamic interplay with components of the tumor microenvironment (TME) which comprises endothelial cells, the immune system, gut microbiome, cancer associated fibroblasts and neuronal innervations (Schmitt and Greten, 2021). Orchestrated crosstalk between the TME and epithelial compartment govern tumor proliferation, stemness, distal dissemination, angiogenesis, immune surveillance and ultimately therapy resistance and relapse (Ganesh and Massague, 2021; Quail and Joyce, 2013; Quante et al., 2013; Schmitt and Greten, 2021). Therefore, research optimization in colon and rectal cancer therapy, such as radiotherapy, shall not merely examine the tumor cells intrinsic properties and hence undermine thorough assessments of the TME contributions at molecular, cellular and systemic levels, given the growing body of evidence on its impacting not only on metastasis yet also therapy response: initial resistance and recurrence (Barker et al., 2015).

1.2 Cancer associated fibroblasts

The most prominent cells in the TME are cancer associated fibroblasts (CAFs), a heterogeneous cell population, derived from various sources including resident fibroblasts, adipocytes, pericytes, endothelial cells, bone-marrow derived mesenchymal cells and stellate cells (Biffi and Tuveson, 2021; Chen et al., 2021; Kalluri, 2016; Sahai *et al.*, 2020). The challenge in defining CAFs resides in the lack of exclusive markers. They are often identified by their spindle shaped mesenchymal morphology, their lacking lineage markers for epithelial cells, endothelial cells and leukocytes, as well as their expressing α-smooth muscle actin (α-SMA), fibroblasts activation protein α (FAP), S100 calcium binding protein A4 (S100A4) and platelet derived growth factor receptor α/β (PDGFRα/β) (Chen *et al.*, 2021; Sahai *et al.*, 2020).

1.2.1 CAFs functions

CAFs play major tumor supportive roles facilitating cancer progression. Their synthetic and secretory properties attributed to their distinct polarization, subtypes and mechanisms of activation, reflect a broad array of functionalities ranging from supporting primary tumors local progression to secondary sites metastasis (Figure 4).

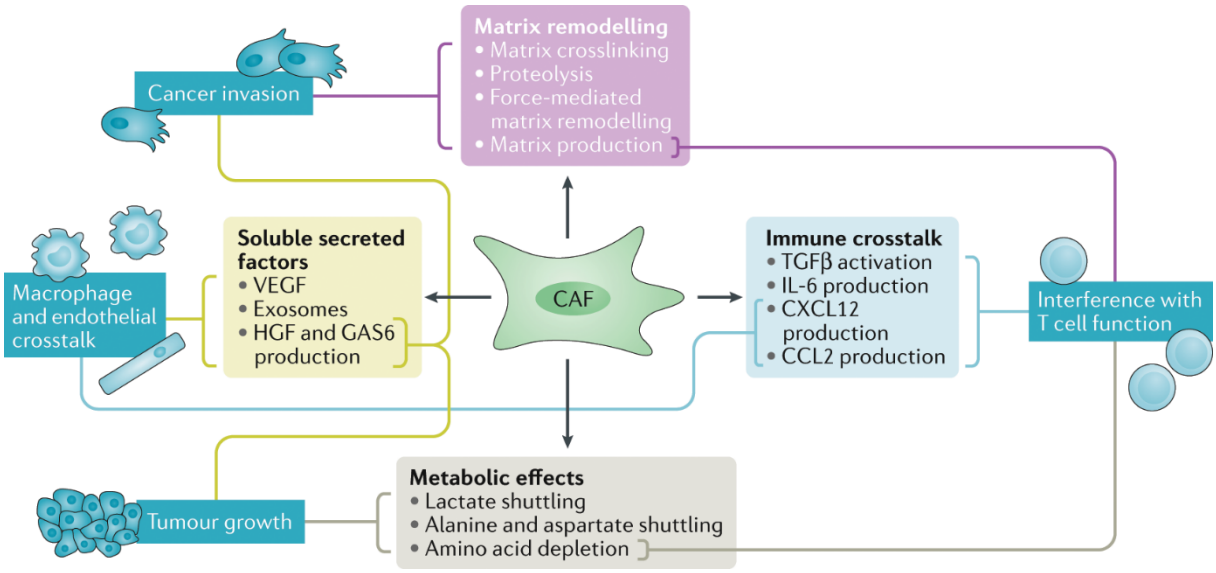

Figure 4: Functional heterogeneity of cancer associated fibroblasts (CAFs). Schematic illustration of the different biologic functions of CAFs attributed to their secretory and synthetic profiles. They have been implicated in tumor growth, progression, metastasis, extracellular matrix remodeling and immunomodulation of the tumor microenvironment that is further influenced by the altered tumor metabolome. CAF, cancer-associated fibroblast; CCL2, CC-chemokine ligand 2;

CXCL12, CXC-chemokine ligand 12; IL-6, interleukin-6; GAS6, growth arrest-specific protein 6; HGF, hepatocyte growth factor; TGFβ, transforming growth factor-β; VEGF, vascular endothelial growth factor. Copied from (Sahai *et al.*, 2020). Open access article.

CAFs secretome consists of growth factors, cytokines, chemokines and exosomes including transforming growth factor beta (TGFβ), leukemia inhibitory factor (LIF), heat shock factor 1 (HSF1), growth arrest-specific protein 6 (GAS6), tumor necrosis factor alpha (TNF-α) and many other soluble factors (Chen and Song, 2019; Kalluri, 2016). Therefore, they do not only provide pro-proliferative signals directly to cancer cells but also impact cancer progression by driving angiogenesis through their production of vascular endothelial growth factor (VEGF) and stromal-cell derived factor 1 (SDF1) (Fukumura et al., 1998; Orimo et al., 2005). The systemic effects of CAFs secretome additionally promote the invasive properties and growth of disseminated cells in metastatic sites (Bruzzese et al., 2014). For instance, in colorectal cancer, activated CAFs release IL-11 which is proven to enhance survival and distant colonization of tumor cells (Calon *et al.*, 2012). The multiple immunomodulatory phenotypes of CAFs are adopted by their ample production of cytokines and chemokines, allowing a dynamic interplay between CAFs and immune cells, promoting evasion of immune surveillance. Generally, CAFs secretome dominant effects are immunosuppressive via IL-6, IL-4, IL-8, TGFβ and CXCL9 of well-assessed roles in hindering immune surveillance (Chomarat et al., 2000; Fearon, 2014; Park et al., 2004; Wan and Flavell, 2007). For instance, CAFs-derived IL-6 has been implicated in suppressing dendritic cells (DCs) maturation and subsequently T cells anergy by promoting monocytes differentiation into macrophages rather than DCs lineage (Chomarat *et al.*, 2000; Park *et al.*, 2004). More recently, in pancreatic cancer, antigen presentation by a CAFs subtype has been reported (Elyada et al., 2019). PDL1 and PDL2 expressions have been reported in subsets of CAFs isolated from lung and breast cancer and were further correlated with regulatory T cells (Tregs) differentiation (Costa et al., 2018; Nazareth et al., 2007). Robust studies unraveling the full and detailed spectrum of CAFs heterogeneous immunosuppressive properties *in vivo*, beyond correlative evidence, are still lacking for the development of solid tumors targeted therapies.

CAFs are a major source for the deposition of cross-linking enzymes and extracellular matrix (ECM) remodeling, an essential component of tissue architecture providing anchorage for resident cells. In mammals, analysis of the core matrisome revealed identification of around 300 proteins, including 43 collagen units, three dozens of proteoglycans, and approximately 200 glycoproteins (Hynes and Naba, 2012). Proteins belonging to the collagen group present

triplet repeats Gly-X-Y, where X is mostly proline and Y is commonly 4-hydroxyproline. Such repeating structure allows the formation of firm, rod like, trimeric, helical loops of variable lengths (Hynes and Naba, 2012). Whereas proteoglycans are glycosaminoglycans glycoproteins, providing not only ECM structural strength, but also lubrication (Sarrazin et al., 2011). The glycoproteins list includes fibronectins and laminins. They confer myriad functions allowing ECM assembly and sequestration of growth factors that can be served as a ready to be released reservoir (Hynes, 2009). Over decades, accumulating evidence revealed the particular role of ECM in cancer progression as a prominent component of TME (van Kempen et al., 2003). Pronounced deposition of ECM is a highly encountered among tumors of worse prognosis (Ramaswamy et al., 2003). As central modulators of tumor tissue architecture, CAFs play crucial part in triggering pro-survival and cell migration cues to cancer cells (Paszek et al., 2005). CAFs-mediated production of matrix proteases allows ECM organization and the generation of permissive trajectories for cancer cells dissemination to metastatic sites (Gaggioli *et al.*, 2007). In addition to their supporting local invasion, CAFs were found engaged the establishment and progression of micro-metastasis at secondary sites. Once tumor cells have migrated to the metastatic niche, *de novo* stimulation of fibroblasts characterized by marked ECM deposition, including tenascin and periostin production, triggers pro-survival and pro-proliferative signals enabling metastasis evolution (Malanchi et al., 2011; Oskarsson et al., 2011). Furthermore, increased tissue stiffness drives hypoxia and reduces drug delivery as well as efficacy of cytotoxic therapies and immunotherapies, hence favoring therapy resistance (Provenzano et al., 2012). Accordingly, CAFs collagen matrix remodeling affects immune cells mobilization and interstitial migration, thus hindering tumors immune surveillance (Kaur et al., 2019). Several *in vivo* studies revealed that targeting FAP^+ CAFs resulted in tumor regression through suppression of collagen synthesis and consequently boosted intratumoral infiltration of $CD8^+$ T cells and cytotoxic eradication of cancer cells (Lo et al., 2015). Targeting CAFs derived ECM components, hence altering tumors mechanical properties is currently highly explored in the therapeutic management of solid tumors (Sahai *et al.*, 2020; Wang et al., 2019).

An emerging avenue through which CAFs pave the way for tumor progression is their dynamic metabolites exchange with tumor cells and their rewiring local and systemic cancer bioenergy (Sanford-Crane et al., 2019). Research on CAFs metabolic reprogramming, initially highlighted their enhanced aerobic glycolysis and reduced oxidative phosphorylation in comparison to normal fibroblasts (Zhang et al., 2015). Consequently, CAFs-mediated pronounced release of lactate in the ECM drives TME acidification thus favoring malignant

transformation of neighboring tumor cells (Fiaschi et al., 2013). Moreover, in the reverse Warburg-effect, CAFs secreted lactate and pyruvate metabolites fuel the bioenergy needs of tumor cells (Knudsen et al., 2016). The dynamic metabolic flux between both cellular compartments is facilitated by the mono-carboxylate transporters (MCT1 and MCT4) and associated with potentiated invasion and metastatic spread of PDAC tumor cells (Knudsen *et al.*, 2016). Accumulating evidence on amino acids metabolism reported the role of glutamine to drive stromal autophagy and subsequently an oxidative mitochondrial metabolism in breast cancer tumor cells favoring tumor cells expansion (Ko et al., 2011). In PDAC, alanine secreted by stellate cells upon autophagy fuels tumor cells tricarboxylic acid cycle (TCA), non-essential amino acids and lipids biosynthesis, thus sustaining their growth and survival in an austere TME (Sousa et al., 2016). Lipidomic rewiring in CAFs and their fatty acid synthase (FAS)-mediated accumulation of fatty acids and phospholipids was also shown to potentiate CRC cells migration (Gong et al., 2020).

1.2.2 CAFs heterogeneity and cancer fibrosis

The diverse functions attributed to CAFs raise the question on their plasticity and distinct polarizations or sub-specializations. Their heterogeneity can be attributed, from one hand, to the cell of origin and in particular for those arising from activated quiescent fibroblasts, and from the other hand, to the type of activating signals (Figure 5). A bulk of cancer studies highlighted that the recruitment of fibroblasts and their distinct polarizations are highly governed by the tumor cells released signals: growth and inflammatory factors (Kalluri, 2016). As tumors are considered “wounds that do not heal” (Dvorak, 1986), an everlasting accumulation of heterogeneous cancer cells generates a chronic healing response with the emergence of distinctly activated fibroblasts culminating in cancer fibrosis or stroma (Kalluri, 2016). Accumulating evidence, with the development of single cells sequencing technologies, supports the presence of distinct mesenchymal subpopulations in breast (Costa *et al.*, 2018; Kieffer et al., 2020) , lung (Hu et al., 2021; Su et al., 2018), colon (Lee et al., 2020; Li et al., 2017) and pancreatic cancer (Elyada *et al.*, 2019; Hutton et al., 2021; Kay and Zanivan, 2021) where two major types of CAFs were identified: myofibroblasts (myCAFs) and inflammatory CAFs (iCAFs) of a contractile phenotype and an inflammatory secretome respectively (Ohlund *et al.*, 2017). Correlative findings highlighted the functional heterogeneity of the distinct CAFs subtypes. In Breast Cancer, the different CAFs populations were differentiated based on the extent of FAP expression. High FAP^{+} CAFs correlated with poor prognosis and were shown

of an immunosuppressive role attributed to their promoting Tregs infiltration (Kraman et al., 2010). Furthermore, their depletion with chimeric antigen receptor (CAR) T cells resulted in a pronounced reduction in ECM deposition (Lo *et al.*, 2015). Additional study revealed a NFκB-driven subtype of $GPR77^+$ and $CD10^+$ CAFs implicated in chemotherapy resistance (Su *et al.*, 2018). A recent report summarized $FGF7^+$ and HGF^+ CAFs association with non-small lung carcinoma (NSCLC) patients poor prognosis and resistance to EGFR-tyrosine kinase inhibitors therapy (Hu *et al.*, 2021).

Among the well-established signals for the recruitment of activated fibroblasts in numerous solid tumors are TGFβ ligands (Su *et al.*, 2018). For instance, CAFs proliferation and invasion is governed by TGFβ availability in the TME (Aoyagi et al., 2004; Lohr et al., 2001). In pancreatic cancer, TGFβ drives activation of a "myCAFs" profile in proximal fibroblasts characterized by a pronounced expression of αSMA and a cytoskeleton contractile phenotype (Ohlund *et al.*, 2017). Physical changes and modulation of tissue mechanics or the ECM were linked to CAFs stimulation through their driving a contractile CAFs phenotype mediated by activation of the transcription factors: serum response factor (SRF) and yes associated protein 1 (YAP1), collectively involved in maintaining tissue stiffness (Calvo et al., 2013; Foster et al., 2017). Moreover, inflammatory signals including IL-6, TNFα and IL-1, emerging from the pathological tissue remodeling, may initiate a pro-inflammatory and tumorigenic profile in fibroblasts through NFκB and STAT complexes (Biffi *et al.*, 2019; Ohlund *et al.*, 2017; Wu et al., 2021). In early lesions of squamous cell carcinoma, IL-1 signaling favors education of dermal fibroblasts through initiation of NFκB signaling into a pro-inflammatory secretome promoting macrophage recruitment, neovascularization, and tumor expansion (Erez et al., 2010). Later on, in pancreatic cancer, similar distal CAFs population of a pro-inflammatory NFκB and STAT3-driven phenotype was reported and identified as an iCAFs subtype (Ohlund *et al.*, 2017). CAFs heterogeneity raises the question on each subtype interconvertibility or stability and calls for a robust understanding of the epigenetic regulation of each state as well as their functional contributions to cancer progression in different solid tumors.

Beyond the above listed triggers of CAFs activation, gathered evidence highlighted the contribution of reactive oxygen species and the associated oxidative DNA damage in resident fibroblast differentiation into an activated "myofibroblasts" state promoting tumor spreading (Albrengues et al., 2015)**.** Moreover, epigenetic- metabolic interconnected rewiring fostered conversion of fibroblasts into pro-invasive CAFs phenotype favoring tumor progression

(Bhagat et al., 2019). The epigenetic landscape underlining CAFs molecular heterogeneity as spotted by single-cell analysis is still undetermined.

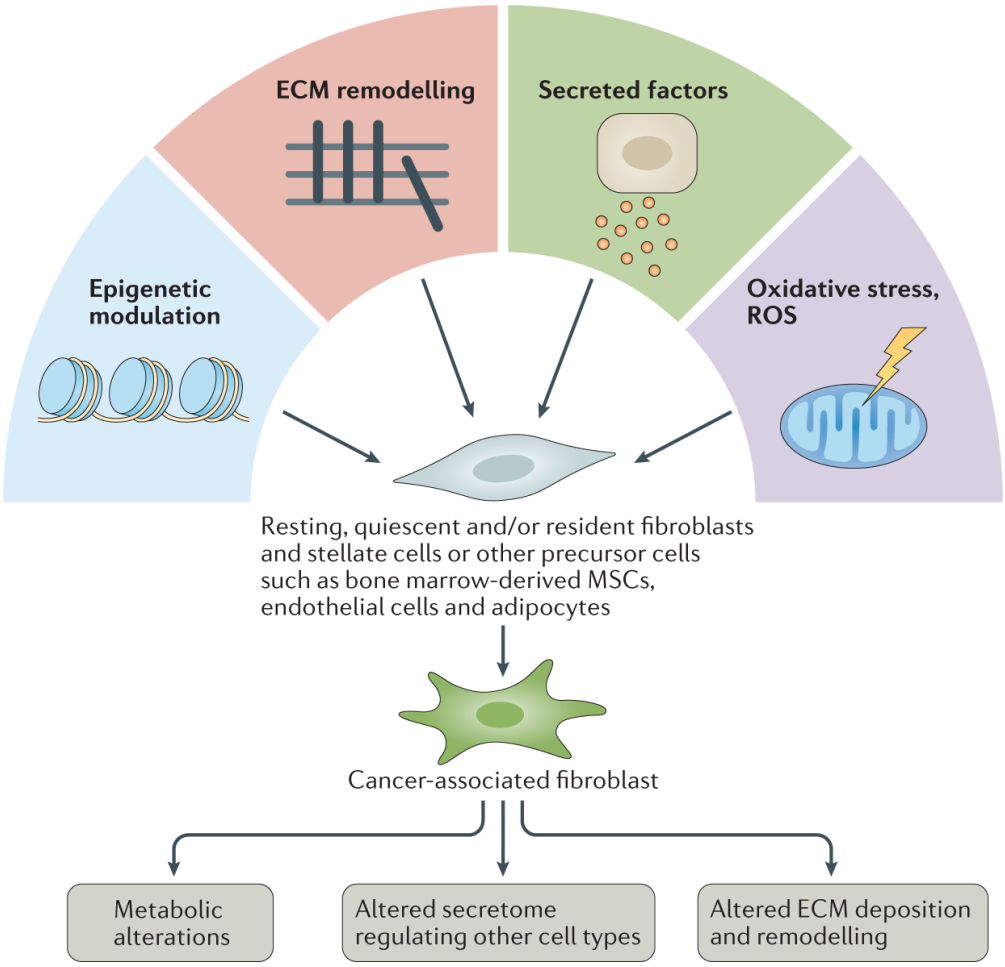

Figure 5: Mechanisms of CAFs activation. Schematic representation of the multiple reported drivers engaged in CAFs activation and recruitment: epigenetic regulators, extracellular matrix (ECM) components, soluble paracrine factors and oxygen reactive species (ROS). CAFs are heterogenous population which is derived from resident fibroblasts, endothelial cells, bone-marrow derived mesenchymal cells, adipocytes and stellate cells. Copied from (Chen *et al.*, 2021). Copyright permission has been obtained.

1.2.3 Therapeutic targeting of CAFs

The robust bulk of accumulated data on the pro-tumorigenic features of CAFs makes them appealing targets for anti-cancer therapy. However, the lack of specific CAFs marker hinders their precise depletion without affecting normal tissues resident fibroblasts. Their heterogenous functions and polarizations pose another challenge in the field of CAFs-therapy. Favorable clinical outcome will require targeting a CAFs subtype, repolarization into normal

or quiescent fibroblasts, targeting CAFs-derived ECM or blocking downstream signals (Figure 6). Therefore, it is essential to address, whether each subtype present an interconvertible state and its functional attributes to cancer progression are well conserved across different tumor types. With the accumulating knowledge on CAFs biology, targeted therapies research is expanding and numerous preclinical trials have been reported (Biffi and Tuveson, 2021; Chen and Song, 2019).

Multiple studies on direct depletion of CAFs by targeting nonspecific markers have been previously reported. In a murine model of PDAC, selective depletion of αSMA^+ CAFs resulted in reduction in tumor angiogenesis yet surprisingly drove aggressive tumor progression and overall survival through hypoxia driven EMT and enhanced stemness (Ozdemir et al., 2014). On the other hand, genetic or pharmacological depletion of FAP^+ CAFs drove deceleration of tumor growth in preclinical models of lung and colon tumors (Santos et al., 2009). Furthermore, FAP targeted immunotherapy by anti-FAP monoclonal antibodies (mAbs) resulted in promising outcomes of long-lasting tumor regression in stroma- rich xenografts of lung, prostate, and head & neck cancers (Ostermann et al., 2008). A humanized FAP mAb showed clear tumor regression in phase I trials for locally advanced tumors yet turned out to be non-beneficial for patients with metastatic colorectal cancers in early phase II trial (Hofheinz et al., 2003). Continuous investigations on more promising FAP antibodies, DNA vaccines or CAR T cells approaches are required. In breast cancer, identification of $CD10^+$ and $GPR77^+$ as novel CAFs markers for the chemotherapy resistance subtype suggested a more specific therapeutic CAFs ablation. Anti-GPR77 mAbs proved promising in reducing tumorigenesis and enhancing chemosensitivity among breast cancer xenografts (Su *et al.*, 2018). The therapeutic value of the dual inhibition of CD10 and GPR77 remains to be addressed in upcoming trials.

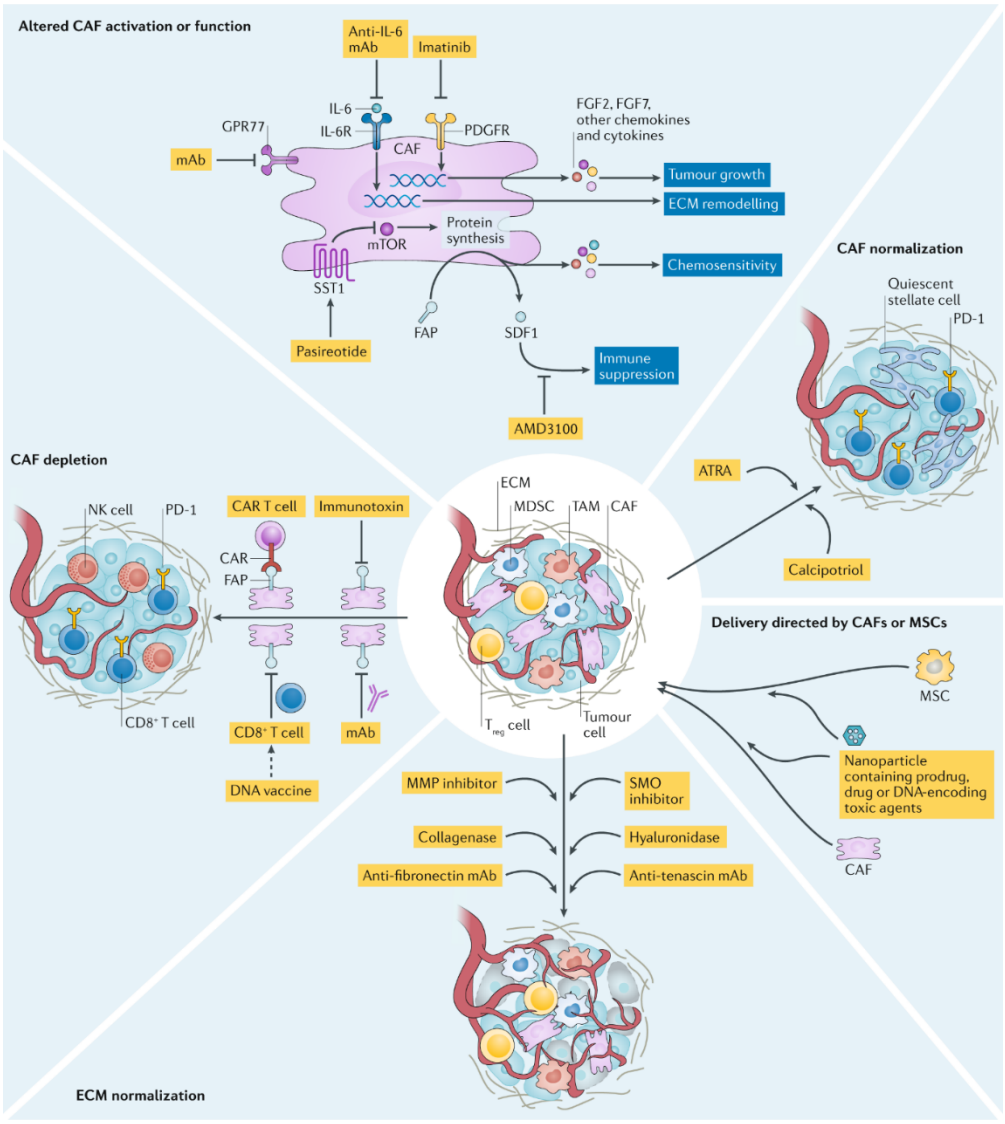

Figure 6: Major therapeutic approaches for targeting CAFs. Overview of the five principal approaches reported and utilized in targeting CAFs. Firstly, inhibiting CAFs upstream signaling regulators including cytokines and growth factors, hence inhibiting CAFs activation. Secondly, normalization of CAF into a more quiescent phenotype through usage of all-*trans* retinoic or calcipotriol molecules. CAFs or mesenchymal stem cells (MSCs)-utilizing therapies ensure specific delivery of cytotoxic drug. Targeting CAFs- derived ECM components and associated biologic effects. Finally, direct depletion of CAFs through targeting extracellular markers via immunotherapies. CAR, chimeric antigen receptor; FAP, fibroblast activation protein; FGF2, fibroblast growth factor 2; GPR77, G protein-coupled receptor 77; IL-6, interleukin-6; IL-6R, IL-6 receptor; mAb, monoclonal antibody; MMP, matrix metalloproteinase; MDSC, myeloid-derived suppressor cell; NK, natural killer; PD-1, programmed cell death 1; PDGFR, platelet-derived growth factor receptor; SDF1, stromal-derived factor 1; SMO, smoothened; TAM, tumor-associated macrophage; Treg cell, regulatory T cell. Adapted from (Chen and Song, 2019). Copyright permission has been obtained.

An appealing approach to target CAFs, apart from their nonspecific and challenging depletion is their conversion back to a normal state or tumor suppressive subtype.

Targeting CAFs-mediated desmoplastic reactions that result in from abundant deposition of ECM modulating factors, represents an appealing therapeutic approach which allows interference with tissue stiffness or vasculature, hence ameliorating tumoral drug deliveries and ultimately prognosis (Chen and Song, 2019; Cox, 2021; Huang et al., 2019). Indeed, scientific findings unraveled a close link between ECM density and angiogenesis via the hypoxia-response axis (Cox, 2021; Subrahmanyam and Ghandehari, 2021). A promising approach is the inhibition of stromal CAFs-derived hyaluronan (HA) which excessive production was found notable in many solid tumors: PDAC (Jacobetz et al., 2013), breast cancer (Chauhan et al., 2013)**,** CRC (Jian et al., 2017), prostate cancer (Simpson et al., 2002) and brain malignancies (Misra et al., 2015)**.** HA increased levels were significantly associated with poor prognosis and aggressive tumor progression by inducing blood vessels compression and hypoxia (Chauhan *et al.*, 2013). Interference with HA extracellular transportation via treatment with ABC –transporter inhibitors failed to show therapeutic benefits in breast cancer cells (Thomas and Brown, 2010). However, a recently recognized molecule PEGPH20, a recombinant HA degrading enzyme, proved to ameliorate patients prognosis in clinical trials, in combination with chemotherapeutic drugs, by ameliorating vascular perfusion (Jacobetz *et al.*, 2013). Accordingly, a phase I clinical trial of combinational PEGPH20 and doxorubicin therapy revealed enhanced OS and DFS among advanced PDAC patients (Hingorani et al., 2016). An alternative way to sensitize solid tumors to chemotherapy can be achieved by targeting the family of lysyl oxidase isoenzymes (LOX) which are crucial for collagen networks stabilization and ECM density (Schutze et al., 2015). For instance, CAFs are prominent source for the elevated detected expression of LOX molecules in many solid tumors and thus directly confer intrinsic therapy resistance in breast, CRC and ovarian cancer (Kirschmann et al., 2002; Murdocca et al., 2019; Sterzynska et al., 2018). LOX inhibition ameliorated diffusion of chemotherapeutics like doxorubicin and enhanced efficacy of cytotoxic agents in a 3D model of fibrosarcoma *in vivo* (Schutze *et al.*, 2015). Therapy resistance was further attributed to ligands that allow tumor cells anchorage to ECM. An example would be integrin β1 which allows adherence to ECM via interaction with fibronectin and lamini thereby providing protective effects for SCLC cells from apoptosis by activation of the prosurvival PI3K/AKT axis and prevention of G2/M arrest in response to conventional CRT (Deng et al., 2016a). Fibronectin targeting by recombinant inhibitory antibodies suppresses tumor vasculature and aggressive progression into metastatic phenotype

(Ebbinghaus et al., 2004). Similarly, inhibition of tenascin C, a well-studied adhesion protein highly associated with metastasis, with iodine-131 mAb showed survival benefits among patients with recurrent and metastatic glioma in phase II study in combination with chemotherapy (Reardon et al., 2006). Finally, essential ECM modulators are matrix metalloproteinases (MMPs). MMPs-mediated ECM proteolysis and collagenolytic activity enhances angiogenesis and malignant cells dissemination, resulting in poor prognosis (Bonnans et al., 2014). Over the last decades, intensive research on therapeutic targeting of MMPs started, and around 50 inhibitors have been developed. Early trials revealed that inhibiting all MMPs simultaneously would be of detrimental outcome (Overall and Kleifeld, 2006; Vandenbroucke and Libert, 2014; Wang *et al.*, 2019). However, none of the clinical trials with MMPs inhibitors succeeded in phase III. Overall, the previous poor performance of MMPs inhibitors in clinical trials has been attributed to: (a) lack of specificity, (b) poor pharmacokinetics, (c) dose-limiting side effects/toxicity and (d) *in vivo* instability (Overall and Kleifeld, 2006; Vandenbroucke and Libert, 2014). An in-depth understanding of each MMP implication in different stages of tumor evolution might culminate in a successful clinical outcome in combination with other treatment regimens.

Targeting CAFs activating signaling and CAFs-derived paracrine pathways have been extensively studied with feasible approaches. For instance, TGFβ signaling, a potent inducer of myCAFs profile, of well-established pleiotropic functions in motility, invasion, ECM deposition and immune modulation, has been assessed in preclinical studies in conjunction with multiple conventional therapies. In a murine model of PDAC, TGFβ signaling inhibition failed to show regression of tumor growth. However, preclinical models of advanced CRC revealed successful tumor regression upon TGFβ signaling inhibition in combination with anti-PD1 immunotherapy (Tauriello *et al.*, 2018). Similarly, in a urothelial cancer mouse model TGFβ expression correlated with resistance to PDL1-directed immunotherapy and poor prognosis. Its inhibition strongly ameliorated cytotoxic T cells infiltration and response to anti-checkpoint therapy (Mariathasan et al., 2018). So far, isolated targeting of TGFβ signaling in clinic didn't prove efficient (Chen and Song, 2019). There are numerous challenges to be carefully addressed in upcoming studies associated with the tumor stage and type given the diverse and opposing effects of TGFβ signaling on tumor cells and the microenvironment (Barker *et al.*, 2015; Chen and Song, 2019; Kalluri, 2016). Activated CAFs secretome, such as human growth factor (HGF), and its paracrine effects in wound healing or tissue regeneration, constitutes another promising target. Studies proposed that CAFs-derived HGF supports

therapy resistance through activation of MET signaling, enhancing invasion and evasion to (Deying et al., 2017; Ding et al., 2018). Anti-MET drugs and HGF antagonists sensitized tumor cells response to radiation therapy (Cui, 2014). Clinical trials targeting MET signaling by anti-HGF or anti-MET antibodies and small molecule inhibitors led to promising outcomes that require further assessments in a combinational therapy context (Huang et al., 2020). An alternative approach for targeting CAFs secretome has been evaluated through inhibition of CAFs mTOR signaling and consequently protein synthesis machinery (Duluc et al., 2015; Moatassim-Billah et al., 2016). An exemplary study demonstrated that αSMA^+ CAFs isolated from PDAC patients present abundant expression of somatostatin receptor and treatment of PDAC xenografts with somatostatin analogue in combination with chemotherapy (gemcitabine) promoted tumor growth breakdown through inhibition of CAFs protein synthesis mTOR/4E-BP1 machinery (Duluc *et al.*, 2015). As IL-6 and its downstream JAK/STAT3 signaling have been implicated in the activation of iCAF inflammatory profile (Ohlund *et al.*, 2017), they have been well explored in numerous scientific reports. In fact, drugs targeting IL-6, IL-6 receptor or JAKs have been approved for autoimmune diseases and myeloproliferative syndromes with ongoing trials in cancer (Johnson et al., 2018). In a phase I clinical study, combining Tocilizumab, an anti-IL-6 antibody, with doxorubicin and interferon α2b was found to be a safe and effective regimen for the treatment of patients with recurrent epithelial ovarian cancer (Dijkgraaf et al., 2015). Novel IL-6, ROCKs and STAT3 inhibitors are currently tested in preclinical studies (Hong et al., 2015; Patel et al., 2012). Apart from IL-6, IL-1α was introduced as an essential upstream activator of CAFs inflammatory profile through JAK/STAT3 and NFκB signaling and hence mentioned as a legitimate therapeutic target in the management of stroma-rich malignancies (Biffi *et al.*, 2019). The effects or functional contributions of iCAFs to therapy responses and their potential targeting through IL-1 signaling inhibition have not been previously addressed neither in preclinical models nor in clinical trials.

1.3. IL1 signaling

A key regulator the inflammatory process is IL1 signaling which is involved in inflammation resolution and the recruitment of hematopoietic cells post cellular stress or injury (Garlanda et al., 2013; Kaneko et al., 2019; Weber et al., 2010). Since the identification of the amino acids sequences of IL-1α and IL-1β in 1985, the IL1 family of cytokines has increased to currently include a total of seven pro-inflammatory ligands (IL-1α, IL-1β, IL-18, IL-33, IL-

36α, IL-36β and IL-36γ), two anti-inflammatory cytokines (IL-37 and IL-38), and two receptors antagonists that ensure a regulation of IL-1 signaling intensified induction of inflammation (IL1RA and IL-36Ra) (Garlanda *et al.*, 2013). The originally identified members of the IL1 family were IL-1α and IL-1β (Figure 7). Extensive findings highlighted the biogenesis, physiological and pathophysiological functions of IL-1β with little evidence on the biogenesis and inflammatory processes mediated by IL-1α (Di Paolo and Shayakhmetov, 2016).

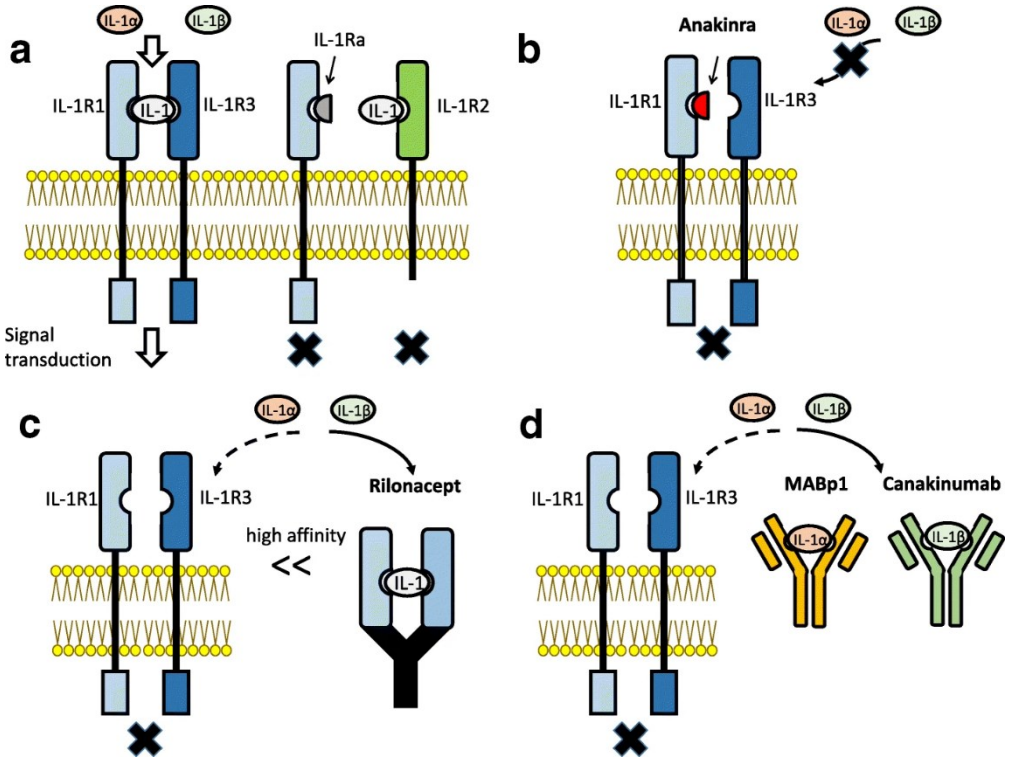

Figure 7: IL1 signaling ligands, antagonists and receptors. **A.** IL-1α and IL-1β ligands bind to IL-1R1 receptor and drive signal activation along the co-receptor IL-1R3 (IL1RAcP). Inhibition of the IL-1 signaling is mediated by IL1RA protein binding to IL-1R1. IL-1R2 is considered as a decoy receptor for lacking a cytoplasmic fraction. **B.** A recombinant form of IL1RA is anakinra which is able to inhibit IL-1α/IL-1β signaling axis. **C.** Rilonacept is a recombinant fusion molecule that includes the extracellular portion of human IL-1R1 and IL-1R3 combined with the Fc region of human IgG1. Its interactions with the IL-1 signaling ligands (IL-1α/IL-1β) drive prolonged inhibitory consequences. **D.** Anti-IL-1α and anti-IL-1β monoclonal antibodies of inhibitory effects are respectively MABp1 and Canakinumab. Copied from (Kaneko *et al.*, 2019). Open access article.

1.3.1 IL-1α and IL-1β ligands distinct properties

Despite being encoded by distinct genes, with a low level of amino acids sequences homology, IL-1α and IL-1β act as ligands for the same IL-1 receptor (IL-1R), recruiting the accessory protein IL1RAcP as well as the myeloid differentiation primary response 88

(MyD88) adaptor protein and consequently promoting activation of immune and pro-inflammatory processes (Weber *et al.*, 2010). Both ligands are synthesized as proforms proteins with a 31 kDa molecular weight and readily cleaved into mature proteins of 17 kDa weight of IL-1R binding potential. The mechanisms of IL-1α and IL-1β isoforms maturation, cell of origin, secretion and cellular localizations are highly distinct (Di Paolo and Shayakhmetov, 2016). While both IL-1α precursor protein and its cleaved smaller form act as active ligands for IL-1R, only cleaved IL-1β is endowed of an IL-1R binding activity (Kim et al., 2013). The functional maturation of IL-1β requires cleavage by caspase-1 downstream of the inflammasome protein complex with no reported activity in mediating IL-1α cleavage (van de Veerdonk et al., 2011). Upon its maturation IL-1β is released and presents a higher affinity for IL-1R. It was further reported to be merely expressed in hematopoietic cells such as blood monocytes, residual macrophages, dendritic cells and brain microglia, upon stimulation by the complement system, Toll-Like Receptors (TLRs) and in response to pro-inflammatory cytokines including TNF-α and the IL-1 signaling itself (Dinarello, 1996). In contrast, IL-1α functions as both a secreted and membrane bound protein and is actively expressed under steady states in both hematopoietic and non-hematopoietic compartments, including the epithelial lineages of the gastrointestinal tract, lungs, liver, endothelial cells and astrocytes (Garlanda *et al.*, 2013). Upon pro-inflammatory or cellular stress stimuli, such as apoptosis or necrosis-linked cues, IL-1α production is potentiated and the ligand acts as an alarmin initiating and potentiating an inflammatory cascade (Rider et al., 2011). Apart from their investigated differences in cellular sources and mechanisms of release, IL-1α and IL-1β additionally differ in their cellular localizations. Accordingly, in contrast to IL-1β, IL-1α was reported to possess an amino acids sequence known as nuclear localization sequence (NLS) promoting its nuclear localization in epithelial, myeloid, and keratinocytes cells as well as its binding to chromatin (Garlanda *et al.*, 2013; Malik and Kanneganti, 2018). Moreover, IL-1α-mediated inflammation is a tightly controlled process as its shuttling between the nucleus and cytosol is highly driven by the upstream activation signals. For instance, during apoptosis, IL-1α is retained within the chromatin and concentrated in nuclear foci (Cohen et al., 2010). However, during ischemic injury, as hypoxic cells undergo necrosis, IL-1α precursor is delocalized from the nucleus to the cytosol and upon its release incites inflammatory processes mediated by myeloid cells recruitment and activation (Cohen *et al.*, 2010)

1.3.2 IL-1α biogenesis and regulation of expression

The constitutive expression of IL-1α or the level of its secretion under homeostatic conditions differs distinctly among cell types and is known to be mediated by the specificity protein 1 (SP1) transcription factors as the *Il1a* promoter lacks Goldberg-Hogness box (TATA) and CAAT regulatory boxes of transcription (McDowell et al., 2005; Wierstra, 2008). Induction of IL-1α expression occurs in response to pro-inflammatory stimuli, cytotoxic stress and growth factors. Such induction is mediated by the transcription factors activator protein 1 (AP1) of identified binding sites on *Il1α* promoter (Alheim et al., 1996; Bailly et al., 1996) and the protein kinases NFκB, JNK and p38 pathways which, cooperatively, drive the expression of IL-1α and its associated inflammatory genes by transcriptional and post-transcriptional mechanisms (Kimura et al., 1998). Consequently, the broad spectrum of stimuli that would drive *Il1α*-inducible expression includes: TLR inflammatory microbial mediators (Weber *et al.*, 2010), pro-inflammatory cytokines upstream of NFκB and p38 complexes (Kimura *et al.*, 1998), redox stress (McCarthy et al., 2013), steroid hormones such as 17-β Estradiol (Itoh et al., 2007) and fatty acids-mediated mitochondrial uncoupling (Freigang et al., 2013).

IL-1α is translated as precursor isoform "pro-IL1α" and subjected to numerous post-translational modifications: phosphorylation at residue Serine 90 (Beuscher et al., 1988), myristylation on Lys82 and acetylation on Lys82 within the 16-kDa N-terminal propiece (Stevenson et al., 1993). Calcium dependent-neutral protein calpain (CANP) promotes calcium-driven cleavage and processing of human pro-IL-1α at phenylalanine residue 118 and mouse pro-IL-1α at serine 115 residue (Carruth et al., 1991). Likewise, pro-IL-1α acts as a substrate for granzyme B, a lymphocyte-derived protease that ensures its cleavage at the aspartic acid residue 103 resulting in a mature C-terminal IL-1α of more potent activity (Afonina et al., 2011). Mature and pro-IL1α share identical biological functions assessed by their comparable potential of triggering pro-inflammatory genes expression and cytokines release among epithelial and hematopoietic cells (Kim *et al.*, 2013). IL-1α is endowed of a unique characteristic membrane-associated feature. For instance, upon exposure of immune cells to pro-inflammatory stimuli, upregulation of IL-1α expression was correlated with its nuclear, cytosolic and plasma membrane localization (Kurt-Jones et al., 1985). Further studies confirmed the full bioactivity of membrane-bound IL-1α through IL-1R in a paracrine manner and its consequently promoting T cell proliferation and chemokines release (Kurt-Jones et al., 1986). In macrophages, pro-IL-1α was shown to be glycosylated via incorporation of a D

[14C]-mannose suggesting a lectin-mediated binding of pro-IL1α to plasma membrane (Brody and Durum, 1989).

1.3.3 IL-1α in inflammation and cancer

Pro- and mature IL-1α are both endowed of full bioactivity and present a constitutive as well as induced expression in a broad array of hematopoietic and non- hematopoietic cells. Accumulated findings depicted IL-1α as a major driver of inflammatory signaling networks, identified it as an "alarmin" molecule and a crucial member of the danger-associated molecular pattern (DAMP) signaling molecules (Malik and Kanneganti, 2018). For instance, in response to cellular stress, including injuries or infectious insults, a passive release of IL-1α is encountered in the extracellular milieu, further triggering activation of an inflammatory cascade through IL-1R which is constitutively expressed in numerous cell types (Di Paolo and Shayakhmetov, 2016). NFκB and MAPK pathways are downstream of IL-1R and drive an IL-1α-dependent expression of pro-inflammatory cytokines and mediators such as IL-6, TNF-α, cyclooxygenase type -2 (COX-2) that supplementary potentiate release of IL-1α and IL-1β. Hence, a sustained or amplified inflammatory loop, initially driven by IL-1α, occurs and results in a pronounced tissue damage (Dinarello, 1996; 2009). Thus, fever, hypotension, vasodilation and increase pain sensitivity are physiological signs of IL-1 signaling (Lee et al., 2004).

IL-1α is known to mediate inflammatory processes in non-hematopoietic cells including fibroblasts (Kawaguchi et al., 2004). Aberrant activation of the IL-1α-IL-1R axis is associated with multiple auto-inflammatory pathologies: cutaneous inflammation (neutrophilic dermatoses) (Milora et al., 2014), cardiovascular disorders (Freigang *et al.*, 2013), neural inflammation (Brough and Denes, 2015) and cancer (Bersudsky et al., 2014). For instance, fibroblasts isolated from human patients with multiple sclerosis (SSc) express pronounced amounts of IL-1α and present increased IL-1R signaling activity associated with enhanced release of pro-inflammatory mediators (IL-6, PDGFα…) and collagen deposition compared to fibroblasts from normal skin (Kawaguchi et al., 1999; Kawaguchi *et al.*, 2004) .

Tumor cells and components of the TME express IL-1α, IL-1β, IL-1R and the receptor antagonist IL1RA. Given the crucial implication of IL-1α in inflammation induction, wound healing and tissue fibrosis, its contributions to cancer pathogenesis and therapy response have been extensively appreciated over the last years. IL-1R signaling dysregulation directly affects tumor initiation and progression at different levels. Stroma-derived IL-1α promotes paracrine

effects on tumor cells, sustaining their proliferation, survival and stemness through promoting expression of stemness like genes (Bmi1 and Nestin) supporting cancer cells renewal and epithelial mesenchymal transition (Li et al., 2012). Moreover, IL-1-driven inflammation associated with enhanced production of growth factors, prostaglandins, cytokines and chemokines activates β-catenin signaling in transformed proliferating cells (Sakurai et al., 2008). A further evidence on IL-1α implication in tumor promotion is the dramatic bowel inflammation with an increased weight loss and mortality rates exhibited in preclinical model of IL-1R8/SIGIRR (a negative regulator of IL1 signaling) deficient mice in response to dextran sulfate sodium salt (DSS) intake reflecting higher susceptibility to tumorigenesis (Garlanda *et al.*, 2013)**.** IL-1 signaling is further implicated in driving tumor cells dissemination and metastasis through promoting NFκB and MAPK-driven expression of ECM modulators: glycoproteins, collagens and proteoglycans as well as ECM-regulators and growth factors (Tjomsland et al., 2013; Zigrino et al., 2009). An immunity suppressing role of IL-1 signaling is attributed to its acting as inflammatory 'emergency' signal accelerating division of hematopoietic stem cells and their subsequent differentiation into myeloid-derived suppressor cells (MDSCs) phenotype (Pietras et al., 2016), hence fostering tumor cells survival and evasion of immune surveillance (Song et al., 2005). Further findings on IL-1α carcinogenic attributes emerged from clinical studies. For head and neck squamous cell carcinoma and gastric cancer patients, higher IL-1α expression and protein levels significantly correlated with poor prognosis and distant metastasis (Leon et al., 2015; Tomimatsu et al., 2001). Blocking the IL-1α feed forward inflammatory loop by recombinant monoclonal antibodies as a cancer therapeutic approach proved of favorable outcome (Garlanda and Mantovani, 2021; Gottschlich et al., 2021).

1.3.4 IL-1 receptor antagonist

IL1RA was originally identified as a suppressor molecule engaged in the inhibition of IL-1-mediated thymocyte proliferation (Dinarello et al., 1981). Further studies reported the presence of IL-1 signaling inhibitory circulating unit in the serum and urine of juvenile arthritis patients (Prieur et al., 1987). The first naturally described receptor inhibitor of any cytokine or hormone-like factors was IL1RA (Dinarello, 2018). In 1987, an inhibitor of IL-1 bioactivity was identified in the urine of febrile patients, providing evidence *in vivo* on direct interference with the ligand binding to its receptor (Seckinger et al., 1987). In 1990, the cloning and properties of recombinant IL1RA were defined (Hannum et al., 1990). The identification of

distinct isoforms of IL1RA, its transcriptional regulation, single nucleotide polymorphisms (SNPs) and crystal structure reflect its unique yet complex roles in the regulation of IL-1 signaling. Research findings identified two distinct isoforms of IL1RA generated by alternative splicing of different first exons (Butcher et al., 1994): a 17-kDa secretory IL1RA (sIL1RA) released from hematopoietic cells and an 18-kDa intracellular form of IL1RA (icIL1RA) retained in the cytoplasm of epithelial, monocytes and fibroblasts (Haskill et al., 1991). Crystal structure and mechanisms of action of IL1RA identified that IL-1β and IL1RA share a similar β-pleated sheet structure binding on the same site of IL-1RI receptor. IL-1R type I and II receptors belong to the family of Ig molecules and present three Ig-like motifs in the extracellular domains (Arend et al., 1998). Receptor structure analysis revealed that IL-1β and IL-1α further interacted with type I IL-1R at two additional sites of the receptor, a β-bulge between strands 4 and 5 and a domain around aspartic acid at residue 145 (Greenfeder et al., 1995). These bounds of the two agonists are responsible for the distinct bioactivity compared to IL1RA and subsequent induction of inflammatory processes in target cells (Boraschi et al., 1995; Evans et al., 1995). An additional unit of the IL-1 receptor complex is the IL-1 accessory protein (IL1RAcP), a 570 amino acids molecule and a member of the Ig family of proteins, forming a complex with the agonists IL-1α and IL-1β and their corresponding receptor type I IL-1R (Greenfeder *et al.*, 1995). IL-1 signaling transduction necessitates intact cytoplasmic motifs of the IL-1R and accessory protein IL-RAcP for downstream activation of interleukin-1 receptor-associated kinase (IRAK) and stress- activated protein kinases (SAP Kinases) (Smith et al., 2003; Wesche et al., 1997).

IL1RA production is induced by an array of inflammatory mediators, infectious products and acute phase proteins reflecting its implication in chronic inflammation and infectious diseases (Dinarello, 2018). Accumulated findings on IL1RA tissue distribution and aberrant expression in transgenic and knockout models, unraveled its function in pathophysiological conditions as regulator of IL-1 signaling and inflammatory feed-forward associated loop. IL1RA secreted and cytoplasmic isoforms are expressed under homeostatic conditions in normal intestine, lungs, kidneys, liver, spleen and skin (Arend and Guthridge, 2000). *In vivo* evidence on IL1RA implication in normal physiology and pathology, demonstrated IL1RA as an endogenous anti-inflammatory protein which downregulation promotes exaggerated IL-1 signaling and amplification of the inflammatory loop favoring the biological functions of the agonists IL-1α and IL-1β (Arend *et al.*, 1998). IL1 signaling-driven chronic inflammatory processes play favoring and crucial roles in enhancing the risk of cancer development and progression with

colitis associated models exemplifying this connotation (Greten and Grivennikov, 2019). Analysis of colonic tissues from patients affected by Chron's disease or IBD revealed a reduced ratio of IL1RA to IL-1β mRNA expression levels compared to tissues from patients with infection driven inflammation (Casini-Raggi et al., 1995). In preclinical models of colitis, administration of anti-IL1RA neutralizing antibodies resulted in a sustained and colonic inflammation and enhanced mortality rate (Ferretti et al., 1994).

1.3.5 IL1 signaling-associated genetic polymorphisms

Genetic evidence exploring the association of IL1 signaling with increased cancer risk, examined reported variants in the agonists-encoding genes as well as the inhibitory unit *IL1RN*. Evaluation of genetic risk factors of ovarian cancer, identified a missense single nucleotide polymorphism (SNP) in *Il1α* gene "rs17561" that results in an alanine to serine substitution at residue 114 (A114S) and a reduced susceptibility to ovarian cancer (Charbonneau et al., 2014). The A114S pro-IL-1α form is highly sensitive to calpain-mediated proteolytic cleavage which leads to reduced levels of the membrane bound pro-IL1α and hence minimizes the signaling associated tumorigenic and metastasis functions (Kawaguchi et al., 2007). Genetic evidence showed further associations between *IL1RN* polymorphisms and numerous types of cancer. Human *IL1RN* maps the long arm of chromosome 2 band q14-q21 (Steinkasserer et al., 1992). In the second intron of *IL1RN* gene, a variable number tandem repeat (VNTR) polymorphism has been identified. Five alleles were identified due to the presence of 2, 3, 4, 5 and 6 repeats of the 86-bp tandem repeat (Clay et al., 1994). In fact, *IL1RN**2 allele has been associated with several human diseases and pathological conditions such as ulcerative colitis (Bioque et al., 1995; Mansfield et al., 1994), ischemic stroke (Worrall et al., 2007), psoriasis (Jesus et al., 2011), gastric carcinoma (Xue et al., 2010), human colorectal cancer (Ibrahimi et al., 2019), ovarian cancer (Sehouli et al., 2003)and cutaneous melanoma (Cauci et al., 2019).

Increased IL-1α production and pro-inflammatory mediators (IL-6, IL-8, CXCL1, CCL2, CCL20…) has been described in aging cells as a senescence associated secretory profile (SASP) which is triggered by activation of transcription complexes, including NFκB, p-38 MAPK and mTOR-MK2 signaling (Alspach et al., 2014; Chien et al., 2011; Di Paolo and Shayakhmetov, 2016; Faget et al., 2019; Freund et al., 2011; Herranz et al., 2015; Laberge et al., 2015). Previous studies highlighted the roles of IL1 signaling as a SASP member sustaining an autocrine feed-forward amplification loop leading to a constitutive activation of NFκB signaling and a self-amplifying SASP production reinforcing growth arrest by aged and

senescent cells (Laberge *et al.*, 2015; Melisi et al., 2009; Niu et al., 2004). Several studies further demonstrated that SASP molecules act in a paracrine fashion inducing a bystander senescence spreading effect in neighboring cells. For instance, cells undergoing any of the three forms of senescence: oncogene, therapy or replicative senescence were able to induce in surrounding cells a senescence phenotype through their IL-1α, TGF-β family ligands (VEGF, CCL2, CCL20…) and IL6 rich secretome in neighboring cells. The paracrine effect was driven by activation of the DNA-Damage Response (DDR) machinery and subsequently JAK/STAT, TGFβ/SMAD and IL1/NFκB signaling pathways (Acosta et al., 2013; Hubackova et al., 2012; Nelson et al., 2018).

1.4 Senescence

Cellular senescence is defined as a stable exist from the cell cycle or an adaptive response promoted by numerous physiological and pathological factors, resulting in a permanent state of cell cycle arrest (Di Micco et al., 2021). Originally, senescence was reported in human diploid fibroblasts (HDF) which following long term in vitro culturing, undergo a sustained proliferative arrest (Hayflick and Moorhead, 1961). Numerous triggers including oncogenes, cytokines, oxidative stress and DNA damage have been implicated in senescence induction and maintenance (Wang et al., 2020; Wyld et al., 2020).

1.4.1 Senescence phenotype: morphology and biomarkers

The identification of senescent cells includes a combination of several markers. Positivity for senescence- associated- β- galactosidase reactivity, due to an altered lysosomal activity, is the "gold hallmark" for senescence. Additional senescence identification markers include: enlarged, flattened shape *in vitro*; exhibition of a disrupted nuclear envelope integrity due to decreased expression of laminin B1; lack of DNA duplication and the cell-cycle-associated Ki67 proliferative protein; pronounced activation of the cyclin-dependent kinase (CDK) inhibitors CDKIs p16INK4a, p21 and p27; chromatin reorganization including the formation of senescence associated heterochromatin foci (SAHF) and increased levels of histone H3 lysine 9 trimethylation (Narita et al., 2003; Serrano et al., 1997) . Many of the listed senescence markers have been validated *in vivo*, in developmental, physiological, pathological and malignant processes (Sharpless and Sherr, 2015).

1.4.2 DNA damage response-associated senescence

Recent advances in senescence research, proved DNA damage response (DDR) generation and activation as a cause of senescence (d'Adda di Fagagna, 2008). Breaks in the DNA backbone culminate in pronounced generation of either single or double strand DNA (DSBs) which trigger the activation of DDR characterized by the recruitment of two specialized complexes and kinases: ataxia telangiectasia and Rad-3 related (ATR) or ataxia telangiectasia mutated (ATM) at the site of DNA damage (Li et al., 2016). Upon their recruitment, ATM and ATR kinases promote local phosphorylation of histone H2AX in a crucial stage in DDR nucleation. At DSBs, phosphorylated γH2AX further recruits ATM complexes in a positive feedback loop, therefore amplifying local ATM activation and therefore magnifying the extent of Chromatin γH2AX. Crucial DDR signal transduction mediators (signal boosters) are downstream kinases DNA-damage checkpoint 1 (MDC1), p53-binding protein 1 (53BP1), CDC25, CHK1 and CHK2 (d'Adda di Fagagna, 2008; Goldberg et al., 2003; Lou et al., 2003). If the encountered DNA damage is promptly and properly fixed, cells will resume normal proliferation. By contrast, upon pronounced DNA damage, cells may undergo either programmed cell death (apoptosis) or initiate senescence. Generation of DNA damage in primary fibroblasts cultures showed a permanent cell cycle arrest (Kollarovic et al., 2016). Accordingly, robust activation of the DDR signaling and generation of DDR foci in senescent cells were shown of causative roles in the establishment of replicative, oncogene-induced, oxidative and therapy-induced senescence.

1.4.3 Replicative senescence

Telomeres are molecular clocks that maintain a record of the cells replications (Harley et al., 1990). They are nucleoprotein complexes composed of specific repeat sequence “5’-TTAGGG-3’” and a multiprotein complex known as “Shelterin” (Fumagalli et al., 2012). Telomeres occupy the end of every chromosome and play a central role in DNA protection by inhibiting enzymes-mediated DNA metabolism (Shay and Wright, 2019). Replicative senescence is encountered through a series of consecutive cell divisions that fail to maintain telomeres. The shortening of telomeres in replicated cells triggers a DNA-damage response (DDR) similar to that formed by external DNA-damaging mediators, such as ionizing irradiation and chemotherapeutic agents. Accordingly, inhibition of ATM/ATR or CHK2/CHK1 complexes delay the onset of replicative senescence and forced expression of telomerase can evade replicative senescence and sustain chromosomal integrity (Bodnar et al.,

1998; d'Adda di Fagagna et al., 2003). Although the exact cutoff of telomers dysfunctions and length within a cell that can elicit replicative senescence is still unclear, a current structural model suggest three telomers states: closed, intermediate and uncapped states (Cesare and Karlseder, 2012). In the "uncapped state", telomers shortening triggers loss of the shelterin protein TRF2 leading to cell crisis characterized by intra- and intrer-chromosomal fusions, a marked genomic instability and cell death. Damage at unprotected telomers is traced by DDR marker proteins: 53BP1 and gamma-H2AX (Herbig et al., 2004). Upon genomic dispersed DNA damage, an irreversible and persistent telomeres damage occurs (Fumagalli *et al.*, 2012). In humans, telomere dysfunction, linked with genetic maladies (for example dyskeratosis congenita), is associated with early commencement of ageing, including pulmonary fibrosis, bone marrow failure and cirrhosis (Armanios, 2013; Lansdorp, 2009).

1.4.4 Oncogene induced senescence

OIS was primarily detected in human fibroblasts upon expression of oncogenic form of RAS (Serrano *et al.*, 1997). This senescence process, with a growing list of about 50 oncogenes (such as *BRAF*, *E2F1* and *MYC*), appears to be independent of telomeres dysfunctions (Gorgoulis and Halazonetis, 2010; Jones et al., 2000). Normal cells initially react to constitutively active oncogene by a hyperproliferation phase which appears to be transient and subsequently triggers an OIS (d'Adda di Fagagna, 2008). The connection between mitosis and senescence induction is the S-phase encountered DDR which is an omnipresent machinery for OIS (Bartkova et al., 2006). Accordingly, oncogenes stress promotes pronounced DNA duplication origins, driving an increase in partially complete replication intermediates, culminating in DNA damage and stimulation of DDR kinases: ATM, ATR, CHK1 and CHK2 (Bartkova *et al.*, 2006; Di Micco et al., 2011). Furthermore, ATM degradation by E3 ubiquitin ligase WD repeat and SOCS box-containing protein 1 (WSB1) leads to the inhibition of OIS and drives pronounced proliferation (Kim et al., 2017a). Studies revealed RB and p53 as two core controllers, which are promoting cell-cycle arrest in OIS (Lin et al., 1998). In view of that, p53 accumulation was reported in cells experiencing OIS, which could be evaded upon p53 inactivation. Findings among lung cancer-bearing mice with oncogenic K-Ras-(G12D) developed demonstrated in premalignant adenomas, with p53 expression, positivity for senescence markers, whereas in aggressive adenocarcinomas, that arose in the absence of p53, senescence markers were not detected (Bieging et al., 2014).

1.4.5 Oxidative stress and therapy-induced senescence

No longer after the finding of OIS, a new form of senescence known as therapy-induced senescence (TIS) emerged as a cellular response to pronounced therapy- induced genotoxic stress: chemotherapeutic drugs and irradiation. Firstly, it was described in tumor cell lines derived from human solid tumors, where adequate doses of doxorubicin induced senescence-like phenotype (SLP) similar to replicative senescence (Chang et al., 1999). TIS is now a recognized outcome to a growing list of chemotherapeutic anti-cancer agents, conventional and targeted: topoisomerase poisons/inhibitors, alkylating agents, platinum-based, antimetabolites, microtubule inhibitors/poisons, hormonal therapy, kinases inhibitors and monoclonal antibodies (Gewirtz et al., 2008; Saleh et al., 2020). In fact, chemotherapeutic drugs drive numerous hallmarks of senescence in malignant cells, including enriched expression of SA-β-gal, sustained growth arrest, and polyploidy (Wang et al., 1998). Moreover, TIS was encountered in human breast cancer samples collected from patients subjected to preoperative neoadjuvant chemotherapy and shown to be positive for SA-β-gal activity and p16 expression (Chang *et al.*, 1999; Cotarelo et al., 2016).

Therapy-induced genotoxic stress by chemotherapeutics and ionizing radiation drives an increase in the levels of oxygen free radicals largely known as reactive oxygen species (ROS) and reactive nitrogen species (RNS). They both have established roles as secondary messengers in intracellular signaling pathways, sustaining oncogenic phenotype of tumor cells, as well as inducing cellular senescence and apoptosis (Valko et al., 2006). Accumulative generation of ROS/RNS through either endogenous or exogenous sources, beyond homeostatic threshold, is termed as oxidative stress or cellular redox imbalance which triggers cellular DNA damage causing either SSBs or DSBs. A subcategory of SSBs may progress into DSBs (Cannan and Pederson, 2016). DSBs are the most harmful DNA lesions mostly restored via non-homologous end joining (NHEJ) (Jacob et al., 2013). The most studied base in oxidative DNA damage is guanine of low oxidative potential, making it highly susceptible to oxygen free radicals and the formation of 8-Oxo-2'-deoxyguanosine (8-OHdG) (Margolin et al., 2006). The causal relationship between cellular oxidants and senescence induction has been introduced with findings on hydrogen peroxide triggering senescence induction in primary cells (Chen and Ames, 1994; Chen et al., 1995). Accordingly, in response to DSBs driven by oxidative stress caused by oxygen or nitrogen species, a complex DDR is induced characterized by the induction of the RAS-RAF-MEK-ERK cascade and subsequent activation of the p38 MAPK, thus collectively promoting transcriptional activity of p53 and p21 (Debacq-Chainiaux et al.,

2010; Sun et al., 2007). The significant role of redox imbalance in senescence induction was additionally verified with antioxidants usage that delayed or prevented senescence. For instance, scavenging H_2O_2 with the antioxidant N-acetylcysteine (NAC) or lowering ambient oxygen levels was sufficient to block p53 activation and reverted cells Ras-induced senescence phenotype (Chen *et al.*, 1995; Lee et al., 1999). Numerous studies reported positive feedbacks loops induced by ROS driving amplification of the induced senescence phenotype through pronounced alterations of cellular secretome via autocrine and paracrine mechanisms.

1.4.6 Senescence-associated secretory phenotype

A hallmark of senescent cells is the harnessing of a complex pro-inflammatory secretome response recognized as senescence associated secretory profile (SASP) (Coppe et al., 2010). Senescent cells dynamically communicate to their surrounding environment and the extracellular matrix through a complex secretome including extracellular proteases, cytokines, chemokines and growth factors (Figure 8) (Coppe *et al.*, 2010; Kuilman and Peeper, 2009). Early studies reported among cultured endothelial cells, undergoing growth arrest, an augmented release of secretory factors, including plasminogen activated protein- 1 which later became a functional marker for senescence (Vaughan et al., 2017). The complexity of the SASP reflects the dynamic and long-term functionality of senescent cells in pathology of ageing related disorders including cancer (Faget *et al.*, 2019). The downstream effects of the SASP depend on its molecular composition, targets, cellular context and type of stress. SASP functions, ascribed to its members, are extremely diverse, ranging from autocrine and paracrine signaling, pro- and anti-tumorigenic, and pro- and anti-inflammatory circuits (Birch and Gil, 2020).

1.4.6.1 Molecular regulation of SASP

Regulation of senescent cells secretome is achieved at numerous levels, both transcriptional and post-translational, resulting in diverse effects (Figure 8) (Faget *et al.*, 2019; Kuilman and Peeper, 2009). Nevertheless, a pronounced and persistent DDR appears critical for the development and regulation of SASP (Coppe *et al.*, 2010)**.** Interestingly, SASP constituents appear to form a hierarchical network for signal transduction and amplifications. For instance, senescence was shown to be closely linked with identified inflammasomes, multimolecular immune complexes, hence playing critical and core role in inflammation (Acosta *et al.*, 2013). Such findings enforced the concept of a SASP master regulator. In view

of that, several SASP components were reported to be up-regulated transcriptionally by two major transcription factors: NFκB and CCAAT/enhancer binding protein-ß (C/EBPß) complexes, which were shown to exhibit increased chromatin binding activity during OIS or TIS and therefore collectively driving the inflammatory profile of senescent cells (Chien *et al.*, 2011; Faget *et al.*, 2019; Flanagan et al., 2018). Additionally, the Janus kinase (JAK)–signal transducer and activator of transcription (STAT) signaling was reported to control a subgroup of immunosuppressive SASP molecules in PTEN deficient prostate cancer mouse model (Toso et al., 2014). Recently, the antiviral cyclic GMP–AMP synthase (cGAS)–stimulator of interferon genes (STING) pathway, known to play a principal role in detection of cytosolic DNA, was shown to induce senescence and SASP phenotype through potential activation of NFκB signaling (Gluck et al., 2017). Furthermore, mTOR signaling in senescent cells regulate SASP profile post-transcriptionally including IL-1α and MK2 (Laberge *et al.*, 2015). Hence, mTOR inhibition by rapamycin decreased SASP. Senescence and SASP expression are associated with epigenetic modifications (Pazolli et al., 2012). Histone deacetylase (HDAC) inhibitors were demonstrated as strong stimulants for the expression of several SASP molecules in human senescent fibroblast (Birch and Gil, 2020). SIRT1 and EZH2 were reported as epigenetic negative regulator of SASP phenotype in senescent cells through post-translational modifications (Hayakawa et al., 2015; Ito et al., 2018). Considerable scientific efforts have been directed over the last years to dissect the epigenetic mechanisms of SASP regulation (Sen et al., 2016).

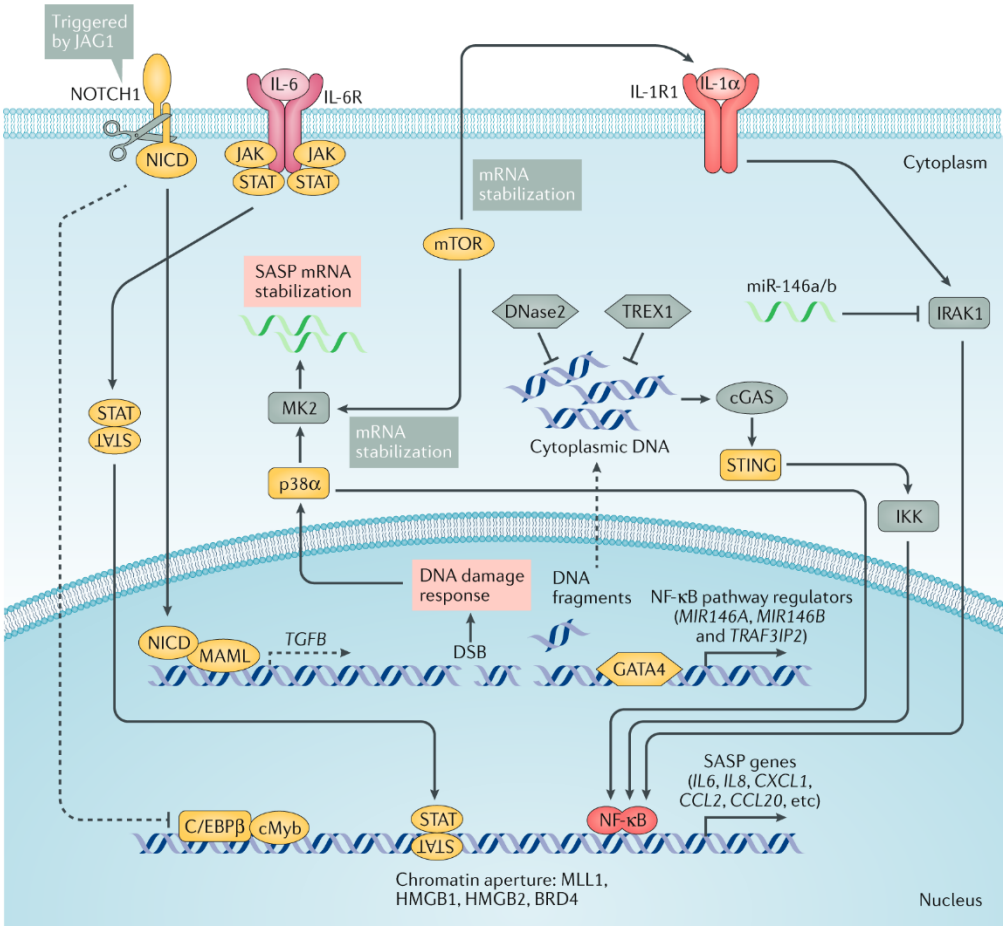

Figure 8: Signaling complexes controlling the senescence associated secretory profile. Numerous pathways regulate SASP through the DDR machinery, such as ATM-ATR, p38MAPK/MAPK-activated protein kinase 2 (MK2) and GATA binding protein GATA4. DDR additionally activates NFκB signaling of pivotal role in regulating the pro-inflammatory secretome of senescent cells. Cyclic GMP-AMP synthase (cGAS) signaling, sensor of cytoplasmic DNA, contributes to SASP response. In NOTCH-induced signaling, SASP molecules are regulated by CCAAT/enhancer-binding protein β (C/EBPβ). Mechanisms of SASP initiation are not yet completely unraveled. cMyb, myeloblastosis oncoprotein; DSB, double strand breaks; IKK, IκB kinase; JAG1, protein jagged-1; JAK, Janus kinase; MAML, mastermind-like transcriptional co-activator; NICD, NOTCH intracellular domain; p38α, p38 mitogen-activated protein kinase-α; STAT, signal transducer and activator of transcription; STING, stimulator of interferon genes; TREX1, three prime repair exonuclease-1. Copied from (Faget *et al.*, 2019). Copyright permission has been obtained.

1.4.6.2.1 Immunity and SASP

Initial findings unraveled anti-tumor immunity effects of SASP factors eliciting the elimination of neoplastic cells by alerted immune cells, hence preserving tissue homeostasis (Xue et al., 2007). Paracrine SASP anti-tumorigenic properties were demonstrated as triggers of "senescence surveillance" in liver associated pathologies including fibrosis and hepatocellular carcinoma. Numerous studies, exploiting distinct mouse models of liver induced

fibrosis and tumorigenesis, revealed the impact of SASP on the myeloid compartment, including M1 macrophage polarization and NK cells activation and mobilization, driving clearance of senescent cells, reduced tissue fibrosis and tumor growth, culminating in decelerated tumor progression (Iannello et al., 2013; Sagiv et al., 2016; Xue *et al.*, 2007). The effects of senescent cells secretome on eliciting an immunosuppressive adaptive immune response was shown in a model of hepatocarcinoma, where OIS of hepatocytes coupled with a SASP signature resulted in stimulation of $CD4^+$ T cells and subsequent cytotoxic $CD8^+$ T cells-mediated elimination of senescent cells (Kang et al., 2011).

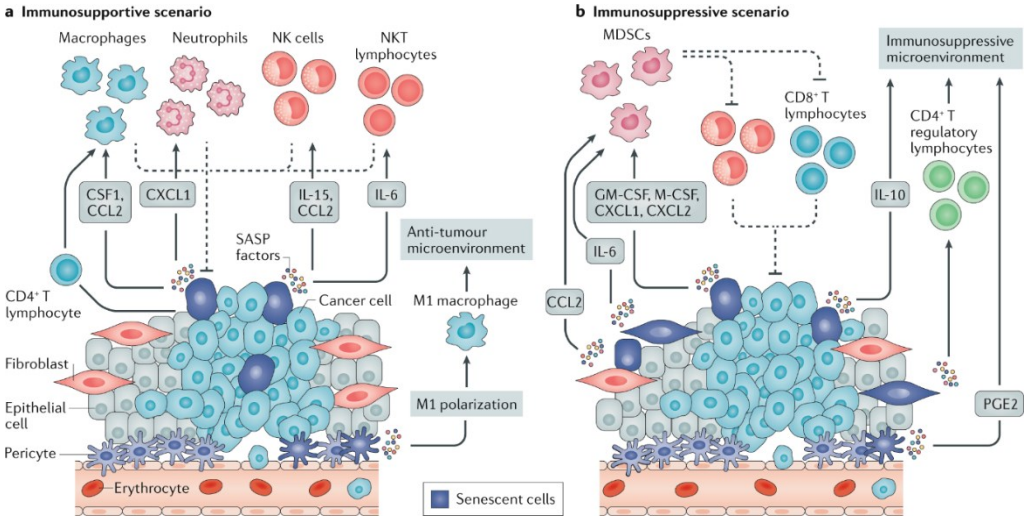

Figure 9: Immunologic properties of senescence-associated secretory profile. **a-** In an immunosupportive microenvironment, SASP molecules released by cancer cells promote activation and infiltration of macrophages, neutrophils, natural killer cells and lymphocytes to mediate phagocytosis and cytotoxic killing of senescent cells. **b-** Immunosuppressive properties of SASP are attributed to its promoting infiltration of myeloid-derived suppressor cells (MDCSs) that hinder the NK and T lymphocytes cytotoxic effects. CCL2, C–C motif chemokine ligand 2; CSF1, colony-stimulating factor 1; CXCL, C–X–C motif chemokine ligand; GM-CSF, granulocyte–macrophage CSF; M-CSF, macrophage CSF; NK, natural killer; NKT, natural killer T lymphocyte; PGE2, prostaglandin. Copied from (Faget *et al.*, 2019). Copyright permission has been obtained.

1.4.6.2.2 SASP and tissue remodeling

Beyond the immunogenic and paracrine effects of SASP, accumulating findings summarized its impact on tissue architecture and integrity (Freitas-Rodriguez et al., 2017). The secretome of senescent cells is highly rich in extracellular matrix proteins including growth factors, proteases and proteoglycans. In tumor progression, SASP factors can drive in angiogenesis through endothelial growth factor (VEGF) and connective tissue growth factor (CTGF) thus contributing to an increased vasculature and neoplastic cells dissemination (Yang

et al., 2005). Studies confirmed, *in vitro*, that SASP molecules (IL-6, IL-8…) can also impact malignant invasion of tumor cells by promoting epithelial-to-mesenchymal transition (EMT) (Ortiz-Montero et al., 2017). The rich matrisome of senescent cells comprising ECM modulators remodeling drives metastasis through tissue architecture remodeling, impacting cellular motility and dissemination to metastatic sites. Accordingly, aged skin fibroblasts display pronounced secretion of MMP-1 and MMP-2, resulting in activation of the serine/threonine protein kinase PAR-1 signaling in tumorigenic keratinocytes and subsequently driving cellular motility (Tandara and Mustoe, 2011). Additionally, in senescent human skin, the reduced expression of hyaluronan and proteoglycan link protein 1 (HAPLN1) was associated with an aligned ECM which endorses dissemination and metastasis of melanoma cells (Ecker et al., 2019). Further evidence in pillar thyroid carcinoma, validated senescent cells role as triggers of collective migration through CXCR4 signaling pathway (Kim et al., 2017b).

Surprisingly, a bulk of studies conveyed striking findings on senescent cells resuming proliferation *in vitro* and *in vivo*, favoring tumor progression and relapses (Demaria et al., 2017; Saleh et al., 2019; Was et al., 2017). Therefore, therapeutic targeting of senescent cells, in an attempt to overcome SASP protumorigneic detrimental and unfavorable effects, has been widely addressed recently.

1.4.7 Senotherapy of cancer

The standardly used cancer therapeutics reported to induce cellular senescence in tumor and non-malignant cells can be categorized into 5 distinct groups: chemotherapy, immunotherapy, epigenetic modulators, CDK5/6 inhibitors and radiotherapy. For instance, *in vitro* and *in vivo* findings in preclinical models demonstrated chemotherapy implication in senescence induction. For instance, topoisomerase inhibitors, alkylating agents, microtubules inhibitors DNA oxidative drugs have been all shown candidates for senescence induction though inflicting unrepairable DNA damage and mitosis impairment in different types of tumors (Ewald et al., 2010). Epigenetic modulators such as inhibitors of DNA methyltransferase (DNMT) were reported to promote senescence through p16 upregulation and activation of p53-p21 pathway in osteosarcoma cells (Widodo et al., 2007). Similarly, histone deacetylase (HDAC) such as suberoylanilide hydroxamic acid (SAHA) conveyed clear senescence- like growth arrest among normal and cancer cell lines such as colon cancer, urothelial carcinoma and leukemia cell lines (Almeida et al., 2017; Elknerova et al., 2011; Xu et al., 2005). In B cells lymphoma cell lines, rituximab, a CD20 targeting antibody, belonging

to the family of immunotherapeutic drug used for the management of leukemia and lymphoma, was shown to increase SA-β-galactosidase activity, p53/p21 network, a DDR response and a SASP phenotype (Dabritz et al., 2016). Further accumulating evidence validated the effect of radiotherapy and the application of high-energy electrically charged ions on DDR signaling activation, and unfavorable induction of senescence profile in cancer and non-malignant surrounding cells (Baskar et al., 2012). Recently, three pharmacological inhibitors of CDK4/CDK6, essential kinases playing important roles in cell proliferation and cell cycle G1 to S phase transition, have been developed and approved as anti-cancer drugs. Increasing number of studies, confirmed the link between cyclin-dependent kinases inhibitors and cell cycle arrest as a phenotype of therapy induced senescence (Kirkland and Tchkonia, 2015; Wang *et al.*, 2020).

Primary cytotoxic cancer treatment options inevitably induce senescence and a SASP of detrimental effects ranging from therapy resistance, therapy-induced adverse effects, cancer progression and relapses with overall negative impact on the health-span of treated patients. The well-established role of the inflammatory SASP in favoring tumor progression through facilitating invasion, metastasis and immune cells evasion, drove a scientific thought on the clearance of senescence cells by senolytics (senolysis) as a legitimate therapeutic opportunity, complementary to conventional regimens, and hence optimizing treatment outcomes through SASP inhibition (senostasis). However, eradication of senescent cells is also thought as a strategy targeting cellular dormancy and promoting resumption of an uncontrolled proliferation and tumor regrowth at primary and distant sites (Wang *et al.*, 2020). Removal of the apoptosis-resistant senescent cells is pharmacologically achieved by senolytics, including small molecules, peptides and antibodies (Kirkland et al., 2017). Identification of senescent cells anti-apoptotic pathways (SCAPs) allowed development of relevant senolytic agents. Transcriptional and proteomic analysis of senescent cells identified five major SCAPs (1- BCL-2 family; 2- PI3Kδ & AKT family; 3- MDM2, p53, p21 & PAI signaling; 4- Ephrins & tyrosine kinases; 5- HIF-1α and 6- HSP-90) and laid the ground for the development of senolytic drugs targeting senescent cells pro-survival pathways (Baar et al., 2017; Chang et al., 2016; Fuhrmann-Stroissnigg et al., 2017; Zhu et al., 2016). The BCL-2 inhibitor "ABT-263" (navitoclax) was among the first developed senolytic drug which was recently approved for the treatment of AML in combination with hypomethylating agents (Chang *et al.*, 2016). Additional senolytic drugs targeting SCAPs , including dasatinib, alvespimycin, obatoclax and venetoclax were demonstrated to reduce β-galactosidase activity, p53/p21 signaling, p16

expression, telomers-associated foci, SASP and senescence associated markers (Kirkland and Tchkonia, 2015; Kirkland *et al.*, 2017). Senolytic effects of mTOR inhibitors (rapamycin, AZD8055 and temsirolimus) have also been shown in xenografts and *in vitro* experimental models as SASP inhibitory effects (Fung et al., 2009; Herranz *et al.*, 2015; Laberge *et al.*, 2015). Senolytic properties have been further attributed to HDAC inhibitors with their promoting successful targeting of chemotherapy-treated NSCLC and HNSCC cell lines (Jenke et al., 2021).

Anti-senescence compounds are currently entering clinical trial for numerous human pathologies. Besides the bulk of *in vivo* and *in vitro* studies on SASP molecules detrimental effects of tumor progression and malignancy, some of the pro-inflammatory SASP hold established roles in anti-tumorigenic effects (Faget *et al.*, 2019). In lymphomas, sarcomas and liver carcinomas reactivation of p53 signaling promoted tumor regression through driving senescence secretory phenotypes (Ventura et al., 2007; Xue *et al.*, 2007) and favoring immune surveillance. In a preclinical PDAC mouse model, combinational therapy with MEK and CDK4/6 inhibitors triggered regression in tumor cells proliferation via induction of RB-induced senescence. Moreover, SASP-mediated endothelial activation and vascular remolding, favored chemotherapeutic drugs delivery and intratumoral T cell infiltration as well sensitivity to anti-PD1immunotherapy (Ruscetti et al., 2020).

The long-time suggested “one-two” punch approach based on a pro-senescence therapy followed by anti-senescence senolytic-based interventions might sound a promising and effective approach. Yet much work should be done on dissecting questions on whether and when a senolytic drug is to be used with strategies taking into consideration differences between adult and young cancer patients. In response to senescence inducing therapy, a senolytic might accelerate tumor regression by elimination of malignant pro-tumorigenic stroma. On the other hand, senolytics might come as an initial cure hindering metastasis through potential targeting of dormant cancer cells at pre-metastatic and secondary sites hence reducing distant recurrences. An exemplary study was encountered in the context of breast cancer where a long term dormancy state of disseminated cells has been reported (Carpenter et al., 2021). Indeed, targeting senescence in cancer, might be of beneficial effects on tumor progression, therapy resistance and metastasis, yet detailed characterization of senescence phenotype in distinct cell and tumor types is essentially required for entering clinical trials with maximum therapeutic outcomes (Wissler Gerdes et al., 2020; Wyld *et al.*, 2020).

2. Results

2.1 Enhanced inflammatory CAFs content among rectal cancer patients and correlation with survival

To assess whether the newly established Consensus Molecular Subtype (CMS) classifier would be predictive of rectal cancer prognosis, a total of 212 rectal cancer patients' transcriptomic data, pre-CRT, were grouped according to three CMS classifiers (CMSclassifier-random forest prediction; CMSclassifier-single sample prediction and CMS caller) (Eide *et al.*, 2017; Guinney *et al.*, 2015). There was a comparable disease-free survival (DFS) outcome for the four different CMS subtypes (Figure 10A). Therefore, among rectal cancer patients, the CMS classifier doesn't predict prognostic outcomes. To unravel the molecular pathways driving patients' resistance to CRT and identify targetable biomarkers, using mass spectrometry, a comprehensive global proteomic analysis was performed on tumor cells isolated from patients' paraffin embedded specimens by laser capture microdissection, pre-therapy. The principal component analysis (PCA) plot of the total 2747 identified proteins revealed no clear segregation of the tumor cells proteomic profiles between complete responders (pCR) and non-responders (non-pCR) patients (Figure 10B). The findings suggest that components of the TME rather than actual tumor cells are central player in therapy resistance and outcome. While the performed multiplexed immunohistochemistry on patients pretherapeutic biopsies revealed no differences in T cells ($CD3^+$, $CD4^+$, $CD8^+$ or $FOXP3^+$), macrophages ($CD163^+$), neutrophils (MPO^+) and proliferative tumor cells ($Ki67^+PanCK^+$), there was a significant enrichment of $vimentin^+$ stromal cells (Figure 10C, D).

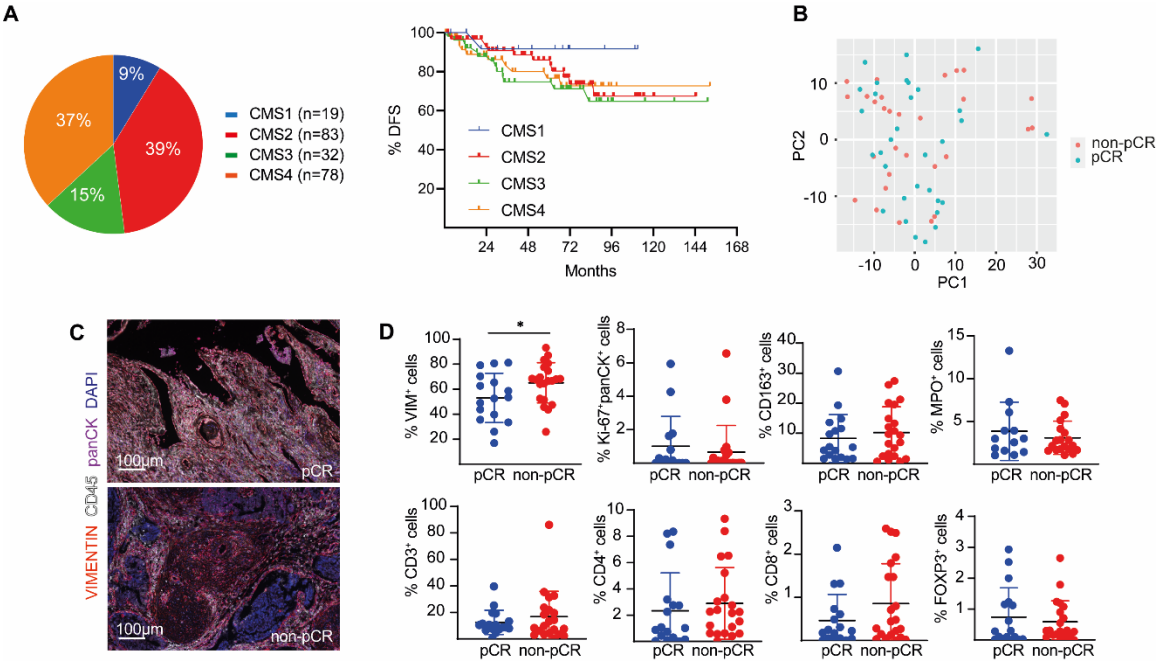

Figure 10: CMS classifier, tumor cells proteomic profile or immune cells content pre-CRT do not predict RCA prognosis. A. Pie chart and Kaplan-Meier DFS curve representative of CMS classification among 212 RCA patients based on their sequencing data pretherapeutic (published cohort: GSE87211 and RCA patients 1st cohort). **B.** PCA plot of global proteomic analysis of RCA patients' tumor cells pretherapeutic (61 RCA patients from second cohort with 29 non-pCR patients and 32 pCR patients) using laser capture microdissection and mass spectrometry. **C.** Representative images and quantifications of vimentin, Ki67, panCK, MPO, CD3, CD4, CD8, CD163 and FOXP3 multiplexed IHC performed on pretherapeutic biopsies from non-pCR and pCR RCA patients before CRT. Data are mean ± SD. *p-value <0.05 by t-test. For MPO IHC: 13 pCR and 19 non-pCR patients (second cohort). For the CAFs multiplexed IHC panel (Vimentin, Ki67 and panCK): 16 pCR and 21 non-pCR patients (second cohort). For the immune multiplexed IHC panel (CD3, CD4, CD8, FOXP3 and CD163): 17 pCR and 21 non-pCR patients (second cohort).

Furthermore, a clear enrichment of CAFs, EMT and inflammatory signatures was detected among non-pCR patients before therapy (Figure 11) (Isella *et al.*, 2015). In contrast, there was no enrichment of endothelial, leukocyte or CMS4 signatures among non-pCR rectal cancer patients before CRT further highlighting the importance of CAFs in impairing therapy response among RCA patients (Figure 11) (Isella *et al.*, 2015; Michels et al., 2019). In an attempt to investigate the implication of a CAF subtype in impairing therapy response among RCA patients, analysis of recently published single-cell RNA sequencing data from 23 colorectal cancer patients was performed and revealed the presence of 18 CAFs clusters among which four were identified as inflammatory CAFs populations (cluster 3, cluster 6, cluster 7 and cluster 17; Figure 12A and Table S2). The most prominent iCAFs cluster_3 presented IL-1, TNFα and NFκB as predicted upstream signature regulators (Figure 12B). Importantly, gene

set enrichment analysis (GSEA) demonstrated a baseline significant enrichment of the most prominent iCAFs cluster among non-pCR patients (Figure 12C). Significantly, scoring RCA patients before therapy for decorin (DCN), a differentially expressed extracellular marker for iCAFs (Table S2) demonstrated that patients with high iCAF/DCN score pretherapeutic had a shorter DFS rates compared to patients with low expression (Figure 11D). These findings support the role of the TME, particularly inflammatory CAFs, in conferring resistance to CRT among RCA patients.

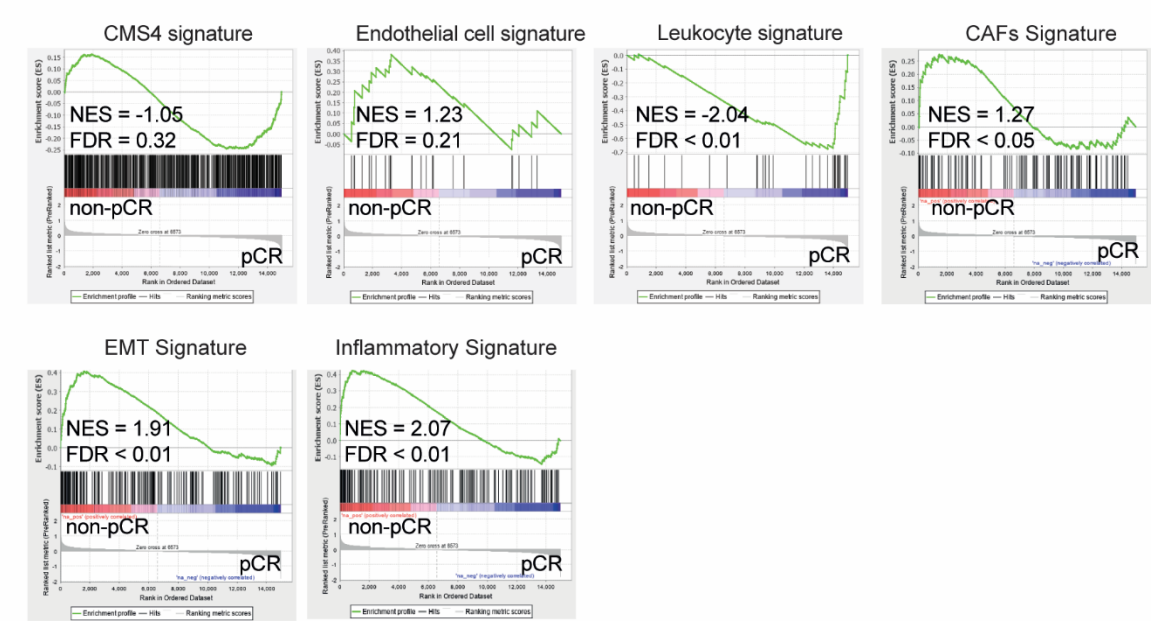

Figure 11: CAFs signature is enriched among non-pCR RCA patients pre-CRT. GSEA plots of CMS4, endothelial cell, leukocytes, CAFs, EMT and inflammatory signatures among RCA patients pretherapeutic (n=105 patients of the first cohort with 26 non-pCR and 79 pCR patients). Significance is considered for FDR q-value >1 and adjusted p-value <0.05.

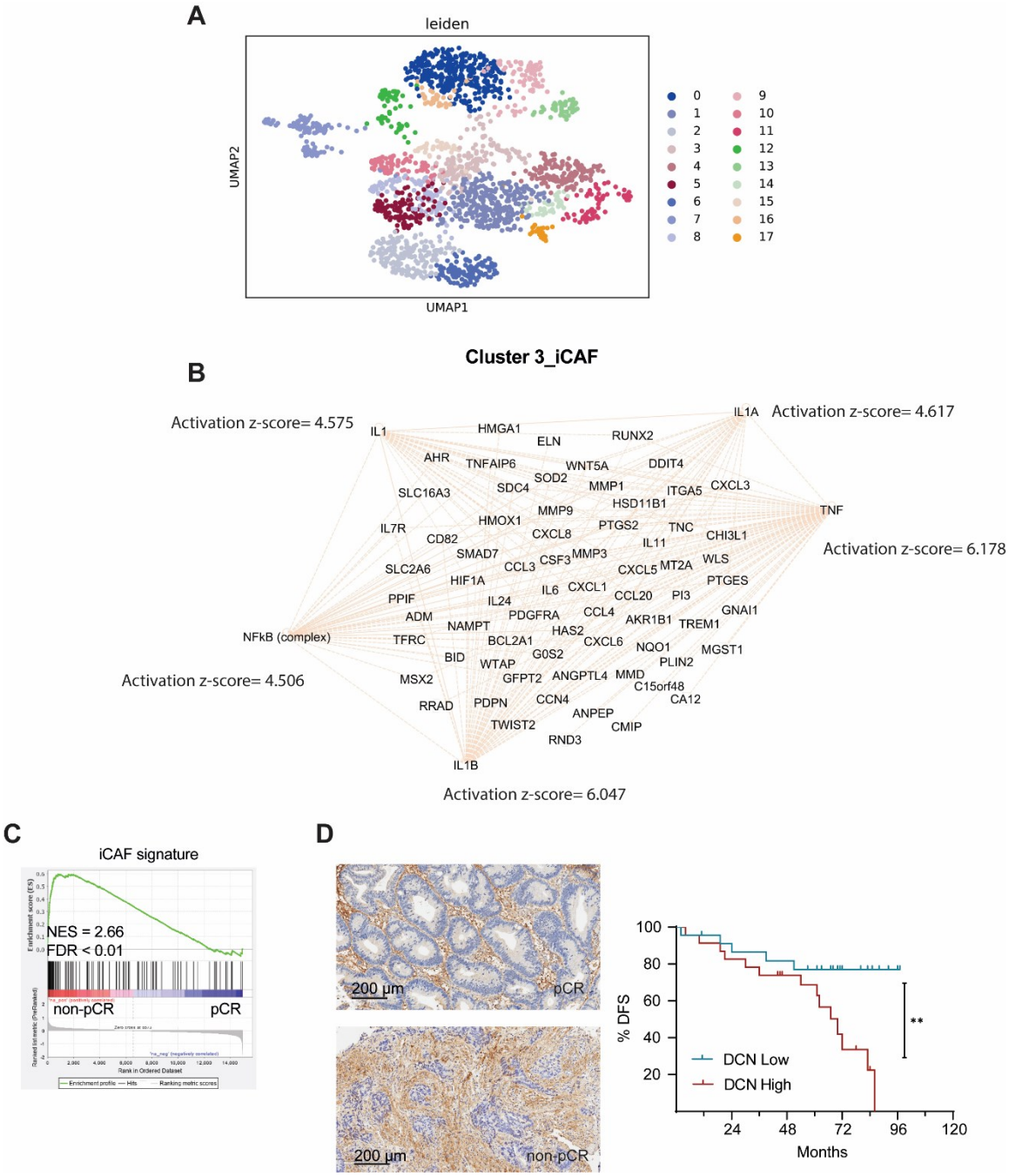

Figure 12: Inflammatory CAFs predict survival of rectal cancer patients. A. UMAP plot illustrating unsupervised clustering of 1936 viable CAFs among 23 CRC patients revealing 18 identified CAFs clusters. **B.** Mechanistic map illustrating Cluster 3 predicted upstream regulators by IPA software and their differentially expressed genes (Log2FoldChange ≥1 and adjusted p-value threshold of 0.05). Activation z-score >1 and p-value of overlap <0.0001. **C.** GSEA plot of iCAFs signature among RCA patients pretherapeutic (n=105 patients of the first cohort with 26 non-pCR and 79 pCR patients). Significance is considered for FDR q-value >1 and adjusted p-value <0.05. **D**. DCN IHC on pretherapeutic biopsies from pCR and non-pCR RCA patients' samples. Scale bars represent 200 µm. Kaplan-Meier DFS curve of patients with DCN high (n=23) and low (n=23) scores pretherapeutic (46 RCA patients from the first cohort). Split of high and low scores was median based. **p-value<0.001 by Log-rank (Mantel-Cox) test.

2.2 Preclinical-orthotopic mouse model of rectal cancer resembles the pretherapeutic stroma enhanced reaction of non-pCR patients

To confirm the functional relevance of iCAFs in therapy resistance of rectal cancer and unravel the underlying molecular mechanism of resistance, a novel preclinical *in vivo* mouse model of rectal cancer and local irradiation was established. Immunocompetent C57BL6/J mice were subjected to dextran sodium sulfate (DSS) induced colitis, followed by transplantation of genetically modified organoids. Two to three weeks post transplantation, tumor growth was confirmed by mini-colonoscopy and mouse was subjected to local irradiation using the small animal radiation research platform (SARRP) (Figure 13). Two different types of genetically modified organoids were transplanted, both mutant for *Apc*, *Trp53*, *Tgfbr2* and *K-ras*^{G12D} with one additionally expressing myristoylated AKT, hence the labeling APTK and APTKA organoids respectively (Figure 13A).

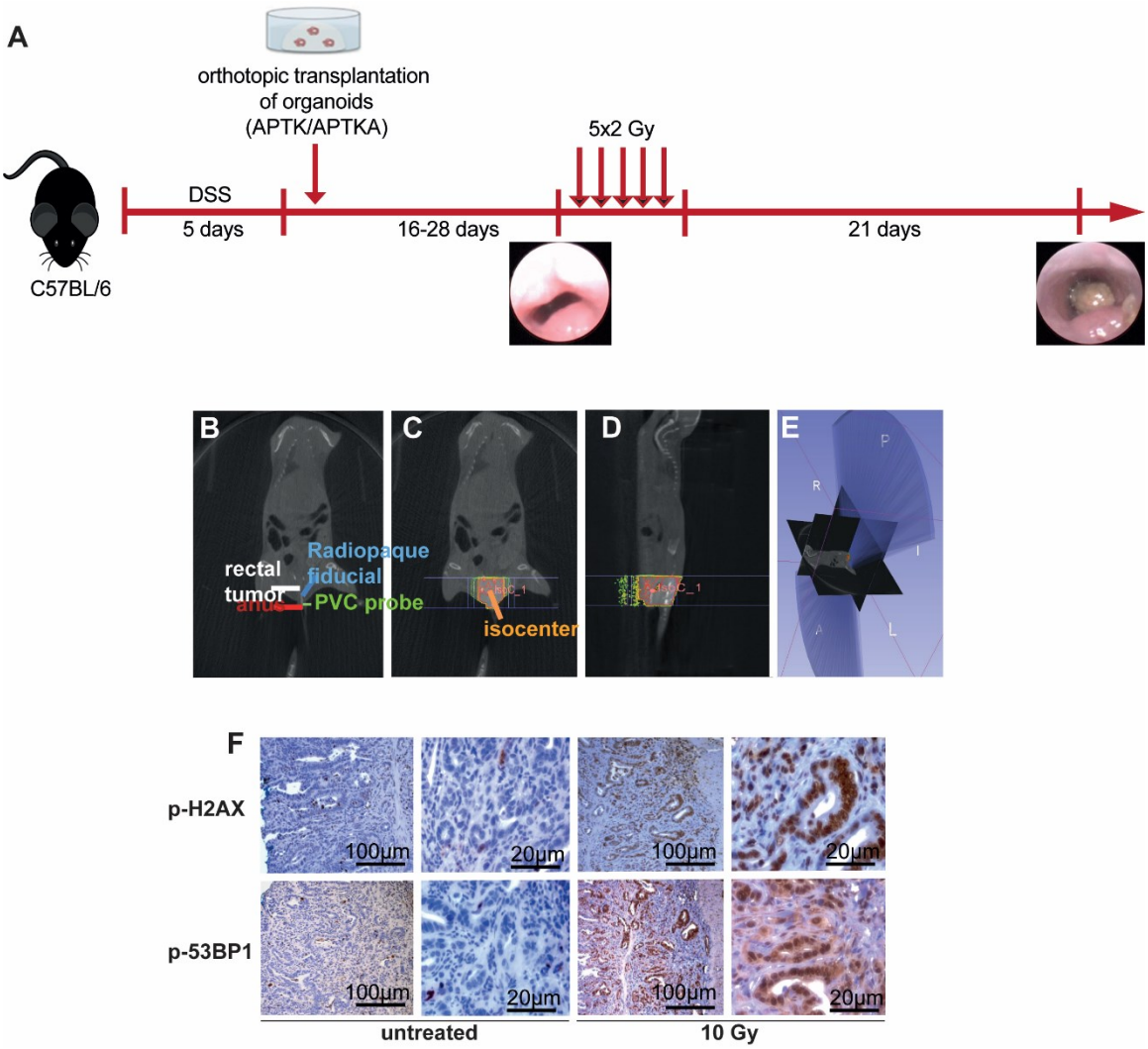

Figure 13: Local radiotherapy in a preclinical orthotopic mouse model of rectal cancer. **A.** Summarizing scheme of APTK and APTKA organoids orthotopic transplantation into C57BL6/J mouse (female) colon following the DSS model. Post-colonoscopy, local fractionated irradiation (5x2Gy) suing SARRP on established tumors was performed. End point colonoscopy was done 21 days post last dose irradiation. **B-E.** Scheme summarizing the local radiotherapy performed by the small animal radiation research platform (SARRP): **B.** CBCT image of the mouse revealing endoluminal insertion of the radiopaque fiducial into the PVC probe and determination of the rectal tumor isocenter; **C, D.** Sagittal and coronal views of the radiotherapy treatment plan illustrating dose distribution (color wash) prescribed to the orthotopic tumor isocenter. **E.** Representation of the radiotherapy arcs applied for the treatment plan. **F.** Representative images of phospho-H2AX and phospho-53BP1 IHC among untreated and 10 Gy irradiated APTKA orthotopic tumors 45 min post irradiation. Scale bars represent 20 and 100 µm.

Interestingly, transcriptomic analysis of APTKA and APTK tumors revealed distinct expression profiles as noted by the PCA plot (Figure 14A). Importantly, APTKA tumors presented a significantly enriched CAFs signature similarly to non-pCR RCA patients (Figure 14B). Moreover, a thorough molecular characterization of CAFs derived from APTKA tumors was performed by single-cell RNA sequencing analysis of 624 sorted $EPCAM^-$, $CD31^-$, $CD45^-$ and $F4/80^-$ primary CAFs. Leiden clustering identified 5 distinct CAFs subtypes labeled according to their predicted upstream regulators: IL-1β, TGF-β, IFNγ, DNMT/EPO/FST and RICTOR CAFs clusters (Figure 14C, D and Table S3). Cluster 0_IL1 was the most prominent subtype with DCN as differentially expressed gene which increased expression among APTKA compared to APTK orthotopic tumors was further confirmed by IHC (Figure 14E, F). Therefore, APTKA tumors provided excellent preclinical model as they resembled the baseline inflammatory stroma enriched rectal tumors of non-pCR patients.

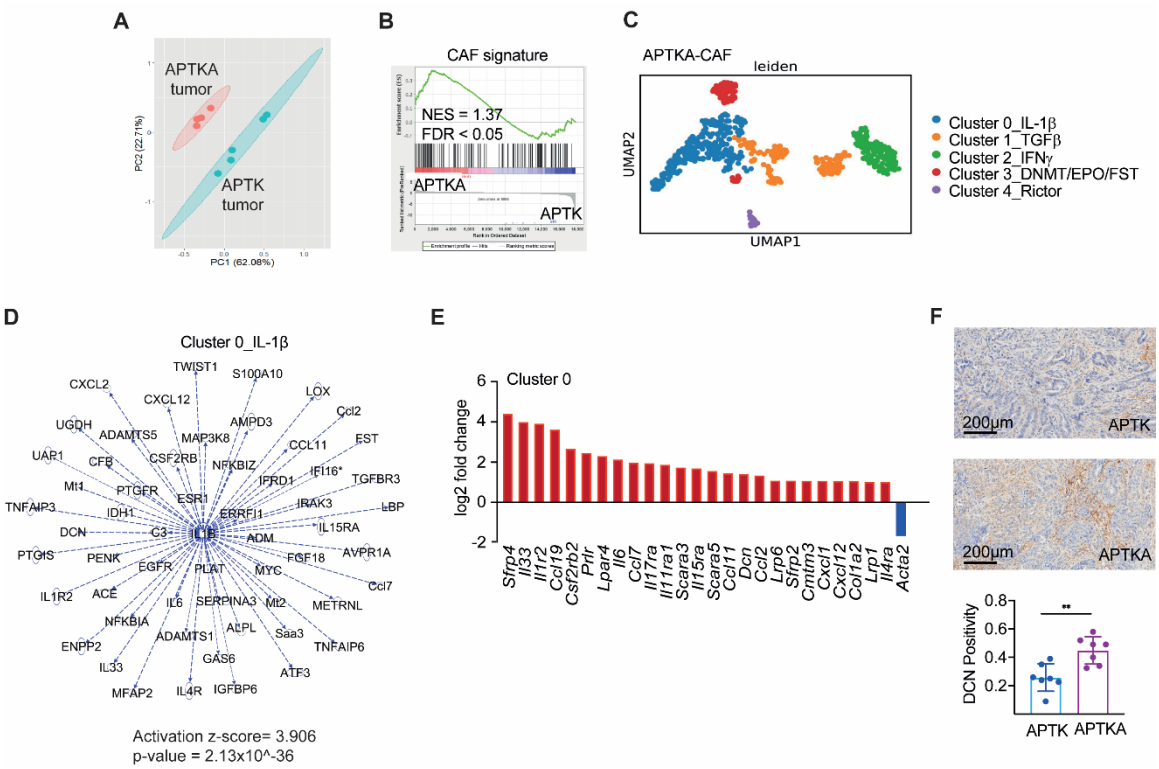

Figure 14: APTKA orthotopic tumors display heterogeneous CAFs populations and an enriched inflammatory stroma. A. PCA plot based on RNA sequencing of APTKA (n=4) and APTK (n=5) orthotopic tumors. **B.** GSEA plot of CAF signature among APTKA (n=4) compared to APTK (n=5) orthotopic tumors using total transcriptomic data. Significance of NES ≥1 and FDR-q-value <0.05. **C.** UMAP plot representing clustering of viable sorted 624 CAFs (EpCAM$^-$, F4/80$^-$, CD31$^-$ and CD45$^-$) from APTKA orthotopic tumors (n=4). **D.** IPA software generated mechanistic network map of APTKA tumors Cluster 0_CAFs depicting IL-1β as upstream signature regulator and its associated differentially upregulated genes (Log2FoldChange ≥1; p-adjusted value threshold of 0.05) compared to remaining CAFs clusters (activation z-score>1 and p-value <0.005). **E.** Representative scheme of cluster 0_IL-1β upregulated cytokines and transmembrane receptors (red bars) of Log2FoldChange ≥1 and adjusted p-value <0.05. Blue bar represents *Acta2* as downregulated gene in Cluster_0 _CAFs compared to remaining clusters. **F.** Representative images and quantification of DCN IHC performed on untreated APTKA (n=7) and APTK (n=7) orthotopic tumors. Scale bars represent 200 µm. Data are mean ±SD. **p-value<0.01 by t-test.

2.3 Stroma-rich orthotopic tumors are resistant to radiotherapy

Attempting to evaluate therapy response among tumors of distinct transcriptional profiles, APTKA and APTK tumors were subjected *in vivo* to local fractionated radiotherapy (5x2Gy) followed by histological analysis of primary tumors and livers 21 days' post last dose irradiation. Interestingly, APTK tumors responded well to radiotherapy and showed a significant reduction in primary tumor growth and complete loss of invasive potential (Figure 15A-C). In striking contrast, inflammatory stroma-rich APTKA tumors were resistant to local

radiotherapy and displayed an increased primary tumor growth, pronounced invasion and accelerated liver metastases post-radiotherapy (Figure 15D-G).

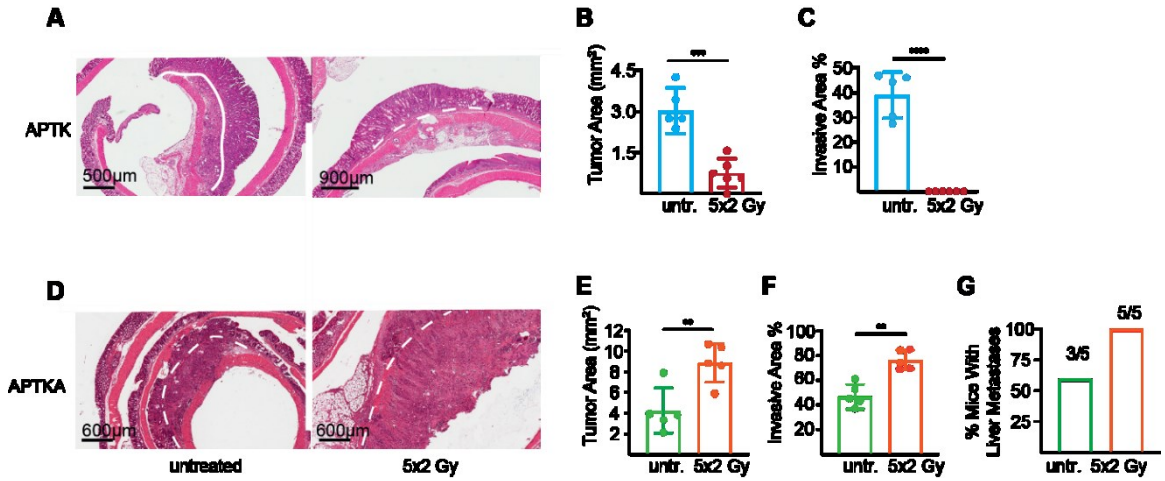

Figure 15: Stroma-rich orthotopic tumors are resistant to local radiotherapy *in vivo*. A. H&E staining of untreated and irradiated APTK tumors 21 days post last dose irradiation (experiment end point). Scale bars represent 500 µm and 900 µm respectively. White lines mark basal membrane and invasion fronts. **B, C.** Quantifications of tumor area (mm^2) and invasive area (%) among untreated (n=5) and 5x2Gy irradiated (n=5) APTK orthotopic tumors with 21 days post last dose RT as experiment end point. Data are mean ± SD. ***p <0.001 and ****p <0.0001 by t-test. **D.** Representative images of H&E staining of untreated and irradiated APTKA orthotopic tumors with scale bars representing 600 µm. **E-G.** Quantifications of tumor area (mm^2), invasive area (%) and % of mice with liver metastases among untreated and 5x2Gy irradiated APTKA tumors (n=5 mice per group). **p-value <0.01 by t-test. Data are mean ± SD.

Histological examination of irradiated APTKA tumors unmasked a distinct aligned morphology of fibroblasts acquired post-therapy suggestive of an increased ECM deposition. In fact, pronounced DCN and collagen (Sirius red) positivity was confirmed by IHC among irradiated APTKA tumors further coupled with a reduced cytotoxic T cells ($CD8^+$) infiltration with no variation in myeloid cells ($F4/80^+$ and $Ly6G^+$) content (Figure 16).

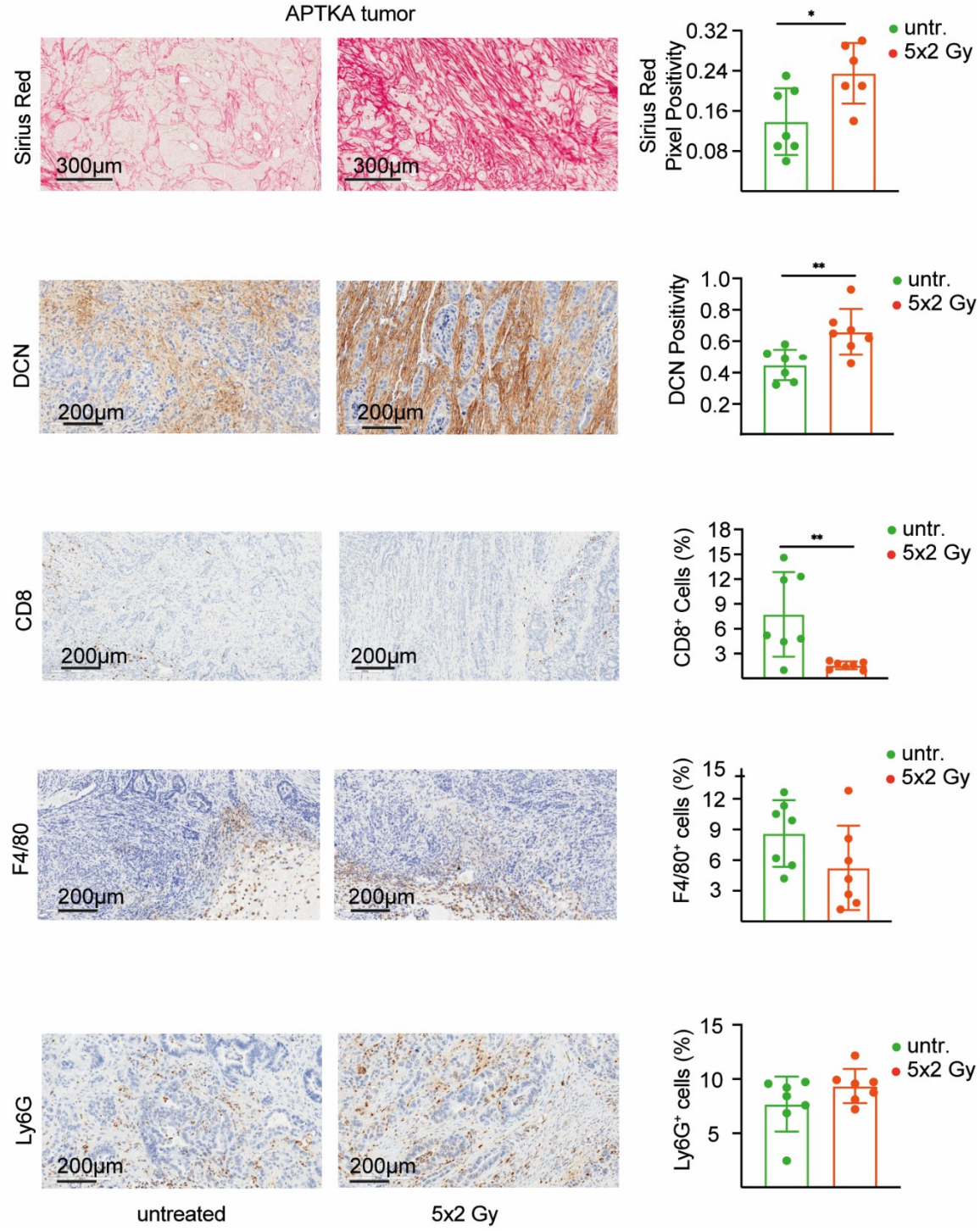

Figure 16: Radiotherapy resistant orthotopic tumors display post therapy increased collagen deposition and reduced cytotoxic T cells infiltration *in vivo*. Representative images and quantifications of Sirius red staining, DCN, CD8, F4/80 and Ly6G IHC among untreated (n=7) and 5x2Gy irradiated (n=6) APTKA orthotopic tumors 21 days post last dose RT. Scale bars represent 300 or 200 µm. Data are mean ±SD and significant *p-value <0.05 and **p-value <0.01 by t-test.

Importantly, both APTKA and APTK organoids, *ex vivo*, were responsive to radiotherapy, displaying reduced viability and seeding capacity post 5x2Gy treatment regimen (Figure 17A,

B). Moreover, organoids irradiated *ex vivo* failed to grow subcutaneously at comparable rates to non-irradiated organoids (Figure 17C). These reported findings support the opinion that APTKA orthotopic tumors therapy resistance *in vivo* was not attributed to organoids intrinsic properties but rather mediated by stroma cells.

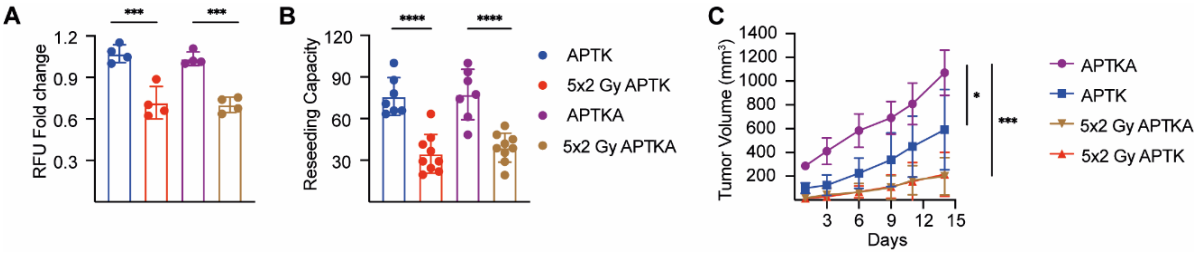

Figure 17: APTKA and APTK organoids sensitivity to radiotherapy. A. Relative fluorescent units of untreated and 5x2Gy irradiated APTKA and APTK organoids *ex vivo*, 6 h post last dose irradiation following resazurin cell viability assay (n=4 experimental replicates per group). Data are mean ± SD. *** p-value <0.001 and **** p-value <0.0001 by one-way ANOVA followed by Tukey's multiple comparisons test. **B.** Number of APTKA and APTK organoids untreated and 5x2Gy irradiated 4 days post reseeding (n=7 or 9 experimental replicates per condition). Data are mean ± SD and p-value <0.05 by one-way ANOVA followed by Tukey's multiple comparisons test. **C.** Subcutaneous tumors growth curves of untreated and 5x2Gy *ex vivo* irradiated APTKA and APTK organoids (n=6 female C57BL6/J mice per group). Data are mean ± SD. * p-value <0.05 and *** p-value <0.001by one-way ANOVA followed by Tukey's multiple comparisons test. Results represent one experiment which has been independently repeated three times.

2.4 Therapy resistant tumors dictate an IL-1α dependent inflammatory polarization of CAFs

To examine whether APTKA and APTK organoids conditioned media influence polarization of fibroblasts directly in a paracrine manner, supernatants were collected from both organoids and subsequently used to treat for 24 h intestinal fibroblasts isolated from unchallenged C57/BL6J mice (Figure 18A). RNA sequencing analysis confirmed distinct transcriptional profiles and clustering in PCA plot of fibroblasts stimulated with the two organoids conditioned media compared to untreated fibroblasts (Figure 18B). GSEA of APTKA conditioned media treated fibroblasts confirmed an inflammatory secretory and synthetic signature (Figure 18C) resembling the *in vivo* APTKA tumors inflammatory CAFs with significant enrichment of IL-1 CAFs Cluster-0 signature but no enrichment of the other clusters: TGFβ, IFNγ, DNMT or RICTOR CAFs (Figure 18D). Cross-species comparison further revealed a significant enrichment of iCAFs from human CRC in APTKA-conditioned medium treated fibroblasts (Figure 18E).

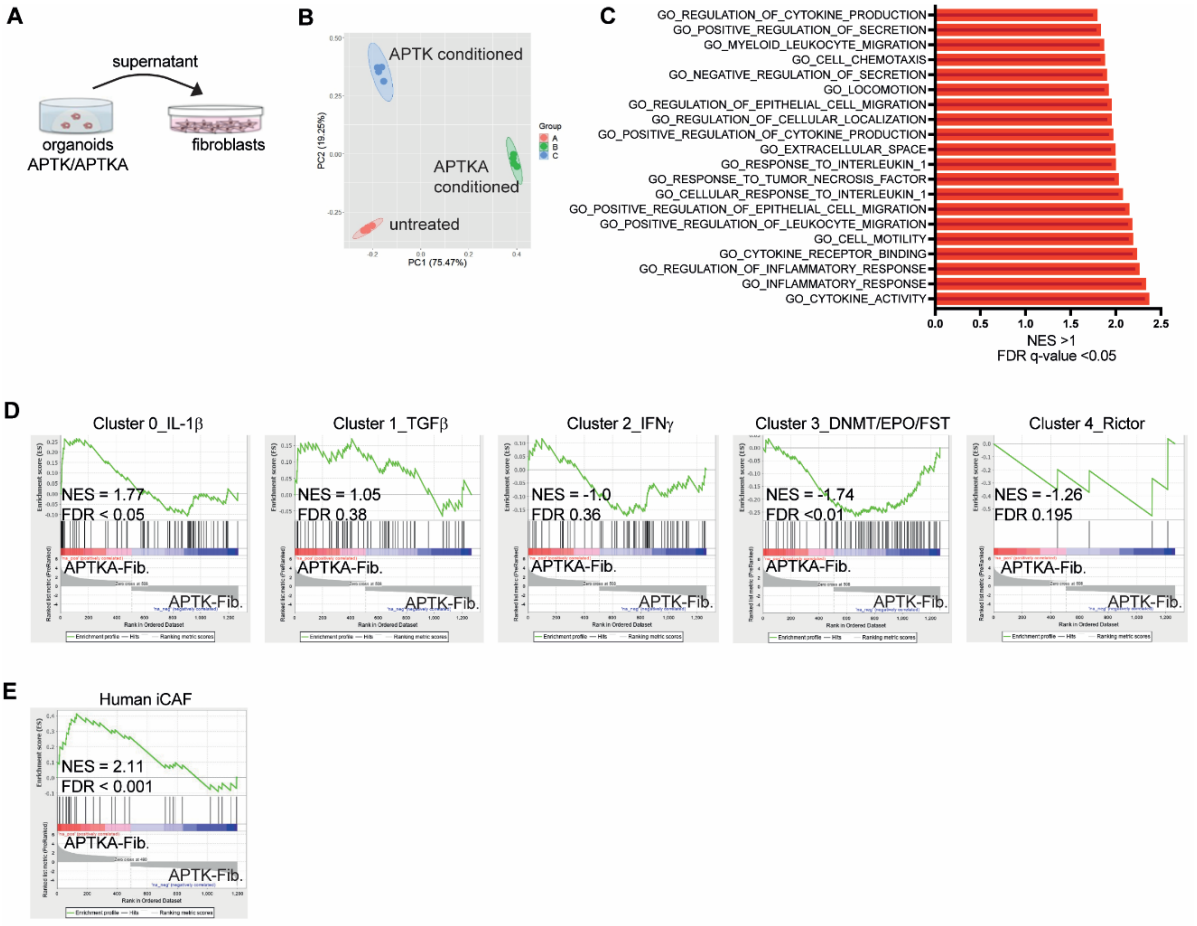

Figure 18: Therapy resistant tumors promote inflammatory polarization of CAFs *ex vivo*. **A.** schematic representation of APTKA and APTK organoids conditioned media collection followed by stimulation of unchallenged colonic fibroblasts isolated from C57BL6/J mice. **B.** PCA plot of the RNA sequencing analyses performed on untreated, APTKA and APTK conditioned media treated mouse fibroblasts 24 h post stimulation (n= 4 biological replicates per group). **C.** Graph summarizing gene ontology (GO) signatures enriched (NES≥1; adjusted p-value< 0.05) among APTKA versus APTK conditioned media treated fibroblasts 24 h post stimulation. **D.** GSEA plots of APTKA orthotopic tumors CAFs clusters signatures: Cluster 0_IL-1β, Cluster 1_TGFβ, Cluster 2_IFNγ, Cluster 3_DNMT/EPO and Cluster 4_Rictor CAFs among APTKA conditioned medium treated fibroblasts 24 h post stimulation. Significant enrichment is considered for NES > 1 and FDR-q-value < 0.05. **E.** GSEA plot of human iCAFs signature enrichment among APTKA compared to APTK conditioned media treated fibroblasts with NES>1 and FDR-q-value <0.05.

Ingenuity-pathway analysis of APTKA-conditioned media-treated fibroblasts identified NFκB and p38 MAPK signaling pathways as upstream regulators of their inflammatory secretory and synthetic signature (Figure 19A). Accordingly, IKKβ inhibitor ML120B or p38 MAPK inhibitor SB203580 significantly reduced APTKA-conditioned medium-mediated induction of inflammatory genes like *Cxcl1*, *Cxcl2*, *Cxcl5*, *Mmp9*, *Mmp13*, *Il1a*, *Il6*, *Tnfa* and *Nos2* (Figure 19B).

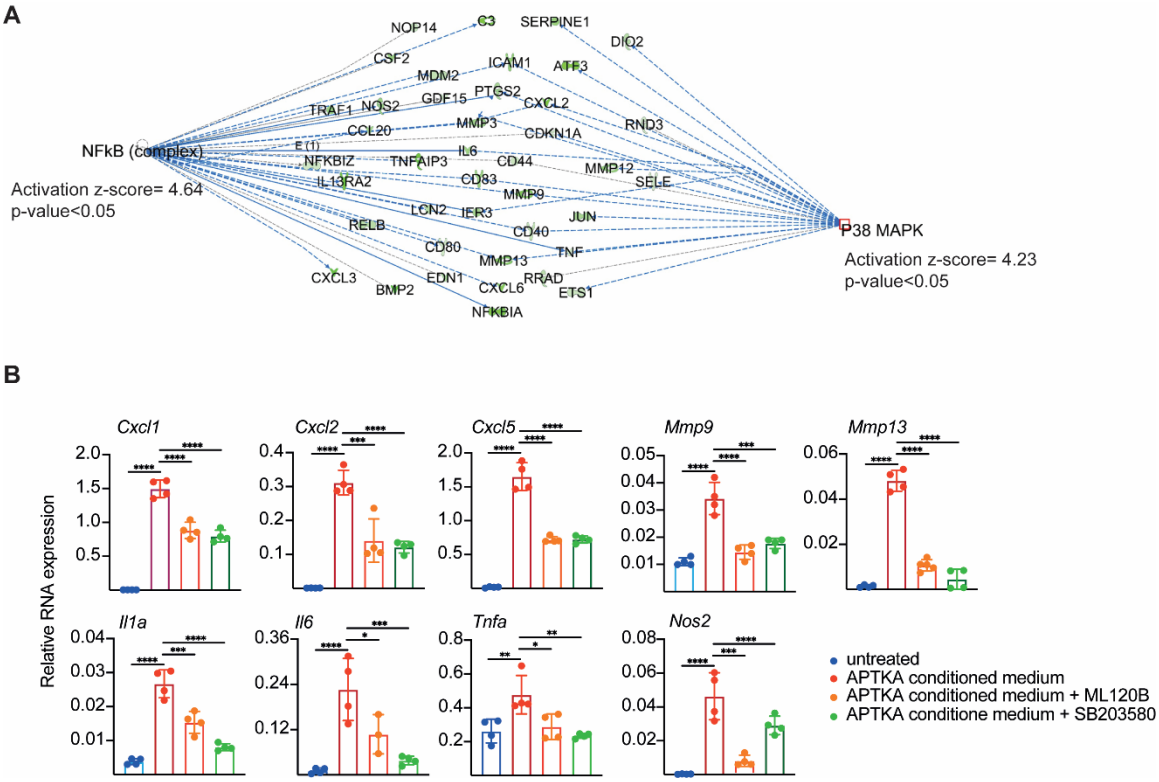

Figure 19: Therapy resistant tumors promote NFκB and p38-MAPK signaling pathways-mediated inflammatory polarization of CAFs *ex vivo*. A. Mechanistic network map generated by IPA software depicting NFκB and p38 MAPK signaling pathways as upstream regulators of APTKA conditioned medium-treated fibroblasts and their differentially expressed genes (activation z-score >1 and p-value <0.05) based on bulk RNA sequencing data generated 24 h post stimulation. **B.** Quantitative RT-PCR of inflammatory markers of untreated and APTKA conditioned medium-treated mouse fibroblasts in the presence or absence of IKKβ inhibitor ML120B (30 µM) and p38 MAPK inhibitor SB203580 (10 µM) 24 h post stimulation (n=4 experimental replicates per group). Data are mean ±SD and significant **** p-value<0.0001 by one-way ANOVA followed by Tukey's multiple comparisons test. Results representative of one experiment which has been repeated three times using independently isolated unchallenged mouse fibroblasts.

In order to identify the secreted molecules that were driving inflammatory polarization of conditioned media-treated fibroblasts, transcriptomic profiling of APTKA and APTK organoids was performed and several differentially expressed candidates encoding cytokines were identified among APTKA organoids (Figure 20A). Inhibition of TNFα, B cell activating factor (BAFF), CXCL16 or IL-33 didn't hinder iCAFs induction upon treatment with APTKA conditioned medium (Figure 20B). Interestingly, only IL-1α inhibition blocked induction of inflammatory genes such as *Cxcl5*, *Cxcl1*, *Cxcl2* and *Il1a* in fibroblasts challenged with APTKA supernatant (Figure 20B). Similarly, stimulation of unchallenged fibroblasts with recombinant IL-1α was sufficient to induce pro-inflammatory genes expression comparable to APTKA organoids conditioned medium (Figure 20C). To examine the potential reversibility of CAFs inflammatory polarization upon IL-1α signaling inhibition, for therapeutic implications, fibroblasts were stimulated for 24 h with APTKA organoids conditioned medium followed by addition of anakinra (recombinant IL1RA), fresh APTKA medium or regular medium for another 24 h. Importantly, replacing APTKA medium by regular medium or blocking IL-1 signaling by anakinra significantly reduced inflammatory genes expression (*Cxcl1*, *Cxcl5* and *Mmp13*) in fibroblasts (Figure 20D). Hence, IL-1α is essential in maintaining inflammatory CAFs polarization.

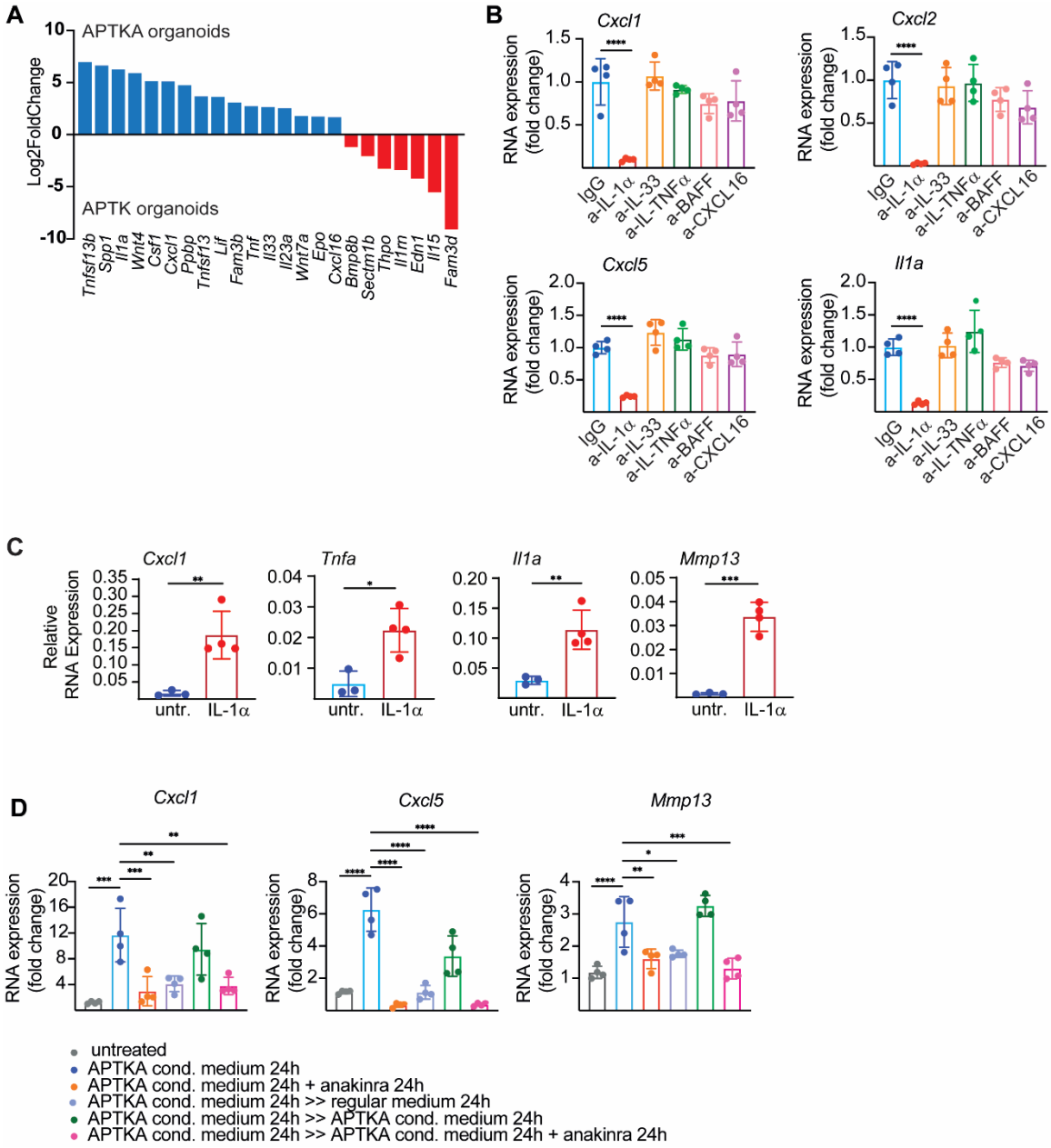

Figure 20: Therapy resistant tumors promote inflammatory polarization of fibroblasts *ex vivo* in an IL-1α dependent manner. A. Graph summarizing differentially expressed inflammatory genes (adjusted p-value <0.05) among APTKA organoids (blue bars; Log2FoldChange ≥ 1) and APTK organoids (red bars; Log2FoldChange ≤ -1) based on organoids bulk RNA sequencing data (n=3 independent replicates per group). **B.** Quantitative RT-PCR analysis of inflammatory genes among APTKA conditioned media treated fibroblasts in the presence of control IgG, anti-IL-1α, anti-IL1-33, anti-TNFα, anti-BAFF or anti-CXCL16 neutralizing antibodies (2 µg/ml) for 24 h (n=4 experimental replicates per group). Results represent one experiment which has been independently repeated three times. Data are mean ± SD and significant p-value <0.05 by one-way ANOVA followed by Tukey's multiple comparisons test. **C.** RNA expression analyses of untreated and IL-1α (1 µg/ml) stimulated fibroblasts (n=4 replicates) for 24 h. Results represent one experiment which has been independently repeated 3 times. **D.** RNA expression levels of inflammatory genes among APTKA conditioned medium-treated fibroblasts for 24 h further subjected for anakinra (10 µg/ml), fresh APTKA medium or regular basic medium for an additional 24 h (n=4 experimental replicates per

condition). Results represent one experiment which has been independently repeated two times. Data are mean ± SD and significant p-value <0.05 by one-way ANOVA followed by Tukey's multiple comparisons test.

2.5 IL-1 polarized cancer associated fibroblasts are central players in therapy resistance

To assess the relevance of *in vivo* IL-1 signaling blockade in improving radiotherapy response of resistant APTKA tumors, mice were treated with recombinant IL1RA (anakinra/ 500 µg/daily) three days before fractionated radiotherapy started, for 10 consecutive days (Figure 21A). Interestingly, anakinra administration alone had no significant impact on tumor growth, invasion or liver metastases (Figure 21B-D). Importantly, in conjunction with radiotherapy, IL-1 signaling blockade by anakinra, markedly reduced tumor growth as well as invasion and metastasis potential (Figure 21B-D). This was further histologically coupled with reduced ECM deposition reflected by a marked decrease in collagen and DCN positivity as well as enhanced $CD8^+$ cytotoxic T cells infiltration while the myeloid compartment ($F4/80^+$ and $Ly6G^+$ cells) was suppressed (Figure 21E).

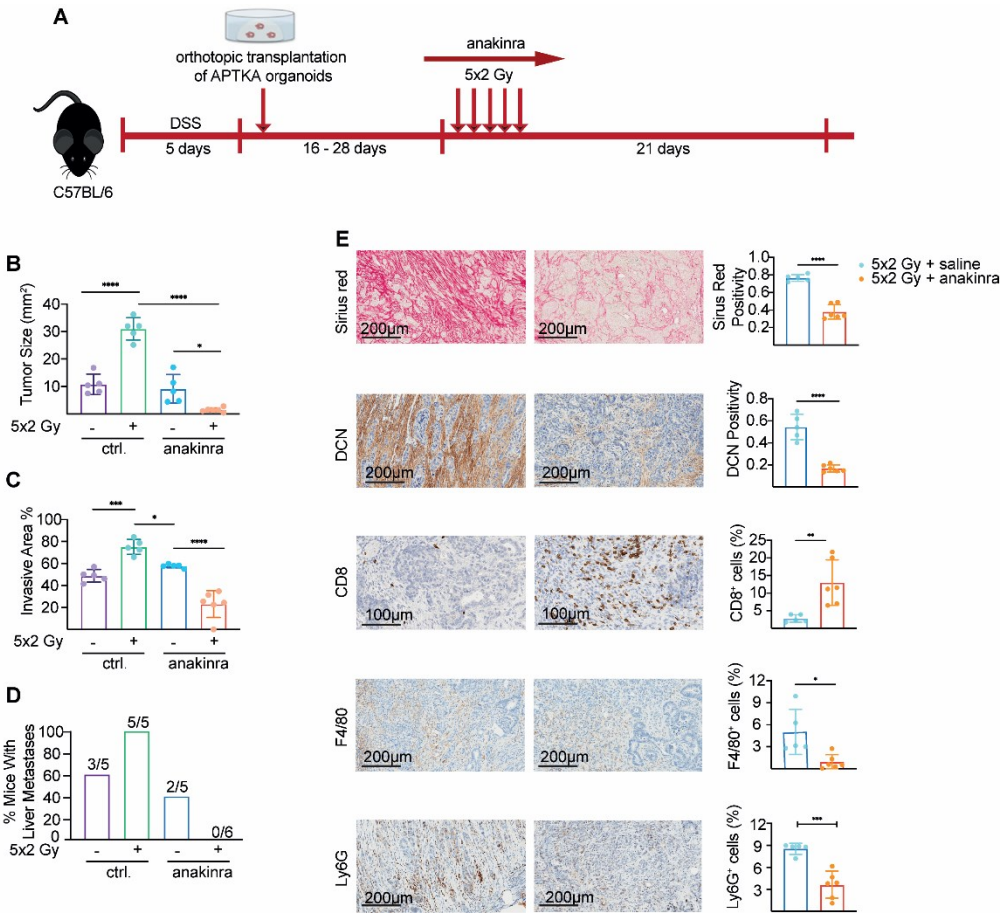

Figure 21: IL-1 signaling blockade by Anakinra sensitizes resistant orthotopic tumors to radiotherapy *in vivo*. A. Schematic representation of anakinra and (5x2Gy) radiotherapy treatment

plan among C57BL6/J mice bearing APTKA orthotopic tumors. Following tumor growth post transplantation, anakinra (500 µg/day) was administered daily, three days before radiotherapy, for 10 consecutive days with experiment end point 21 days post last dose RT. **B-D.** Tumor size (mm^2), invasive area (%) and % mice with liver metastases quantifications of untreated, anakinra treated or irradiated APTKA tumors in the presence or absence of anakinra. Experiment included 5 to 6 female C57BL6/J mice per group. Data are mean ± SD. Significant p-value<0.05 by one-way ANOVA followed by Tukey's multiple comparisons test. **E.** Representative images and quantifications of Sirius red, DCN, CD8, F4/80 and Ly6G IHC among irradiated APTKA orthotopic tumors in the presence or absence of anakinra (500 µg; daily). Scale bars represent 100 or 200 µm. Significant p-value <0.05 by t-test.

In line with these findings, employing a genetic preclinical mouse model of IL-1 receptor specific depletion in fibroblasts (*Col1a2*CreER^{T2}; *Il1r*$^{F/F}$) sensitized tumors to radiotherapy *in vivo* with a clear reduction in tumor growth, invasion, liver metastases, CAFs activation, myeloid cells infiltration and a marked intratumoral CD8$^+$ T cells infiltration (Figure 22A-D). Hence, these data further corroborate the central role of CAFs IL-1 signaling in promoting therapy resistance and hindering successful cytotoxic T cells infiltration.

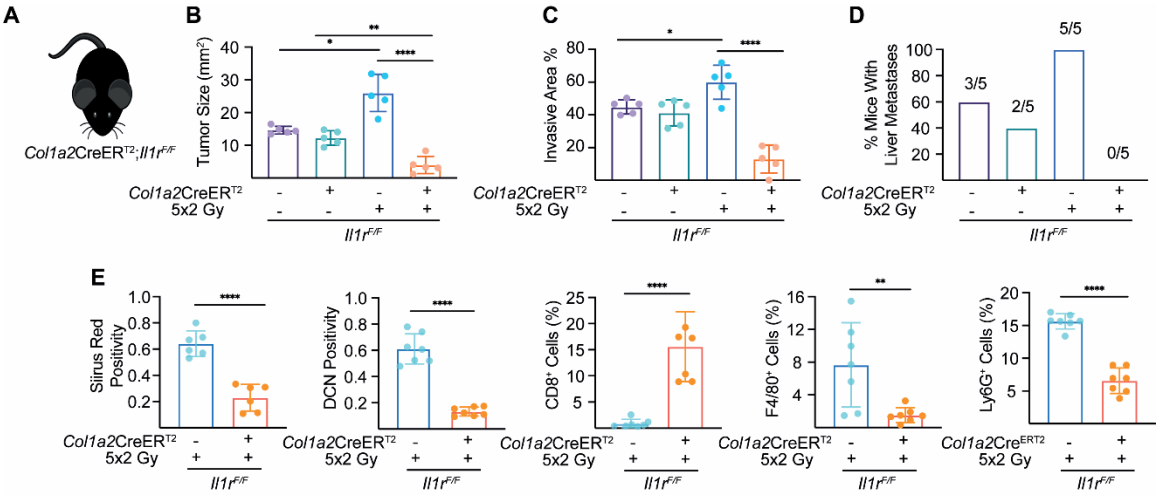

Figure 22: Conditional deletion of IL-1 signaling in fibroblasts sensitizes tumors to radiotherapy response *in vivo*. **A.** Irradiation of APTAK orthotopic tumors in *Col1a2*CreER^{T2}; *Il1r*$^{F/F}$ mice subjected to tamoxifen food 4 days before irradiation for 21 days (experiment end point). **B-D.** Overall tumor size (mm^2), invasive area (%) and % mice with liver metastases among untreated APTAK tumors transplanted in *Il1r*$^{F/F}$ WT (n=5 females) or *Col1a2*CreER^{T2} *Il1r*$^{F/F}$ KO (n=5 females) mice and 5x2Gy irradiated APTKA orthotopic tumors transplanted in *Il1r*$^{F/F}$ WT (n=5 females) or *Col1a2*CreER^{T2} *Il1r*$^{F/F}$ KO (n=5 females) mice. Data are mean ± SD. Significant p-value <0.05 by one-way ANOVA followed by Tukey's multiple comparisons test. **E.** Sirius red, DCN, CD8, F4/80 and Ly6G IHC quantifications among 5x2Gy irradiated APTKA tumors transplanted orthotopically in *Il1r*$^{F/F}$ WT or *Col1a2*CreER^{T2} *Il1r*$^{F/F}$ KO mice (n= 6 to 7 mice per group). Data are mean ± SD. Significant p-value <0.05 by t-test.

Moreover, in radiotherapy sensitive organoids, *Il1a* overexpression was performed by CRISPRa/Cas9 and increased IL-1α protein level was confirmed by ELISA in APTKA-sg-IL-

1α conditioned medium (Figure 23A, B). Fibroblasts treated with APTK-sg-*Il1a* organoids supernatant displayed increased expression of pro-inflammatory genes comparable to APTKA conditioned medium treated fibroblasts (Figure 23C). Importantly, greater IL-1α production by APTK organoids rendered them *in vivo* resistant to radiotherapy. Irradiated APTK-sg-*Il1a* orthotopic tumors, similarly to irradiated APTKA tumors, displayed enhanced growth, invasion, metastases and stroma reaction characterized by pronounced collagen/DCN positivity as well as reduced $CD8^+$ T cells infiltration (Figure 23D-G). In conclusion, tumor cells drive IL-1α polarization of CAFs towards an inflammatory profile, culminating in resistance to radiotherapy.

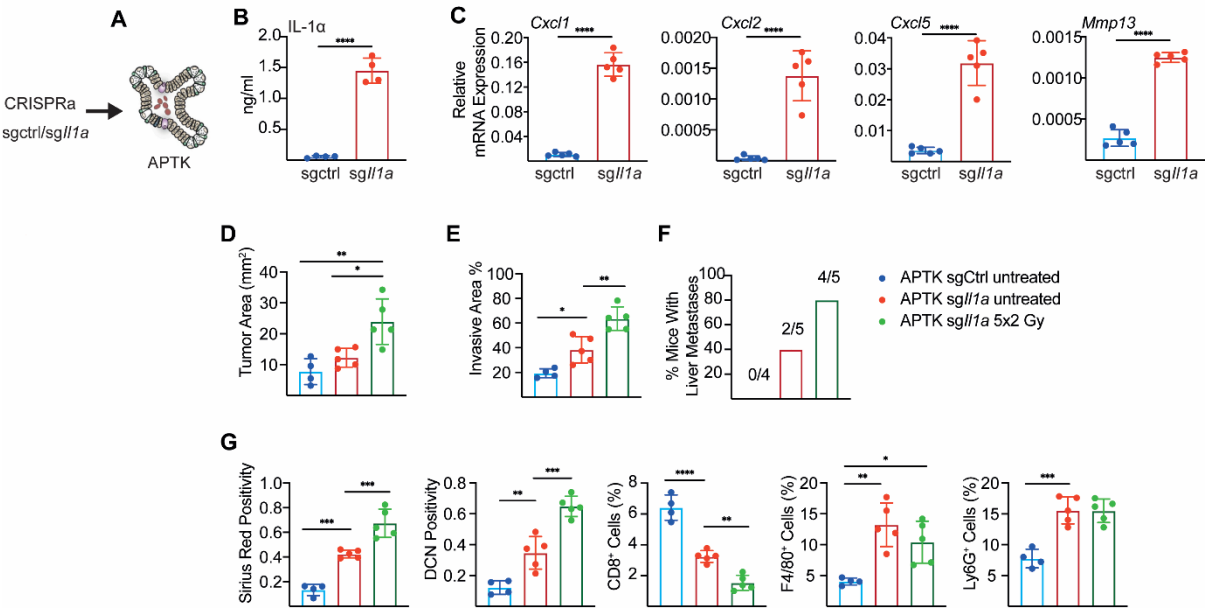

Figure 23: IL-1 signaling overexpression renders responsive tumors resistant to radiotherapy *in vivo*. A. IL-1α overexpression in APTK organoids by CRISPRa/dCas9 approach. **B.** ELISA based quantification of IL-1α protein levels (ng/ml) in conditioned media of control (sgctrl) APTK and *Il1a* overexpressing (sg*Il1a*) APTK organoids (n=4 biological replicates per group). Data are mean ± SD. ****p-value<0.0001 by t-test. **C.** quantitative RT-PCR analysis of inflammatory genes among sgctrl and sg*Il1a* APTK organoids. Data are mean ± SD. Significant p-value <0.05 by t-test. Each group include 5 biological replicates. Results represent one experiment which has been independently repeated two times. **D-F.** Quantifications of tumor size (mm^2), % invasive area and frequency of liver metastases among C57BL6/J mice transplanted with either untreated sgctrl or untreated and 5x2Gy irradiated sg*Il1a* APTK organoids (n= 4 to 5 females per group). Data are mean ± SD. Significant p-value <0.05 by one-way ANOVA followed by Tukey's multiple comparison test. **G.** Quantifications of Sirius red, DCN, CD8, F4/80 and Ly6G IHC among untreated sgctrl-APTK (n=4), untreated (n=5) and 5x2Gy irradiated (n=5) sg-*Il1a* APTK orthotopic tumors transplanted into C57BL6/J mice. Data are mean ± SD. ** p-value<0.01 and *p-value <0.05 by one-way ANOVA followed by Tukey's multiple comparisons test.

2.6 IL-1α sensitizes inflammatory CAFs to therapy-induced senescence *ex vivo* and *in vivo* in a p53-dependent manner

To dissect the molecular mechanism underlying CAFs-mediated resistance to radiotherapy *in vivo* and to which extent such resistance is attributed to irradiation of tumor cells, intestinal wildtype fibroblasts were exposed to conditioned media from irradiated APTKA or APTK organoids (Figure 24A). RNA sequencing analyses revealed no significant changes in the transcriptomic profiles of fibroblasts subjected to untreated or 5x2Gy irradiated organoids (Figure 24B), suggesting that radiotherapy has direct and differential effects on distinctly polarized fibroblasts. Accordingly, primary intestinal fibroblasts were initially treated with either APTKA or APTK conditioned media followed by their being subjected to 3x2Gy irradiation leading to pronounced morphological differences between the distinct fibroblasts with irradiated APTKA polarized fibroblasts presenting a distinctive elongated morphology comparable to that encountered among irradiated APTKA orthotopic tumors (Figure 24C, D). To get molecular insights on the observed therapy induced morphological changes, matrisome profiling of untreated and 3x2Gy irradiated APTKA-polarized fibroblasts was performed by mass spectrometry (Naba *et al.*, 2015; Naba *et al.*, 2017)**.** In line with the aligned morphology, irradiation of inflammatory CAFs led to significant increase in ECM deposition, comprising ECM glycoproteins, collagens, proteoglycans, growth factors and ECM regulators (Figure 24E).

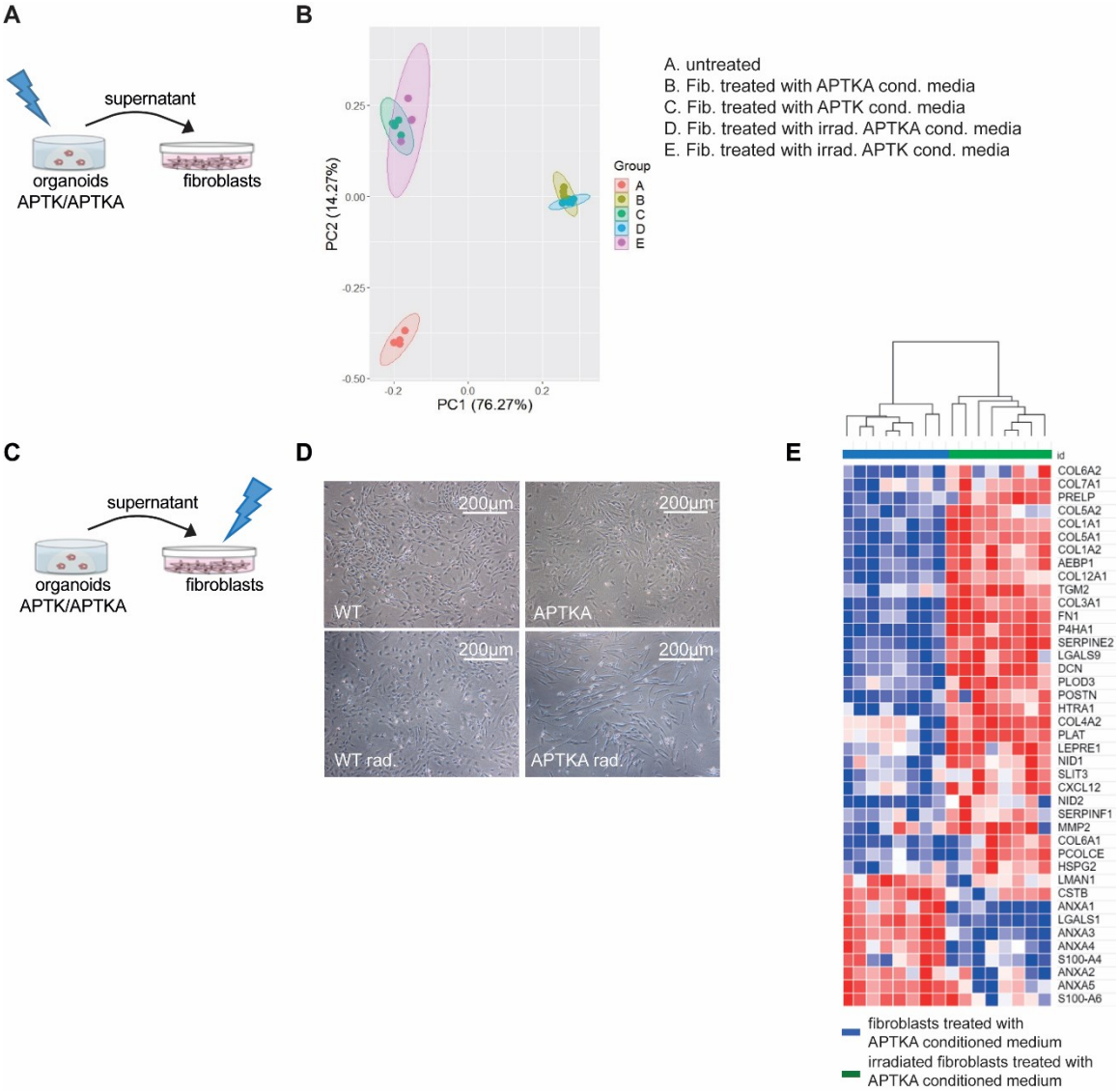

Figure 24. *Ex vivo* irradiation of IL-1α polarized iCAFs drives an aligned morphology and an enhanced ECM deposition. A. Scheme illustrating *ex vivo* 5x2Gy irradiation of APTKA or APTK organoids, followed by supernatant collection 6 h post last dose irradiation and stimulation of unchallenged mouse fibroblasts for 24 h. **B**. PCA plot based on the total RNA sequencing of untreated, APTKA, irradiated APTKA, APTK and irradiated APTK conditioned media stimulated fibroblasts for 24 h (n=4 biological replicates per group). **C.** Scheme representing treatment of unchallenged mouse fibroblasts with APTKA conditioned media for 12 h followed by 3x2Gy irradiation for 3 consecutive days. Proteomic, transcriptomic and microscopic IF or IHC analysis were performed 6 h post last dose irradiation. **D.** Microscopic captures of untreated or 3x2Gy irradiated wildtype and APTKA conditioned medium-treated fibroblasts. scale bars represent 200 µm. **E.** Heatmap of significantly enriched ECM proteins (student's t-test q-value <0.05) among 3x2Gy irradiated (n=4; 2 replicates per sample) or untreated (n=4; 2 replicates per sample) APTKA conditioned medium-treated fibroblasts as assessed by mass spectrometry 6 h post last dose RT.

Consistently, genes expression analysis of untreated and 3x2Gy irradiated APTKA-polarized CAFs reflected a significantly enriched senescence transcriptome in treated fibroblasts with

pronounced downregulation of cell cycle and cell cycle checkpoint associated genes (Figure 25A, B) compared to untreated iCAFs. In agreement with RNA sequencing findings, immunoblot analyses confirmed iCAFs growth arrest upon therapy with an upregulation of p21, CDK4, Cyclin D2 and a downregulation of CDK1 and Cyclin A while p16INK4a levels remained unchanged (Figure 25C). Moreover, immunofluorescence analyses validated a p21 nuclear accumulation and a pronounced phospho-H2AX positivity reflective of DNA damage while the SA-β-gal staining positivity corroborated a clear senescence program induction in IL-1α iCAFs upon irradiation *ex vivo* (Figure 25D). In attempt to examine senescence profile *in vivo*, SA-β-gal staining was performed on untreated and irradiated APTKA orthotopic tumors with a clear stroma positivity in conjunction with pronounced nuclear p21 staining in irradiated tumors implying a senescence program initiation *in vivo* (Figure 25E).

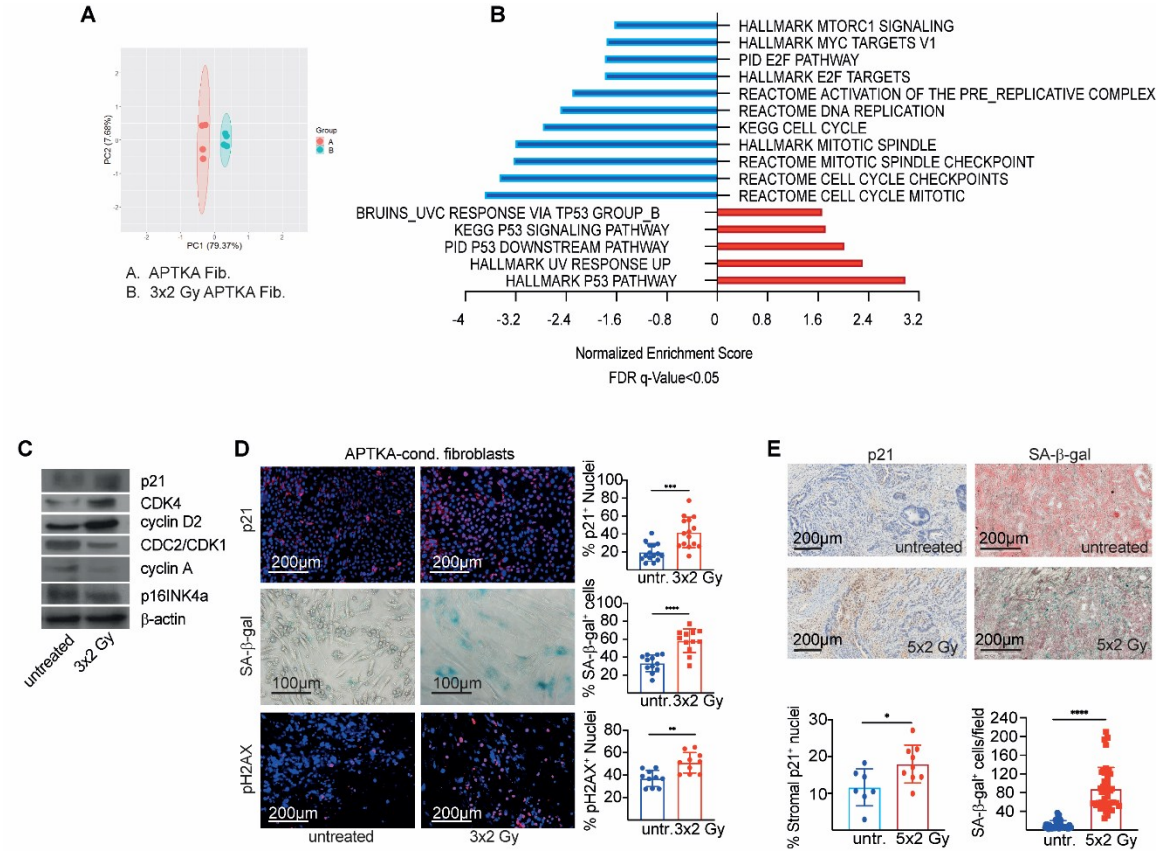

Figure 25: IL-1α sensitizes iCAFs to radiotherapy-induced senescence *ex vivo* and *in vivo*. **A.** PCA plot of the RNA sequencing data of untreated and 3x2Gy irradiated APTKA conditioned media treated fibroblasts (n=4 biological replicates per group). **B.** Graph summarizing significant signatures downregulated (NES≤-1 and FDR_q_value<0.05; blue bars) and upregulated (NES≥1 and FDR_q_value<0.05; red bars) in APTKA-conditioned medium-polarized fibroblasts upon 3x2Gy irradiation *ex vivo.* **C.** Immunoblot analyses of untreated and irradiated APTKA-conditioned medium polarized fibroblasts 6 h post last dose RT. **D.** Representative images and quantifications of p21,

pH2AX IF and SA_β_gal staining of untreated and 3x2Gy irradiated APTKA-conditioned medium treated fibroblasts 6 h post last dose RT. Scale bars represent 100 µm and 200 µm. Results represent three independent experiments. Significant p-value<0.05 by t-test. **E.** Representative images and quantifications of p21 IHC among untreated (n=7) and 5x2Gy irradiated (n=9) APTKA orthotopic tumors 21 days post last dose RT. SA_β_gal staining representative images and quantifications among untreated (n=5) and 5x2Gy irradiated APTKA orthotopic tumors 21 days post last dose RT with at least 10 independent microscopic fields quantified per tumor. Scale bars represent 200 µm. data are mean ±SD. Significant p-value<0.05 by t-test.

Bearing in mind that rectal cancer patients are subjected to a combination treatment plan of fractionated radiotherapy and chemotherapy, 5-fluorouracil (5-FU)-mediated effects on APTKA conditioned medium treated fibroblasts (iCAFs) were further examined. *Ex vivo*, 5 FU- treatment of APTKA conditioned medium treated mouse fibroblasts and IL-1α stimulated human fibroblasts drove a clear senescence induction confirmed by SA-β-gal positivity reflecting a central role of IL-1α in iCAFs polarization and sensitization to genotoxic therapy-induced senescence (Figure 26A, B).

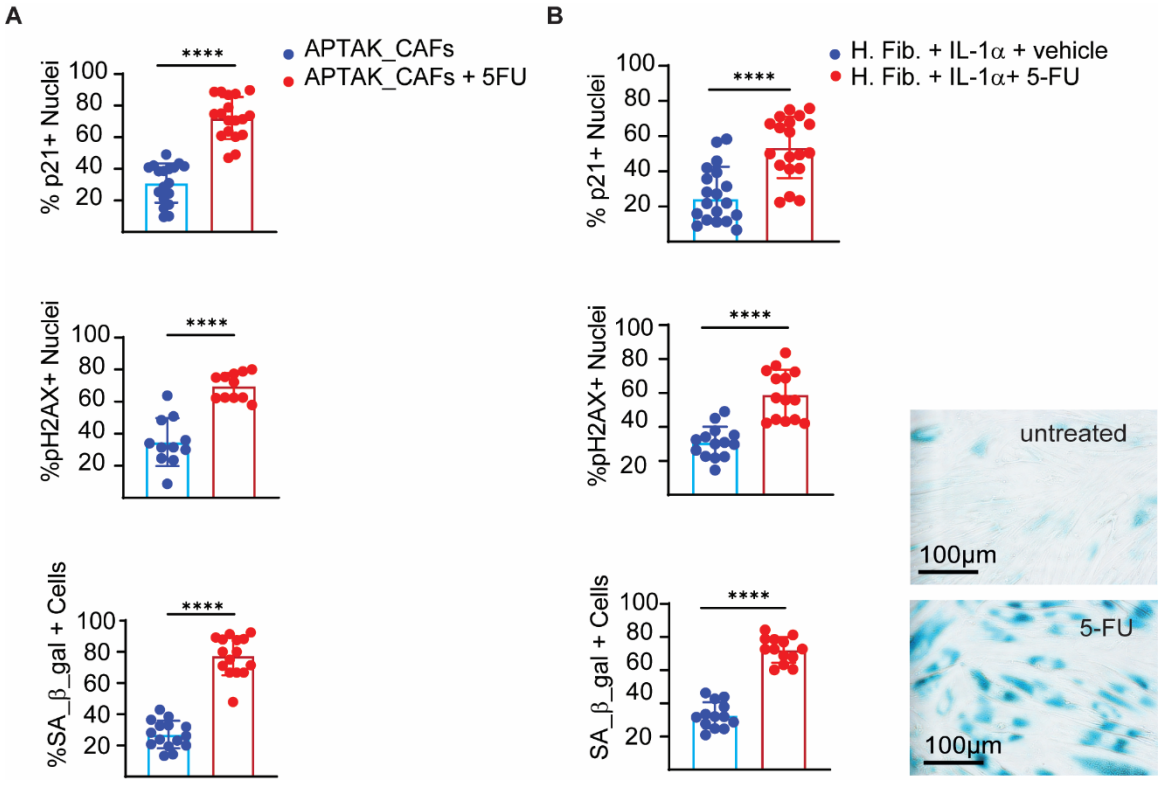

Figure 26: IL-1α sensitizes iCAFs to chemotherapy induced senescence *ex vivo*. A, B. Quantifications of p21, pH2Ax IF and SA-β-gal staining of untreated and 5-FU (10 µM) treated APTKA-conditioned medium polarized mouse fibroblasts and IL-1α (1 µg/ml) stimulated human fibroblasts. Results represent 4 independent experiments. Significant p-value<0.05 by t-test. Scale bars = 100µm.

Given that p53 was predicted as upstream regulator of the senescence program encountered *ex vivo* upon APTKA-CAFs irradiation (Figure 27A), to functionally confirm *in vivo* its implication and consequently the relevance of iCAFs senescence in therapy resistance, *Trp53* knockout mice were employed (Figure 27B). Orthotopic APTKA tumors transplanted in *Trp53*$^{-/-}$ mice responded well to radiotherapy which led to a significant reduction in tumor size, invasive area and ECM deposition as depicted by reduced collagen and DCN positivity along a pronounced intratumoral CD8^{+} T cells infiltration (Figure 27C, D). Further confirmation *ex vivo* included usage of *Trp53* deficient fibroblasts which upon stimulation with APTKA conditioned medium and further 3x2Gy irradiation didn't display a therapy-induced senescence program (Figure 27E).

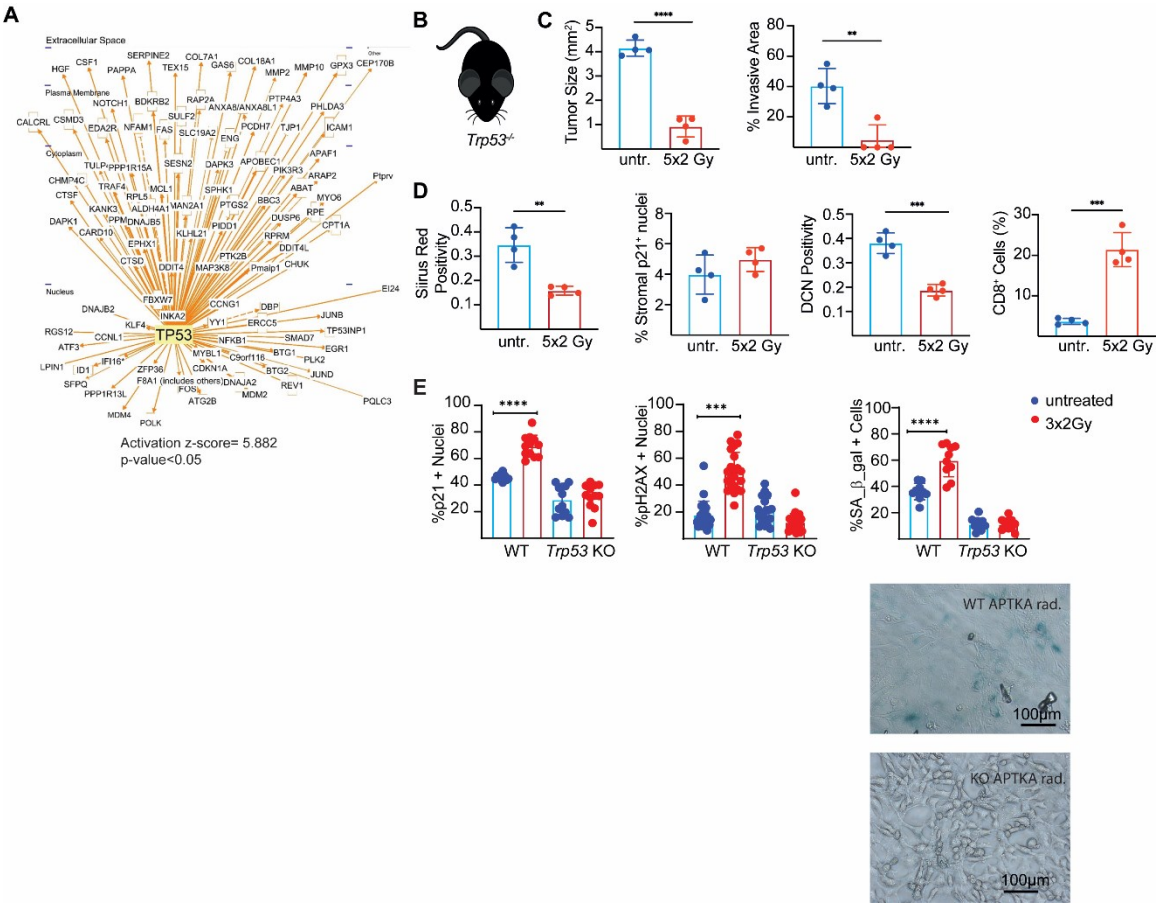

Figure 27: IL-1α sensitizes iCAFs to p53 signaling-mediated therapy induced senescence *in vivo*. A. Mechanistic network map of p53 signaling pathway (activation z-score= 5.882 and p-value<0.05) as predicted upstream regulators of 3x2Gy irradiated APTKA conditioned medium treated fibroblasts and its differentially expressed genes (adjusted p- value<0.05) as predicted by IPA software. **B.** APTKA organoids orthotopic transplantation into *Trp53* knockout mice (males) following the brush EDTA model described in "materials and methods". **C.** Quantifications of tumor size (mm^2) and % invasive area among untreated (n=4) and 5x2Gy irradiated (n=4) APTKA orthotopic tumors transplanted into Tp53 knockout mice 21 days' post last dose irradiation. Data are mean ± SD. *p-

value,0.05 by t-test. **D.** Quantifications of Sirius red, p21, DCN and CD8 staining among untreated and 5x2Gy irradiated APTKA orthotopic tumors transplanted in p53 knockout mice (n=4 mice per group) 21 days' post last dose RT. Data are mean ± SD. Significant p-value<0.05 by t-test. **E.** Quantifications and representative images of SA-β-gal staining as well p21 and phospho-H2AX IF among untreated and 3x2Gy irradiated APTKA conditioned medium- polarized WT and *Trp53* knockout fibroblasts *ex vivo*. Results represent 4 independent experiments. Data are mean ± SD. Scale bars =100 µm. Significant p-value <0.05 one-way ANOVA followed by Tukey's multiple comparison analysis.

Moreover, to pharmacologically block senescence *in vivo*, Venetoclax was administered as 100mg/kg of mouse daily in combination with fractionated radiotherapy of APTKA orthotopic tumors. Senotherapy via Venetoclax, along radiotherapy, reverted APTKA tumors resistance and directed a pronounced decrease in tumor burden, invasion and liver metastases (Figure 28A-D). Such a therapy response was accompanied by a decrease in collagen deposition, DCN content and importantly enhanced $CD8^{+}$T cells infiltration, similarly to anakinra effects on irradiated APTKA tumors *in vivo* (Figure 28E). *Ex vivo*, Venetoclax further inhibited senescence induction among iCAFs upon irradiation (Figure 28F).

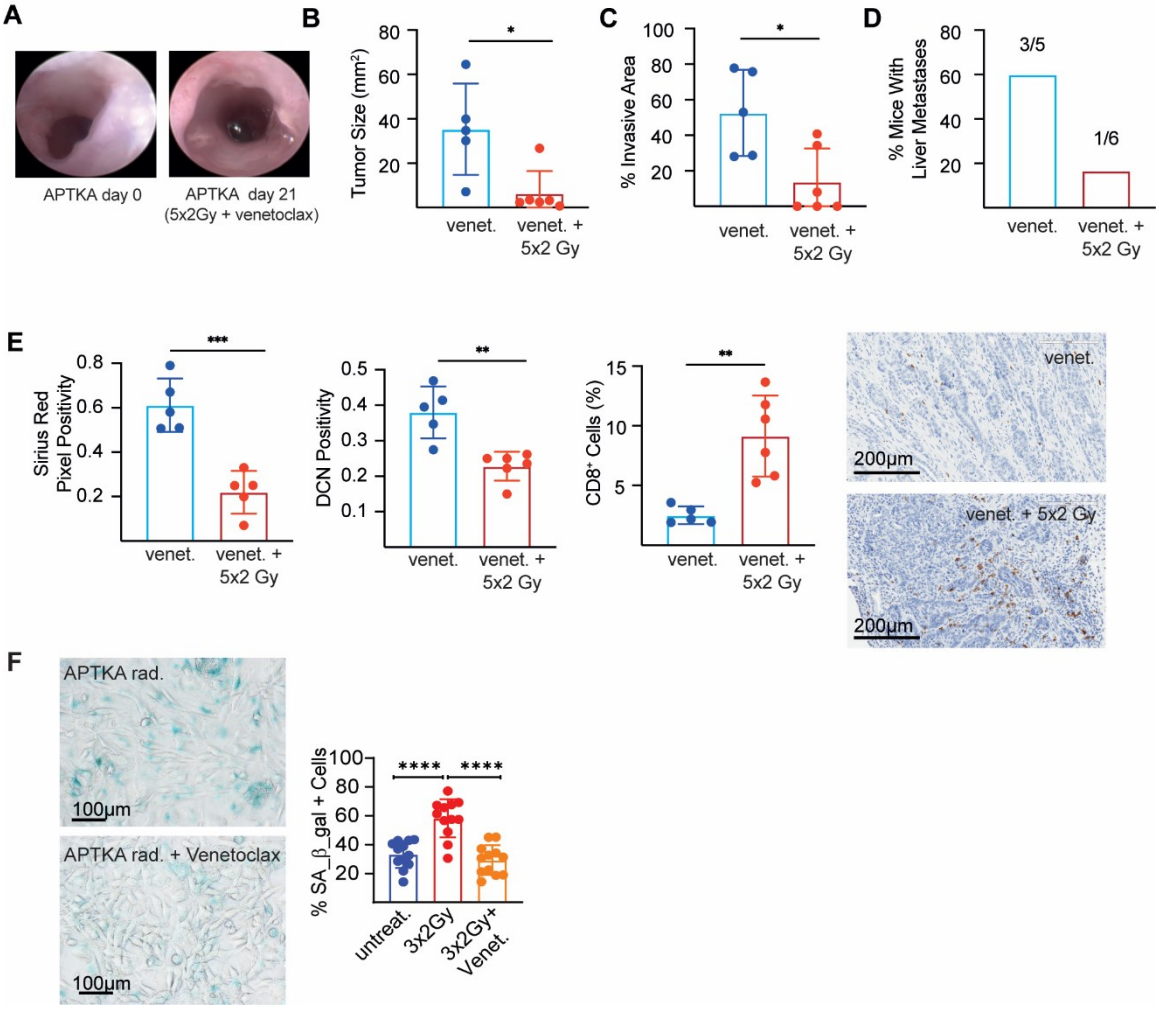

Figure 28: Senotherapy of resistant orthotopic tumors renders them responsive to radiotherapy *in vivo*. **A.** APTKA organoids orthotopic transplantation into C57BL6/J mice (females) following the DSS model described in "materials and methods" and subjected to Venetoclax therapy (oral gavage of 100 mg/kg/day) with or without local 5x2Gy radiotherapy. **B-D.** Quantifications of tumor size (mm^2), % invasive area and frequency of liver metastases among untreated (n=5) and 5x2 Gy irradiated (n=6) Venetoclax-treated APTKA orthotopic tumors transplanted into C57BL6/J mice 21 days' post last dose irradiation. Data are mean ± SD. *p-value<0.05 by t-test. **E.** Quantifications of Sirius red, DCN and CD8 staining among Venetoclax treated APTKA orthotopic in the presence or absence of local irradiation (5x2Gy) 21 days' post last dose RT. Data are mean ± SD (n=5 or 6 mice per group). Significant **p-value <0.01 and ***p-value <0.001 by t-test. Representative images at 200 µm. **F.** SA_β_gal quantifications and representative images (100 µm) among untreated and irradiated APTKA conditioned medium treated fibroblasts in the presence or absence of Venetoclax (500 nM). Results represent three independent experiments. Significant **** p-value <0.0001 by one-way ANOVA followed by Tukey's multiple comparison analysis.

2.7 IL-1α mobilizes a nitrite-mediated oxidative DNA damage sensitizing iCAFs to senescence induction upon chemoradiotherapy

To understand how IL-1α promotes therapy induced senescence in inflammatory CAFs, it was hypothesized that IL-1α mediated accumulation of reactive oxygen and nitrogen species (ROS and NOS), mobilizes a DNA damage machinery prompting iCAFs susceptibility to senescence upon therapy. Accordingly, mitochondrial activity in APTKA-conditioned medium treated fibroblasts was reduced and in agreement with reduced proliferation and enhanced quiescence, cells exhibited lower OCR, ECAR, maximal respiration, reserve respiratory capacity as well as basal glycolysis and compensatory glycolysis (Figure 29A-C). While ROS levels remained unchanged among WT versus APTKA or APTK conditioned media treated fibroblasts (Figure 30A), importantly, higher nitrite levels were detected in conditioned medium from APTKA and recombinant IL-1α stimulated fibroblasts in agreement with their enhanced *Nos2* expression (Figure 30B, C). Parallelly, an enhanced oxidative DNA damage was reported by 8-OHdG immunofluorescence (Figure 30D). Application of the NOS2 inhibitor W1400 or anakinra mediated inhibition of IL-1 signaling resulting in blockade of nitrite release, prevention of oxidative DNA damage and subsequently senescence induction in APTKA-conditioned medium treated fibroblasts (Figure 30D, E). In summary, the reported findings revealed the role of IL-1α in NOS induction and subsequent DNA damage further predisposing inflammatory CAFs to senescence programs activation upon therapy. Jointly, these findings validated the notion that IL-1α mediated polarization of iCAFs culminate in nitrite production and NOS-mediated DNA damage. Further genotoxic stress driven by irradiation or chemotherapy triggers a p53-dependent senescence program characterized by active secretion

of cytokines and ECM deposition, counteracting T cells mediated immunosurveillance yet favoring tumor progression and distant dissemination.

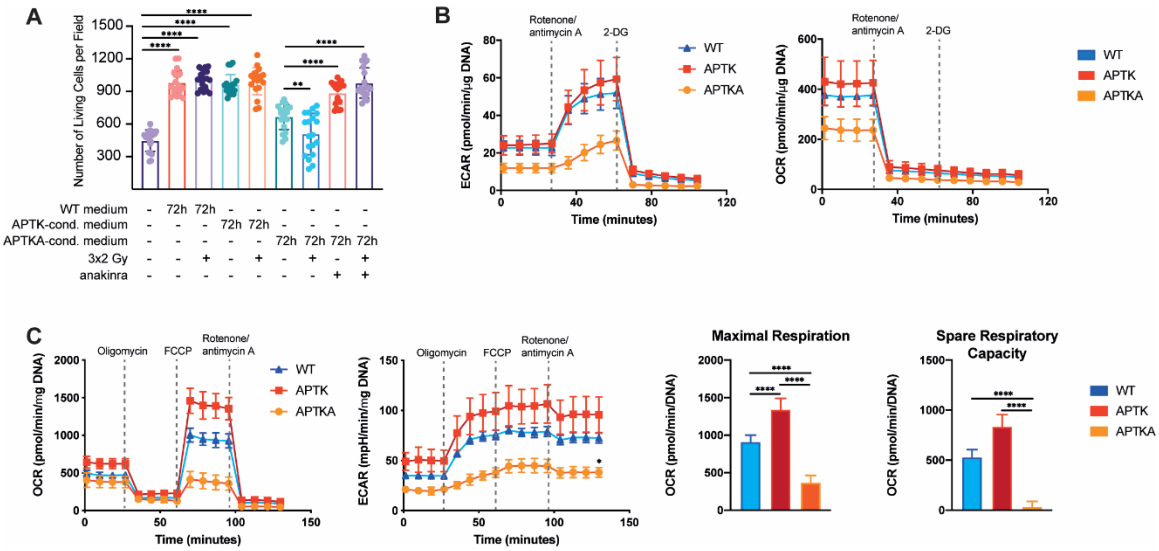

Figure 29: Inflammatory CAFs display a reduced mitochondrial activity along a decreased proliferation and increased quiescent profile. A. Quantifications of the number of living cells per field of untreated, APTK and APTKA conditioned media treated fibroblasts in the presence or absence of anakinra (20 µg/ml), with or without *ex vivo* 3x2Gy irradiation. Data are mean ± SD. * p <0.05, ** p <0.01, *** p <0.001 and **** p <0.0001. by one-way ANOVA followed by Tukey's multiple comparisons test. Results represent three independent experiments. **B.C.** Extracellular acidification rate (ECAR) and oxygen consumption rate (OCR) among non-irradiated WT, APTK and APTKA conditioned media treated fibroblasts for 72 h. Measurements were performed in real time under basal conditions and in response to indicated compounds using mitostress and glycolytic rate kits. Data are mean ± SD. Results represent two independent experiments with 6 to 7 replicates. Significant **** p-value<0.0001 by one-way ANOVA followed by Tukey's multiple comparison test.

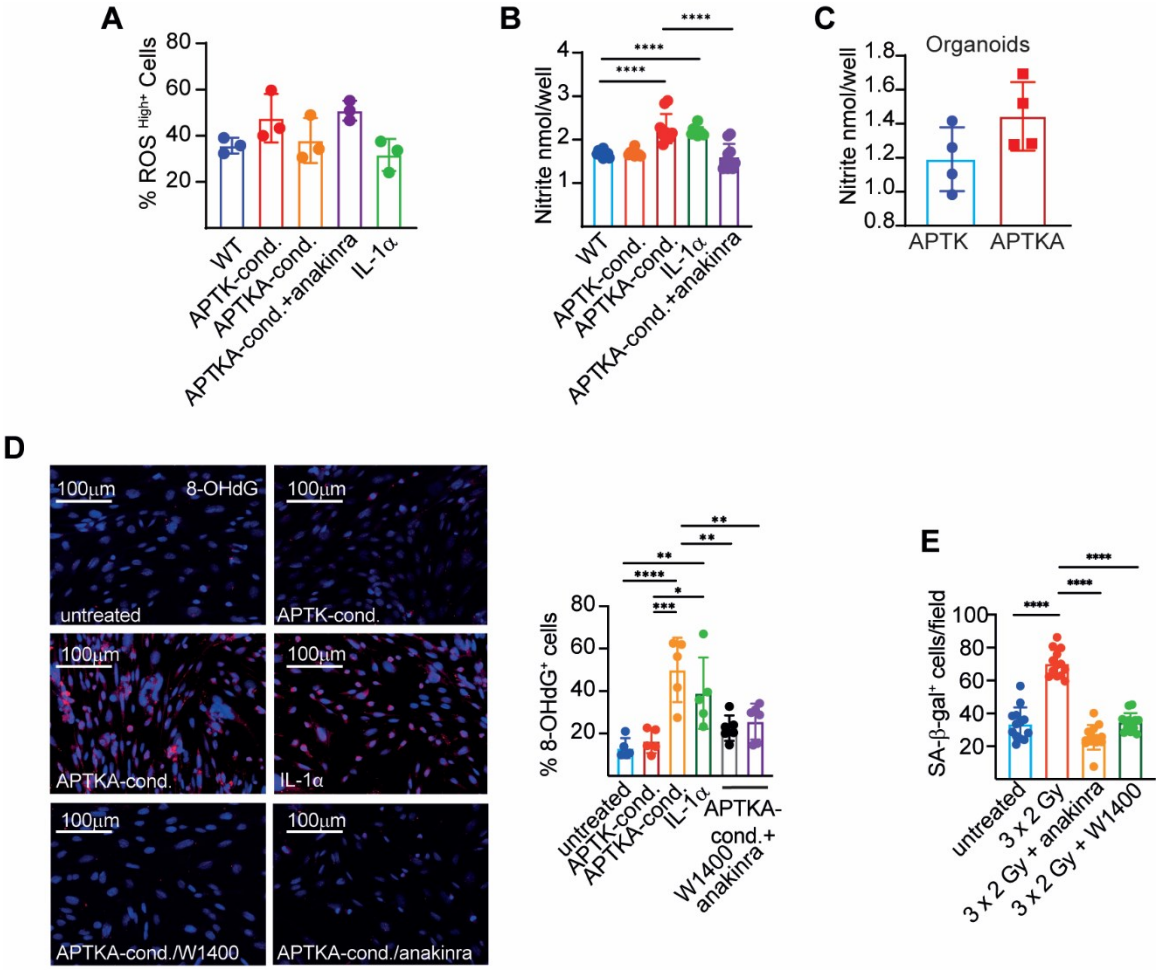

Figure 30: IL-1α sensitizes inflammatory CAFs to therapy induced senescence through a NOS-mediated DNA damage. A. ROS ^{high} (+) cells (%) among untreated, APTKA, APTK, APTKA conditioned media plus anakinra (20 µg/ml) and IL-1α (1 µg/ml) stimulated fibroblasts for 72 h. Results represent 3 independent experiments. Data are mean ± SD. No statistical significance by one-way ANOVA followed by Tukey's multiple comparison analysis. **B, C.** Nitrite levels (nmol/well) determined by Griess assay in supernatants of organoids (APTKA and APTK), WT, APTK medium, APTKA medium, IL-1α (1 µg/ml) and APTKA medium plus anakinra (20 µg/ml) treated fibroblasts for 72 h. Results representative of three independent experiment. Data are mean ± SD. ****p <0.05 by one-way ANOVA followed by Tukeys' multiple comparisons analysis. **D.** Representative images and quantifications of 8-OHdG IF staining among WT, IL-1α (1 µg/ml), APTK conditioned medium, APTKA conditioned medium treated fibroblasts for 72 h in the presence or absence of W1400 (1 mM) inhibitor or anakinra (20 µg/ml). Scale bars represent 200 µm. Data are mean ± SD. Results representative of one experiment with 5 to 6 technical replicates per condition. Experiment repeated three times. *p <0.05, **p <0.01, **p <0.001 and ****p <0.0001 by one-way ANOVA followed by Tukey's multiple comparison analysis. **E.** Quantification of SA-β-gal staining among untreated and 3x2Gy irradiated APTKA conditioned medium polarized fibroblasts in the presence or absence of anakinra (20 µg/ml) and W1400 (1 mM) for 72 h. Results represent three independent experiments. Data are mean ± SD. **** p-value <0.0001 by one-way ANOVA followed by Tukey's multiple comparisons test.

2.8 Reduced IL1RA levels augment IL-1 signaling among rectal cancer patients and drive iCAFs therapy induced senescence

To examine the relevance of the reported findings in the preclinical mouse model and their potential association with rectal cancer prognosis, proteome profiling of patients' serum samples, pre-CRT, was performed using Luminex Bio-Plex assay allowing determination of serum circulating levels of inflammatory cytokines, chemokines and growth factors. There were no observed differences in the circulating levels of IL-1β or any of the remaining cytokines, chemokines or growth factors with IL-1α levels being below detection range (Figure 31A). Significantly, pretherapeutic serum IL1RA levels were significantly reduced among poor prognosis non-pCR patients with lymph nodes and distal metastasis post CRT (Figure 31A). To understand IL1RA levels variability among RCA patients, two *IL1RN* polymorphisms were examined: rs4251961 (T/C) and rs579543 (G/A) SNPs. Higher IL1RA levels were detected among patients of homozygous T/T genotype for the rs4251961 polymorphism while there was no observed correlation between IL1RA and rs579543 genotypes (Figure 31B). In line with the proteomic findings, pretherapeutic, lower *IL1RN* expression levels in RCA patients' biopsies was associated with significantly shorter DFS supporting the value of an enhanced IL-1 signaling in conferring therapy resistance among these patients (Figure 31C).

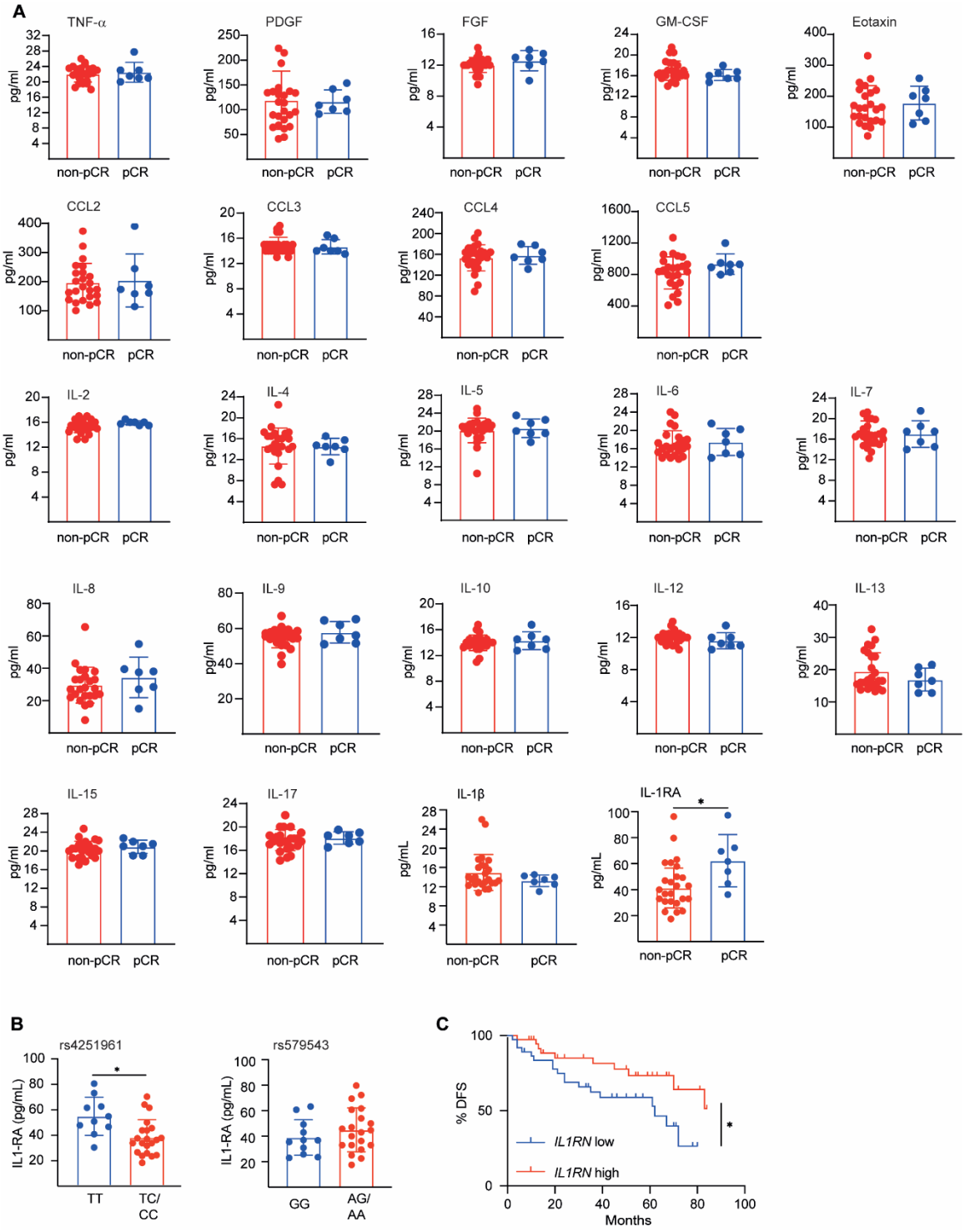

Figure 31: Baseline IL1RA serum levels are markedly reduced among non-pCR patients. **A.** Serum protein levels (pg/ml) of cytokines, chemokines and growth factors among RCA patients pretherapeutic (7 pCR and 25 non-pCR patients). Data are mean ± SD. *p-value<0.05 by t-test. **B.** Association analyses of RCA patients pretherapeutic IL1RA serum levels (pg/ml) and SNPs: rs4251961 and rs579543 using DNA isolated from 31 RCA patients (first and third cohorts) peripheral blood mononuclear cells. Data are mean ± SD. **p-value <0.05 by t-test. **C.** Kaplan-Meier DFS curve (median split) of RCA patients of low (n=37) and high (n=37*) IL1RN* expression score based on transcriptomic data of pretherapeutic biopsies (first patients' cohort). *p-value <0.05 by Log-rank (Mantel-Cox) test.

Comparative paired analysis of non-pCR patients' transcriptomic profiles before and after CRT, similarly to the resistant APTKA tumors, revealed an induction, post CRT, of an EMT, ECM and collagen signature in patients' surgical specimens (Figure 32A, B). A further cross species analysis showed a significant enrichment of the senescence program detected among irradiated APTKA polarized CAFs and a pronounced expression of their acquired matrisome signature post therapy (Figure 32B). Therapy-induced senescence among non-pCR patients was further validated by an augmented p21 stromal staining, and collagen as well as DCN deposition in response to CRT hence strongly stressing on a link among RCA patients between IL-1 signaling and therapy induced senescence (Figure 32C-E).

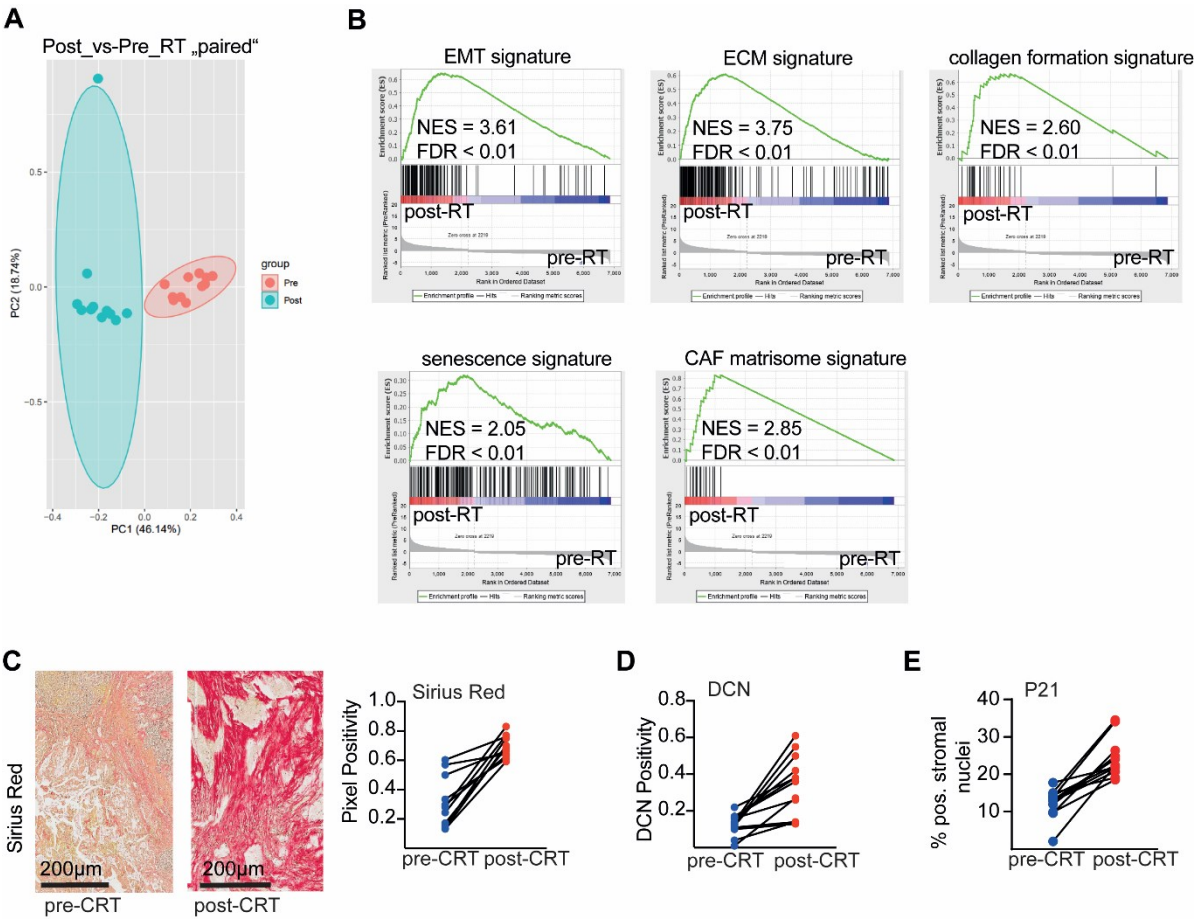

Figure 32: Enhanced ECM deposition and induced senescence profile among non-pCR rectal cancer patients pre-CRT. A. PCA plot generated based on the comparative analysis of RCA patients total transcriptomic profiles before (biopsies samples) and post CRT (surgical samples). Analysis included 11 RCA non-pCR patients of the first cohort. **B.** GSEA plots of EMT, ECM, collagen formation, senescence and CAF matrisome signatures among post-CRT samples of RCA patients compared to pre-CRT transcriptomic data (n=11 RCA non-pCR patients; paired analysis). Significant NES≥2 and FDR-q-value<0.05. **C-E.** Paired analysis of post-CRT versus pre-CRT Sirius red, DCN and

p21 staining among RCA patients (n=11 or 12 RCA patients from first cohort). Scale bars represent 200 µm.

To further support this notion, PDOs were established from pre-CRT biopsies collected from six distinct non-pCR RCA patients characterized by different IL1RA yet of comparable IL-1α in their conditioned media (Figure 33A). Stimulation of non-patient matched fibroblasts isolated from normal rectal biopsies with supernatants from "IL1RA low" organoids promoted a higher inflammatory profile and nitrite production then conditioned media from "IL1RA high" PDOs (Figure 33B, C). Similarly, higher nitrite production was detected upon stimulation of human fibroblasts with recombinant IL-1α (Figure 33D). These findings were associated with a stronger senescence induction, as reflected by SA-β-gal staining of fibroblasts, in "IL1RA low" conditioned media-treated fibroblasts upon radiotherapy. Such senescence program was blocked by anakinra confirming among human RCA inflammatory CAFs an IL-1 mediated therapy-induced senescence (Figure 33E).

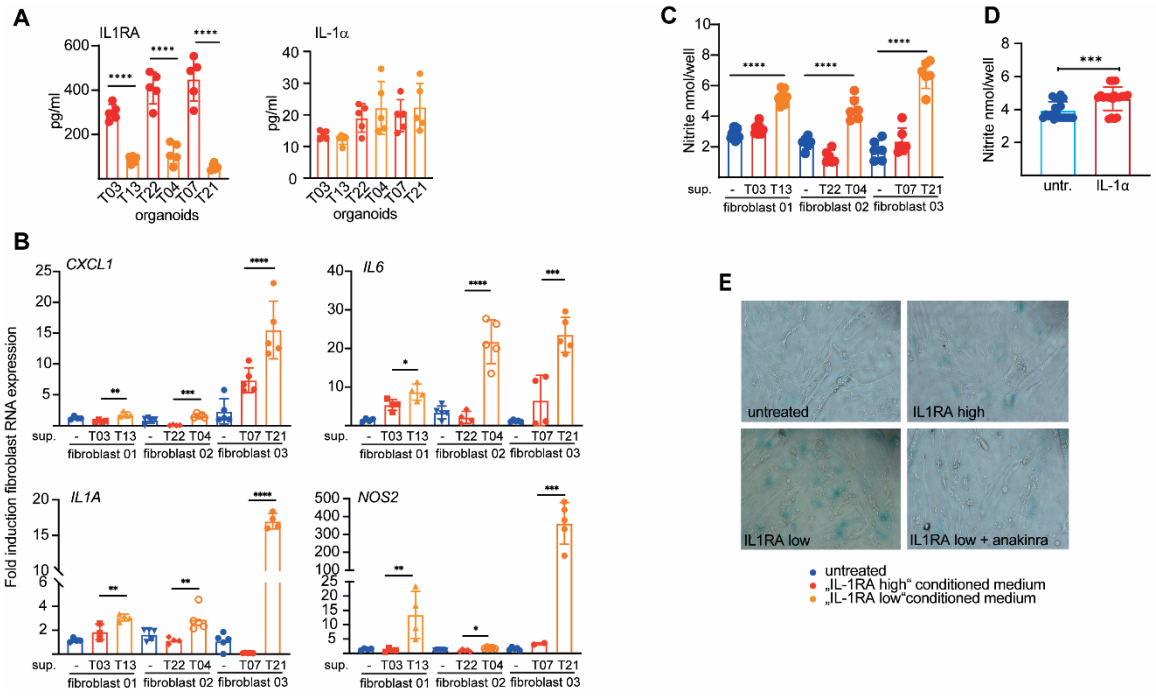

Figure 33: PDOs of low IL1RA levels drive inflammatory polarization of CAFs and sensitize them to radiotherapy-induced senescence *ex vivo*. A. IL1-RA and IL-1α protein levels (pg/ml) determined by ELISA in conditioned media derived from six different patients-derived organoids (n=5 independently collected organoids). ****p-value <0.0001 by one-way ANOVA followed by multiple Tukey's comparison analyses. **B.** Gene expression analysis performed by RT-qPCR of inflammatory genes among IL1RA high and IL1RA low conditioned media treated human fibroblasts isolated from normal rectal biopsies. A total of three distinct normal human fibroblasts were included. Results confirmed in four independent experiments. Data are mean ± SD. *p <0.05, **p <0.01, ***p <0.001 and ****p <0.0001 by one-way ANOVA followed by Tukey's multiple

comparisons test. **C.** Nitrite levels (nmol/well) in supernatants of IL1RA low and IL1RA high PDOs conditioned media treated human non-matching fibroblasts as determined by Griess assay. Results represent four independent experiments. Data are mean ± SD. ***p-value <0.001 and ****p <0.0001 by one-way ANOVA followed by Tukey's multiple comparisons test. **D.** Nitrite levels (nmol/well) determined by Griess assay in supernatants of untreated and IL-1α (1 μg/ml) stimulated human fibroblasts for 72 h. Results represent four independent experiments. Data are mean ± SD. Significant p-value<0.05 by t-test. **E.** Representative images of SA-β-gal staining among 3x2Gy irradiated WT, IL1RA high, IL1-RA low and IL1RA low plus anakinra (20 μg/ml) conditioned media-treated human fibroblasts for 72 h.

3. Discussion

3.1 Inflammatory CAFs predict survival of rectal cancer patients

After colon cancer, rectal cancer constitutes the second most common cancer of the large intestine and represents a particularly good example of the successful employment of a multimodal therapeutic approach in cancer management (Fazeli and Keramati, 2015; Fokas *et al.*, 2020). The standard of care among patients with locally advanced disease is neoadjuvant chemoradiotherapy prior to surgical resection leading to partially improved survival rates (Fokas *et al.*, 2018; Fokas *et al.*, 2017). Despite the implementation of modern methods in radiotherapy and conventional chemotherapy, tumors of identical stages, respond heterogeneously after preoperative CRT. Accordingly, patient response ranges from pathologically complete tumor regression to tumor progression post-CRT (Fokas *et al.*, 2020). Therefore, a thorough understanding of the cellular and molecular basis that would predict individual tumor response is an urgent need that will improve clinical outcome and further select patients for organ preservation. For instance, patients stratification based on whole tumor transcriptomic profile was made possible in CRC with the recently established consensus molecular subtype classification (CMS) that enables categorization of most tumors into one of the four robust subtypes (Dienstmann *et al.*, 2017; Guinney *et al.*, 2015). Correlative analysis revealed that one subtype (CMS4) is associated with poorer DFS when compared to remaining subtypes and histologically included an advanced desmoplastic reaction (Eide *et al.*, 2017; Guinney *et al.*, 2015). However, among 212 RCA patients, employing three CMS classifier algorithms (CMSclassifier random forest, CMScaller, and CMSclassifier-single) didn't allow prediction of patients' response patterns or DFS (Figure 10) (Eide *et al.*, 2017; Guinney *et al.*, 2015; Michels *et al.*, 2019). In an attempt to identify possible predictive markers and signaling pathways responsible for therapy resistance, a mass spectrometry-based comprehensive global proteomic analysis of laser microdissected tumor cells from pretherapeutic biopsies of patients with either pCR (excellent prognosis) or non-pCR was performed. PCA plot and heatmap analysis revealed no clear segregation of patients suggesting potential implication of TME cellular components in determining CRT response. For decades, radiotherapy and radiobiology-related research largely focused on the intrinsic properties of tumor cells with limited accumulated evidence on the implication of TME cellular components in initial therapy resistance and recurrence. Clearly, a detailed multiplexed immunohistochemistry of pretherapeutic biopsies revealed an enhanced content of vimentin^{+} mesenchymal cells while there were no differences in T cells (CD3^{+}, CD8^{+}, CD4^{+}, FOXP3^{+}), macrophages (CD163^{+})

and neutrophils (MPO^+) infiltrations or proliferative tumor cells ($Ki67^+$ $panCK^+$ cells) (Figure 10). Furthermore, transcriptionally, non-pCR patients, pretherapeutic, presented an enrichment of inflammatory, EMT and cancer associated fibroblasts signatures further highlighting the relevance of CAFs in impairing therapy response among RCA patients (Figure 11). Previous studies on CAFs implication in predicting RCA therapy response restrictedly highlighted that morphological categorization or scoring of fibrotic cancer stroma in advanced rectal cancer as immature stroma significantly correlated with poorer patients survival and T cells infiltration (Ueno et al., 2004). Moreover, high expression of a CAFs- specific stromal signature correlated with poor CRC prognosis and resistance to radiotherapy among rectal cancer patients (Isella *et al.*, 2015). Such reports lacked further characterization of the CAFs molecular heterogeneity among RCA and their potential functional heterogeneity in dictating therapy response (Goncalves-Ribeiro et al., 2017; Ueno *et al.*, 2004). In fact, recent single cell RNA sequencing (scRNAseq) studies highlighted the heterogeneity of CAFs in different types of solid malignancies that seemingly correlated with better or poor survival. For instance, the emergence of single cell technologies supported CAFs molecular heterogeneity and identified distinct subclusters in breast (Costa *et al.*, 2018; Kieffer *et al.*, 2020; Wu et al., 2020), lung (Hu *et al.*, 2021; Lambrechts et al., 2018), head and neck (Puram et al., 2017), colorectal cancer (Lee *et al.*, 2020; Li *et al.*, 2017) and pancreatic cancer (Elyada *et al.*, 2019). Overall, the most consistent observation on CAFs molecular heterogeneity across distinct types of tumors appeared to be the presence of a myofibroblastic ACTA2+ population with an ECM signature and a non-myofibroblastic subtype endowed of a secretory inflammatory phenotype (Biffi and Tuveson, 2021; Chen *et al.*, 2021). Among CRC patients, the earliest single-cell analysis report employed only 26 viable sorted CAFs from tumor biopsies and identified two CRC CAFs populations: myofibroblastic with a significantly enriched ACTA2 expression and non-myofibroblastic population (Li *et al.*, 2017). Likewise, $ACTA2^+$ myofibroblasts CAFs, exhibiting a TGF-β-driven signature, were identified among breast (Kieffer *et al.*, 2020) and pancreatic cancer (Elyada *et al.*, 2019) patients samples which additionally presented an inflammatory CAFs subset characterized by a significant downregulation of *ACTA2* expression yet an enhanced pro-inflammatory transcriptome. The small number of analyzed CRC CAFs hindered accurate insights on CAFs subpopulations molecular heterogeneity and associated differential genes signatures. Therefore, a large-scale analysis on 1936 CAFs derived from 23 CRC patients was performed here and highlighted the presence of 18 CAFs subpopulations among which four were identified to be of inflammatory phenotype (Cluster 3, cluster 6, cluster 7 and cluster 17) (Figure 12 and Table S2). Signature of the most prominent inflammatory IL-

1/TNFα subtype was significantly enriched among non-responders RCA patients (Figure 12). Similarly, to the earliest report among CRC, decorin (DCN) was a significantly upregulated marker among three of the four iCAFs subtypes (iCAFs 3, 6 and 17) and interestingly, scoring patients before CRT by DCN IHC, demonstrated a reduced DFS for patients with high baseline iCAFs/DCN score (Figure 12). Collectively these data strongly supported the observation that a CAFs subtype, particularly iCAFs confers CRT resistance among RCA patients.

3.2 Stroma-enriched orthotopic tumors in the preclinical mouse model are resistant to local radiotherapy

To functionally assess the implication of a particular CAFs subtype, iCAFs, in radiotherapy response, beyond the descriptive and correlative issued reports, a novel preclinical orthotopic model of rectal cancer was established. The study became increasingly aware of the previously published models' limitations. From one hand, the PDOs which response to therapy has been recently correlated with patient outcome, undermine the contribution and complexity of the TME (Ganesh et al., 2019; Yao et al., 2020). From the other hand, xenografts, employed in multiple *in vivo* studies, lack intact immune compartment and thus hinder robust assessment of well-reported parameters in radiotherapy outcomes such as hypoxia, vascularization and T cells infiltration (Lin et al., 2013). Furthermore, xenografts rarely metastasize in contrast to human disease where distant metastasis are encountered among 30% of patients and impose a real challenge to successful prognostic outcomes (Coleman et al., 2016; Kahn et al., 2012; Lin *et al.*, 2013). Therefore, the project aimed successful establishment and characterization of a preclinical mouse model of rectal cancer characterized by distal transplantation of genetically modified organoids into the lumen of immunocompetent C57BL/6 mice. Two weeks following transplantation, distal tumor growth was confirmed by colonoscopy and established tumors were subjected to fractionated local radiotherapy using the SARRP platform (Figure 13). The novelty of the model resided in its large resemblance of the clinical scenario, with one distal tumor, locally irradiated by a fractionated modality in immunocompetent mice. Hence, it provided a thorough understanding of therapy resistance and optimal translational outcomes through promising clinical trials. Two different types of organoids were included: APTK and APTKA, both gathering the well reported mutations among CRC patients: *Apc*, *Trp53*, *Tgfbr2* knockout, gain of function *K-ras*^{G12D} mutation and an additional expression of myristoylated AKT in APTKA organoids. In line with previous findings, AKT hyperactivation culminated in a more pronounced stromal response associated with a higher aggressive phenotype and

frequency of liver metastasis among APTKA tumors which transcriptionally presented a significant enrichment of CAFs signature compared to APTK tumors, mimicking the profile of human non-pCR patients' biopsies (Varga and Greten, 2017) (Figures 13 and 14). Moreover, CAFs heterogeneity was confirmed in the employed mouse preclinical APTKA orthotopic tumors, confined as revealed by scRNASeq data of sorted CAFs to five subtypes with the inflammatory IL-1 dependent cluster, attributed as C0 Cluster, being the most prominent (Figure 13 and Table S3). Interestingly, this cluster, similarly to human CRC IL-1-CAFs subtype (Figure 12), presented *Dcn* as differentially expressed gene with a significant downregulation of *Acta2* expression, a marker of TGFβ1-myCAFs as highlighted in breast cancer (Kieffer *et al.*, 2020), PDAC (Elyada *et al.*, 2019) and CRC ((Li *et al.*, 2017) emerging evidence on CAFs distinct polarization. DCN higher positivity among CAFs-enriched APTKA tumors was further validated by IHC. Importantly, upon radiotherapy, iCAFs-enriched APTKA tumors were resistant to radiotherapy and displayed *in vivo* an enhanced primary tumor growth, invasion and accelerated liver metastases post-therapy, thus corroborating their relevance as valuable models mimicking the mesenchymal composition of non-pCR patients' biopsies. Of interest to mention that APTKA tumors in a subcutaneous model of C57BL6/J immunocompetent mice showed positive outcome upon fractionated radiotherapy (5x2Gy) characterized by reduced tumor growth compared to untreated group (data not shown). Variances in therapy response between the orthotopic versus the subcutaneous model might be attributed to tumor architecture, TME cellular components and microbiome composition differences between tumors grown subcutaneously versus those transplanted orthotopically into the mouse colon.

3.3 Tumor cells drive inflammatory polarization of fibroblasts through IL-1α in a paracrine manner

Addressing drivers of molecular heterogeneity of CAFs has been the scope of interest of the following study as well as numerous others as diverse and myriad functions of CAFs are ascribed to their distinct polarizations and sub-specializations (Chen *et al.*, 2021). Generally, in literature, from one hand, CAFs heterogeneity has been attributed to their cells of origin as they arise from various sources including adipocytes, pericytes, stellate cells, endothelial cells, bone-marrow derived mesenchymal cells or resident fibroblasts (Biffi and Tuveson, 2021; Chen and Song, 2019; Sahai *et al.*, 2020). A recent report employed single cell transcriptomic data across numerous disease and healthy tissues of mouse as well as human species to

construct fibroblasts atlases and identified dermatopontin+ (Dpt) universal fibroblasts as a resource lineage for the diverse fibroblasts subtypes across tissues (Buechler et al., 2021). In this study, Dpt+ universal fibroblasts, endowed of functional plasticity, were speculated to undergo differentiation upon inflammation or during developmental processes into activated fibroblasts (Buechler *et al.*, 2021). From the other hand, the paracrine signals (growth and inflammatory factors) received by the tumor cells were found to highly govern their differential recruitment, in particular those arising from activated quiescent lineages (Kalluri 2016). Since tumors are for long thought as "wounds that do not heal", an everlasting accumulation of heterogeneous tumor cells drives a chronic wound healing response from which emerges distinctly polarized fibroblasts dictating cancer fibrosis or stroma remodeling (Dvorak, 1986). Importantly, the following study demonstrated that indeed distinct tumor cells harvesting differential mutational profile drive distinct polarization of treated intestinal fibroblasts in a paracrine manner (Figure 18). RNA sequencing and GSEA analysis confirmed differential transcriptomic profiles in fibroblasts exposed to conditioned media from APTK and APTKA organoids which drove a clear inflammatory polarization of fibroblasts mimicking the IL-1-Cluster-0 iCAFs reported *in vivo* in whole tumors (Figure 18). The thesis findings through detailed profiling of the tumor cells secretome, suggested multiple candidate inflammatory upstream regulators that would drive NFκB and p38 signaling pathways activation among iCAFs (Figure 19). Employing neutralizing antibodies and anakinra confirmed that the inflammatory polarization of CAFs is mediated by tumor-derived IL-1α (Figure 19). Furthermore, rectal PDOs of low IL1RA conditioned media promoted an inflammatory profile among treated human fibroblasts reflected by increased expression of inflammatory markers (Figure 33). Earlier reports summarized findings on IL-6 and TNFα pro-inflammatory signals initiating a tumorigenic profile in fibroblasts through NFκB and STAT signaling activation (Heichler et al., 2020; Hendrayani et al., 2014; Ohlund *et al.*, 2017). However, blockade of neither IL-6 nor TNFα inhibited iCAFs profile induction which seemed to be entirely driven by IL-1α upon treatment with APTKA organoids conditioned media (Figure 19). Similarly, in early lesions of squamous cell carcinoma, IL-1 signaling educates dermal fibroblasts into a pro-inflammatory secretome driving neovascularization and myeloid lineage recruitment (Erez *et al.*, 2010). Moreover, in a preclinical model of PDAC, pancreatic stellate cells stimulated with IL-1 exhibited iCAFs polarization (Biffi *et al.*, 2019).

3.4 IL-1α sensitizes iCAFs to therapy-induced senescence through driving a nitrite-mediated oxidative DNA damage

Attempts to explore how iCAFs confer therapy resistance, included initial histologic examination of irradiated resistant orthotopic tumors which displayed an aligned morphological pattern of CAFs, post-therapy, characterized by extensive ECM deposition (Figure 16). Likewise, paired analysis of pre- versus post-CRT biopsies of RCA patients revealed increased ECM deposition post-therapeutic among non-responders (Figure 32). Similarly, *ex vivo*, iCAFs or IL-1α polarized fibroblasts displayed the same elongated, spindle shaped morphology that resembled the *in vivo* observed phenotype, hence clearly demonstrating an IL-1 dependent morphological modification (Figure 24). Through in-depth proteomic and transcriptomic analysis, the study unraveled a detailed molecular mechanism that was rigorously characterized driving CAFs-mediated therapy resistance. Accordingly, IL1-driven inflammatory polarization of CAFs induces iNOS and a subsequent nitrite production which leads to an oxidative DNA damage and ultimately sensitization of iCAFs to TIS mediated by p53 signaling activation among RCA patients and the preclinical model (Figures 30, 31). Limited studies explored baseline oxidative stress in CAFs. An example would be the published results reporting oxidative DNA damage in CAFs through loss of caveolin-1 that further triggers an oxidative stress, mitochondrial dysfunction, mitophagy, and aerobic glycolysis collectively acting as a metabolic and mutagenic feedforward loop for stroma-epithelial tumor cells coevolution (Martinez-Outschoorn et al., 2010). Likewise, in a model of mammary carcinogenesis, a chronic oxidative stress was reported to be induced by JunD inactivation in CAFs and further driving metastatic spread via activation of HIF and CXCL12 (Toullec et al., 2010). However, these studies lacked the mechanistic insights unraveled here of the therapeutic context, sub-cellularization of the oxidative damage across the distinct subtypes of CAFs and its molecular drivers. Here, the results shed light on a different role of IL-1α as a core trigger of TIS and genotoxic stress by chemotherapeutics and ionizing radiation among an inflammatory subset of CAFs through increased levels of RNS causing oxidative DNA damage beyond homeostatic threshold as assessed by 8-OHdG positivity (Figure 30). Although bulk of evidence recognized TIS as an outcome of a growing list of chemotherapeutic anti-cancer agents and ionizing radiation, there was no discrimination in the extent of senescence induction among different cellular components of the TME. The following project highlighted senescence induction among the inflammatory subtype of CAFs, with no clear evidence of β-galactosidase positivity among irradiated unchallenged fibroblasts

or non-inflammatory CAFs. And the causal relationship between IL-1α, oxidative stress and senescence has been further verified with the usage of anakinra and NOS inhibitor W1400 that blocked oxidative DNA damage and senescence induction upon radiotherapy among iCAFs (Figure 30). Previous reports didn't stress the role of IL-1α as a senescence driver yet as a SASP member which is triggered by the activation of pro-inflammatory transcription complexes such as NFκB, p38-MAPK and mTOR-MK2 signaling. Particularly, they highlighted IL-1 signaling as a SASP protein sustaining an autocrine feed-forward amplification loop leading to a constitutive activation of NFκB signaling and a self-amplifying SASP production reinforcing growth arrest by aged and senescent cells (Laberge et al., 2015; Melisi et al., 2009; Niu et al., 2004).

Indeed, additionally to NOS, countless findings implicated mitochondrial dysfunctions and ROS in the ageing process upon its accumulative generation, prompting DSBs and induction of the DDR complex characterized by inflammatory signaling activations and ultimately irreversible loss of replicative capacity (Passos et al., 2013). However, the TIS phenotype in inflammatory fibroblasts *in vivo* and *ex vivo* was confined to RNS-mediated oxidative DNA damage, as there was no detected difference in ROS levels among the different CAFs subtypes (Figure 30). In fact, IL-1α, in the following report, importantly seems to metabolically shape iCAFs and mitochondrial function. A metabolic heterogeneity among distinctly polarized fibroblasts was encountered with findings on a reduced mitochondrial activity among iCAFs in line with their exhibiting a lower OCR and ECAR compared to non-inflammatory counterparts and remarkably a lower basal and compensatory glycolysis reflecting unexplored metabolic shifts among this subpopulation (Figure 29). In line with decreased glycolysis, an increased quiescence was detected among iCAFs mirrored by a reduced baseline proliferation rate in comparison to unchallenged fibroblasts (Figure 29). Indeed, earlier reports recognized decelerated proliferation rates among iCAFs in comparison to myofibroblasts without further dissection of the metabolic or epigenetic attributes of such observation (Davidson et al., 2020). In fact, emerging preliminary reports described metabolic adaptation of CAFs to substantial variations in oxygen and nutrients availability at the primary site and their rewiring local and systemic cancer bioenergy (Sanford-Crane et al., 2019). Research on CAFs metabolism, initially emphasized their enhanced aerobic glycolysis and reduced oxidative phosphorylation in comparison to normal fibroblasts (Zhang et al., 2015). Consequently, in the reverse Warburg-effect, CAFs-released lactate and pyruvate fuel a dynamic CAFs-tumor cells metabolic flux facilitated by the mono-carboxylate transporters: MCT1 and MCT4 (Knudsen

et al., 2016). Accumulating evidence on amino acids metabolism highlighted the role of glutamine in inducing stromal autophagy and driving mitochondrial oxidative metabolism as well as tumor cells expansion though glutamine importers such as SLC6A14 (Ko et al., 2011). In PDAC, autophagy-mediated secretion of alanine by stellate cells supports tumor cells tricarboxylic acid cycle (TCA) and sustains their survival in an austere TME (Sousa et al., 2016). Besides well-known glycolysis and glutamine metabolism, there is a sign of a lipidomic rewiring in CAFs favoring CRC tumor cells migration (Gong et al., 2020). While scientific reports on tumor cells and immune metabolism are emerging, thorough understanding and metabolic mapping of bioenergy orchestration among distinct CAFs subtypes is still lacking. The study introduced findings call for metabolic mapping of energy circuits among distinct CAFs subtypes and comprehensive analysis of the upstream regulators in tissue specific and therapeutic contexts.

3.5 Senescent iCAFs secretome drives remodeling of extracellular matrix composition

To explore how senescent iCAFs would counteract therapy cytotoxic effects yet rather confer disease progression and accelerated dissemination, an in-depth proteomic and transcriptomic characterization of a so called "iCAFs-specific senescence profile" was performed. In fact, ongoing inquiries are endeavoring to dissect SASP diverse composition and consequently pathophysiologic functions ranging from reported detrimental effects on tumor evolution to surprisingly well established anti-tumorigenic effects (Birch and Gil, 2020; Faget *et al.*, 2019; Wang *et al.*, 2020). An example of the SASP decelerating impacts on cancer progression are the published findings in lymphoma, sarcoma and liver carcinoma where p53 reactivation drove senescence secretory phenotypes favoring immune surveillance and eventually tumor regression (Iannello *et al.*, 2013; Sagiv *et al.*, 2016; Xue *et al.*, 2007). Moreover, recently, SASP was reported to mediate endothelial activation and vascular remolding, favoring chemotherapeutic drugs delivery and intratumoral T cell infiltration as well sensitivity to anti-PD1 immunotherapy (Ruscetti et al., 2020). In contrast, the thesis characterized, among irradiated iCAFs, a pro-tumorigenic p53-mediated matrisome senescence profile characterized by a marked deposition of ECM glycoproteins, collagens, proteoglycans, growth factors and ECM regulators, in addition to the well conserved pro-inflammatory cytokines-based secretory profile (Figures 24, 25). Senescent iCAFs secretome was shown to favor, from one hand, irradiated tumor cells survival and proliferation (data not shown). From the other hand, it hindered immune cells interstitial mobilization or immune surveillance as corroborated by significantly reduced $CD8^+$ T cells intratumoral infiltration among irradiated APTKA

orthotopic tumors (Figure 16). Cross-species mouse to human analysis, further confirmed among non-responders RCA patients, a significant enrichment of ECM, EMT and collagen signatures post therapeutic (Figure 32). In fact, accumulative findings stressed on SASP-driven remodeling of tissue architecture, integrity and stiffness (Freitas-Rodriguez *et al.*, 2017). For instance, aged skin fibroblasts were found to display pronounced release of MMP-1 and MMP-2 and further stimulating tumorigenic keratinocytes collective migration though PAR-1 (protease activator receptor-1) activation (Malaquin et al., 2013). In Line with this report, arrested cells, in papillary thyroid carcinoma, triggered tumor cells dissemination and motility through activation of CXCR4 signaling cascade (Kim *et al.*, 2017b).

Here, contribution of iCAFs SASP matrisome to the accelerated metastasis phenotype encountered post-therapy *in vivo*, might be attributed to its effects on tissue vasculature, endothelial cells growth, tumor cells-platelets interaction, matrix remodeling, the establishment of premetastatic niche (Cox, 2021). The *in vivo* and *ex-vivo* encountered IL-1α-dependent aligned distinctive morphological pattern of senescent iCAFs is further suggestive of their acting as “leader cells” supporting multiple aspects of collective invasion which has been recently recognized as a pivotal mechanism in the progression of solid malignancies (Vilchez Mercedes et al., 2021). Though multiple invasion modes have been reported, including mesenchymal single cells invasion and multicellular streaming or collective migration, it became evident that aggregates of cancer cells are endowed with a higher metastatic capacity than individual cells (Liotta et al., 1976). The prominent matrisome signature of senescent iCAFs corroborates their histologically spotted capability to populate the invading fronts, generate disseminative tracks steering the invasion route, and further create a low-resistance path while coordinating with follower tumor cells (Figure 16). Indeed, CAFs were previously found to assist tumor cells in parting from primary sites through heterotypic E-cadherin/N-cadherin-based adhesions, promoting a spatially organized invasion in the form of sprouts patterns which have been recognized among examined human samples specimens by IHC (Friedl et al., 2012; Labernadie et al., 2017). In line with the previously mentioned insights on CAFs metabolome, the project didn’t explore neither the metabolic resources senescent iCAFs garner while leading the highly energy-intensive task of collective migration nor their employed signals to engage following cancer cells at the invasive margins. Further insights on senescent iCAFs secretome and matrisome-mediated modulation of the premetastatic niche were also not thoroughly addressed. All these aspects need further

assessments as we embark into a systematic understanding of tumor architecture and mechanics for an effective metastatic spreading and ultimately targeting.

In an attempt to hinder the unfavorable effects of senescent iCAFs, targeting senescent iCAFs-driven desmoplastic reaction represented an attractive approach to interfere with tissue stiffness and its side effects post therapy. In fact, over the last decades, intensive preclinical work was conveyed on the promising therapeutic inhibition of ECM molecules (LOX, integrins, MMPs, TN-C, HA and SMO) in an attempt to overcome post-radiotherapy fibrosis, delay ECM modifications driving tumor spreading and ameliorate intratumoral drug delivery and consequently prognosis (Barker *et al.*, 2015). As the mass spectrometry analysis of senescent iCAFs revealed enrichment of multiple ECM (Figure 24), there was no rational to target one protein but rather the upstream driver and complexes of the secretory phenotype. Thus, prevention of CAFs senescence was approached by either *Trp53* depletion or senotherapy *in vivo* via usage of venetoclax in conjunction with radiotherapy, which reverted tumors therapy resistance and drove a significant regression in primary and distant tumor growth coupled with increased T cells infiltrations and reduced ECM deposition (Figures 27, 28). *Ex vivo* venetoclax treated iCAFs lacked an oxidative DNA damage reflected by reduced levels of -8OHdG and consequently therapy-induced senescence (Figure 28). Hence, it was shown here whether and when in a novel preclinical model of rectal cancer, senotherapy can be employed with evidence on successful implementation of the long-time suggested “one-two” punch approach based on a pro-senescence therapy followed by anti-senescence senolytic interventions (Carpenter *et al.*, 2021; Kirkland and Tchkonia, 2015; Kirkland *et al.*, 2017; Wang *et al.*, 2020).

3.6 IL-1 signaling blockade sensitizes tumors to radiotherapy *in vivo*

While CAFs heterogeneity has been addressed with the emergence of scRNASeq platforms, exact functional properties of the distinct subtypes in tumorigenesis and particularly therapy response is far from being understood. The following study provided the first evidence that one CAFs subtype, iCAFs, is a core player in the response to neoadjuvant CRT. And thus, valuably introduced functional heterogeneity among CAFs subsets beyond the bulk of descriptive and correlative studies that recently appeared among solid malignancies with scRNA Seq platforms, yet lacked molecular insights and therapeutic assessments in convenient models. For example, in breast and lung cancer, $GPR77^{+}$ $CD10^{+}$ CAFs subtype was found to correlate with chemoresistance by providing a supportive IL-6 and IL8-dependent niche essential for cancer stem cells (CSCs) survival (Su *et al.*, 2018). In CRC, TGFβ-CAFs

correlated with pronounced tumor aggressiveness, poor survival and therapy resistance (Calon *et al.*, 2012). In contrast, later study correlated phospho-STAT3^{+} CAFs garnering a pro-angiogenic transcriptome with worse CRC patients prognosis (Heichler *et al.*, 2020). In breast cancer, abundance of TGFβ-myCAFs, at diagnosis, correlated with resistance to immunotherapy in NSCLC and melanoma, ascribed to their *ex vivo* capacity to enhance CTLA4 and PD1 expression in regulatory T cells (Kieffer *et al.*, 2020). Moreover, a recent report among NSCLC patients, through an established biobank of patients-derived CAFs, identified three subtypes differing in their intrinsic TGFβ signaling with two high FGF7^{+} and HGF^{+} CAFs subtypes associated with patient's poor response to EGFR TK1 therapy and prognosis (Hu *et al.*, 2021).

This project conveyed the first evidence that one CAF subset, IL-1α-CAFs, is a core player in the response to neoadjuvant CRT. For instance, IL-1α overexpression in irradiation-sensitive APTK organoids promoted paracrine induction of iCAFs polarization *ex vivo* and rendered tumors resistant to irradiation *in vivo* (Figure 23). Hence, it laid the ground for a clinically novel and approachable combinational CAFs subtype-targeted therapy, a juvenile field which success was hindered by multiple limitations (Figure 6). Correspondingly, earlier attempts to target CAFs included non-specific depletion of cell surface markers with unfavorable outcomes attributed back then to the limited knowledge on CAFs molecular heterogeneity and further functional heterogeneity in neoplasms evolution and therapy. For instance, CAFs nonspecific targeting via direct depletion of ubiquitous CAFs markers such as α-SMA, despite reducing angiogenesis, surprisingly promoted tumor progression through hypoxia and enhanced stemness phenotypes (Ozdemir *et al.*, 2014). In contrast, while in preclinical models, anti-FAP CAFs targeted immunotherapy proved of promising antitumorigenic effects, in early phase II clinical trials, it turned out to be non-beneficial for patients with advanced metastasis CRC (Hofheinz *et al.*, 2003). On the whole, the foremost investigated strategies for CAF-directed anticancer therapy included: targeting the upstream activation and effector signals such (chemokines, growth factors, cytokines) hence blocking CAFs activation; inhibition of abundance ECM deposition (collagen, fibronectin, MMPs and LOX); CAFs normalization through usage of APTRA or calcitriol molecules and CAFs targeted immunotherapies such as CAR-T cells and monoclonal antibodies. Accordingly, CAFs conversion to a normal (less active) state or tumor suppressive subtype is an appealing approach which has been previously explored in multiple preclinical mouse models. Promising findings were reported in PDAC, where restoration of retinols levels in pancreatic stellate cells

(PSCs) by administration of the pleiotropic agent all-*trans* retinoic acid (ATRA) resulted in their inactivation and subsequent regression in tumor growth attributed to $CD8^+$ cytotoxic T cells immunity and suppression of the tumor WNT-ß-catenin signaling (Froeling et al., 2011). Furthermore, PSCs reprogramming into quiescent phenotype was successfully managed by treatment with vitamin D receptor (VDR) ligand, and promoted tumor suppression as well as reversion of chemoresistance in a preclinical PDAC model (Sherman et al., 2014). Targeting myCAFs TGF signaling showed promising anti-tumor effects in PDAC (Biffi *et al.*, 2019) and reduced liver metastasis in combination with anti-PDL1 immunotherapy in CRC (Tauriello *et al.*, 2018). Therefore, the best aimed approaches are those targeting a subset of CAFs which unraveled functionality proved to be of detrimental effect on patients' prognosis, through its normalization into a more quiescent-less active phenotype. Importantly, the shared novel findings on iCAFs potential reversibility into a more quiescent like phenotype upon anakinra therapy introduces an attractive therapeutic opportunity in the field of CAFs targeted therapies (Figure 20). Indeed, iCAFs targeting has been previously described in PDAC through usage of the JAK inhibitor AZD1480 in an attempt to block their STAT3-mediated inflammatory polarization (Biffi *et al.*, 2019). The reported findings demonstrated iCAFs interconversion to a myCAFs-TGFβ-like phenotype upon JAK inhibition with an increased ECM deposition in PDAC tumors and claimed favorable outcomes of reduced tumor growth. However, in CRC, stromal TGFβ has established roles in cancer progression through conferring survival advantage to migratory tumor cells as well as metastatic initiation and its blockade by Galunisertib renders immunologically cold CRC susceptible to anti-PD-1-PDL-1 therapy (Calon *et al.*, 2012; Tauriello *et al.*, 2018)**.** Therefore, JAK inhibitors, in this study's context, were unfavorable options for iCAFs targeting. Furthermore, neither Human iCAFs subpopulation nor its counterpart in the preclinical mouse model seemed to be dependent on a STAT3 but rather NFκB signaling activation (Figures 12, 19). Moreover, addressing downstream complexes would not secure broad inhibition of iCAFs inflammatory profiles given the presence of overlapping signaling pathways as assessed by reported findings including NFκB and p38 MAPK signaling inhibition with partial effects on iCAFs inflammatory phenotype (Figure 19). Additionally, JAK inhibitors were found of anti-proliferative effects on cytotoxic T cells, a challenge not be undermined in combinational immunotherapies, potentially hindering promising successes in clinical trials (Burger et al., 2009)**.** Therefore, in hampering iCAFs roles, the upstream driver of the inflammatory polarization, IL-1 signaling was targeted as the most appealing option.

In fact, IL1 blocking agents were originally designed for the treatment of auto-inflammatory and autoimmune disorders. The four different approaches in blocking IL1 signaling include: IL-1α neutralizing antibodies, IL-1β antagonists, recombinant IL1RA and IL1RAP inhibitors (Litmanovich et al., 2018). The anti-IL-1α human monoclonal antibody, known as Xilonix, MABp1 or bermekimab, showed encouraging results in phase 1 and phase 2 clinical trials regarding safety, tolerability and pharmacokinetic profile. A phase III clinical trial on 40 patients with refractory metastatic CRC who failed oxaliplatin or irinotecan-based chemotherapy demonstrated encouraging outcome with 39% better OS among Xilonix treated patients compared to the placebo group and a reduced death risk (Fisher, 2015). Xilonix-treated patients displayed reduced platelets count which might be considered as a key outcome given the well-established supportive role of platelets in tumor progression and metastasis (Huong et al., 2019). The last Xilonix completed study included a total of 333 unresectable metastatic CRC patients which received a higher dose of Xilonix compared to the placebo group. More anti-IL1α treated patients reached the endpoint in comparison to the control group with stable/improved lean body mass (LBM). Reduced IL-1α levels and platelets count were further reported in the treatment group. Yet, the trial didn't reveal clear differences in OS among the two patients groups (Hickish et al., 2017). Therefore, a phase I clinical trial is currently conducted for assessment of a combinational therapy using Xilonix, in addition to standard doses of Onivyde (nanoliposomal irinotecan) and 5- fluorouracil (5-FU) for the treatment of locally advanced pancreatic cancer patients (Litmanovich et al., 2018). On the other hand, IL-1β-driven signaling is targeted by Canakinumab, additionally known as ACZ885, a human IgG1/κ mAb developed by Novartis Pharma and specifically targeting the IL-1RI binding motif of IL-1β hence preventing the agonist-receptor signaling cascade (Rondeau et al., 2015). IL-1β antagonist is already authorized for the treatment of systemic juvenile idiopathic arthritis (SJIA) and gouty arthritis. The potential implication of IL-1β antagonist in the treatment of cancer patients originally emerged from a study that recruited 10,061 patients with atherosclerosis and no previous cancer diagnosis (Ridker et al., 2017). The trial primary aim was assessment of anti-IL-1β treatment impacts on cardiovascular diseases, myocardial infarction and strokes. An additional outcome of the "canakinumab anti-inflammatory thrombosis outcomes study" (CANTOS), was evaluation of IL-1β potential correlation with cancer incidence. The findings surprisingly revealed, during a follow-up of 3.7 years, a significantly lower lung cancer incidence among the canakinumab treated-patients compared to the placebo group (Ridker et al., 2017b). The study suggested blockade of IL-1β-mediated inflammatory processes as an appealing approach to reduce cancer incidence and mortality of

lung cancer as well as other potential solid malignancies. More formally designed trials in a proper clinical cancer screening and treatment settings are further required. Numerous cancer-related clinical trials on canakinumab are currently ongoing, including phase I clinical trials for CRC, triple negative breast cancer (TNBC) and NSCLC patients in combination with checkpoint inhibitors (PDR001) (Garlanda and Mantovani, 2021; Gottschlich et al., 2021). Additionally, phase 3 clinical trials are currently assessing canakinumab and PDR001 synergetic effects among patients with unresectable or metastatic melanoma (Litmanovich et al., 2018). A third approach for inhibiting IL1 signaling includes targeting the IL1-RAP unit by inhibitory antibodies. Nidanilimab is an anti-IL1RAP human mAb reported to drive a pronounced antibody-dependent cell-mediated cytotoxicity (ADCC) response in treated acute myeloid leukemia xenografts (Agerstam et al., 2015). Early phases clinical trials are designed to assess the safety of tolerability of anti-IL1RAP antibody among patients with different tumors types (Garlanda and Mantovani, 2021; Gottschlich et al., 2021). A fourth approach for targeting IL-1 signaling resides in mimicking the biological ability of IL1RA to downregulate IL-1α and IL-1β activity as an anti-inflammatory agent (Dinarello and Thompson, 1991). Accordingly, anakinra (Kineret) is a recombinant non-glycosylated IL1RA clinically approved for the treatment of rheumatoid arthritis and neonatal-onset multisystem inflammatory disease (NOMID). Findings in smoldering multiple myeloma (SMM), an early precursor to multiple myeloma, identified two groups of patients on the basis of bone-marrow stromal cells ability to produce IL-6 as a surrogate marker for IL-1β biological activity (Xiong et al., 2006). One group of SMM patients were high producers of IL-6 levels comparable to active MM patients. This observation promoted the conduction of a phase 2 clinical trial on SMM patients attempting to inhibit IL1 signaling axis by anakinra and prolong their progression free survival (PFS) (Lust et al., 2009). Anakinra treatment was continued for patients of clinical improvement, whereas patients with stable or cancer progression, in addition to anakinra, received a low dose dexamethasone. The follow-up findings were highly encouraging. Anakinra-mediated IL1 inhibition among SMM patients decreased patients high sensitivity C-Reactive Protein (hs-CRP) levels and the risk of developing active MM while improving PFS rates. The long-term follow-up further confirmed these findings with reported significantly improved OS and PFS among anakinra treated SMM patients exhibiting 40% reduction in their hs-CRP levels (Lust et al., 2016).

In targeting IL-1 signaling, this study didn't employ anti-IL-1α (Xilonix), anti-IL-1β (canakinumab) monoclonal antibodies or the novel IL1RA expressing CRISPR-Cas9

engineered implants recently assessed in a preclinical rheumatoid arthritis model and shown to yield favorable outcomes in disease management (Choi et al., 2021). The project rather approached by using recombinant IL1RA or anakinra, as a pharmacologically well characterized drug. In fact, the rational of blocking IL-1 signaling by anakinra was based on the analysis of RCA patients' proteins levels by multiplexed cytokine profiling. Significantly, RCA patients demonstrated no difference in their pre-CRT serum levels of IL-1β or candidate cytokines, chemokines or growth factors (Figure 31). However, they clearly differed in their circulating IL1RA levels, with reduced IL1RA among non-pCR patients pre-CRT and further correlation of low *IL1RN* gene expression levels with poorer DFS rates (Figure 31). Several lines of evidence unraveled crucial roles of IL1 signaling and IL1RA in cancer-associated inflammatory processes such as IBD where reduced IL1RA production correlated with higher IBD incidence (Casini-Raggi *et al.*, 1995; Hyams et al., 1995). The relevance of IL-1 and IL1RA in IBD pathogenesis has been further demonstrated with findings associating low levels of IL1RA with IL-1RN allele 2 polymorphism and disease severity (Cominelli and Pizarro, 1996; Tountas et al., 1999). In exploring the association of IL1 signaling with cancer development and progression, most studies examined genetic evidence reporting variants in the agonists encoding genes *Il-1α* and the inhibitory unit *IL1RN* which reduced levels have been frequently associated with two SNPs rs4251961 T/C and rs579543 G/A. Interestingly, the following study found that low IL1RA serum levels were associated with the rs4251961 T/C SNP with higher IL1RA protein levels being noticed among homozygous rs4251961 T/T carriers (Figure 31). Moreover, all the analyzed pCR patients were carriers of the protective rs4251961 T/T or T/C alleles and none of them presented a homozygous C/C genotype. Correspondingly, advanced patients with metastatic CRC, carriers of the rs4251961 T/T genotypes were classified as high producer of IL1RA with a better median survival times compared to the non-T/T genotype carriers (Graziano et al., 2009).

Hence the clinical significance of using recombinant IL1RA to downregulate the exaggerated IL-1 signaling and the amplification of the inflammatory pro-tumorigenic loop mediated by the agonists IL-1α and IL-1β. In line with the medical report mentioned above on Xilonix anti-IL-1α human monoclonal antibody failing to show OS advantages among 333 unrespectable metastasis CRC patients in comparison to placebo treated group, remarkably, IL-1 signaling blockade alone by anakinra in the preclinical orthotopic mouse model here, had no effect on tumor progression yet its combination with conventional radiotherapy allowed successful therapeutic response with a clear reduction in primary tumor growth, distant metastases and

massive mobilization of cytotoxic T cells intratumoral infiltration (Figure 21). Hence the rational of conducting clinical trials with prompt design assessing among different solid malignancies anakinra implementation in conjunction with standard of care CRT regimens as well as the emerging immunotherapy. Indeed, anakinra-based cancer therapy studies are currently ongoing as phase 1 clinical trials for metastatic tumors, breast cancer and pancreatic cancer as well as phase 2 clinical trials for CRC patients in conjunction with chemotherapy and anti-PD1/PDL1 inhibitors (Garlanda and Mantovani, 2021; Gottschlich *et al.*, 2021). Comparably, this project paved the way for a clinical trial that recently recruited RCA patients for anakinra therapy as combinational regimen with conventional CRT.

4. Materials and Methods

4.1 Mice

4.1.1 Mouse models

For subcutaneous and orthotopic transplantations C57BL6/J (Janvier Labs) female mice aged 8 to 10 weeks old were included. To selectively block IL-1R signaling in fibroblasts, *Il1r*$^{F/F}$ floxed mice (The Jackson Laboratory; stock 028398) possessing LoxP sites flanking exons 3-4 of the *Il1r1* gene were bred to *Col1a2*CreER^{T2} (The Jackson Laboratory; stock 029235) mice carrying a transgene with tamoxifen inducible Cre recombinase. For APTKA organoids orthotopic transplantations *Col1a2*CreER^{T2} *Il1r*$^{F/F}$ and *Il1r*$^{F/F}$ female mice aged 8 to 10 weeks old were included in the experiments following the DSS model of orthotopic transplantation detailed below. Male *Trp53*$^{-/-}$ mice (The Jackson Laboratory; stock 002101), presenting a neomycin cassette replacing exons 2-6 including the start codon of the *Trp53* gene, aged 8 to 10 weeks' old were included in the orthotopic transplantations of APTKA organoids following the brush EDTA model described below. To isolate colon fibroblasts, IL1 receptor knockout mice, *Il1r1*^{tm1Imx} (The Jackson Laboratory; stock 003245) and *Trp53*^{tm1Brn} mice were used (The Jackson Laboratory; stock 008462) having loxP sites flanking exons 2-10 of the transformation related protein 53 gene.

4.1.2 Genotyping

To perform genotyping, genomic DNA was collected from the mice tails which were incubated in 5% proteinase K/lysis buffer overnight at 60°C. Heat inactivation for 10 min at 95°C was then performed to stop the enzymatic reaction. Samples dilution (1:10) with distilled water was further performed followed by centrifugation for 10 min and DNA rich supernatant collection. Polymerase chain reaction (PCR) was performed with 20µl PCR reaction mix, run on 1.5% agarose gel and bands visualization was performed using ethidium bromide solution with Gel Doc XR imaging system (BioRad).

Reagents	Volume
PCR buffer (10x)	2 µl
$MgCl_2$ (50 mM)	0.8 µl
dNTP mix (10 mM)	0.4 µl
Forward primer (20 pM)	0.5 µl
Reverse primer (20 pM)	0.5 µl
Taq Polymerase (5U/µl)	0.15 µL
H_2O	14.5 µl
DNA	1.5 µl

Table 1: Mouse genotyping reaction mixture.

Mouse Strain	Primers Sequence 5'----- 3'
Trp53$^{-/-}$	Common: TGG ATG GTG GTA TAC TCA GAG C Mutant Forward: CAG CCT CTG TTC CAC ATA CAC T Wild type Forward: AGG CTT AGA GGT GCA AGC TG
Trp53^{tm1Brn}	Forward: GGT TAA ACC CAG CTT GAC CA Reverse: GGA GGC AGA GAC AGT TGG AG
Il1r$^{F/F}$	Forward: GAA AAG TGC TAG AAC ATC CTT TGA G Reverse: GTA CCA ATG GAG GCC AGA AG
Il1r1^{tm1Imx}	Common: TTC TGT GCA TGC TGG AAA AC Mutant Forward: CTC GTG CTT TAC GGT ATC GC Wild type Forward: GGT GCA ACT TCA TAG AGA GAT GA
*Col1a2*CreER^{T2}	Transgene Reverse Cre: CAT GTC CAT CAG GTT CTT GC Internal positive control forward: TGA AAA AGT CCA CTA ATT AAA ACC A Internal positive control reverse: CTA ACA ACC CTT TCT CTC AAG GT Transgene Forward Col1a2: CAG GAG GTT TCG ACT AAG TTG G

Table 2: Mouse genotyping primers list.

4.1.3. Subcutaneous model

Untreated and 5x2Gy irradiated APTKA and APTK organoids were subcutaneously injected into C57BL6/J mice. Briefly, 6 h post last dose irradiation, organoids were collected in cold PBS, mechanically disrupted by pipetting with 1 mL pipet tip and centrifuged at 800 rpm for 5 min. The pellet was resuspended into sterile PBS and 100 µl was subcutaneously injected into C57BL6/J mouse (~$6x10^5$ cells/ 100 µl). Approximately, two weeks post injections, tumor development started and measurements were performed three times per week with tumor volumes calculated according to the following formula: Volume (mm^3) = 0.5 x (length x $width^2$). Mice were sacrificed when tumor volume reached a maximum size of 1000 mm^3. Tumor samples were further processed for histological analysis.

4.1.4 Orthotopic transplantations

For orthotopic transplantation of genetically modified organoids APTK and APTKA, C57 BL6/J, *Il1r*$^{F/F}$ and *Col1a2CreER*^{T2}*Il1r*$^{F/F}$ mice, females of 8 to 10 weeks' old were given 4% dextran sodium sulfate (DSS) (ThermoFischer Scientific; 9011-18-1) in drinking water for 5 consecutive days with daily monitoring of weight loss. On day 7, healthy APTKA and APTK organoids were processed for collection by cold PBS for transplantation, mechanically disrupted by 1mL pipet tip, centrifuged at 800 rpm for 5 min and pellet resuspended in cold PBS supplemented with 20% Matrigel. Mice anesthesia was performed using ketamine/xylazine solution. Organoids were injected as 100 µl volume (1~2 x 10^6/100 µl/ mouse) into the rectum using an inserted 1.5 cm deep catheter. Post-injection, mouse anus was sealed with Vaseline to prevent leakage.

For *Trp53*$^{-/-}$ knockout mice, a previously published EDTA/Brush protocol for orthotopic transplantation was performed (Sugimoto et al., 2018). Briefly, homozygous males mice aged 8 to 10 weeks old, were subjected to isoflurane anesthesia and using flexible catheters, colons were flushed with cold PBS to remove feces. The colon was further flushed with warm 250 mM EDTA/PBS using a handmade catheter mounted with a small balloon and injected 1 cm deep into the mouse rectum. Using a gently half circle vibrating electric toothbrush (EW-DL22), inserted 1.5 cm deep, the colon epithelial layer was removed ensuring a local colon injury. Approximately 100 µl APTKA organoids, collected as previously mentioned by mechanic disruption, were injected orthotopically (1-2 x 10^6 cells/100 µl/ mouse), within 2 h post epithelial injury, using a flexible catheter. To prevent organoids leakage and successful transplantation, the anus was sealed with surgical glue for 6h and manually removed under isoflurane anesthesia.

Three weeks post transplantation; successful tumor growth was assessed by small- animal endoscope imaging on ketamine/xylazine anesthetized mice. Tumor depth was measured with the endoscopic probe as the distance of the lower tumor margin from the anus of the mouse. Tumors of approximately 2/3 endoluminal growth were considered for irradiation. If tumors didn't reach the required size (~2/3 of the lumen) another colonoscopy was performed a week later. Optimum tumor size for therapy was encountered 21 to 40 days' post transplantation.

4.1.5. Orthotopic tumors irradiation and chemotherapy

When orthotopic tumors reached adequate size, radiotherapy was performed using the small animal radiation research platform (SARRP by Xstrahl). With 2Gy irradiation dose daily for 5 consecutive days. Shortly, a PVC probe of 2 mm diameter equipped with an endoluminal 1 mm-diameter radiopaque line (S-SPOT CT simulation marker, Berkley Medical, USA) was inserted inside the PVC tube. The PVC probe was then inserted into the mouse rectum. A cone-beam computer tomography (CBCT) imaging was then performed and acquired images were processed using SARRP reconstruction software. Radiotherapy treatment plan was determined using the built-in Muriplan software (SARRP, Xstrahl, Surrey, UK) and locally applied. To assess tumor response to radiotherapy, a colonoscopy was performed 7, 14 and 21 days post last dose RT. Mice were sacrificed 21 days post last dose- experiment end point and tumors processed for histologic analysis.

5-Fluorouracil (5-FU) (Merck; 51-21-8) chemotherapy was applied as a dose of 20mg/kg of mouse injected intraperitoneal at day 1 and day 4 RT. Three days before first dose irradiation, anakinra (Kineret) treatment of APTKA orthotopic tumors started. Anakinra was applied intraperitoneally, 500 µg/mouse with 250 µg morning and 250 µg evening dose for a total of 10 consecutive days. Venetoclax (ABT-199; Selleckchem; S8048) was dissolved in 5% DMSO, 50% PEG30, 5% Tween 80 and distilled water. Venetoclax therapy started two days before radiotherapy and was administered by oral gavage daily (100 mg/kg/day) for 21 consecutive days. To selectively delete IL-1 receptor in fibroblasts, *Col1a2*CreER^{T2} *Il1r*$^{F/F}$ and *Il1r*$^{F/F}$ mice were subjected to tamoxifen diet (GENOdiet CreActive T400 with 400mg/kg tamoxifen citrate; GENOBIOS; #GEN16/T400-R) 4 days before RT started for 21 consecutive days (experiment end point). All mice were sacrificed at day 21 post last dose irradiation for histologic, proteomic and transcriptomic analyses and experiments were previously approved and reviewed by Regierungspräsidium Darmstadt, Germany.

4. 2. Cell Culture

4.2.1. Organoids culture

4.2.1.1 Human organoids

Human organoids were generated from normal and tumor biopsies of rectal cancer patients before chemoradiotherapy obtained from the University Cancer Center Frankfurt (UCT). All patients received a written informed consent and the study was approved by the UCT ethics board. Tumor and normal biopsies were cut into smaller fragments, cleaned with sterile PBS supplemented with 1% penicillin/streptomycin ten times, and further incubated with 5 mM EDTA (ThermoFisher Scientific; AM9260G)/ PBS for 30 min on ice with several vortexing cycles and supernatant collected and kept on ice. A second round of incubation with 5mM EDTA/PBS was performed at 37°C for 30 min with constant agitation on a rocking platform. The remaining pieces were allowed to settle and processed for fibroblasts isolation. Both fractions of collected supernatants were mixed and centrifuged at 800 rpm for 5 min. To the pellet adequate volume of Matrigel (Corning; 356231) was added. Isolated crypts were seeded as droplets of 100 µl Matrigel in 12 wells suspension plates. Matrigel was allowed to solidify for 30 min at 37°C in the incubator. Post solidification, 1ml human tumor or normal organoids media was added to each well (media composition below). Human organoids passaging was performed every second week with a splitting ratio of 1:4 per well. For passaging, upon confluency, normal and tumor rectal organoids were collected in PBS, mechanically disrupted using a 1 ml pipette tip for 15 times, centrifuged at 800 rpm for 5 min and pellet resuspended into Matrigel and seeding was performed into 12 wells suspension plates with 100 µl Matrigel droplet per well.

Reagent Name	Volume/ Concentration
Reduced media: Advanced DMEM F12 (ThermoFisher Scientific; 12634010) + 1% Glutamax (ThermoFisher Scientific; 35050061) + 1% HEPES (ThermoFisher Scientific; 15630080) + 1% Penicillin/ Streptomycin (ThermoFisher Scientific; 15070063)	35 ml
B-27 supplement (ThermoFisher Scientific; #12587010)	1 ml
R-spondin	10 ml
Noggin	5 ml
human EGF (Peprotech; #AF-100-15)	50 ng/ml
N-Acetylcysteine (Sigma-Aldrich; #A9165)	2 mM
TGF-ß inhibitior A-83-01 (Tocris; #2939/10)	500 nM
p38 MAPK inhibitor SB202190 (Biotrend; #S7067)	10 µM

Table 3: Medium composition of human tumor organoids.

4.2.1.2 Mouse organoids

Generation of APTKA and APTK organoids was previously described (Drost et al., 2015). Briefly, the colon of *Trp53*$^{F/F}$ *Tgfbr2*$^{F/F}$ (The Jackson Laboratory; 008462 and 012603 respectively) mouse was collected and an organoid culture was established as described above. The established organoids harbor *loxP* sites flanking exon 4 of the *Tgfbr2* gene as well as the exons 2 and 10 of the *Trp53* gene and were cultured in a medium containing advanced DMEM F12 supplemented with B27, nicotinamide, N-acetylcysteine, noggin, R-spondin 1, EGF and TGF-β type I receptor inhibitor A83-01. The *Apc* mutation was introduced using CRISPR/Cas9 transgenesis and organoids were kept in the medium described above yet lacking R-spondin. The obtained *Apc* knockout organoids (A) were transfected with Cre-IRES-puroR plasmid (Addgene plasmid, #30205) that encodes Cre recombinase to ablate *Trp53* and *Tgfbr2* genes. The transfected organoids were maintained in a medium further deprived from Noggin and supplemented with 5 µM of TGFβ (Peprotech; 100-21) and 5 µM of MDM2 inhibitor, Nutlin-3 (Biomole; 10004372) to ensure an enrichment of the organoids carrying a loss of function mutations of *Tgfbr2* and *Trp53* genes, respectively (ATP organoids). Finally, *K-ras*^{G12D} gain of function mutation was obtained by overexpressing the murine version of *K-ras* gene (*K-ras*^{G12D}; cloned in-house based on Addgene plasmid #111164; Map-S5) by retroviral transduction in the ATP organoids to obtain APTK organoids which were kept in a medium further deprived from EGF and supplemented with 2 µg/ml of puromycin to maintain the *K-ras*^{G12D} expression. Human myristoylated AKT was cloned downstream of IRES and

hygromycin in rtTA3-PGK-Hygro retroviral vector (a gift from Lars Zender laboratory) and APTK organoids were transduced, selected with 200 µg/ml hygromycin containing media to obtain and maintain APTKA organoids.

Reagent Name	Volume/ Concentration
Reduced media: Advanced DMEM F12 (ThermoFisher Scientific; 12634010) + 1% Glutamax (ThermoFisher Scientific; 35050061) + 1% HEPES (ThermoFisher Scientific; 15630080) + 1% Penicillin/ Streptomycin (ThermoFisher Scientific; 15070063)	38 ml
B-27 supplement (ThermoFisher Scientific; 12587010)	1 ml
N-2 supplement (ThermoFisher Scientific; 17502048)	400 µl
N-Acetylcysteine (Sigma-Aldrich; A9165)	2 mM
Puromycin (Merck; 58-58-2)	2 µg/ml
Hygromycin (ThermoFisher Scientific; 10687010)	200 µg/ml

Table 4: Medium composition of APTKA and APTK organoids

For the generation of APTK organoids overexpressing IL-1α, organoids transduction with lentiviral constructs encoding CRISPR components for gene activation was performed: sgRNAs with MS2 loops at tetraloop and stemloop 2 (addgene; 61427), MS2-P65-HSF1 activator helper complex (addgene; 61426) and dCas9-VP64 (addgene; 61425). Insertion of sgRNAs into lenti-sgRNA (MS2) _zeobackbone (addgene; 61427) was performed at BsmBI restrictions sites via Golden Gate reaction. Three sgRNAs from Caprano mouse activation library (sequences below) (Sanson et al., 2018). Control sg-APTK were generated based on three random sequences non-mouse targeting sequences retrieved similarly from Caprano mouse activation library.

sgRNA Target	Oligonucleotides_Sequence
Il1a sgRNA I:	ATGTTCATTCTGCCTGATAC
Il1a sgRNA II:	GTGTGTCACTGGGAATTTAC
Il1a sgRNA III:	TCTGCCTGATA CCGGCCAGA
Ctrl sgRNA I:	AGGGCAATCGCGTGCCCAAC
Ctrl sgRNA II:	AGTAGAGTCGCGAACGCTAC
Ctrl sgRNA III:	ATAAAGTCCAGGTGCGCGC

Table 5: Oligonucleotides sequences employed for the generation of *Il1a* overexpressing APTK organoids.

4.2.2 Organoids irradiation experiments

For irradiation experiments, APTK and APTKA organoids were seeded in BME type II (R&D Systems; 3533-005-02P) into 6 wells suspension plates as 3 droplets of 100 µl size each per well. 24 h post seeding, organoids were subjected to 2Gy irradiation for 5 consecutive days (5x2Gy) in the presence or absence of Venetoclax supplemented 1h-before and 48 h-post first dose irradiation (500 nM; Selleckchem; S8048). Irradiation was performed using the radiation platform Biobeam 2000 (Eckert & Ziegler BEBIG GmbH). 6 h post last dose irradiation, control and treated organoids were split at equal ratios and 4 days' post first reseeding, number of organoids (reseeding capacity) was determined for the control and the treated groups.

4.2.3 Organoids survival assay

Resazurin (alamar blue) assay was performed to determine organoids viability post 5x2Gy irradiation (Cell Signaling Technology; 11884S). Briefly, APTKA and APTK organoids were seeded in 6 wells suspension plates with 3 droplets of 100 µl volume per each well. One-day post seeding, organoids irradiation started and was performed for 5 consecutive days with 2Gy irradiation dose daily using the radiation platform Biobeam 2000 (Eckert & Ziegler BEBIG GmbH). 6 h post last dose irradiation, untreated and 5x2Gy treated organoids media were changed into resazurin solution and incubation was performed for 6 h (1 ml per well). Using a plate reader with 560/590 nm (ex/em) filter settings, relative fluorescent units (RFU) were measured.

4.2.4 Fibroblasts isolation and treatments

After isolating crypts from normal human rectal biopsies, remaining tissue pieces were seeded in 6 wells plate that was previously coated with 1 ml of advanced DMEM F12 supplemented with 2% BME. Few days later, fibroblasts dissemination and attachment were observed. Fibroblasts medium was changed every second day. Mouse fibroblasts were isolated from the colons of unchallenged C57BL6/J, *Trp53*^{tm1Brn} (The Jackson Laboratory, stock #008462) and *Il1r1*^{tm1Imx} knockout mice (The Jackson Laboratory, stock #003245). The colons were collected, opened longitudinally, cleaned with sterile PBS and cut into small sized fragments. After 10 times washing with PBS supplemented with 1% penicillin/streptomycin, the small tissue pieces were incubated with 10 mM EDTA/PBS on ice for 15 min and supernatant discarded. An additional incubation cycle with 10mM EDTA/PBS was performed for another 15 min at 37°C on a rocking platform and supernatant discarded. The settled tissue pieces were

cut into smaller fragments of 1 to 2 mm^2, washed three times with cold PBS and seeded in 10 cm tissue culture dishes with low fibroblasts volume media (4-5 ml) (description below). Three days' post seeding, under the microscope, fibroblasts spreading was observed. Upon confluence, human and mouse fibroblasts were washed with PBS, collected by trypsinization using 0.05% EDTA/Trypsin and seeded into 6 wells tissue culture plates previously coated with 1% Matrigel/advanced DMEM F12 (1ml/well). *Trp53*^{tm1Brn} fibroblasts were transduced with Cre-IRES-puroR lentiviral plasmid (addgene; #30205) and successfully transduced *Trp53*$^{-/-}$ knockout fibroblasts were selected for puromycin resistance (2 µg/ml) and further validated by qRT-PCR.

Advanced DMEM F12	500 ml
Glutamax	5 ml
HEPES	5 ml
Penicillin/Streptomycin	5 ml
FCS	20 ml

Table 6: Medium composition of human and mouse intestinal fibroblast.

Conditioned media experiments with PDOs, were performed as three independent experiments with three distinct fibroblasts isolated from three normal non-matching biopsies from different patients (one line for each experiment). Fibroblasts of 70% confluence, seeded in 6 wells tissue culture plates were washed with PBS and further stimulated with either advanced DMEM F12 supplemented with 1%FCS, PDO IL1RA high media or PDO IL1RA low medium. 24 h post stimulation, adherent fibroblasts were collected by trypsinization with 0.05% EDTA/Trypsin, centrifugation at 1200 rpm for 5 min and pellet processed for RNA isolation and RT-PCR analysis. 72 h post stimulation, fibroblasts supernatants were collected, filtered using 0.45 µm filters and processed for nitrite levels assessments using Griess assay.

For transcriptomic analysis of polarized mouse fibroblasts, Wildtype mouse fibroblasts isolated from unchallenged C57BL6/J mouse colon, seeded in 6 wells tissue culture plates till reaching 70% confluence, were treated with either APTKA or APTK conditioned media for 24 h. The control untreated group included fibroblasts treated with advanced DMEM F12 supplemented with 1%FCS, similarly, for 24 h. Fibroblasts were collected by trypsinization with 0.05% EDTA/Trypsin, followed by centrifugation at 1200 rpm for 5 min, and pellets processing for either RNA or protein isolation.

To perform neutralization experiments, Wildtype mouse fibroblasts, isolated from unchallenged C57BL6/J mouse colon, were seeded in 6 wells tissue culture plates for three days, till reaching an approximately 70% confluence. Fibroblasts media removal was performed, followed by two times washing with cold PBS and stimulation for 24 h with APTKA organoids conditioned media (1.3 ml/well) supplemented with one the listed neutralizing antibodies at a concentration of 2 µg/ml each. At experiment end point, supernatants of each well were collected, filtered with 0.45 µm and frozen at -20°C for further analysis. For RNA isolation and subsequent RT-PCR analysis, fibroblasts were collected by trypsinization with 0.05% EDTA/Trypsin and centrifuged at 1200 rpm for 5 min. Pellets were processed for RNA isolation.

IKKβ inhibitor, p38 MAPK inhibitor and anakinra, in short-term experiments (24 h) were used at 30 µM, 10 µM and 10 µg/ml concentrations respectively. The inhibitors were applied 30 min before fibroblasts stimulation with organoids conditioned media. For long-term and irradiation experiments (~72 h), human and Wildtype mouse fibroblasts, isolated from normal rectal biopsies and unchallenged C57BL6/J colon respectively, were seeded into 6 wells tissue culture plates and treated upon reaching 70% confluence with advanced DMEM F12 media supplemented with 1%FCS with or without recombinant IL-1α (1 µg/ml) or APTKA conditioned media in the presence or absence of the following daily applied inhibitors: anakinra (20 µg/ml), Venetoclax (500 nM) and W1400 (1 mM) for 12 h followed by either 2Gy irradiation for 3 consecutive days (3x2Gy) or two consecutive daily doses of 5 FU (10 µM). Anakinra and Venetoclax were applied 30 min before fibroblasts stimulation with organoids conditioned media while W1400 inhibitor was applied 1 h before. Microscopic, proteomic and transcriptomic analysis were performed 6 h post first dose irradiation or 24 h post 2nd dose 5-FU therapy.

Reagent Name	Application	Manufacturer	Catalogue number	Concentration
Control Goat IgG	Neutralizing antibody	R&D Systems	AB-108	2 µg/ml
Anti-mIL-1α	Neutralizing antibody	R&D Systems	AF-400	2 µg/ml
Anti-mIL-33	Neutralizing antibody	R&D Systems	AF3626	2 µg/ml
Anti-mTNFα	Neutralizing antibody	R&D Systems	AF-410	2 µg/ml
Anti-mBAFF	Neutralizing antibody	R&D Systems	AF2106	2 µg/ml
Anti-mCXCL16	Neutralizing antibody	R&D Systems	AF503	2 µg/ml
ML120B	IKKβ- inhibitor	Sigma-Aldrich	SML1174	30 µM
SB203580	P38 MAPK-inhibitor	Selleckchem	S1076	10 µM
Anakinra	Recombinant IL1RA	Kineret		10 µg/ml 20 µg/ml
W1400	NOS inhibitor	Selleckchem	S8337	1 mM
Venetoclax/ ABT-199	BCL-2 inhibitor	Selleckchem	S8048	500 nM
IL-1α	Recombinant human protein	R&D Systems	200-LA-010/CF	1 µg/ml
IL-1α	Recombinant mouse protein	R&D Systems	400-ML-005/CF	1 µg/ml
5- Fluorouracil (5-FU)	Cytotoxic chemotherapeutic drug	Sigma-Aldrich	51-21-8	10 µM

Table 7: List of neutralizing antibodies, inhibitors and chemicals employed in human and mouse fibroblasts therapy *ex vivo.*

4.3 Histology

4.3.1 Paraffin embedding and scoring

Quantification of overall tumor size and % of invasive area were performed on control and untreated colons 21 days' post last dose irradiation. The collected colons were fixed as swiss rolls in 4 % paraformaldehyde (PFA) for 24 h and subsequently washed with PBS and kept in 70 % ethanol for another 24 h before being embedded in paraffin and serially sectioned at 200 µm. On serial sections, hematoxylin and eosin (H&E) staining was performed. The sections were further scanned by Aperio Scan Scope CS2 (Leica) and quantified by ImageScope Leica software. For each section, the overall tumor area (mm^2) and invasive area were calculated. For detecting and scoring liver metastases, collected liver tissues were fixed for 24 h in 4% PFA, before being incubated overnight with 70 % ethanol, paraffin embedded and further serially sectioned at 200 µm. H&E staining was performed on a total of 15 serial sections that were carefully examined for histological evidence of micro-metastases.

4.3.2 Immunohistochemistry

The automated Bond-Max autostainer by Leica was used to perform immunohistochemistry for the following antibodies listed below. For the detection of the primary antibody staining, Leica bond polymer refine detection kit was used. The staining was carefully examined and analyzed using ImageScope software by Leica. DCN and Sirius red positivity quantifications were performed using Aperio ImageScope 12.4.3 software algorithm of positive pixel count.

Antibody	Manufacturer	Catalogue number	Dilution	Application
Phospho-53BP1 (Ser1778)	Cell Signaling Technology	2675	1:100	IHC
Phospho-H2A.X (Ser139)	Cell Signaling Technology	9718	1:200	IHC
MPO	Abcam	ab134132	1:200	IHC
Ly6G	Abcam	ab25377	1:1000	IHC
Anti- F4/80	ThermoFischer Scientific	MF48000	1:200	IHC
Anti- CD8	Novus Biologicals	NBP2-297475	1:500	IHC
Anti- DCN	Novus Biologicals	AF143	1:500	IHC
Anti- p21	Santa Cruz	sc-397	1:100	IHC
IL1R1	ThermoFisher Scientific	PA5-97866	1:100	IHC

Table 8: List of antibodies used for immunohistochemistry.

Visualization of connective tissue, collagen I and II was performed using picros Sirius red stain by Sigma-Aldrich (#2610-10-8). In summary, after tissue deparaffinization and hydration, slides were incubated with 0.04% Sirius red solution for 1 h at RT. Then they were rinsed quickly with two changes of acetic acid solution (0.5%), absolute alcohol and finally dehydrated and covered with mounting media. Stained slides were scanned with Aperio ScanScope CS2 (Leica) and analyzed by ImageScope-Leica software using positive pixel macro.

4.3.3 Immunofluorescence

On untreated and irradiated fibroblasts, immunofluorescent staining was performed 72 h post last dose irradiation. Briefly, fibroblasts seeded in 8 wells staining chambers (by Sarstedt), were washed with cold PBS, fixed for 10 min in 4% PFA at RT, further washed with PBS and blocked with 3% bovine serum albumin (BSA) for 40 min at RT. Post blocking, fibroblasts were incubated overnight with the following primary antibodies listed below diluted in 3%

BSA/PBS. Next day, stained cells were washed with PBS and treated for 1 h at RT with anti-species specific 1:1000 diluted secondary antibody Alexa Fluor 596 (ThermoFischer Scientific) diluted in 3% BSA/PBS. DAPI (4′,6-diamidino-2-phenylindole) blue fluorescent DNA staining was performed for 5 min before slides being covered with coverslips and microscopically examined using Zeiss microscope.

Antibody	Manufacturer	Catalogue number	Dilution	Application
p21	Santa Cruz	sc-397	1:100	IF
phospho- H2AX (Ser139)	Cell Signaling Technology	cst-2577	1:100	IF
8OHdG	Santa Cruz	sc-393871	1:100	IF

Table 9: List of antibodies used for immunofluorescence.

4.3.4 Phenoptics

Phenoptics or multiplex IHC was performed using PerkinElmer Opal 7 color kit (NEL801001KT) on FFPE tissue sections obtained from human baseline rectal cancer biopsies pre-chemoradiotherapy. Tumor sections were stained with Opal 7-Color Automation IHC Kits (Akoya Biosciences, Menlo Park, CA, USA) in the BOND-RX Multiplex IHC Stainer (Leica, Wetzlar). For the visualization of immune cells and CAFs, two IHC panels were performed using the following primary antibodies listed below. Nuclei were counterstained with DAPI and mounted with Fluoromount-G (SouthernBiotech, Birmingham, AL, USA). The slides were visualized and further analyzed using Vectra3 imaging system and its corresponding inForm 2.4.9 software (Akoya Biosciences, Mentlo Park, CA, USA).

	Antibody	Manufacturer	Catalogue Number	Antigen Retrieving (Kit)	Dilution	Fluorochrome
Immune Human Phenoptics Panel	CD4	Abcam	ab133616	AR6	1:100	520
	CD3	VENTANA	790-4341	AR6	1:1	540
	PD1	Abcam	ab137132	AR6	1:500	650
	CD163	Abcam	ab182422	AR9	1:250	570
	CD8	Abcam	ab4055	AR6	1:200	620
	FoxP3	Abcam	ab20034	AR6	1:100	690
CAF Human Phenoptics Panel	PanCyto	Abcam	ab7753	AR6	1:200	620
	CD45	Abcam	ab10558	AR6	1:100	650
	Ki67	Abcam	ab16667	AR9	1:500	540
	Vimentin	Abcam	ab92547	AR6	1:100	570

Table 10: List of antibodies used in the immune and CAFs phenoptics.

4.3.5 SA-β- Galactosidase assay

For the validation of senescence induction upon therapy among fibroblasts, SA-ß-galactosidase assay was performed 6 h post last dose irradiation or 24 h post 2nd dose chemotherapy 5-FU dose following kit manufacturer's instructions (Cell Signaling Technology; #9860). Briefly, fibroblasts seeded in 6 wells tissue culture (TC) plates were washed with PBS and fixed for 10 min at RT with 1X PFA solution (1 ml/well). Post fixation, fibroblasts were washed again with PBS and plates were covered with aluminum foil and further incubated overnight with a pH~6 SA-ß-gal solution (description below) at 37ºC in a dry, CO_2 free incubator, with constant agitation. Staining visualization was performed 24 or 48 h post incubation using light microscopy. Quantification of number of positive cells per field were performed using ImageJ software.

SA-ßgal Solution (pH~6)	
1X Staining Solution	930 µl
100X Solution A	10 µl
100X Solution B	10 µl
20mg/mL X-gal stock solution (in Dimethylformamide)	50 µl

Table 11: SA-β-galactosidase reaction mixture.

For *in vivo* detection of senescent cells, irradiated and untreated APTKA tumors were collected 21 days post last dose irradiation (experiment end point), washed three times in clean 1X PBS, fixed for 2 h at RT in 4%PFA, incubated for 4 h at 4ºC in 15% sucrose/PBS (Sigma Aldrich; #57-50-1) and finally incubated overnight at 4ºC in 30% sucrose/PBS. Next day, fixed tumors were washed with PBS and embedded for cryosections in transparent histo-casettes using Tissue-Tek O.C.T gel (SAKURA; #4583). SA-β-gal staining assay was performed on freshly sectioned 6 µm cryosections as following: slides were incubated for 10 min RT in PBS, fixed at RT for 15 min with 150 µl 1X fixative solution, washed again with PBS then stained overnight with ~150 µl of the previously described SA-ß gal staining solution (pH~6) in a dry incubator at 37ºC with constant agitation. Next day, slides were washed with PBS and visualized under light microscopy for senescent cells positivity (blue coloration). Counterstaining with fast red nuclear stain (Sigma Aldrich; #6409-77-4) was performed for 5 min followed by slides rinsing in distilled water and mounting in aqueous mounting media. The Aperio digital pathology slide scanner by Leica was used to scan the stained slides that were analyzed using the Aperio ImageScope Software (Leica Biosystems). Quantifications were performed as number of positive cells per field with at least 10 independent microscopic fields captured per tumor.

4.4 Protein Analysis

4.4.1 Immunoblot analysis

For immunoblot analysis, on irradiated and untreated APTKA- conditioned media fibroblasts 6 h post last dose irradiation proteins samples were collected by trypsinization of fibroblasts using 0.05% EDTA-Trypsin (ThermoFischer Scientific; #25300062) followed by centrifugation at 1200 rpm for 5 min. Complete lysis buffer (description below) was added to the collected pellets. Cellular disruption using Precellys 24 homogenizer (Bertin Technologies) was performed. Protein concentrations in collected lysates were measured at a wavelength of 595 nm using a spectrophotometer (Nanodrop, Thermo Scientific) by mixing 2 µl of the lysate with 1 ml of 1:5 diluted Bradford protein assay solution (BioRad). A total of 30 µg of protein were prepared in a total volume of 30 µl lysis buffer supplemented with 1x laemmli buffer and 5% β-mercaptoethanol were prepared for each sample followed by protein denaturation at 95ºC for 5 min.

Protein lysis buffer	50 mM Tris (Roth), pH 7.8 250 mM NaCl (Sigma) 30 mM EDTA (Sigma) 25 mM Sodium-pyrophosphate (Sigma) 1% Triton-X100 (Sigma) 0.5% NP40 (Sigma) 10% Glycerol 1 mM DTT (Sigma) 50 mM ß-glycerophosphate (Sigma) 25 mM Sodium fluoride (Sigma) 5 mM Sodium orthovanadate (Sigma) 2 nM PMSF (Sigma) 1 tablet of complete protease inhibitor cocktail (Roche) per 50 mL
Running buffer (10x)	9.5 M Glycine (Roth) 0.25 M Tris (Roth) 35 mM SDS
Transfer buffer 10x	9.5 M Glycine 0.25 M Tris
Transfer buffer 1x	100 mL 10x Transfer buffer 200 mL Methanol (Merck) 700 mL distilled water

Table 12: Western blot buffers composition.

Protein lysates were separated by 12% SDS-PAGE in 1x running buffer at 120 Volt. Protein gel transfer to methanol activated polyvinylidene difluoride (PVDF) membrane was performed using the Mini Trans-Blot Cell system (BioRad) in 1x transfer buffer for 90 min at 280 mA. Membranes blocking was performed for 40 min at RT with 5% milk-PBS supplemented with 1% Tween 20 (Promega). Incubations with primary antibodies (listed below) diluted in 3% BSA/PBS-1% Tween 20 were performed at 4ºC overnight on a rocking platform. Next day, membranes were washed three times with 1% Tween 20/PBS and further incubated for 30 min at RT with corresponding HRP labeled secondary antibodies diluted in 3% BSA-PBST (α-rabbit/α-mouse/α-goat, GE Healthcare). Next, the membranes were washed 3 times with PBS-T. ECL solution was applied on the membrane for 1 min for protein band detection. X-ray films

were subsequently exposed for few seconds up to 15 min, and placed into films developer machine.

Antibody	Manufacturer	Catalogue number	Dilution
Anti- p21	Santa Cruz	sc-471	1:500
Anti- CDK4	Santa Cruz	sc-260	1:500
Anti- Cyclin D2	Santa Cruz	sc-593	1:500
Anti- Cyclin A	Santa Cruz	sc-751	1:500
Anti- CDK1	Merck	PC25	1:500
Anti- p16INK4a	ThermoFischer Scientific	PAI-46220	1:1000

Table 13: List of antibodies used in western blot analysis.

4.4.2 Enzyme Linked Immunosorbent Assay (ELISA)

To determine IL-1α protein levels in rectal cancer PDOs supernatant, sgCtrl and sg*Il1a* APTK mouse organoids supernatants, the following ELISA kits (R&D Systems) were used respectively: DY200-05 and DY400-05. To determine IL1RA protein levels in PDOs supernatant an ELISA kit was used (R&D Systems; DY280-05). To collect mouse or human organoids supernatants, organoids were seeded into 12 wells plates with 200 µL droplet size per well and 2 days post splitting, their media was changed into advanced DMEM F12 supplemented with 1% glutamax, 1% HEPES, 1% penicillin/streptomycin and 1% FCS (1 ml/ well). Three days later, media collection and filtering using 0.45 µm filters were performed. ELISA was performed following manufacturer's protocol with 200µl sample volume per well.

4.4.3 Bio-Plex pro-human cytokine array

Quantification of circulating chemokines, cytokines, and growth factors protein levels in RCA patients serum pre-CRT was performed using the Bio-Plex Pro Human Cytokine 27-Plex Assay kit (Bio-Rad; m500kcaf0y) following manufacturer's instructions manual (Bio-Rad; 10014905). The loaded human RCA serum samples were 1:4 diluted as recommended by the manufacturer. Briefly, reconstituted 1x beads were added into the plate (50 µl/well) and washed two times for 1 min each using Bio-Plex Handheld Magnetic Washer (Bio-Rad). Standards, blanks and serum samples (1:4 diluted) were added (50 µl/well) and incubated with the beads at RT on 850 rpm rocking platform. The plate was then washed for three times using a magnetic washer and incubation with 1x detection antibody (25 µl/well) was performed at RT for 30 min with constant shaking at 850 rpm. After washing the plate three times, streptavidin-PE (1x)

incubation was performed (50 µl/well) at RT for 10 min with constant agitation at 850 rpm. Finally, the plate was washed three times and beads were resuspended in 125 µl/well assay buffer. Data were acquired on the Bio-Plex manager software version 6 (Bio-Rad).

4.4.5 Mass spectrometry analysis

Baseline RCA biopsies were obtained from the University Medical Center Gottingen-department of General, Visceral and Pediatric Surgery with the approval of the university Ethics committee. From each participating patient, an informed consent was obtained. Mass spectrometry analysis was conducted following described published protocol (Bohnenberger et al., 2018). 5 to 10 µm histology sections were mounted on film-covered membrane slides, allowed to dry for 1 h at 37°C. Deparaffinization in xylene followed and subsequent treatment with 100% ethanol, 70% ethanol, and water were performed for 1 min each. A final hematoxylin staining for 20 s was done and slides were rinsed with tap water. MMI cell cut-laser microdissection system allowed collection of tumor epithelial cells following manufacturer's instructions. Human proteomics data can be found under the accession number PXD030422.

Irradiated (3x2Gy) and untreated APTKA-conditioned medium polarized fibroblasts were subjected to ECM proteins isolation 6 h post last dose RT using Millipore compartment protein extraction kit (Millipore, #2145) following manufacturer's instructions and published protocols. Briefly, collected pellets (4 replicates per group) were homogenized and subjected to sequential proteins extraction to remove (1) cytosolic (2), nuclear (3), membrane (4), cytoskeletal and finally insoluble ECM proteins. Mass spectrometry analysis of ECM proteins was then performed following published protocols. Initially, samples solubilization with urea lysis buffer (2.5 mM sodium pyrophosphate, 1 mM ß-glycerophosphate, 20 mM HEPES, 9 M urea and 0.1 sodium orthovanadate pH 8.0) was performed and BCA assay allowed determination of protein concentration for each sample. For 80 µg of protein, sample volume was adjusted to 120 µl with urea buffer. Further incubation with 10 mM DTT for 1 h at 37ºC ensured reduction of disulfide bonds. Subsequently, alkylation with 25 mM Iodoacetamide (IAA) was performed for 15 min at 37ºC. For deglycosylation, samples were treated with PNGase F for 2 h at 37ºC. Sequential sample digestion was performed by incubation with 1:50 enzyme- substrate diluted Lys-C for 2 h at 37ºC followed by another incubation round with trypsin (1:100 dilution) for 16 h at 37ºC. Acidification of peptides mixture was performed followed by a clean-up with C18 spin tips and a vacuum configuration-based drying step.

Samples reconstitution in 50 Mm TEAB followed and peptide concentrations were determined using a fluorometric peptide assay by ThermoFisher Scientific. For each sample, a tandem mass tag (TMT) labeling was performed followed by a vacuum centrifugation-based drying, sample reconstitution in 01% TFA and pre-fractionation using high-PH C18 reversed phase kit (Thermofisher Scientific). The peptide mixtures analysis was achieved on a Q Exactive HF orbitrap mass spectrometer coupled online to an Ultimate 3000 RSLCnano HPLC system (ThermoFisher Scientific). The MaxQuant software (version 1.6.5.0) was employed in processing the raw mass spectrometry data. For protein identification, the mouse protein database UniProt was employed to search for MS/MS spectra along the Andromeda search engine supplemented with 245 frequently observed contaminants. Variable modifications included the following: proline oxidation to pyroglutamic acid, hydroxylation of lysine and proline, oxidation of methionine and acetylation on the protein N-terminus and Deamidation (N). For peptide and protein, a 1% value was set for the false discovery rate (FDR). Data analysis was performed using Perseus software (version 1.6.0.7, Max Plank Institute for Biochemistry). For replicate measurements, reporter intensities were normalized to an internal reference of comparable amount for each sample (Plubell et al., 2017). Mouse mass spectrometry data can be accessed through PXD020871.

4.5 Griess assay

Measurements of nitrite levels in untreated, irradiated and IL-1α stimulated fibroblasts were performed using the Griess assay kit (abcam; 234044). Briefly, fibroblasts supernatants were collected 6 h post last dose irradiation, filtered using 0.45 µm filters, processed fresh for nitrite measurements and loaded as 100 µl sample mixed with 1:10 diluted Griess reagent I and 1:10 diluted Griess reagent II per well in 96 wells plate with clear flat bottom. The plate was incubated for 15 min at RT followed by absorbance measurements at 540 nm. Each sample nitrite level was presented as nmol/well by applying corrected OD levels to the standard curve.

4.6 Real-time metabolomic analysis

XFe24 Extracellular Flux Analyzer (Agilent) along pre-hydrated XFe24 Sensor Cartridges (Agilent; 102340-100) were used to measure fibroblasts oxygen consumption rate (OCR) and extracellular acidification rate (ECAR). Seahorse V7 24-wells assay plate were pre-coated with Gelatin (Merck; G1393; 30µl/well). Unstimulated mouse fibroblasts, isolated from unchallenged C57BL6/J mouse, were seeded at a density of 30 000 cells/ well into the assay

plate. Two days' post seeding, upon reaching a 70% confluence, fibroblasts were washed and 500 µl regular media supplemented with 1%FCS, APTKA or APTK conditioned medium was added per well for 72 h. On the day of the assay, fibroblasts were washed three times with assay medium: 10 mM glucose (Sigma, G8270), 1mM sodium pyruvate (Gibco, 11360070), Agilent Seahorse XF Minimal DMEM media (Agilent, 103575-100) and 2 mM glutamax (Gibco, 35050061). Then addition of 500 µl assay medium per well and subsequent incubation for 1 h in a CO_2 free incubator was performed. Glycolytic rates and mitochondrial respiration were measured using XF Glycolytic Rate Assay kit (Agilent; 103344-100) and XF Cell Mito Stress kit (Agilent; 103015-100) respectively. Upon completion of OCR and ECAR measurements, assay medium was discarded and plates were frozen overnight at -80°C. ECAR and OCR measurements were standardized to DNA content measured by CyQUANT cell proliferation assay (Invitrogen; C7026) in thawed plates. Briefly, 200 µl of 1:1 mixed CyQUANT fluorescent GR dye with CyQUANT GR lysis buffer was added per well. Post cellular lysis by pipetting, lysate was transferred to 96 wells plate (200 µl lysate/ well) of clear flat-bottom. Measurements of absorbance were performed with Fluostar Optima microplate reader at 485/520 nm wavelength. Using generated standard curve, DNA concentrations were generated and values were used for ECAR and OCR measurements normalization to 1µg DNA.

4.7 Patients

Patients samples were collected from the Clinic for General, Visceral and Pediatric Surgery of the University Medical Center Göttingen and Frankfurt. Approval for obtaining RCA patients materials was given by the Ethics Committees of the University Medical Center at Göttingen and Frankfurt. Pretherapeutic staging of patients was performed based on a multislice CT thorax/abdomen and MERI pelvis, colorectoscopy and biopsy. Rectal cancer (RCA) patients of histologically identified rectal tumor with perirectal fat infiltration (cT3-T4) or lymph node metastasis (N+) were included in the study. All patients received preoperative chemoradiotherapy (CRT). Patients were subjected to fractionated radiotherapy receiving each 50.4 Gy total dose delivered as 1.8 Gy daily in 28 fractions. Simultaneously, during radiotherapy, chemotherapy was administered, as 5-fluorouracil (5-FU) alone or in combination with oxaliplatin. 4 to 6 weeks after CRT, RCA patient was subjected to surgical resection. The records of all patients' cohorts included in the following study were summarized in supplementary table S1. A total of three different cohorts were included in data analysis based on samples availability and quality: a transcriptomic cohort consisting of 105 patients

before CRT, a proteomic cohort (n=61 patients) and a rectal cancer patient derived organoids (PDO) cohort (n=17).

4.8 Gene expression analyses

4.8.1 RNA isolation

Collected untreated APTKA and APTK mouse orthotopic tumors were incubated with 1% β-mercaptoethanol RNA lysis buffer (Qiagen; 74106) and homogenized for three cycles using Precellys 24 homogenizer (Bertin Technologies). To collect RNA from fibroblasts, a trypsinization using EDTA-Trypsin was performed, followed by centrifugation for 5 min at 1200 rpm for pellet collection. Processing organoids for RNA isolation included their collection in cold PBS, followed by mechanical disruption using 1 ml pipette tip and centrifugation at 800 rpm for 5 min. RNA isolation from orthotopic tumors, fibroblasts and organoids was performed using Qiagen RNeasy Mini Kit (Qiagen; 74106). Assessment of RNA quality and concentration was performed using Nanodrop spectrophotometer. From human pretherapeutic RCA samples, total RNA was isolated from patient's formalin fixed paraffin embedded biopsies before CRT, following Qiagen RNeasy FFPE kit (Qiagen; 73504) protocol followed by next generation sequencing (NSG).

4.8.2 cDNA synthesis and quantitative real time- PCR

For quantitative real time polymerase chain reaction (qRT-PCR), complementary DNA (cDNA) synthesis was performed from 1000 ng RNA, using Superscript II reverse transcriptase (Invitrogen; 18080044) in a total reaction volume of 20 µl. Initially, 1000 ng RNA was incubated with 1µl OligoDT (Invitrogen; N8080128) and 1 µl DNTP (Invitrogen; AM8200) in a total volume of 13 µl reaction for 5 min at 65°C followed by 5 min incubation on ice. Secondly, to each samples 4µl (1x) reaction buffer (Invitrogen; 18064014), 1 µl DTT (Invitrogen; 18064014), 1 µl recombinant ribonuclease inhibitor_RNAseout (Invitrogen; 10777019) and 1µl Superscript II reverse transcriptase (Invitrogen; 18064014) were added and incubation followed at 42°C for 60 min. Before being processed into gene expression analysis, synthesized cDNA samples were 1:5 diluted in nuclease free water (ThermoFisher Scientific; R0582). For qRT-PCR, in a total reaction mixture of 20 µl, 1 µl of CDNA was mixed with 1x SYBR Green Master Mix (Roche), 2 mM forward and 2 mM reverse primers (list below). Samples were processed with the 96 wells StepOne real time PCR machine (Applied

Biosystems). Normalization of genes expression levels was performed with respect to the housekeeping gene *Ppia* (cyclophilin) expression level.

Gene	Forward	Reverse
mCxcl1	GCCAATGAGCTGCGCTGT	CCTTCAAGCTCTGGATGTTCTTG
mCxcl2	AAGGCAAGGCTAACTGACCT	CATCAGGTACGATCCAGGCT
mCxcl5	TCCATCTCGCCATTCATG C	GATGCTGCGGCAGCGT
mMmp9	CAGCTGGCAGAGGCATACTTG	GCTTCTCTCCCATCATCTGGG
mMmp13	ACAAGCAGTTCCAAAGGCTACAA	AGTGATCCAGACCTAGGGAGTGG
mIl1a	CACAACTGTTCGTGAGCGCT	TTGGTGTTTCTGGCAACTCCT
mIl6	ATGGTACTCCAGAAGACCAGAGGA	GTATGAACAACGATGATGCACTTG
mTnfa	ACTCCAGGCGGTGCCTATG	GAGCGTGGTGGCCCT
mNos2	CCCTCCTGATCTTGTGTTGGA	CAACCCGAGCTCCTGGAAC
mIl1b	GTG GCT GTG GAG AAG CTG TG	GAA GGT CCA CGG GAA AGA CAC
mIl1r1	AGACCCCCATATCAGCGGA	TGGCAGGTACAAACCAAAGATGT
mCdkn2a	CCCAAGGCCCCGAACTC	TGTGAACGTTGCCCATCATC
mTrp53	AGATCCGCGGGCGTAAAC	TCTGTAGCATGGGCATCCTTT
hCXCL1	CGCCCAAACCGAAGTCATAG	GGATGCAGGATTGAGGCAAG
hCXCL5	TACAGACCACGCAAGGAGTT	GAGGCTACCACTTCCACCTT
hMMP9	TGTAAATCCCCACTGGGACC	CACTCCTCCCTTTCCTCCAG
hMMP3	GCAGTTTGCTCAGCCTATCC	CAAGGTTCATGCTGGTGTCC
hIL1A	TCTCCTTTCAGGCCAATCCC	AGAACCAAAATGTGGCCTGG
hIL6	AGACAGCCACTCACCTCTTC	TTGTTTTCTGCCAGTGCCTC
hNOS2	ATGCCAAGAACGTGTTCACC	GCCATCCTCACAGGAGAGTT

Table 14: List of quantitative real time PCR analysis primers.

4.9 RNA sequencing and data analysis

Single cell RNA sequencing data, proteomic data and total RNA sequencing data were deposited online as summarized in the table below.

Dataset	Repository	Accession number
APTKA and APTK orthotopic tumors and organoids total RNA sequencing data	NCBI-Bioproject	PRJNA656937
Mouse fibroblasts	NCBI-GEO	GSE190006
Mass spectrometry of untreated and irradiated APTKA-CAFs	ProteomeXchange	PXD020871
RCA patients baseline proteome	ProteomeXchange	PXD030422
RCA patients total RNA sequencing pre- and post-CRT	NCBI-GEO	GSE190826
RCA patients total RNA sequencing pre-CRT_ published cohort (Hu et al., 2018)	NCBI-GEO	GSE87211
Mouse single cell RNA sequencing data	NCBI-GEO	GSE191093
CRC single cell RNA sequencing data_ published cohort (Lee *et al.*, 2020)	NCBI-GEO	GSE132465

Table 15: Deposited transcriptomic and proteomic data.

4.9.1 Single-cell RNA sequencing

4.9.1.1 CAFs fluorescent-activated cell sorting

Untreated APTKA orthotopic tumors, transplanted in C57BL6/J mice were isolated at experiment end point and washed in sterile cold PBS supplemented with 1% penicillin/streptomycin. Collected tumors were cut into small pieces and enzymatically digested in 15 ml Advanced DMEM-F12 supplemented with 10% FCS, 1 mg/ml collagenase-II (Sigma-Aldrich; C6885), 1mg/ml dispase-II (Sigma-Aldrich; 9003-98-9) for 20 min at 37°C with constant agitation on a rocking platform. Two successive digestions were performed and for each, cells rich supernatant was collected, quenched with Advanced DMEM-F12 and filtered using 70 µm filters. 5 Mm EDTA was used to stop the digestion reaction. Cells fractions collected from both digestion cycles were pooled together into one 50 ml falcon tube, followed by centrifugation at 1200 rpm speed/ 4°C for 10 min. Cells surface staining was performed with 20 min/4°C Fc receptor block with anti-mouse CD16/CD32 antibody followed by 30 min incubation at 4°C with staining antibodies listed in the table below. APTKA tumors CAFs were sorted in pre-labeled 384 wells plates as alive cells negative for the following markers: CD31, CD45, EpCAM and F4/80 and stored at -80°C till further processing. RNA isolation, library preparation, single cell RNA sequencing and raw data acquisition was performed by Single Cell Discoveries (SCD, Utrecht- Netherlands).

FACS Antibody	Manufacturer	Catalogue number	Dilution
Anti-CD326 (EpCAM)	ThermoFisher Scientific	G8.8-PE 12-5791-82	1:200
Anti-CD45	ThermoFisher Scientific	30-F11-eFluor450 48-0451-82	1:200
Anti-CD31	Biolegend	PerCP/Cyanine5.5 102419	1:200
Anti-F4/80	ThermoFisher Scientific	FITC 11-4801-82	1:200

Table 16: List of antibodies used in FACs sorting of CAFs from APTKA orthotopic tumors.

4.9.1.2 Mouse scRNASeq data analysis

Data analysis of scRNASeq mouse CAFs included a total of 658 viable CAFs. The following criteria were considered in the performed quality control: 1) overall reads number >1000; 2) % of reads that presented ERCC spike-ins mapping <20% and 3) mitochondrial reads mapping <5%. Hence, the final analysis included 624 CAFs. Normalization of expression was performed to overall reads per cell with target sum of 1e4. CITE, a dispersion-based method was adopted to identify highly variable genes. Dispersion normalization was achieved by scaling with the mean and standard deviation of the dispersions for genes falling into a given bin for mean expression. Standard values for minimum/maximum cut-offs for mean of 0.0125 and 3 were adopted, along 20 bins, and a span of 0.3. Highly variable genes were considered for minimum dispersion higher than 0.5. Cells stratification into subpopulations was performed using the Leiden algorithm with UMAP-based map visualization (McInnes et al., 2018; Traag et al., 2019). Wilcoxon rank sum test served for the DE analysis. The signature of each cluster was identified as the set of DE genes with a log2FoldChange ≥1 and an adjusted p-value threshold of 0.05. To identify upstream regulators of each cluster, IPA software by Qiagen was used. Results were summarized in supplementary table S3. Mouse scRNASeq data can be found at NCBI-GEO under the accession number: GSE191093.

4.9.1.3 Human scRNASeq data analysis

Single cell RNA sequencing data of colorectal cancer patients was generated based on the published data of 23 colorectal cancer patients (Lee *et al.*, 2020) (NCBI-GEO; GSE132465). Unsupervised clustering of a total of 1936 CAFs was performed based on 4469 highly variable genes (identified as above) using the Leiden algorithm (Traag *et al.*, 2019). Gene signature of each cluster including iCAFs Cluster C3 was identified as the list of differentially expressed

genes of Log2FoldChange ≥1 and an adjusted p-value threshold of 0.05. Differential expression analysis was performed using the Wilcoxon rank sum test. All analyses were performed using scanpy (Wolf et al., 2018). Identification of clusters upstream signature regulators was performed by IPA software (Qiagen) and results were summarized in supplementary Table S2.

4.9.2 Human bulk transcriptomic analysis

Total RNA was isolated from paraffin blocks of 105 rectal cancer patients following described protocol above followed by ribosomal RNA depletion to prepare libraries for next generation sequencing. RNA isolation, library preparation and data analysis were performed by GENEWIZ, LLC (South Plainfield, NJ, USA). Samples sequencing was performed at 2 x 150 paired end configuration after quality control (TapeStation, Agilent Technologies, Palo Alto, CA, USA) and quality assessed as ≥80% of bases of ≥Q3. NGS was performed by GENEWIZ, LLC (South Plainfield, NJ, USA). The using of Trimmomatic V.0.36 ensured elimination of poor-quality nucleotides and adapter sequences. The using of the STAR aligner v.2.5.2b ensured reads mapping to the human reference genome (Homo sapiens GRCh38) available on ENSEMBL. The Subread package v.1.5.2 was used for unique counts. Extracted gene counts were used for further analysis of differentially expressed genes. Comparison between non-pCR and pCR patients as well as preCRT versus CRT samples was performed via DESeq2 analysis. Log2Fold changes and p-values were generated through the Wald test. GSEA were performed using version v.4.0.3 software by the Broad Institute. Significantly enriched signatures were counted of NES ≥1 and FDR-q-value ≤0.05. Gene expression levels were implicated in calculating *IL1RN* Z-score followed by a median split of high versus low scores to generate Kaplan-Meier DFS curve with a long-term follow-up survival of 85 months.

4.9.3 CMS classification

In the addition to the 105 baseline RCA RNA sequencing data (patients first cohort), the microarray expression GSE87211 data was downloaded from NCBI-GEO repository and included in the analysis using GEoquery R package (Hu *et al.*, 2018). Genes expression levels were summarized and further log2 transformed. Using biomaRt R package, the probes were annotated and those of highest intensity were chosen as gene expression representative. Genes expressions value were processed using three published CMS classifiers: random forest, single sample prediction methods as well as CMScaller R packages (Guinney *et al.*, 2015). The CMS

classifier of each patient was assigned only if at least two classification algorithms identified the same subtype, otherwise the classification was considered unclear.

4.9.4 Mouse bulk transcriptomic analysis

4.9.4.1 Library preparation for directional mRNA-sequencing

Using Illumina's TruSeq stranded RNA library prep kit, mRNA-focused RNA libraries were prepared. Poly(A)-positive mRNA transcripts were collected from total RNA by binding to magnetic oligo(d)T beads and subsequently fragmented and reverse transcribed throughout initial and second strand synthesis to produce double-stranded cDNA. The disjointed cDNA was then end-repaired and adenylated then a ligation of the proper six-nucleotide TruSeq RNA Single Index (Illumina) or eight-nucleotide NEXTFLEX DNA barcode adapter (PerkinElmer) was performed. The last ligation product was amplified via PCR. AMPure XP beads (Beckman Coulter) were employed for intermediate and final library purifications. The quality and quantity of the library was evaluated by Qubit dsDNA HS Assay Kit (Invitrogen) and the Agilent High Sensitivity DNA kit.

4.9.4.2 Sequencing

Paired-end sequencing mode (2 x 50 nt) on an Illumina NovaSeq 6000 instrument was performed culminating in a minimum of 20 million distinct sequencing reads per library.

4.9.4.3 Gene annotation and RPKM computation

Genes quantification was performed with the Ensembl v84 mouse transcript annotation (January 2012/GRCm38/mm10) following three steps: 1) quality control using FastQC and cleaning of low quality reads 2) alignment to the reference genome using STAR aligner and 3) reads overlapping with exonic coordinates, counting and normalization to Reads Per Kilobase Million (RPKM).

4.9.4.4 Analysis of differentially expressed genes

For normalization and differential expression (DE) analysis, R software package DESeq2 was used (Love et al., 2014). Ingenuity pathway analysis software (Qiagen) was further used for the identification of canonical pathways and upstream regulators. To perform GSEA and for the generation of enrichment plots, the preranked tool was employed (version 4.0.3; Broad

Institute). Signatures of significant enrichment were considered for a normalized enrichment score (NES) ≥1 and FDR q-value <0.05.

4.10 Genotyping assay

4.10.1 PBMCs collection and DNA isolation

For the collection of peripheral blood monocytes (PBMCs), from RCA patients, blood samples were retrieved in EDTA tubes and subjected to 1:2 dilution (in PBS) followed by further 1:2 dilution in Biocoll solution (BIOCHROM; L6113) and centrifugation for 20 min at 400 g. The lymphocytes-rich fraction (interphase) was collected, diluted in PBS to a total volume of 50 mL and centrifuged for 10 min at 300 g. To the pellet, a 1 M ammonium chloride solution was added, followed by incubation for 1 min and subsequent centrifugation at 300 g for 7 min. The collected pellet was further mixed in PBS and centrifuged for 10 min at 300 g. The collected PBMCs rich pellet was resuspended in 1 mL FACs buffer and number of cells was determined. The samples were further frozen at -80°C. To extract DNA from PBMCs, the Qiagen DNA mini kit (Qiagen, 51104) was used following manufacturer's instructions. Nanodrop spectrophotometer was used to determine quality and concentration of the isolated DNA.

4.10.2 SNP genotyping

For the SNPs genotyping, 31 DNA samples isolated from patients PBMCs pre-CRT were used using the following TaqMan genotyping probes: C_32060323_20 and C_8737959_10 for the IL1RA rs4251961 T/C and rs579543 G/A SNPs respectively (ThermoFisher Scientific; #4351379). In a reaction of 12 µl volume, a total of 12.5 ng DNA was amplified in the presence of 1X TaqMan Universal PCR Master Mix (ThermoFisher Scientific, 4304437) and 1X TaqMan SNP genotyping assay. The following steps summarize the amplification cycle:

- 50°C for 2 min
- 95°C for 10 min
- 40 cycles: 95°C for 15 s and 60°C for 1 min

PCR reactions were run on the 96 wells Applied Biosystems StepOnePlus™ Fast Real-Time PCR System. Post reaction analysis and genotypes determination was performed using the TaqMan® Genotyper™ Software.

References

Acosta, J.C., Banito, A., Wuestefeld, T., Georgilis, A., Janich, P., Morton, J.P., Athineos, D., Kang, T.W., Lasitschka, F., Andrulis, M., et al. (2013). A complex secretory program orchestrated by the inflammasome controls paracrine senescence. Nat Cell Biol *15*, 978-990. 10.1038/ncb2784.

Afonina, I.S., Tynan, G.A., Logue, S.E., Cullen, S.P., Bots, M., Luthi, A.U., Reeves, E.P., McElvaney, N.G., Medema, J.P., Lavelle, E.C., and Martin, S.J. (2011). Granzyme B-dependent proteolysis acts as a switch to enhance the proinflammatory activity of IL-1alpha. Mol Cell *44*, 265-278. 10.1016/j.molcel.2011.07.037.

Albrengues, J., Bertero, T., Grasset, E., Bonan, S., Maiel, M., Bourget, I., Philippe, C., Herraiz Serrano, C., Benamar, S., Croce, O., et al. (2015). Epigenetic switch drives the conversion of fibroblasts into proinvasive cancer-associated fibroblasts. Nat Commun *6*, 10204. 10.1038/ncomms10204.

Alheim, K., McDowell, T.L., Symons, J.A., Duff, G.W., and Bartfai, T. (1996). An AP-1 site is involved in the NGF induction of IL-1 alpha in PC12 cells. Neurochem Int *29*, 487-496. 10.1016/0197-0186(96)00017-4.

Almeida, L.O., Guimaraes, D.M., Martins, M.D., Martins, M.A.T., Warner, K.A., Nor, J.E., Castilho, R.M., and Squarize, C.H. (2017). Unlocking the chromatin of adenoid cystic carcinomas using HDAC inhibitors sensitize cancer stem cells to cisplatin and induces tumor senescence. Stem Cell Res *21*, 94-105. 10.1016/j.scr.2017.04.003.

Alspach, E., Flanagan, K.C., Luo, X., Ruhland, M.K., Huang, H., Pazolli, E., Donlin, M.J., Marsh, T., Piwnica-Worms, D., Monahan, J., et al. (2014). p38MAPK plays a crucial role in stromal-mediated tumorigenesis. Cancer Discov *4*, 716-729. 10.1158/2159-8290.CD-13-0743.

Aoyagi, Y., Oda, T., Kinoshita, T., Nakahashi, C., Hasebe, T., Ohkohchi, N., and Ochiai, A. (2004). Overexpression of TGF-beta by infiltrated granulocytes correlates with the expression of collagen mRNA in pancreatic cancer. Br J Cancer *91*, 1316-1326. 10.1038/sj.bjc.6602141.

Arend, W.P., and Guthridge, C.J. (2000). Biological role of interleukin 1 receptor antagonist isoforms. Ann Rheum Dis *59 Suppl 1*, i60-64. 10.1136/ard.59.suppl_1.i60.

Arend, W.P., Malyak, M., Guthridge, C.J., and Gabay, C. (1998). Interleukin-1 receptor antagonist: role in biology. Annu Rev Immunol *16*, 27-55. 10.1146/annurev.immunol.16.1.27.

Armanios, M. (2013). Telomeres and age-related disease: how telomere biology informs clinical paradigms. J Clin Invest *123*, 996-1002. 10.1172/JCI66370.

Baar, M.P., Brandt, R.M.C., Putavet, D.A., Klein, J.D.D., Derks, K.W.J., Bourgeois, B.R.M., Stryeck, S., Rijksen, Y., van Willigenburg, H., Feijtel, D.A., et al. (2017). Targeted Apoptosis of Senescent Cells Restores Tissue Homeostasis in Response to Chemotoxicity and Aging. Cell *169*, 132-147 e116. 10.1016/j.cell.2017.02.031.

Bach, S.P., Hill, J., Monson, J.R., Simson, J.N., Lane, L., Merrie, A., Warren, B., Mortensen, N.J., Association of Coloproctology of Great, B., and Ireland Transanal Endoscopic Microsurgery, C. (2009). A predictive model for local recurrence after transanal endoscopic microsurgery for rectal cancer. Br J Surg *96*, 280-290. 10.1002/bjs.6456.

Bailly, S., Fay, M., Israel, N., and Gougerot-Pocidalo, M.A. (1996). The transcription factor AP-1 binds to the human interleukin 1 alpha promoter. Eur Cytokine Netw *7*, 125-128.

Barker, H.E., Paget, J.T., Khan, A.A., and Harrington, K.J. (2015). The tumour microenvironment after radiotherapy: mechanisms of resistance and recurrence. Nat Rev Cancer *15*, 409-425. 10.1038/nrc3958.

Bartkova, J., Rezaei, N., Liontos, M., Karakaidos, P., Kletsas, D., Issaeva, N., Vassiliou, L.V., Kolettas, E., Niforou, K., Zoumpourlis, V.C., et al. (2006). Oncogene-induced senescence is part of the tumorigenesis barrier imposed by DNA damage checkpoints. Nature *444*, 633-637. 10.1038/nature05268.
Baskar, R., Lee, K.A., Yeo, R., and Yeoh, K.W. (2012). Cancer and radiation therapy: current advances and future directions. Int J Med Sci *9*, 193-199. 10.7150/ijms.3635.
Bersudsky, M., Luski, L., Fishman, D., White, R.M., Ziv-Sokolovskaya, N., Dotan, S., Rider, P., Kaplanov, I., Aychek, T., Dinarello, C.A., et al. (2014). Non-redundant properties of IL-1alpha and IL-1beta during acute colon inflammation in mice. Gut *63*, 598-609. 10.1136/gutjnl-2012-303329.
Beuscher, H.U., Nickells, M.W., and Colten, H.R. (1988). The precursor of interleukin-1 alpha is phosphorylated at residue serine 90. J Biol Chem *263*, 4023-4028.
Bhagat, T.D., Von Ahrens, D., Dawlaty, M., Zou, Y., Baddour, J., Achreja, A., Zhao, H., Yang, L., Patel, B., Kwak, C., et al. (2019). Lactate-mediated epigenetic reprogramming regulates formation of human pancreatic cancer-associated fibroblasts. Elife *8*. 10.7554/eLife.50663.
Bieging, K.T., Mello, S.S., and Attardi, L.D. (2014). Unravelling mechanisms of p53-mediated tumour suppression. Nat Rev Cancer *14*, 359-370. 10.1038/nrc3711.
Biffi, G., Oni, T.E., Spielman, B., Hao, Y., Elyada, E., Park, Y., Preall, J., and Tuveson, D.A. (2019). IL1-Induced JAK/STAT Signaling Is Antagonized by TGFbeta to Shape CAF Heterogeneity in Pancreatic Ductal Adenocarcinoma. Cancer Discov *9*, 282-301. 10.1158/2159-8290.CD-18-0710.
Biffi, G., and Tuveson, D.A. (2021). Diversity and Biology of Cancer-Associated Fibroblasts. Physiol Rev *101*, 147-176. 10.1152/physrev.00048.2019.
Bioque, G., Crusius, J.B., Koutroubakis, I., Bouma, G., Kostense, P.J., Meuwissen, S.G., and Pena, A.S. (1995). Allelic polymorphism in IL-1 beta and IL-1 receptor antagonist (IL-1Ra) genes in inflammatory bowel disease. Clin Exp Immunol *102*, 379-383. 10.1111/j.1365-2249.1995.tb03793.x.
Birch, J., and Gil, J. (2020). Senescence and the SASP: many therapeutic avenues. Genes Dev *34*, 1565-1576. 10.1101/gad.343129.120.
Bodnar, A.G., Ouellette, M., Frolkis, M., Holt, S.E., Chiu, C.P., Morin, G.B., Harley, C.B., Shay, J.W., Lichtsteiner, S., and Wright, W.E. (1998). Extension of life-span by introduction of telomerase into normal human cells. Science *279*, 349-352. 10.1126/science.279.5349.349.
Bohnenberger, H., Kaderali, L., Strobel, P., Yepes, D., Plessmann, U., Dharia, N.V., Yao, S., Heydt, C., Merkelbach-Bruse, S., Emmert, A., et al. (2018). Comparative proteomics reveals a diagnostic signature for pulmonary head-and-neck cancer metastasis. EMBO Mol Med *10*. 10.15252/emmm.201708428.
Bonnans, C., Chou, J., and Werb, Z. (2014). Remodelling the extracellular matrix in development and disease. Nat Rev Mol Cell Biol *15*, 786-801. 10.1038/nrm3904.
Boraschi, D., Bossu, P., Ruggiero, P., Tagliabue, A., Bertini, R., Macchia, G., Gasbarro, C., Pellegrini, L., Melillo, G., Ulisse, E., et al. (1995). Mapping of receptor binding sites on IL-1 beta by reconstruction of IL-1ra-like domains. J Immunol *155*, 4719-4725.
Braendengen, M., Tveit, K.M., Berglund, A., Birkemeyer, E., Frykholm, G., Pahlman, L., Wiig, J.N., Bystrom, P., Bujko, K., and Glimelius, B. (2008). Randomized phase III study comparing preoperative radiotherapy with chemoradiotherapy in nonresectable rectal cancer. J Clin Oncol *26*, 3687-3694. 10.1200/JCO.2007.15.3858.
Brody, D.T., and Durum, S.K. (1989). Membrane IL-1: IL-1 alpha precursor binds to the plasma membrane via a lectin-like interaction. J Immunol *143*, 1183-1187.
Brough, D., and Denes, A. (2015). Interleukin-1alpha and brain inflammation. IUBMB Life *67*, 323-330. 10.1002/iub.1377.

Bruzzese, F., Hagglof, C., Leone, A., Sjoberg, E., Roca, M.S., Kiflemariam, S., Sjoblom, T., Hammarsten, P., Egevad, L., Bergh, A., et al. (2014). Local and systemic protumorigenic effects of cancer-associated fibroblast-derived GDF15. Cancer Res *74*, 3408-3417. 10.1158/0008-5472.CAN-13-2259.
Budinska, E., Popovici, V., Tejpar, S., D'Ario, G., Lapique, N., Sikora, K.O., Di Narzo, A.F., Yan, P., Hodgson, J.G., Weinrich, S., et al. (2013). Gene expression patterns unveil a new level of molecular heterogeneity in colorectal cancer. J Pathol *231*, 63-76. 10.1002/path.4212.
Buechler, M.B., Pradhan, R.N., Krishnamurty, A.T., Cox, C., Calviello, A.K., Wang, A.W., Yang, Y.A., Tam, L., Caothien, R., Roose-Girma, M., et al. (2021). Cross-tissue organization of the fibroblast lineage. Nature *593*, 575-579. 10.1038/s41586-021-03549-5.
Bujko, K., Nowacki, M.P., Nasierowska-Guttmejer, A., Michalski, W., Bebenek, M., and Kryj, M. (2006). Long-term results of a randomized trial comparing preoperative short-course radiotherapy with preoperative conventionally fractionated chemoradiation for rectal cancer. Br J Surg *93*, 1215-1223. 10.1002/bjs.5506.
Burger, R., Le Gouill, S., Tai, Y.T., Shringarpure, R., Tassone, P., Neri, P., Podar, K., Catley, L., Hideshima, T., Chauhan, D., et al. (2009). Janus kinase inhibitor INCB20 has antiproliferative and apoptotic effects on human myeloma cells in vitro and in vivo. Mol Cancer Ther *8*, 26-35. 10.1158/1535-7163.MCT-08-0149.
Butcher, C., Steinkasserer, A., Tejura, S., and Lennard, A.C. (1994). Comparison of two promoters controlling expression of secreted or intracellular IL-1 receptor antagonist. J Immunol *153*, 701-711.
Calon, A., Espinet, E., Palomo-Ponce, S., Tauriello, D.V., Iglesias, M., Cespedes, M.V., Sevillano, M., Nadal, C., Jung, P., Zhang, X.H., et al. (2012). Dependency of colorectal cancer on a TGF-beta-driven program in stromal cells for metastasis initiation. Cancer Cell *22*, 571-584. 10.1016/j.ccr.2012.08.013.
Calvo, F., Ege, N., Grande-Garcia, A., Hooper, S., Jenkins, R.P., Chaudhry, S.I., Harrington, K., Williamson, P., Moeendarbary, E., Charras, G., and Sahai, E. (2013). Mechanotransduction and YAP-dependent matrix remodelling is required for the generation and maintenance of cancer-associated fibroblasts. Nat Cell Biol *15*, 637-646. 10.1038/ncb2756.
Cannan, W.J., and Pederson, D.S. (2016). Mechanisms and Consequences of Double-Strand DNA Break Formation in Chromatin. J Cell Physiol *231*, 3-14. 10.1002/jcp.25048.
Carpenter, V.J., Saleh, T., and Gewirtz, D.A. (2021). Senolytics for Cancer Therapy: Is All That Glitters Really Gold? Cancers (Basel) *13*. 10.3390/cancers13040723.
Carruth, L.M., Demczuk, S., and Mizel, S.B. (1991). Involvement of a calpain-like protease in the processing of the murine interleukin 1 alpha precursor. J Biol Chem *266*, 12162-12167.
Casini-Raggi, V., Kam, L., Chong, Y.J., Fiocchi, C., Pizarro, T.T., and Cominelli, F. (1995). Mucosal imbalance of IL-1 and IL-1 receptor antagonist in inflammatory bowel disease. A novel mechanism of chronic intestinal inflammation. J Immunol *154*, 2434-2440.
Cauci, S., Buligan, C., Rocchi, F., Salvador, I., Xodo, L., and Stinco, G. (2019). Interleukin 1 receptor antagonist gene variable number of tandem repeats polymorphism and cutaneous melanoma. Oncol Lett *18*, 5759-5768. 10.3892/ol.2019.10923.
Cesare, A.J., and Karlseder, J. (2012). A three-state model of telomere control over human proliferative boundaries. Curr Opin Cell Biol *24*, 731-738. 10.1016/j.ceb.2012.08.007.
Chang, B.D., Broude, E.V., Dokmanovic, M., Zhu, H., Ruth, A., Xuan, Y., Kandel, E.S., Lausch, E., Christov, K., and Roninson, I.B. (1999). A senescence-like phenotype distinguishes tumor cells that undergo terminal proliferation arrest after exposure to anticancer agents. Cancer Res *59*, 3761-3767.
Chang, J., Wang, Y., Shao, L., Laberge, R.M., Demaria, M., Campisi, J., Janakiraman, K., Sharpless, N.E., Ding, S., Feng, W., et al. (2016). Clearance of senescent cells by ABT263 rejuvenates aged hematopoietic stem cells in mice. Nat Med *22*, 78-83. 10.1038/nm.4010.

Charbonneau, B., Block, M.S., Bamlet, W.R., Vierkant, R.A., Kalli, K.R., Fogarty, Z., Rider, D.N., Sellers, T.A., Tworoger, S.S., Poole, E., et al. (2014). Risk of ovarian cancer and the NF-kappaB pathway: genetic association with IL1A and TNFSF10. Cancer Res *74*, 852-861. 10.1158/0008-5472.CAN-13-1051.
Chauhan, V.P., Martin, J.D., Liu, H., Lacorre, D.A., Jain, S.R., Kozin, S.V., Stylianopoulos, T., Mousa, A.S., Han, X., Adstamongkonkul, P., et al. (2013). Angiotensin inhibition enhances drug delivery and potentiates chemotherapy by decompressing tumour blood vessels. Nat Commun *4*, 2516. 10.1038/ncomms3516.
Chen, Q., and Ames, B.N. (1994). Senescence-like growth arrest induced by hydrogen peroxide in human diploid fibroblast F65 cells. Proc Natl Acad Sci U S A *91*, 4130-4134. 10.1073/pnas.91.10.4130.
Chen, Q., Fischer, A., Reagan, J.D., Yan, L.J., and Ames, B.N. (1995). Oxidative DNA damage and senescence of human diploid fibroblast cells. Proc Natl Acad Sci U S A *92*, 4337-4341. 10.1073/pnas.92.10.4337.
Chen, X., and Song, E. (2019). Turning foes to friends: targeting cancer-associated fibroblasts. Nat Rev Drug Discov *18*, 99-115. 10.1038/s41573-018-0004-1.
Chen, Y., McAndrews, K.M., and Kalluri, R. (2021). Clinical and therapeutic relevance of cancer-associated fibroblasts. Nat Rev Clin Oncol. 10.1038/s41571-021-00546-5.
Chien, Y., Scuoppo, C., Wang, X., Fang, X., Balgley, B., Bolden, J.E., Premsrirut, P., Luo, W., Chicas, A., Lee, C.S., et al. (2011). Control of the senescence-associated secretory phenotype by NF-kappaB promotes senescence and enhances chemosensitivity. Genes Dev *25*, 2125-2136. 10.1101/gad.17276711.
Chomarat, P., Banchereau, J., Davoust, J., and Palucka, A.K. (2000). IL-6 switches the differentiation of monocytes from dendritic cells to macrophages. Nat Immunol *1*, 510-514. 10.1038/82763.
Cisel, B., Pietrzak, L., Michalski, W., Wyrwicz, L., Rutkowski, A., Kosakowska, E., Cencelewicz, A., Spalek, M., Polkowski, W., Jankiewicz, M., et al. (2019). Long-course preoperative chemoradiation versus 5 x 5 Gy and consolidation chemotherapy for clinical T4 and fixed clinical T3 rectal cancer: long-term results of the randomized Polish II study. Ann Oncol *30*, 1298-1303. 10.1093/annonc/mdz186.
Clay, F.E., Cork, M.J., Tarlow, J.K., Blakemore, A.I., Harrington, C.I., Lewis, F., and Duff, G.W. (1994). Interleukin 1 receptor antagonist gene polymorphism association with lichen sclerosus. Hum Genet *94*, 407-410. 10.1007/BF00201602.
Cohen, I., Rider, P., Carmi, Y., Braiman, A., Dotan, S., White, M.R., Voronov, E., Martin, M.U., Dinarello, C.A., and Apte, R.N. (2010). Differential release of chromatin-bound IL-1alpha discriminates between necrotic and apoptotic cell death by the ability to induce sterile inflammation. Proc Natl Acad Sci U S A *107*, 2574-2579. 10.1073/pnas.0915018107.
Coleman, C.N., Higgins, G.S., Brown, J.M., Baumann, M., Kirsch, D.G., Willers, H., Prasanna, P.G., Dewhirst, M.W., Bernhard, E.J., and Ahmed, M.M. (2016). Improving the Predictive Value of Preclinical Studies in Support of Radiotherapy Clinical Trials. Clin Cancer Res *22*, 3138-3147. 10.1158/1078-0432.CCR-16-0069.
Cominelli, F., and Pizarro, T.T. (1996). Interleukin-1 and interleukin-1 receptor antagonist in inflammatory bowel disease. Aliment Pharmacol Ther *10 Suppl 2*, 49-53; discussion 54. 10.1046/j.1365-2036.1996.22164020.x.
Coppe, J.P., Desprez, P.Y., Krtolica, A., and Campisi, J. (2010). The senescence-associated secretory phenotype: the dark side of tumor suppression. Annu Rev Pathol *5*, 99-118. 10.1146/annurev-pathol-121808-102144.
Costa, A., Kieffer, Y., Scholer-Dahirel, A., Pelon, F., Bourachot, B., Cardon, M., Sirven, P., Magagna, I., Fuhrmann, L., Bernard, C., et al. (2018). Fibroblast Heterogeneity and

Immunosuppressive Environment in Human Breast Cancer. Cancer Cell *33*, 463-479 e410. 10.1016/j.ccell.2018.01.011.
Cotarelo, C.L., Schad, A., Kirkpatrick, C.J., Sleeman, J.P., Springer, E., Schmidt, M., and Thaler, S. (2016). Detection of cellular senescence within human invasive breast carcinomas distinguishes different breast tumor subtypes. Oncotarget *7*, 74846-74859. 10.18632/oncotarget.12432.
Cox, T.R. (2021). The matrix in cancer. Nat Rev Cancer *21*, 217-238. 10.1038/s41568-020-00329-7.
Cui, J.J. (2014). Targeting receptor tyrosine kinase MET in cancer: small molecule inhibitors and clinical progress. J Med Chem *57*, 4427-4453. 10.1021/jm401427c.
d'Adda di Fagagna, F. (2008). Living on a break: cellular senescence as a DNA-damage response. Nat Rev Cancer *8*, 512-522. 10.1038/nrc2440.
d'Adda di Fagagna, F., Reaper, P.M., Clay-Farrace, L., Fiegler, H., Carr, P., Von Zglinicki, T., Saretzki, G., Carter, N.P., and Jackson, S.P. (2003). A DNA damage checkpoint response in telomere-initiated senescence. Nature *426*, 194-198. 10.1038/nature02118.
Dabritz, J.H., Yu, Y., Milanovic, M., Schonlein, M., Rosenfeldt, M.T., Dorr, J.R., Kaufmann, A.M., Dorken, B., and Schmitt, C.A. (2016). CD20-Targeting Immunotherapy Promotes Cellular Senescence in B-Cell Lymphoma. Mol Cancer Ther *15*, 1074-1081. 10.1158/1535-7163.MCT-15-0627.
Davidson, S., Efremova, M., Riedel, A., Mahata, B., Pramanik, J., Huuhtanen, J., Kar, G., Vento-Tormo, R., Hagai, T., Chen, X., et al. (2020). Single-Cell RNA Sequencing Reveals a Dynamic Stromal Niche That Supports Tumor Growth. Cell Rep *31*, 107628. 10.1016/j.celrep.2020.107628.
De Sousa, E.M.F., Wang, X., Jansen, M., Fessler, E., Trinh, A., de Rooij, L.P., de Jong, J.H., de Boer, O.J., van Leersum, R., Bijlsma, M.F., et al. (2013). Poor-prognosis colon cancer is defined by a molecularly distinct subtype and develops from serrated precursor lesions. Nat Med *19*, 614-618. 10.1038/nm.3174.
Debacq-Chainiaux, F., Boilan, E., Dedessus Le Moutier, J., Weemaels, G., and Toussaint, O. (2010). p38(MAPK) in the senescence of human and murine fibroblasts. Adv Exp Med Biol *694*, 126-137. 10.1007/978-1-4419-7002-2_10.
Demaria, M., O'Leary, M.N., Chang, J., Shao, L., Liu, S., Alimirah, F., Koenig, K., Le, C., Mitin, N., Deal, A.M., et al. (2017). Cellular Senescence Promotes Adverse Effects of Chemotherapy and Cancer Relapse. Cancer Discov *7*, 165-176. 10.1158/2159-8290.CD-16-0241.
Deng, Q.F., Su, B.O., Zhao, Y.M., Tang, L., Zhang, J., and Zhou, C.C. (2016a). Integrin beta1-mediated acquired gefitinib resistance in non-small cell lung cancer cells occurs via the phosphoinositide 3-kinase-dependent pathway. Oncol Lett *11*, 535-542. 10.3892/ol.2015.3945.
Deng, Y., Chi, P., Lan, P., Wang, L., Chen, W., Cui, L., Chen, D., Cao, J., Wei, H., Peng, X., et al. (2016b). Modified FOLFOX6 With or Without Radiation Versus Fluorouracil and Leucovorin With Radiation in Neoadjuvant Treatment of Locally Advanced Rectal Cancer: Initial Results of the Chinese FOWARC Multicenter, Open-Label, Randomized Three-Arm Phase III Trial. J Clin Oncol *34*, 3300-3307. 10.1200/JCO.2016.66.6198.
Deying, W., Feng, G., Shumei, L., Hui, Z., Ming, L., and Hongqing, W. (2017). CAF-derived HGF promotes cell proliferation and drug resistance by up-regulating the c-Met/PI3K/Akt and GRP78 signalling in ovarian cancer cells. Biosci Rep *37*. 10.1042/BSR20160470.
Di Micco, R., Krizhanovsky, V., Baker, D., and d'Adda di Fagagna, F. (2021). Cellular senescence in ageing: from mechanisms to therapeutic opportunities. Nat Rev Mol Cell Biol *22*, 75-95. 10.1038/s41580-020-00314-w.
Di Micco, R., Sulli, G., Dobreva, M., Liontos, M., Botrugno, O.A., Gargiulo, G., dal Zuffo, R., Matti, V., d'Ario, G., Montani, E., et al. (2011). Interplay between oncogene-induced DNA

damage response and heterochromatin in senescence and cancer. Nat Cell Biol *13*, 292-302. 10.1038/ncb2170.
Di Paolo, N.C., and Shayakhmetov, D.M. (2016). Interleukin 1alpha and the inflammatory process. Nat Immunol *17*, 906-913. 10.1038/ni.3503.
Dienstmann, R., Vermeulen, L., Guinney, J., Kopetz, S., Tejpar, S., and Tabernero, J. (2017). Consensus molecular subtypes and the evolution of precision medicine in colorectal cancer. Nat Rev Cancer *17*, 79-92. 10.1038/nrc.2016.126.
Dijkgraaf, E.M., Santegoets, S.J., Reyners, A.K., Goedemans, R., Wouters, M.C., Kenter, G.G., van Erkel, A.R., van Poelgeest, M.I., Nijman, H.W., van der Hoeven, J.J., et al. (2015). A phase I trial combining carboplatin/doxorubicin with tocilizumab, an anti-IL-6R monoclonal antibody, and interferon-alpha2b in patients with recurrent epithelial ovarian cancer. Ann Oncol *26*, 2141-2149. 10.1093/annonc/mdv309.
Dinarello, C.A. (1996). Biologic basis for interleukin-1 in disease. Blood *87*, 2095-2147.
Dinarello, C.A. (2009). Immunological and inflammatory functions of the interleukin-1 family. Annu Rev Immunol *27*, 519-550. 10.1146/annurev.immunol.021908.132612.
Dinarello, C.A. (2018). Overview of the IL-1 family in innate inflammation and acquired immunity. Immunol Rev *281*, 8-27. 10.1111/imr.12621.
Dinarello, C.A., Rosenwasser, L.J., and Wolff, S.M. (1981). Demonstration of a circulating suppressor factor of thymocyte proliferation during endotoxin fever in humans. J Immunol *127*, 2517-2519.
Ding, X., Ji, J., Jiang, J., Cai, Q., Wang, C., Shi, M., Yu, Y., Zhu, Z., and Zhang, J. (2018). HGF-mediated crosstalk between cancer-associated fibroblasts and MET-unamplified gastric cancer cells activates coordinated tumorigenesis and metastasis. Cell Death Dis *9*, 867. 10.1038/s41419-018-0922-1.
Drost, J., van Jaarsveld, R.H., Ponsioen, B., Zimberlin, C., van Boxtel, R., Buijs, A., Sachs, N., Overmeer, R.M., Offerhaus, G.J., Begthel, H., et al. (2015). Sequential cancer mutations in cultured human intestinal stem cells. Nature *521*, 43-47. 10.1038/nature14415.
Duluc, C., Moatassim-Billah, S., Chalabi-Dchar, M., Perraud, A., Samain, R., Breibach, F., Gayral, M., Cordelier, P., Delisle, M.B., Bousquet-Dubouch, M.P., et al. (2015). Pharmacological targeting of the protein synthesis mTOR/4E-BP1 pathway in cancer-associated fibroblasts abrogates pancreatic tumour chemoresistance. EMBO Mol Med *7*, 735-753. 10.15252/emmm.201404346.
Dvorak, H.F. (1986). Tumors: wounds that do not heal. Similarities between tumor stroma generation and wound healing. N Engl J Med *315*, 1650-1659. 10.1056/NEJM198612253152606.
Ebbinghaus, C., Scheuermann, J., Neri, D., and Elia, G. (2004). Diagnostic and therapeutic applications of recombinant antibodies: targeting the extra-domain B of fibronectin, a marker of tumor angiogenesis. Curr Pharm Des *10*, 1537-1549. 10.2174/1381612043384808.
Ecker, B.L., Kaur, A., Douglass, S.M., Webster, M.R., Almeida, F.V., Marino, G.E., Sinnamon, A.J., Neuwirth, M.G., Alicea, G.M., Ndoye, A., et al. (2019). Age-Related Changes in HAPLN1 Increase Lymphatic Permeability and Affect Routes of Melanoma Metastasis. Cancer Discov *9*, 82-95. 10.1158/2159-8290.CD-18-0168.
Edge, S.B., and Compton, C.C. (2010). The American Joint Committee on Cancer: the 7th edition of the AJCC cancer staging manual and the future of TNM. Ann Surg Oncol *17*, 1471-1474. 10.1245/s10434-010-0985-4.
Eide, P.W., Bruun, J., Lothe, R.A., and Sveen, A. (2017). CMScaller: an R package for consensus molecular subtyping of colorectal cancer pre-clinical models. Sci Rep *7*, 16618. 10.1038/s41598-017-16747-x.

Elknerova, K., Myslivcova, D., Lacinova, Z., Marinov, I., Uherkova, L., and Stockbauer, P. (2011). Epigenetic modulation of gene expression of human leukemia cell lines - induction of cell death and senescence. Neoplasma *58*, 35-44. 10.4149/neo_2011_01_35.
Elyada, E., Bolisetty, M., Laise, P., Flynn, W.F., Courtois, E.T., Burkhart, R.A., Teinor, J.A., Belleau, P., Biffi, G., Lucito, M.S., et al. (2019). Cross-Species Single-Cell Analysis of Pancreatic Ductal Adenocarcinoma Reveals Antigen-Presenting Cancer-Associated Fibroblasts. Cancer Discov *9*, 1102-1123. 10.1158/2159-8290.CD-19-0094.
Erez, N., Truitt, M., Olson, P., Arron, S.T., and Hanahan, D. (2010). Cancer-Associated Fibroblasts Are Activated in Incipient Neoplasia to Orchestrate Tumor-Promoting Inflammation in an NF-kappaB-Dependent Manner. Cancer Cell *17*, 135-147. 10.1016/j.ccr.2009.12.041.
Erlandsson, J., Holm, T., Pettersson, D., Berglund, A., Cedermark, B., Radu, C., Johansson, H., Machado, M., Hjern, F., Hallbook, O., et al. (2017). Optimal fractionation of preoperative radiotherapy and timing to surgery for rectal cancer (Stockholm III): a multicentre, randomised, non-blinded, phase 3, non-inferiority trial. Lancet Oncol *18*, 336-346. 10.1016/S1470-2045(17)30086-4.
Evans, R.J., Bray, J., Childs, J.D., Vigers, G.P., Brandhuber, B.J., Skalicky, J.J., Thompson, R.C., and Eisenberg, S.P. (1995). Mapping receptor binding sites in interleukin (IL)-1 receptor antagonist and IL-1 beta by site-directed mutagenesis. Identification of a single site in IL-1ra and two sites in IL-1 beta. J Biol Chem *270*, 11477-11483. 10.1074/jbc.270.19.11477.
Ewald, J.A., Desotelle, J.A., Wilding, G., and Jarrard, D.F. (2010). Therapy-induced senescence in cancer. J Natl Cancer Inst *102*, 1536-1546. 10.1093/jnci/djq364.
Faget, D.V., Ren, Q., and Stewart, S.A. (2019). Unmasking senescence: context-dependent effects of SASP in cancer. Nat Rev Cancer *19*, 439-453. 10.1038/s41568-019-0156-2.
Fazeli, M.S., and Keramati, M.R. (2015). Rectal cancer: a review. Med J Islam Repub Iran *29*, 171.
Fearon, D.T. (2014). The carcinoma-associated fibroblast expressing fibroblast activation protein and escape from immune surveillance. Cancer Immunol Res *2*, 187-193. 10.1158/2326-6066.CIR-14-0002.
Fearon, E.R. (2011). Molecular genetics of colorectal cancer. Annu Rev Pathol *6*, 479-507. 10.1146/annurev-pathol-011110-130235.
Ferretti, M., Casini-Raggi, V., Pizarro, T.T., Eisenberg, S.P., Nast, C.C., and Cominelli, F. (1994). Neutralization of endogenous IL-1 receptor antagonist exacerbates and prolongs inflammation in rabbit immune colitis. J Clin Invest *94*, 449-453. 10.1172/JCI117345.
Fiaschi, T., Giannoni, E., Taddei, M.L., Cirri, P., Marini, A., Pintus, G., Nativi, C., Richichi, B., Scozzafava, A., Carta, F., et al. (2013). Carbonic anhydrase IX from cancer-associated fibroblasts drives epithelial-mesenchymal transition in prostate carcinoma cells. Cell Cycle *12*, 1791-1801. 10.4161/cc.24902.
Flanagan, K.C., Alspach, E., Pazolli, E., Parajuli, S., Ren, Q., Arthur, L.L., Tapia, R., and Stewart, S.A. (2018). c-Myb and C/EBPbeta regulate OPN and other senescence-associated secretory phenotype factors. Oncotarget *9*, 21-36. 10.18632/oncotarget.22940.
Fokas, E., Fietkau, R., Hartmann, A., Hohenberger, W., Grutzmann, R., Ghadimi, M., Liersch, T., Strobel, P., Grabenbauer, G.G., Graeven, U., et al. (2018). Neoadjuvant rectal score as individual-level surrogate for disease-free survival in rectal cancer in the CAO/ARO/AIO-04 randomized phase III trial. Ann Oncol *29*, 1521-1527. 10.1093/annonc/mdy143.
Fokas, E., Glynne-Jones, R., Appelt, A., Beets-Tan, R., Beets, G., Haustermans, K., Marijnen, C., Minsky, B.D., Ludmir, E., Quirke, P., et al. (2020). Outcome measures in multimodal rectal cancer trials. Lancet Oncol *21*, e252-e264. 10.1016/S1470-2045(20)30024-3.
Fokas, E., Liersch, T., Fietkau, R., Hohenberger, W., Beissbarth, T., Hess, C., Becker, H., Ghadimi, M., Mrak, K., Merkel, S., et al. (2014). Tumor regression grading after preoperative

chemoradiotherapy for locally advanced rectal carcinoma revisited: updated results of the CAO/ARO/AIO-94 trial. J Clin Oncol *32*, 1554-1562. 10.1200/JCO.2013.54.3769.
Fokas, E., Strobel, P., Fietkau, R., Ghadimi, M., Liersch, T., Grabenbauer, G.G., Hartmann, A., Kaufmann, M., Sauer, R., Graeven, U., et al. (2017). Tumor Regression Grading After Preoperative Chemoradiotherapy as a Prognostic Factor and Individual-Level Surrogate for Disease-Free Survival in Rectal Cancer. J Natl Cancer Inst *109*. 10.1093/jnci/djx095.
Foster, C.T., Gualdrini, F., and Treisman, R. (2017). Mutual dependence of the MRTF-SRF and YAP-TEAD pathways in cancer-associated fibroblasts is indirect and mediated by cytoskeletal dynamics. Genes Dev *31*, 2361-2375. 10.1101/gad.304501.117.
Freigang, S., Ampenberger, F., Weiss, A., Kanneganti, T.D., Iwakura, Y., Hersberger, M., and Kopf, M. (2013). Fatty acid-induced mitochondrial uncoupling elicits inflammasome-independent IL-1alpha and sterile vascular inflammation in atherosclerosis. Nat Immunol *14*, 1045-1053. 10.1038/ni.2704.
Freitas-Rodriguez, S., Folgueras, A.R., and Lopez-Otin, C. (2017). The role of matrix metalloproteinases in aging: Tissue remodeling and beyond. Biochim Biophys Acta Mol Cell Res *1864*, 2015-2025. 10.1016/j.bbamcr.2017.05.007.
Freund, A., Patil, C.K., and Campisi, J. (2011). p38MAPK is a novel DNA damage response-independent regulator of the senescence-associated secretory phenotype. EMBO J *30*, 1536-1548. 10.1038/emboj.2011.69.
Friedl, P., Locker, J., Sahai, E., and Segall, J.E. (2012). Classifying collective cancer cell invasion. Nat Cell Biol *14*, 777-783. 10.1038/ncb2548.
Froeling, F.E., Feig, C., Chelala, C., Dobson, R., Mein, C.E., Tuveson, D.A., Clevers, H., Hart, I.R., and Kocher, H.M. (2011). Retinoic acid-induced pancreatic stellate cell quiescence reduces paracrine Wnt-beta-catenin signaling to slow tumor progression. Gastroenterology *141*, 1486-1497, 1497 e1481-1414. 10.1053/j.gastro.2011.06.047.
Fuhrmann-Stroissnigg, H., Ling, Y.Y., Zhao, J., McGowan, S.J., Zhu, Y., Brooks, R.W., Grassi, D., Gregg, S.Q., Stripay, J.L., Dorronsoro, A., et al. (2017). Identification of HSP90 inhibitors as a novel class of senolytics. Nat Commun *8*, 422. 10.1038/s41467-017-00314-z.
Fukumura, D., Xavier, R., Sugiura, T., Chen, Y., Park, E.C., Lu, N., Selig, M., Nielsen, G., Taksir, T., Jain, R.K., and Seed, B. (1998). Tumor induction of VEGF promoter activity in stromal cells. Cell *94*, 715-725. 10.1016/s0092-8674(00)81731-6.
Fumagalli, M., Rossiello, F., Clerici, M., Barozzi, S., Cittaro, D., Kaplunov, J.M., Bucci, G., Dobreva, M., Matti, V., Beausejour, C.M., et al. (2012). Telomeric DNA damage is irreparable and causes persistent DNA-damage-response activation. Nat Cell Biol *14*, 355-365. 10.1038/ncb2466.
Fung, A.S., Wu, L., and Tannock, I.F. (2009). Concurrent and sequential administration of chemotherapy and the Mammalian target of rapamycin inhibitor temsirolimus in human cancer cells and xenografts. Clin Cancer Res *15*, 5389-5395. 10.1158/1078-0432.CCR-08-3007.
Gaggioli, C., Hooper, S., Hidalgo-Carcedo, C., Grosse, R., Marshall, J.F., Harrington, K., and Sahai, E. (2007). Fibroblast-led collective invasion of carcinoma cells with differing roles for RhoGTPases in leading and following cells. Nat Cell Biol *9*, 1392-1400. 10.1038/ncb1658.
Ganesh, K., and Massague, J. (2021). Targeting metastatic cancer. Nat Med *27*, 34-44. 10.1038/s41591-020-01195-4.
Ganesh, K., Wu, C., O'Rourke, K.P., Szeglin, B.C., Zheng, Y., Sauve, C.G., Adileh, M., Wasserman, I., Marco, M.R., Kim, A.S., et al. (2019). A rectal cancer organoid platform to study individual responses to chemoradiation. Nat Med *25*, 1607-1614. 10.1038/s41591-019-0584-2.
Garlanda, C., Dinarello, C.A., and Mantovani, A. (2013). The interleukin-1 family: back to the future. Immunity *39*, 1003-1018. 10.1016/j.immuni.2013.11.010.

Garlanda, C., and Mantovani, A. (2021). Interleukin-1 in tumor progression, therapy, and prevention. Cancer Cell *39*, 1023-1027. 10.1016/j.ccell.2021.04.011.
Gerard, J.P., Ortholan, C., Benezery, K., Ginot, A., Hannoun-Levi, J.M., Chamorey, E., Benchimol, D., and Francois, E. (2008). Contact X-ray therapy for rectal cancer: experience in Centre Antoine-Lacassagne, Nice, 2002-2006. Int J Radiat Oncol Biol Phys *72*, 665-670. 10.1016/j.ijrobp.2008.01.030.
Gewirtz, D.A., Holt, S.E., and Elmore, L.W. (2008). Accelerated senescence: an emerging role in tumor cell response to chemotherapy and radiation. Biochem Pharmacol *76*, 947-957. 10.1016/j.bcp.2008.06.024.
Gluck, S., Guey, B., Gulen, M.F., Wolter, K., Kang, T.W., Schmacke, N.A., Bridgeman, A., Rehwinkel, J., Zender, L., and Ablasser, A. (2017). Innate immune sensing of cytosolic chromatin fragments through cGAS promotes senescence. Nat Cell Biol *19*, 1061-1070. 10.1038/ncb3586.
Glynne-Jones, R., and Hughes, R. (2012). Critical appraisal of the 'wait and see' approach in rectal cancer for clinical complete responders after chemoradiation. Br J Surg *99*, 897-909. 10.1002/bjs.8732.
Glynne-Jones, R., Wyrwicz, L., Tiret, E., Brown, G., Rodel, C., Cervantes, A., Arnold, D., and Committee, E.G. (2017). Rectal cancer: ESMO Clinical Practice Guidelines for diagnosis, treatment and follow-up. Ann Oncol *28*, iv22-iv40. 10.1093/annonc/mdx224.
Goldberg, M., Stucki, M., Falck, J., D'Amours, D., Rahman, D., Pappin, D., Bartek, J., and Jackson, S.P. (2003). MDC1 is required for the intra-S-phase DNA damage checkpoint. Nature *421*, 952-956. 10.1038/nature01445.
Goncalves-Ribeiro, S., Sanz-Pamplona, R., Vidal, A., Sanjuan, X., Guillen Diaz-Maroto, N., Soriano, A., Guardiola, J., Albert, N., Martinez-Villacampa, M., Lopez, I., et al. (2017). Prediction of pathological response to neoadjuvant treatment in rectal cancer with a two-protein immunohistochemical score derived from stromal gene-profiling. Ann Oncol *28*, 2160-2168. 10.1093/annonc/mdx293.
Gong, J., Lin, Y., Zhang, H., Liu, C., Cheng, Z., Yang, X., Zhang, J., Xiao, Y., Sang, N., Qian, X., et al. (2020). Reprogramming of lipid metabolism in cancer-associated fibroblasts potentiates migration of colorectal cancer cells. Cell Death Dis *11*, 267. 10.1038/s41419-020-2434-z.
Goodman, K.A., Patton, C.E., Fisher, G.A., Hoffe, S.E., Haddock, M.G., Parikh, P.J., Kim, J., Baxter, N.N., Czito, B.G., Hong, T.S., et al. (2016). Appropriate customization of radiation therapy for stage II and III rectal cancer: Executive summary of an ASTRO Clinical Practice Statement using the RAND/UCLA Appropriateness Method. Pract Radiat Oncol *6*, 166-175. 10.1016/j.prro.2015.11.014.
Gorgoulis, V.G., and Halazonetis, T.D. (2010). Oncogene-induced senescence: the bright and dark side of the response. Curr Opin Cell Biol *22*, 816-827. 10.1016/j.ceb.2010.07.013.
Gottschlich, A., Endres, S., and Kobold, S. (2021). Therapeutic Strategies for Targeting IL-1 in Cancer. Cancers (Basel) *13*. 10.3390/cancers13030477.
Grasso, C.S., Giannakis, M., Wells, D.K., Hamada, T., Mu, X.J., Quist, M., Nowak, J.A., Nishihara, R., Qian, Z.R., Inamura, K., et al. (2018). Genetic Mechanisms of Immune Evasion in Colorectal Cancer. Cancer Discov *8*, 730-749. 10.1158/2159-8290.CD-17-1327.
Graziano, F., Ruzzo, A., Canestrari, E., Loupakis, F., Santini, D., Rulli, E., Humar, B., Galluccio, N., Bisonni, R., Floriani, I., et al. (2009). Variations in the interleukin-1 receptor antagonist gene impact on survival of patients with advanced colorectal cancer. Pharmacogenomics J *9*, 78-84. 10.1038/tpj.2008.16.
Greenfeder, S.A., Nunes, P., Kwee, L., Labow, M., Chizzonite, R.A., and Ju, G. (1995). Molecular cloning and characterization of a second subunit of the interleukin 1 receptor complex. J Biol Chem *270*, 13757-13765. 10.1074/jbc.270.23.13757.

Greten, F.R., and Grivennikov, S.I. (2019). Inflammation and Cancer: Triggers, Mechanisms, and Consequences. Immunity *51*, 27-41. 10.1016/j.immuni.2019.06.025.
Guinney, J., Dienstmann, R., Wang, X., de Reynies, A., Schlicker, A., Soneson, C., Marisa, L., Roepman, P., Nyamundanda, G., Angelino, P., et al. (2015). The consensus molecular subtypes of colorectal cancer. Nat Med *21*, 1350-1356. 10.1038/nm.3967.
Hannum, C.H., Wilcox, C.J., Arend, W.P., Joslin, F.G., Dripps, D.J., Heimdal, P.L., Armes, L.G., Sommer, A., Eisenberg, S.P., and Thompson, R.C. (1990). Interleukin-1 receptor antagonist activity of a human interleukin-1 inhibitor. Nature *343*, 336-340. 10.1038/343336a0.
Harley, C.B., Futcher, A.B., and Greider, C.W. (1990). Telomeres shorten during ageing of human fibroblasts. Nature *345*, 458-460. 10.1038/345458a0.
Haskill, S., Martin, G., Van Le, L., Morris, J., Peace, A., Bigler, C.F., Jaffe, G.J., Hammerberg, C., Sporn, S.A., Fong, S., and et al. (1991). cDNA cloning of an intracellular form of the human interleukin 1 receptor antagonist associated with epithelium. Proc Natl Acad Sci U S A *88*, 3681-3685. 10.1073/pnas.88.9.3681.
Hayakawa, T., Iwai, M., Aoki, S., Takimoto, K., Maruyama, M., Maruyama, W., and Motoyama, N. (2015). SIRT1 suppresses the senescence-associated secretory phenotype through epigenetic gene regulation. PLoS One *10*, e0116480. 10.1371/journal.pone.0116480.
Hayflick, L., and Moorhead, P.S. (1961). The serial cultivation of human diploid cell strains. Exp Cell Res *25*, 585-621. 10.1016/0014-4827(61)90192-6.
Heichler, C., Scheibe, K., Schmied, A., Geppert, C.I., Schmid, B., Wirtz, S., Thoma, O.M., Kramer, V., Waldner, M.J., Buttner, C., et al. (2020). STAT3 activation through IL-6/IL-11 in cancer-associated fibroblasts promotes colorectal tumour development and correlates with poor prognosis. Gut *69*, 1269-1282. 10.1136/gutjnl-2019-319200.
Hendrayani, S.F., Al-Khalaf, H.H., and Aboussekhra, A. (2014). The cytokine IL-6 reactivates breast stromal fibroblasts through transcription factor STAT3-dependent up-regulation of the RNA-binding protein AUF1. J Biol Chem *289*, 30962-30976. 10.1074/jbc.M114.594044.
Herbig, U., Jobling, W.A., Chen, B.P., Chen, D.J., and Sedivy, J.M. (2004). Telomere shortening triggers senescence of human cells through a pathway involving ATM, p53, and p21(CIP1), but not p16(INK4a). Mol Cell *14*, 501-513. 10.1016/s1097-2765(04)00256-4.
Herranz, N., Gallage, S., Mellone, M., Wuestefeld, T., Klotz, S., Hanley, C.J., Raguz, S., Acosta, J.C., Innes, A.J., Banito, A., et al. (2015). mTOR regulates MAPKAPK2 translation to control the senescence-associated secretory phenotype. Nat Cell Biol *17*, 1205-1217. 10.1038/ncb3225.
Hervas Moron, A., Garcia de Paredes, M.L., and Lobo Martinez, E. (2010). Multidisciplinary management in rectal cancer. Clin Transl Oncol *12*, 805-818. 10.1007/s12094-010-0602-9.
Hingorani, S.R., Harris, W.P., Beck, J.T., Berdov, B.A., Wagner, S.A., Pshevlotsky, E.M., Tjulandin, S.A., Gladkov, O.A., Holcombe, R.F., Korn, R., et al. (2016). Phase Ib Study of PEGylated Recombinant Human Hyaluronidase and Gemcitabine in Patients with Advanced Pancreatic Cancer. Clin Cancer Res *22*, 2848-2854. 10.1158/1078-0432.CCR-15-2010.
Hofheinz, R.D., al-Batran, S.E., Hartmann, F., Hartung, G., Jager, D., Renner, C., Tanswell, P., Kunz, U., Amelsberg, A., Kuthan, H., and Stehle, G. (2003). Stromal antigen targeting by a humanised monoclonal antibody: an early phase II trial of sibrotuzumab in patients with metastatic colorectal cancer. Onkologie *26*, 44-48. 10.1159/000069863.
Hofheinz, R.D., Wenz, F., Post, S., Matzdorff, A., Laechelt, S., Hartmann, J.T., Muller, L., Link, H., Moehler, M., Kettner, E., et al. (2012). Chemoradiotherapy with capecitabine versus fluorouracil for locally advanced rectal cancer: a randomised, multicentre, non-inferiority, phase 3 trial. Lancet Oncol *13*, 579-588. 10.1016/S1470-2045(12)70116-X.
Hong, D., Kurzrock, R., Kim, Y., Woessner, R., Younes, A., Nemunaitis, J., Fowler, N., Zhou, T., Schmidt, J., Jo, M., et al. (2015). AZD9150, a next-generation antisense oligonucleotide

inhibitor of STAT3 with early evidence of clinical activity in lymphoma and lung cancer. Sci Transl Med *7*, 314ra185. 10.1126/scitranslmed.aac5272.
Hu, H., Piotrowska, Z., Hare, P.J., Chen, H., Mulvey, H.E., Mayfield, A., Noeen, S., Kattermann, K., Greenberg, M., Williams, A., et al. (2021). Three subtypes of lung cancer fibroblasts define distinct therapeutic paradigms. Cancer Cell. 10.1016/j.ccell.2021.09.003.
Hu, Y., Gaedcke, J., Emons, G., Beissbarth, T., Grade, M., Jo, P., Yeager, M., Chanock, S.J., Wolff, H., Camps, J., et al. (2018). Colorectal cancer susceptibility loci as predictive markers of rectal cancer prognosis after surgery. Genes Chromosomes Cancer *57*, 140-149. 10.1002/gcc.22512.
Huang, T.X., Guan, X.Y., and Fu, L. (2019). Therapeutic targeting of the crosstalk between cancer-associated fibroblasts and cancer stem cells. Am J Cancer Res *9*, 1889-1904.
Huang, X., Li, E., Shen, H., Wang, X., Tang, T., Zhang, X., Xu, J., Tang, Z., Guo, C., Bai, X., and Liang, T. (2020). Targeting the HGF/MET Axis in Cancer Therapy: Challenges in Resistance and Opportunities for Improvement. Front Cell Dev Biol *8*, 152. 10.3389/fcell.2020.00152.
Hubackova, S., Krejcikova, K., Bartek, J., and Hodny, Z. (2012). IL1- and TGFbeta-Nox4 signaling, oxidative stress and DNA damage response are shared features of replicative, oncogene-induced, and drug-induced paracrine 'bystander senescence'. Aging (Albany NY) *4*, 932-951. 10.18632/aging.100520.
Hunter, C.J., Garant, A., Vuong, T., Artho, G., Lisbona, R., Tekkis, P., Abulafi, M., and Brown, G. (2012). Adverse features on rectal MRI identify a high-risk group that may benefit from more intensive preoperative staging and treatment. Ann Surg Oncol *19*, 1199-1205. 10.1245/s10434-011-2036-1.
Hutton, C., Heider, F., Blanco-Gomez, A., Banyard, A., Kononov, A., Zhang, X., Karim, S., Paulus-Hock, V., Watt, D., Steele, N., et al. (2021). Single-cell analysis defines a pancreatic fibroblast lineage that supports anti-tumor immunity. Cancer Cell *39*, 1227-1244 e1220. 10.1016/j.ccell.2021.06.017.
Hyams, J.S., Fitzgerald, J.E., Wyzga, N., Muller, R., Treem, W.R., Justinich, C.J., and Kreutzer, D.L. (1995). Relationship of interleukin-1 receptor antagonist to mucosal inflammation in inflammatory bowel disease. J Pediatr Gastroenterol Nutr *21*, 419-425. 10.1097/00005176-199511000-00008.
Hynes, R.O. (2009). The extracellular matrix: not just pretty fibrils. Science *326*, 1216-1219. 10.1126/science.1176009.
Hynes, R.O., and Naba, A. (2012). Overview of the matrisome--an inventory of extracellular matrix constituents and functions. Cold Spring Harb Perspect Biol *4*, a004903. 10.1101/cshperspect.a004903.
Iannello, A., Thompson, T.W., Ardolino, M., Lowe, S.W., and Raulet, D.H. (2013). p53-dependent chemokine production by senescent tumor cells supports NKG2D-dependent tumor elimination by natural killer cells. J Exp Med *210*, 2057-2069. 10.1084/jem.20130783.
Ibrahimi, M., Moossavi, M., Mojarad, E.N., Musavi, M., Mohammadoo-Khorasani, M., and Shahsavari, Z. (2019). Positive correlation between interleukin-1 receptor antagonist gene 86bp VNTR polymorphism and colorectal cancer susceptibility: a case-control study. Immunol Res *67*, 151-156. 10.1007/s12026-018-9034-3.
Inamura, K. (2018). Colorectal Cancers: An Update on Their Molecular Pathology. Cancers (Basel) *10*. 10.3390/cancers10010026.
Isella, C., Terrasi, A., Bellomo, S.E., Petti, C., Galatola, G., Muratore, A., Mellano, A., Senetta, R., Cassenti, A., Sonetto, C., et al. (2015). Stromal contribution to the colorectal cancer transcriptome. Nat Genet *47*, 312-319. 10.1038/ng.3224.

Ito, T., Teo, Y.V., Evans, S.A., Neretti, N., and Sedivy, J.M. (2018). Regulation of Cellular Senescence by Polycomb Chromatin Modifiers through Distinct DNA Damage- and Histone Methylation-Dependent Pathways. Cell Rep *22*, 3480-3492. 10.1016/j.celrep.2018.03.002.
Itoh, Y., Hayashi, H., Miyazawa, K., Kojima, S., Akahoshi, T., and Onozaki, K. (2007). 17beta-estradiol induces IL-1alpha gene expression in rheumatoid fibroblast-like synovial cells through estrogen receptor alpha (ERalpha) and augmentation of transcriptional activity of Sp1 by dissociating histone deacetylase 2 from ERalpha. J Immunol *178*, 3059-3066. 10.4049/jimmunol.178.5.3059.
Jacob, K.D., Noren Hooten, N., Trzeciak, A.R., and Evans, M.K. (2013). Markers of oxidant stress that are clinically relevant in aging and age-related disease. Mech Ageing Dev *134*, 139-157. 10.1016/j.mad.2013.02.008.
Jacobetz, M.A., Chan, D.S., Neesse, A., Bapiro, T.E., Cook, N., Frese, K.K., Feig, C., Nakagawa, T., Caldwell, M.E., Zecchini, H.I., et al. (2013). Hyaluronan impairs vascular function and drug delivery in a mouse model of pancreatic cancer. Gut *62*, 112-120. 10.1136/gutjnl-2012-302529.
Jenke, R., Ressing, N., Hansen, F.K., Aigner, A., and Buch, T. (2021). Anticancer Therapy with HDAC Inhibitors: Mechanism-Based Combination Strategies and Future Perspectives. Cancers (Basel) *13*. 10.3390/cancers13040634.
Jesus, A.A., Osman, M., Silva, C.A., Kim, P.W., Pham, T.H., Gadina, M., Yang, B., Bertola, D.R., Carneiro-Sampaio, M., Ferguson, P.J., et al. (2011). A novel mutation of IL1RN in the deficiency of interleukin-1 receptor antagonist syndrome: description of two unrelated cases from Brazil. Arthritis Rheum *63*, 4007-4017. 10.1002/art.30588.
Jian, Y.S., Chen, C.W., Lin, C.A., Yu, H.P., Lin, H.Y., Liao, M.Y., Wu, S.H., Lin, Y.F., and Lai, P.S. (2017). Hyaluronic acid-nimesulide conjugates as anticancer drugs against CD44-overexpressing HT-29 colorectal cancer in vitro and in vivo. Int J Nanomedicine *12*, 2315-2333. 10.2147/IJN.S120847.
Johnson, D.E., O'Keefe, R.A., and Grandis, J.R. (2018). Targeting the IL-6/JAK/STAT3 signalling axis in cancer. Nat Rev Clin Oncol *15*, 234-248. 10.1038/nrclinonc.2018.8.
Jones, C.J., Kipling, D., Morris, M., Hepburn, P., Skinner, J., Bounacer, A., Wyllie, F.S., Ivan, M., Bartek, J., Wynford-Thomas, D., and Bond, J.A. (2000). Evidence for a telomere-independent "clock" limiting RAS oncogene-driven proliferation of human thyroid epithelial cells. Mol Cell Biol *20*, 5690-5699. 10.1128/mcb.20.15.5690-5699.2000.
Junginger, T., Goenner, U., Hitzler, M., Trinh, T.T., Heintz, A., Wollschlaeger, D., and Blettner, M. (2016). Long-term Oncologic Outcome After Transanal Endoscopic Microsurgery for Rectal Carcinoma. Dis Colon Rectum *59*, 8-15. 10.1097/DCR.0000000000000509.
Kahn, J., Tofilon, P.J., and Camphausen, K. (2012). Preclinical models in radiation oncology. Radiat Oncol *7*, 223. 10.1186/1748-717X-7-223.
Kalluri, R. (2016). The biology and function of fibroblasts in cancer. Nat Rev Cancer *16*, 582-598. 10.1038/nrc.2016.73.
Kaneko, N., Kurata, M., Yamamoto, T., Morikawa, S., and Masumoto, J. (2019). The role of interleukin-1 in general pathology. Inflamm Regen *39*, 12. 10.1186/s41232-019-0101-5.
Kang, T.W., Yevsa, T., Woller, N., Hoenicke, L., Wuestefeld, T., Dauch, D., Hohmeyer, A., Gereke, M., Rudalska, R., Potapova, A., et al. (2011). Senescence surveillance of pre-malignant hepatocytes limits liver cancer development. Nature *479*, 547-551. 10.1038/nature10599.
Kaur, A., Ecker, B.L., Douglass, S.M., Kugel, C.H., 3rd, Webster, M.R., Almeida, F.V., Somasundaram, R., Hayden, J., Ban, E., Ahmadzadeh, H., et al. (2019). Remodeling of the Collagen Matrix in Aging Skin Promotes Melanoma Metastasis and Affects Immune Cell Motility. Cancer Discov *9*, 64-81. 10.1158/2159-8290.CD-18-0193.

Kawaguchi, Y., Hara, M., and Wright, T.M. (1999). Endogenous IL-1alpha from systemic sclerosis fibroblasts induces IL-6 and PDGF-A. J Clin Invest *103*, 1253-1260. 10.1172/JCI4304.
Kawaguchi, Y., McCarthy, S.A., Watkins, S.C., and Wright, T.M. (2004). Autocrine activation by interleukin 1alpha induces the fibrogenic phenotype of systemic sclerosis fibroblasts. J Rheumatol *31*, 1946-1954.
Kawaguchi, Y., Tochimoto, A., Hara, M., Kawamoto, M., Sugiura, T., Saito, S., and Kamatani, N. (2007). Contribution of single nucleotide polymorphisms of the IL1A gene to the cleavage of precursor IL-1alpha and its transcription activity. Immunogenetics *59*, 441-448. 10.1007/s00251-007-0213-y.
Kay, E.J., and Zanivan, S. (2021). Two opposing sub-populations of fibroblasts decide progression of pancreatic cancer. Cancer Cell *39*, 1175-1177. 10.1016/j.ccell.2021.07.022.
Keller, D.S., Berho, M., Perez, R.O., Wexner, S.D., and Chand, M. (2020). The multidisciplinary management of rectal cancer. Nat Rev Gastroenterol Hepatol *17*, 414-429. 10.1038/s41575-020-0275-y.
Kieffer, Y., Hocine, H.R., Gentric, G., Pelon, F., Bernard, C., Bourachot, B., Lameiras, S., Albergante, L., Bonneau, C., Guyard, A., et al. (2020). Single-Cell Analysis Reveals Fibroblast Clusters Linked to Immunotherapy Resistance in Cancer. Cancer Discov *10*, 1330-1351. 10.1158/2159-8290.CD-19-1384.
Kim, B., Lee, Y., Kim, E., Kwak, A., Ryoo, S., Bae, S.H., Azam, T., Kim, S., and Dinarello, C.A. (2013). The Interleukin-1alpha Precursor is Biologically Active and is Likely a Key Alarmin in the IL-1 Family of Cytokines. Front Immunol *4*, 391. 10.3389/fimmu.2013.00391.
Kim, J.J., Lee, S.B., Yi, S.Y., Han, S.A., Kim, S.H., Lee, J.M., Tong, S.Y., Yin, P., Gao, B., Zhang, J., and Lou, Z. (2017a). WSB1 overcomes oncogene-induced senescence by targeting ATM for degradation. Cell Res *27*, 274-293. 10.1038/cr.2016.148.
Kim, Y.H., Choi, Y.W., Lee, J., Soh, E.Y., Kim, J.H., and Park, T.J. (2017b). Senescent tumor cells lead the collective invasion in thyroid cancer. Nat Commun *8*, 15208. 10.1038/ncomms15208.
Kimura, H., Inukai, Y., Takii, T., Furutani, Y., Shibata, Y., Hayashi, H., Sakurada, S., Okamoto, T., Inoue, J., Oomoto, Y., and Onozaki, K. (1998). Molecular analysis of constitutive IL-1alpha gene expression in human melanoma cells: autocrine stimulation through NF-kappaB activation by endogenous IL-1alpha. Cytokine *10*, 872-879. 10.1006/cyto.1998.0369.
Kirkland, J.L., and Tchkonia, T. (2015). Clinical strategies and animal models for developing senolytic agents. Exp Gerontol *68*, 19-25. 10.1016/j.exger.2014.10.012.
Kirkland, J.L., Tchkonia, T., Zhu, Y., Niedernhofer, L.J., and Robbins, P.D. (2017). The Clinical Potential of Senolytic Drugs. J Am Geriatr Soc *65*, 2297-2301. 10.1111/jgs.14969.
Kirschmann, D.A., Seftor, E.A., Fong, S.F., Nieva, D.R., Sullivan, C.M., Edwards, E.M., Sommer, P., Csiszar, K., and Hendrix, M.J. (2002). A molecular role for lysyl oxidase in breast cancer invasion. Cancer Res *62*, 4478-4483.
Knudsen, E.S., Balaji, U., Freinkman, E., McCue, P., and Witkiewicz, A.K. (2016). Unique metabolic features of pancreatic cancer stroma: relevance to the tumor compartment, prognosis, and invasive potential. Oncotarget *7*, 78396-78411. 10.18632/oncotarget.11893.
Ko, Y.H., Lin, Z., Flomenberg, N., Pestell, R.G., Howell, A., Sotgia, F., Lisanti, M.P., and Martinez-Outschoorn, U.E. (2011). Glutamine fuels a vicious cycle of autophagy in the tumor stroma and oxidative mitochondrial metabolism in epithelial cancer cells: implications for preventing chemotherapy resistance. Cancer Biol Ther *12*, 1085-1097. 10.4161/cbt.12.12.18671.
Kollarovic, G., Studencka, M., Ivanova, L., Lauenstein, C., Heinze, K., Lapytsko, A., Talemi, S.R., Figueiredo, A.S., and Schaber, J. (2016). To senesce or not to senesce: how primary

human fibroblasts decide their cell fate after DNA damage. Aging (Albany NY) *8*, 158-177. 10.18632/aging.100883.
Kraman, M., Bambrough, P.J., Arnold, J.N., Roberts, E.W., Magiera, L., Jones, J.O., Gopinathan, A., Tuveson, D.A., and Fearon, D.T. (2010). Suppression of antitumor immunity by stromal cells expressing fibroblast activation protein-alpha. Science *330*, 827-830. 10.1126/science.1195300.
Kuilman, T., and Peeper, D.S. (2009). Senescence-messaging secretome: SMS-ing cellular stress. Nat Rev Cancer *9*, 81-94. 10.1038/nrc2560.
Kurt-Jones, E.A., Beller, D.I., Mizel, S.B., and Unanue, E.R. (1985). Identification of a membrane-associated interleukin 1 in macrophages. Proc Natl Acad Sci U S A *82*, 1204-1208. 10.1073/pnas.82.4.1204.
Kurt-Jones, E.A., Virgin, H.W.t., and Unanue, E.R. (1986). In vivo and in vitro expression of macrophage membrane interleukin 1 in response to soluble and particulate stimuli. J Immunol *137*, 10-14.
Laberge, R.M., Sun, Y., Orjalo, A.V., Patil, C.K., Freund, A., Zhou, L., Curran, S.C., Davalos, A.R., Wilson-Edell, K.A., Liu, S., et al. (2015). MTOR regulates the pro-tumorigenic senescence-associated secretory phenotype by promoting IL1A translation. Nat Cell Biol *17*, 1049-1061. 10.1038/ncb3195.
Labernadie, A., Kato, T., Brugues, A., Serra-Picamal, X., Derzsi, S., Arwert, E., Weston, A., Gonzalez-Tarrago, V., Elosegui-Artola, A., Albertazzi, L., et al. (2017). A mechanically active heterotypic E-cadherin/N-cadherin adhesion enables fibroblasts to drive cancer cell invasion. Nat Cell Biol *19*, 224-237. 10.1038/ncb3478.
Lambrechts, D., Wauters, E., Boeckx, B., Aibar, S., Nittner, D., Burton, O., Bassez, A., Decaluwe, H., Pircher, A., Van den Eynde, K., et al. (2018). Phenotype molding of stromal cells in the lung tumor microenvironment. Nat Med *24*, 1277-1289. 10.1038/s41591-018-0096-5.
Lansdorp, P.M. (2009). Telomeres and disease. EMBO J *28*, 2532-2540. 10.1038/emboj.2009.172.
Lee, A.C., Fenster, B.E., Ito, H., Takeda, K., Bae, N.S., Hirai, T., Yu, Z.X., Ferrans, V.J., Howard, B.H., and Finkel, T. (1999). Ras proteins induce senescence by altering the intracellular levels of reactive oxygen species. J Biol Chem *274*, 7936-7940. 10.1074/jbc.274.12.7936.
Lee, H.O., Hong, Y., Etlioglu, H.E., Cho, Y.B., Pomella, V., Van den Bosch, B., Vanhecke, J., Verbandt, S., Hong, H., Min, J.W., et al. (2020). Lineage-dependent gene expression programs influence the immune landscape of colorectal cancer. Nat Genet *52*, 594-603. 10.1038/s41588-020-0636-z.
Lee, J.K., Kim, S.H., Lewis, E.C., Azam, T., Reznikov, L.L., and Dinarello, C.A. (2004). Differences in signaling pathways by IL-1beta and IL-18. Proc Natl Acad Sci U S A *101*, 8815-8820. 10.1073/pnas.0402800101.
Leon, X., Bothe, C., Garcia, J., Parreno, M., Alcolea, S., Quer, M., Vila, L., and Camacho, M. (2015). Expression of IL-1alpha correlates with distant metastasis in patients with head and neck squamous cell carcinoma. Oncotarget *6*, 37398-37409. 10.18632/oncotarget.6054.
Li, H., Courtois, E.T., Sengupta, D., Tan, Y., Chen, K.H., Goh, J.J.L., Kong, S.L., Chua, C., Hon, L.K., Tan, W.S., et al. (2017). Reference component analysis of single-cell transcriptomes elucidates cellular heterogeneity in human colorectal tumors. Nat Genet *49*, 708-718. 10.1038/ng.3818.
Li, Y., Wang, L., Pappan, L., Galliher-Beckley, A., and Shi, J. (2012). IL-1beta promotes stemness and invasiveness of colon cancer cells through Zeb1 activation. Mol Cancer *11*, 87. 10.1186/1476-4598-11-87.

Li, Z., Pearlman, A.H., and Hsieh, P. (2016). DNA mismatch repair and the DNA damage response. DNA Repair (Amst) *38*, 94-101. 10.1016/j.dnarep.2015.11.019.
Lin, A.W., Barradas, M., Stone, J.C., van Aelst, L., Serrano, M., and Lowe, S.W. (1998). Premature senescence involving p53 and p16 is activated in response to constitutive MEK/MAPK mitogenic signaling. Genes Dev *12*, 3008-3019. 10.1101/gad.12.19.3008.
Lin, S.H., George, T.J., Ben-Josef, E., Bradley, J., Choe, K.S., Edelman, M.J., Guha, C., Krishnan, S., Lawrence, T.S., Le, Q.T., et al. (2013). Opportunities and challenges in the era of molecularly targeted agents and radiation therapy. J Natl Cancer Inst *105*, 686-693. 10.1093/jnci/djt055.
Liotta, L.A., Saidel, M.G., and Kleinerman, J. (1976). The significance of hematogenous tumor cell clumps in the metastatic process. Cancer Res *36*, 889-894.
Lo, A., Wang, L.S., Scholler, J., Monslow, J., Avery, D., Newick, K., O'Brien, S., Evans, R.A., Bajor, D.J., Clendenin, C., et al. (2015). Tumor-Promoting Desmoplasia Is Disrupted by Depleting FAP-Expressing Stromal Cells. Cancer Res *75*, 2800-2810. 10.1158/0008-5472.CAN-14-3041.
Lohr, M., Schmidt, C., Ringel, J., Kluth, M., Muller, P., Nizze, H., and Jesnowski, R. (2001). Transforming growth factor-beta1 induces desmoplasia in an experimental model of human pancreatic carcinoma. Cancer Res *61*, 550-555.
Lou, Z., Minter-Dykhouse, K., Wu, X., and Chen, J. (2003). MDC1 is coupled to activated CHK2 in mammalian DNA damage response pathways. Nature *421*, 957-961. 10.1038/nature01447.
Love, M.I., Huber, W., and Anders, S. (2014). Moderated estimation of fold change and dispersion for RNA-seq data with DESeq2. Genome Biology *15*, 550. 10.1186/s13059-014-0550-8.
Lynch, H.T., and Smyrk, T.C. (1998). Classification of familial adenomatous polyposis: a diagnostic nightmare. Am J Hum Genet *62*, 1288-1289. 10.1086/301890.
Maas, M., Nelemans, P.J., Valentini, V., Das, P., Rodel, C., Kuo, L.J., Calvo, F.A., Garcia-Aguilar, J., Glynne-Jones, R., Haustermans, K., et al. (2010). Long-term outcome in patients with a pathological complete response after chemoradiation for rectal cancer: a pooled analysis of individual patient data. Lancet Oncol *11*, 835-844. 10.1016/S1470-2045(10)70172-8.
Malanchi, I., Santamaria-Martinez, A., Susanto, E., Peng, H., Lehr, H.A., Delaloye, J.F., and Huelsken, J. (2011). Interactions between cancer stem cells and their niche govern metastatic colonization. Nature *481*, 85-89. 10.1038/nature10694.
Malaquin, N., Vercamer, C., Bouali, F., Martien, S., Deruy, E., Wernert, N., Chwastyniak, M., Pinet, F., Abbadie, C., and Pourtier, A. (2013). Senescent fibroblasts enhance early skin carcinogenic events via a paracrine MMP-PAR-1 axis. PLoS One *8*, e63607. 10.1371/journal.pone.0063607.
Malik, A., and Kanneganti, T.D. (2018). Function and regulation of IL-1alpha in inflammatory diseases and cancer. Immunol Rev *281*, 124-137. 10.1111/imr.12615.
Mansfield, J.C., Holden, H., Tarlow, J.K., Di Giovine, F.S., McDowell, T.L., Wilson, A.G., Holdsworth, C.D., and Duff, G.W. (1994). Novel genetic association between ulcerative colitis and the anti-inflammatory cytokine interleukin-1 receptor antagonist. Gastroenterology *106*, 637-642. 10.1016/0016-5085(94)90696-3.
Margolin, Y., Cloutier, J.F., Shafirovich, V., Geacintov, N.E., and Dedon, P.C. (2006). Paradoxical hotspots for guanine oxidation by a chemical mediator of inflammation. Nat Chem Biol *2*, 365-366. 10.1038/nchembio796.
Mariathasan, S., Turley, S.J., Nickles, D., Castiglioni, A., Yuen, K., Wang, Y., Kadel, E.E., III, Koeppen, H., Astarita, J.L., Cubas, R., et al. (2018). TGFbeta attenuates tumour response to PD-L1 blockade by contributing to exclusion of T cells. Nature *554*, 544-548. 10.1038/nature25501.

Marisa, L., de Reynies, A., Duval, A., Selves, J., Gaub, M.P., Vescovo, L., Etienne-Grimaldi, M.C., Schiappa, R., Guenot, D., Ayadi, M., et al. (2013). Gene expression classification of colon cancer into molecular subtypes: characterization, validation, and prognostic value. PLoS Med *10*, e1001453. 10.1371/journal.pmed.1001453.
McCarthy, D.A., Ranganathan, A., Subbaram, S., Flaherty, N.L., Patel, N., Trebak, M., Hempel, N., and Melendez, J.A. (2013). Redox-control of the alarmin, Interleukin-1alpha. Redox Biol *1*, 218-225. 10.1016/j.redox.2013.03.001.
McDowell, T.L., Symons, J.A., and Duff, G.W. (2005). Human interleukin-1 alpha gene expression is regulated by Sp1 and a transcriptional repressor. Cytokine *30*, 141-153. 10.1016/j.cyto.2004.12.010.
McInnes, L., Healy, J., and Melville, J. (2018). Umap: Uniform manifold approximation and projection for dimension reduction. arXiv preprint arXiv:1802.03426.
Melisi, D., Niu, J., Chang, Z., Xia, Q., Peng, B., Ishiyama, S., Evans, D.B., and Chiao, P.J. (2009). Secreted interleukin-1alpha induces a metastatic phenotype in pancreatic cancer by sustaining a constitutive activation of nuclear factor-kappaB. Mol Cancer Res *7*, 624-633. 10.1158/1541-7786.MCR-08-0201.
Michels, B.E., Mosa, M.H., Grebbin, B.M., Yepes, D., Darvishi, T., Hausmann, J., Urlaub, H., Zeuzem, S., Kvasnicka, H.M., Oellerich, T., and Farin, H.F. (2019). Human colon organoids reveal distinct physiologic and oncogenic Wnt responses. J Exp Med *216*, 704-720. 10.1084/jem.20180823.
Milora, K.A., Miller, S.L., Sanmiguel, J.C., and Jensen, L.E. (2014). Interleukin-1alpha released from HSV-1-infected keratinocytes acts as a functional alarmin in the skin. Nat Commun *5*, 5230. 10.1038/ncomms6230.
Misra, S., Hascall, V.C., Markwald, R.R., and Ghatak, S. (2015). Interactions between Hyaluronan and Its Receptors (CD44, RHAMM) Regulate the Activities of Inflammation and Cancer. Front Immunol *6*, 201. 10.3389/fimmu.2015.00201.
Moatassim-Billah, S., Duluc, C., Samain, R., Jean, C., Perraud, A., Decaup, E., Cassant-Sourdy, S., Bakri, Y., Selves, J., Schmid, H., et al. (2016). Anti-metastatic potential of somatostatin analog SOM230: Indirect pharmacological targeting of pancreatic cancer-associated fibroblasts. Oncotarget *7*, 41584-41598. 10.18632/oncotarget.9296.
Murdocca, M., Capuano, R., Pucci, S., Cicconi, R., Polidoro, C., Catini, A., Martinelli, E., Paolesse, R., Orlandi, A., Mango, R., et al. (2019). Targeting LOX-1 Inhibits Colorectal Cancer Metastasis in an Animal Model. Front Oncol *9*, 927. 10.3389/fonc.2019.00927.
Murphy, N., Norat, T., Ferrari, P., Jenab, M., Bueno-de-Mesquita, B., Skeie, G., Dahm, C.C., Overvad, K., Olsen, A., Tjonneland, A., et al. (2012). Dietary fibre intake and risks of cancers of the colon and rectum in the European prospective investigation into cancer and nutrition (EPIC). PLoS One *7*, e39361. 10.1371/journal.pone.0039361.
Naba, A., Clauser, K.R., and Hynes, R.O. (2015). Enrichment of Extracellular Matrix Proteins from Tissues and Digestion into Peptides for Mass Spectrometry Analysis. J Vis Exp, e53057. 10.3791/53057.
Naba, A., Clauser, K.R., Whittaker, C.A., Carr, S.A., Tanabe, K.K., and Hynes, R.O. (2014). Extracellular matrix signatures of human primary metastatic colon cancers and their metastases to liver. BMC Cancer *14*, 518. 10.1186/1471-2407-14-518.
Naba, A., Pearce, O.M.T., Del Rosario, A., Ma, D., Ding, H., Rajeeve, V., Cutillas, P.R., Balkwill, F.R., and Hynes, R.O. (2017). Characterization of the Extracellular Matrix of Normal and Diseased Tissues Using Proteomics. J Proteome Res *16*, 3083-3091. 10.1021/acs.jproteome.7b00191.
Narita, M., Nunez, S., Heard, E., Narita, M., Lin, A.W., Hearn, S.A., Spector, D.L., Hannon, G.J., and Lowe, S.W. (2003). Rb-mediated heterochromatin formation and silencing of E2F target genes during cellular senescence. Cell *113*, 703-716. 10.1016/s0092-8674(03)00401-x.

Nazareth, M.R., Broderick, L., Simpson-Abelson, M.R., Kelleher, R.J., Jr., Yokota, S.J., and Bankert, R.B. (2007). Characterization of human lung tumor-associated fibroblasts and their ability to modulate the activation of tumor-associated T cells. J Immunol *178*, 5552-5562. 10.4049/jimmunol.178.9.5552.
Nelson, G., Kucheryavenko, O., Wordsworth, J., and von Zglinicki, T. (2018). The senescent bystander effect is caused by ROS-activated NF-kappaB signalling. Mech Ageing Dev *170*, 30-36. 10.1016/j.mad.2017.08.005.
Network, C.G.A. (2012). Comprehensive molecular characterization of human colon and rectal cancer. Nature *487*, 330.
Ngan, S.Y., Burmeister, B., Fisher, R.J., Solomon, M., Goldstein, D., Joseph, D., Ackland, S.P., Schache, D., McClure, B., McLachlan, S.A., et al. (2012). Randomized trial of short-course radiotherapy versus long-course chemoradiation comparing rates of local recurrence in patients with T3 rectal cancer: Trans-Tasman Radiation Oncology Group trial 01.04. J Clin Oncol *30*, 3827-3833. 10.1200/JCO.2012.42.9597.
Niu, J., Li, Z., Peng, B., and Chiao, P.J. (2004). Identification of an autoregulatory feedback pathway involving interleukin-1alpha in induction of constitutive NF-kappaB activation in pancreatic cancer cells. J Biol Chem *279*, 16452-16462. 10.1074/jbc.M309789200.
Ohlund, D., Handly-Santana, A., Biffi, G., Elyada, E., Almeida, A.S., Ponz-Sarvise, M., Corbo, V., Oni, T.E., Hearn, S.A., Lee, E.J., et al. (2017). Distinct populations of inflammatory fibroblasts and myofibroblasts in pancreatic cancer. J Exp Med *214*, 579-596. 10.1084/jem.20162024.
Orimo, A., Gupta, P.B., Sgroi, D.C., Arenzana-Seisdedos, F., Delaunay, T., Naeem, R., Carey, V.J., Richardson, A.L., and Weinberg, R.A. (2005). Stromal fibroblasts present in invasive human breast carcinomas promote tumor growth and angiogenesis through elevated SDF-1/CXCL12 secretion. Cell *121*, 335-348. 10.1016/j.cell.2005.02.034.
Ortiz-Montero, P., Londono-Vallejo, A., and Vernot, J.P. (2017). Senescence-associated IL-6 and IL-8 cytokines induce a self- and cross-reinforced senescence/inflammatory milieu strengthening tumorigenic capabilities in the MCF-7 breast cancer cell line. Cell Commun Signal *15*, 17. 10.1186/s12964-017-0172-3.
Oskarsson, T., Acharyya, S., Zhang, X.H., Vanharanta, S., Tavazoie, S.F., Morris, P.G., Downey, R.J., Manova-Todorova, K., Brogi, E., and Massague, J. (2011). Breast cancer cells produce tenascin C as a metastatic niche component to colonize the lungs. Nat Med *17*, 867-874. 10.1038/nm.2379.
Ostermann, E., Garin-Chesa, P., Heider, K.H., Kalat, M., Lamche, H., Puri, C., Kerjaschki, D., Rettig, W.J., and Adolf, G.R. (2008). Effective immunoconjugate therapy in cancer models targeting a serine protease of tumor fibroblasts. Clin Cancer Res *14*, 4584-4592. 10.1158/1078-0432.CCR-07-5211.
Overall, C.M., and Kleifeld, O. (2006). Tumour microenvironment - opinion: validating matrix metalloproteinases as drug targets and anti-targets for cancer therapy. Nat Rev Cancer *6*, 227-239. 10.1038/nrc1821.
Ozdemir, B.C., Pentcheva-Hoang, T., Carstens, J.L., Zheng, X., Wu, C.C., Simpson, T.R., Laklai, H., Sugimoto, H., Kahlert, C., Novitskiy, S.V., et al. (2014). Depletion of carcinoma-associated fibroblasts and fibrosis induces immunosuppression and accelerates pancreas cancer with reduced survival. Cancer Cell *25*, 719-734. 10.1016/j.ccr.2014.04.005.
Park, S.J., Nakagawa, T., Kitamura, H., Atsumi, T., Kamon, H., Sawa, S., Kamimura, D., Ueda, N., Iwakura, Y., Ishihara, K., et al. (2004). IL-6 regulates in vivo dendritic cell differentiation through STAT3 activation. J Immunol *173*, 3844-3854. 10.4049/jimmunol.173.6.3844.
Paschke, S., Jafarov, S., Staib, L., Kreuser, E.D., Maulbecker-Armstrong, C., Roitman, M., Holm, T., Harris, C.C., Link, K.H., and Kornmann, M. (2018). Are Colon and Rectal Cancer

Two Different Tumor Entities? A Proposal to Abandon the Term Colorectal Cancer. Int J Mol Sci *19*. 10.3390/ijms19092577.
Paszek, M.J., Zahir, N., Johnson, K.R., Lakins, J.N., Rozenberg, G.I., Gefen, A., Reinhart-King, C.A., Margulies, S.S., Dembo, M., Boettiger, D., et al. (2005). Tensional homeostasis and the malignant phenotype. Cancer Cell *8*, 241-254. 10.1016/j.ccr.2005.08.010.
Patel, R.A., Forinash, K.D., Pireddu, R., Sun, Y., Sun, N., Martin, M.P., Schonbrunn, E., Lawrence, N.J., and Sebti, S.M. (2012). RKI-1447 is a potent inhibitor of the Rho-associated ROCK kinases with anti-invasive and antitumor activities in breast cancer. Cancer Res *72*, 5025-5034. 10.1158/0008-5472.CAN-12-0954.
Pazolli, E., Alspach, E., Milczarek, A., Prior, J., Piwnica-Worms, D., and Stewart, S.A. (2012). Chromatin remodeling underlies the senescence-associated secretory phenotype of tumor stromal fibroblasts that supports cancer progression. Cancer Res *72*, 2251-2261. 10.1158/0008-5472.CAN-11-3386.
Perez-Villamil, B., Romera-Lopez, A., Hernandez-Prieto, S., Lopez-Campos, G., Calles, A., Lopez-Asenjo, J.A., Sanz-Ortega, J., Fernandez-Perez, C., Sastre, J., Alfonso, R., et al. (2012). Colon cancer molecular subtypes identified by expression profiling and associated to stroma, mucinous type and different clinical behavior. BMC Cancer *12*, 260. 10.1186/1471-2407-12-260.
Pietras, E.M., Mirantes-Barbeito, C., Fong, S., Loeffler, D., Kovtonyuk, L.V., Zhang, S., Lakshminarasimhan, R., Chin, C.P., Techner, J.M., Will, B., et al. (2016). Chronic interleukin-1 exposure drives haematopoietic stem cells towards precocious myeloid differentiation at the expense of self-renewal. Nat Cell Biol *18*, 607-618. 10.1038/ncb3346.
Plubell, D.L., Wilmarth, P.A., Zhao, Y., Fenton, A.M., Minnier, J., Reddy, A.P., Klimek, J., Yang, X., David, L.L., and Pamir, N. (2017). Extended Multiplexing of Tandem Mass Tags (TMT) Labeling Reveals Age and High Fat Diet Specific Proteome Changes in Mouse Epididymal Adipose Tissue. Mol Cell Proteomics *16*, 873-890. 10.1074/mcp.M116.065524.
Prieur, A.M., Kaufmann, M.T., Griscelli, C., and Dayer, J.M. (1987). Specific interleukin-1 inhibitor in serum and urine of children with systemic juvenile chronic arthritis. Lancet *2*, 1240-1242. 10.1016/s0140-6736(87)91854-x.
Provenzano, P.P., Cuevas, C., Chang, A.E., Goel, V.K., Von Hoff, D.D., and Hingorani, S.R. (2012). Enzymatic targeting of the stroma ablates physical barriers to treatment of pancreatic ductal adenocarcinoma. Cancer Cell *21*, 418-429. 10.1016/j.ccr.2012.01.007.
Puram, S.V., Tirosh, I., Parikh, A.S., Patel, A.P., Yizhak, K., Gillespie, S., Rodman, C., Luo, C.L., Mroz, E.A., Emerick, K.S., et al. (2017). Single-Cell Transcriptomic Analysis of Primary and Metastatic Tumor Ecosystems in Head and Neck Cancer. Cell *171*, 1611-1624 e1624. 10.1016/j.cell.2017.10.044.
Quail, D.F., and Joyce, J.A. (2013). Microenvironmental regulation of tumor progression and metastasis. Nat Med *19*, 1423-1437. 10.1038/nm.3394.
Quante, M., Varga, J., Wang, T.C., and Greten, F.R. (2013). The gastrointestinal tumor microenvironment. Gastroenterology *145*, 63-78. 10.1053/j.gastro.2013.03.052.
Rafiq, S., Stevens, K., Hurst, A.J., Murray, A., Henley, W., Weedon, M.N., Bandinelli, S., Corsi, A.M., Guralnik, J.M., Ferrucci, L., et al. (2007). Common genetic variation in the gene encoding interleukin-1-receptor antagonist (IL-1RA) is associated with altered circulating IL-1RA levels. Genes Immun *8*, 344-351. 10.1038/sj.gene.6364393.
Ramaswamy, S., Ross, K.N., Lander, E.S., and Golub, T.R. (2003). A molecular signature of metastasis in primary solid tumors. Nat Genet *33*, 49-54. 10.1038/ng1060.
Reardon, D.A., Akabani, G., Coleman, R.E., Friedman, A.H., Friedman, H.S., Herndon, J.E., 2nd, McLendon, R.E., Pegram, C.N., Provenzale, J.M., Quinn, J.A., et al. (2006). Salvage radioimmunotherapy with murine iodine-131-labeled antitenascin monoclonal antibody 81C6

for patients with recurrent primary and metastatic malignant brain tumors: phase II study results. J Clin Oncol *24*, 115-122. 10.1200/JCO.2005.03.4082.
Rider, P., Carmi, Y., Guttman, O., Braiman, A., Cohen, I., Voronov, E., White, M.R., Dinarello, C.A., and Apte, R.N. (2011). IL-1alpha and IL-1beta recruit different myeloid cells and promote different stages of sterile inflammation. J Immunol *187*, 4835-4843. 10.4049/jimmunol.1102048.
Ridker, P.M., MacFadyen, J.G., Thuren, T., Everett, B.M., Libby, P., Glynn, R.J., and Grp, C.T. (2017). Effect of interleukin-1 beta inhibition with canakinumab on incident lung cancer in patients with atherosclerosis: exploratory results from a randomised, double-blind, placebo-controlled trial. Lancet *390*, 1833-1842. 10.1016/S0140-6736(17)32247-X.
Rodel, C., Graeven, U., Fietkau, R., Hohenberger, W., Hothorn, T., Arnold, D., Hofheinz, R.D., Ghadimi, M., Wolff, H.A., Lang-Welzenbach, M., et al. (2015). Oxaliplatin added to fluorouracil-based preoperative chemoradiotherapy and postoperative chemotherapy of locally advanced rectal cancer (the German CAO/ARO/AIO-04 study): final results of the multicentre, open-label, randomised, phase 3 trial. Lancet Oncol *16*, 979-989. 10.1016/S1470-2045(15)00159-X.
Rodel, C., Hofheinz, R., and Fokas, E. (2016). Rectal cancer: Neoadjuvant chemoradiotherapy. Best Pract Res Clin Gastroenterol *30*, 629-639. 10.1016/j.bpg.2016.06.004.
Rodel, C., Liersch, T., Becker, H., Fietkau, R., Hohenberger, W., Hothorn, T., Graeven, U., Arnold, D., Lang-Welzenbach, M., Raab, H.R., et al. (2012). Preoperative chemoradiotherapy and postoperative chemotherapy with fluorouracil and oxaliplatin versus fluorouracil alone in locally advanced rectal cancer: initial results of the German CAO/ARO/AIO-04 randomised phase 3 trial. Lancet Oncol *13*, 679-687. 10.1016/S1470-2045(12)70187-0.
Roeder, F., Meldolesi, E., Gerum, S., Valentini, V., and Rodel, C. (2020). Recent advances in (chemo-)radiation therapy for rectal cancer: a comprehensive review. Radiat Oncol *15*, 262. 10.1186/s13014-020-01695-0.
Roepman, P., Schlicker, A., Tabernero, J., Majewski, I., Tian, S., Moreno, V., Snel, M.H., Chresta, C.M., Rosenberg, R., Nitsche, U., et al. (2014). Colorectal cancer intrinsic subtypes predict chemotherapy benefit, deficient mismatch repair and epithelial-to-mesenchymal transition. Int J Cancer *134*, 552-562. 10.1002/ijc.28387.
Ruscetti, M., Morris, J.P.t., Mezzadra, R., Russell, J., Leibold, J., Romesser, P.B., Simon, J., Kulick, A., Ho, Y.J., Fennell, M., et al. (2020). Senescence-Induced Vascular Remodeling Creates Therapeutic Vulnerabilities in Pancreas Cancer. Cell *181*, 424-441 e421. 10.1016/j.cell.2020.03.008.
Sadanandam, A., Lyssiotis, C.A., Homicsko, K., Collisson, E.A., Gibb, W.J., Wullschleger, S., Ostos, L.C., Lannon, W.A., Grotzinger, C., Del Rio, M., et al. (2013). A colorectal cancer classification system that associates cellular phenotype and responses to therapy. Nat Med *19*, 619-625. 10.1038/nm.3175.
Sagiv, A., Burton, D.G., Moshayev, Z., Vadai, E., Wensveen, F., Ben-Dor, S., Golani, O., Polic, B., and Krizhanovsky, V. (2016). NKG2D ligands mediate immunosurveillance of senescent cells. Aging (Albany NY) *8*, 328-344. 10.18632/aging.100897.
Sahai, E., Astsaturov, I., Cukierman, E., DeNardo, D.G., Egeblad, M., Evans, R.M., Fearon, D., Greten, F.R., Hingorani, S.R., Hunter, T., et al. (2020). A framework for advancing our understanding of cancer-associated fibroblasts. Nat Rev Cancer *20*, 174-186. 10.1038/s41568-019-0238-1.
Sakurai, T., He, G., Matsuzawa, A., Yu, G.Y., Maeda, S., Hardiman, G., and Karin, M. (2008). Hepatocyte necrosis induced by oxidative stress and IL-1 alpha release mediate carcinogen-induced compensatory proliferation and liver tumorigenesis. Cancer Cell *14*, 156-165. 10.1016/j.ccr.2008.06.016.

Saleh, T., Bloukh, S., Carpenter, V.J., Alwohoush, E., Bakeer, J., Darwish, S., Azab, B., and Gewirtz, D.A. (2020). Therapy-Induced Senescence: An "Old" Friend Becomes the Enemy. Cancers (Basel) *12*. 10.3390/cancers12040822.
Saleh, T., Tyutyunyk-Massey, L., Murray, G.F., Alotaibi, M.R., Kawale, A.S., Elsayed, Z., Henderson, S.C., Yakovlev, V., Elmore, L.W., Toor, A., et al. (2019). Tumor cell escape from therapy-induced senescence. Biochem Pharmacol *162*, 202-212. 10.1016/j.bcp.2018.12.013.
Sanford-Crane, H., Abrego, J., and Sherman, M.H. (2019). Fibroblasts as Modulators of Local and Systemic Cancer Metabolism. Cancers (Basel) *11*. 10.3390/cancers11050619.
Sanson, K.R., Hanna, R.E., Hegde, M., Donovan, K.F., Strand, C., Sullender, M.E., Vaimberg, E.W., Goodale, A., Root, D.E., Piccioni, F., and Doench, J.G. (2018). Optimized libraries for CRISPR-Cas9 genetic screens with multiple modalities. Nat Commun *9*, 5416. 10.1038/s41467-018-07901-8.
Santos, A.M., Jung, J., Aziz, N., Kissil, J.L., and Pure, E. (2009). Targeting fibroblast activation protein inhibits tumor stromagenesis and growth in mice. J Clin Invest *119*, 3613-3625. 10.1172/JCI38988.
Sarrazin, S., Lamanna, W.C., and Esko, J.D. (2011). Heparan sulfate proteoglycans. Cold Spring Harb Perspect Biol *3*. 10.1101/cshperspect.a004952.
Sauer, R., Becker, H., Hohenberger, W., Rodel, C., Wittekind, C., Fietkau, R., Martus, P., Tschmelitsch, J., Hager, E., Hess, C.F., et al. (2004). Preoperative versus postoperative chemoradiotherapy for rectal cancer. N Engl J Med *351*, 1731-1740. 10.1056/NEJMoa040694.
Sauer, R., Liersch, T., Merkel, S., Fietkau, R., Hohenberger, W., Hess, C., Becker, H., Raab, H.R., Villanueva, M.T., Witzigmann, H., et al. (2012). Preoperative versus postoperative chemoradiotherapy for locally advanced rectal cancer: results of the German CAO/ARO/AIO-94 randomized phase III trial after a median follow-up of 11 years. J Clin Oncol *30*, 1926-1933. 10.1200/JCO.2011.40.1836.
Schmitt, M., and Greten, F.R. (2021). The inflammatory pathogenesis of colorectal cancer. Nat Rev Immunol *21*, 653-667. 10.1038/s41577-021-00534-x.
Schutze, F., Rohrig, F., Vorlova, S., Gatzner, S., Kuhn, A., Ergun, S., and Henke, E. (2015). Inhibition of Lysyl Oxidases Improves Drug Diffusion and Increases Efficacy of Cytotoxic Treatment in 3D Tumor Models. Sci Rep *5*, 17576. 10.1038/srep17576.
Seckinger, P., Lowenthal, J.W., Williamson, K., Dayer, J.M., and MacDonald, H.R. (1987). A urine inhibitor of interleukin 1 activity that blocks ligand binding. J Immunol *139*, 1546-1549.
Sehouli, J., Mustea, A., Koensgen, D., and Lichtenegger, W. (2003). Interleukin-1 receptor antagonist gene polymorphism in epithelial ovarian cancer. Cancer Epidemiol Biomarkers Prev *12*, 1205-1208.
Sen, P., Shah, P.P., Nativio, R., and Berger, S.L. (2016). Epigenetic Mechanisms of Longevity and Aging. Cell *166*, 822-839. 10.1016/j.cell.2016.07.050.
Serrano, M., Lin, A.W., McCurrach, M.E., Beach, D., and Lowe, S.W. (1997). Oncogenic ras provokes premature cell senescence associated with accumulation of p53 and p16INK4a. Cell *88*, 593-602. 10.1016/s0092-8674(00)81902-9.
Seshagiri, S., Stawiski, E.W., Durinck, S., Modrusan, Z., Storm, E.E., Conboy, C.B., Chaudhuri, S., Guan, Y., Janakiraman, V., Jaiswal, B.S., et al. (2012). Recurrent R-spondin fusions in colon cancer. Nature *488*, 660-664. 10.1038/nature11282.
Sharpless, N.E., and Sherr, C.J. (2015). Forging a signature of in vivo senescence. Nat Rev Cancer *15*, 397-408. 10.1038/nrc3960.
Shay, J.W., and Wright, W.E. (2019). Telomeres and telomerase: three decades of progress. Nat Rev Genet *20*, 299-309. 10.1038/s41576-019-0099-1.
Sherman, M.H., Yu, R.T., Engle, D.D., Ding, N., Atkins, A.R., Tiriac, H., Collisson, E.A., Connor, F., Van Dyke, T., Kozlov, S., et al. (2014). Vitamin D receptor-mediated stromal

reprogramming suppresses pancreatitis and enhances pancreatic cancer therapy. Cell *159*, 80-93. 10.1016/j.cell.2014.08.007.
Siegel, R., Desantis, C., and Jemal, A. (2014). Colorectal cancer statistics, 2014. CA Cancer J Clin *64*, 104-117. 10.3322/caac.21220.
Simpson, M.A., Wilson, C.M., and McCarthy, J.B. (2002). Inhibition of prostate tumor cell hyaluronan synthesis impairs subcutaneous growth and vascularization in immunocompromised mice. Am J Pathol *161*, 849-857. 10.1016/S0002-9440(10)64245-9.
Sjoblom, T., Jones, S., Wood, L.D., Parsons, D.W., Lin, J., Barber, T.D., Mandelker, D., Leary, R.J., Ptak, J., Silliman, N., et al. (2006). The consensus coding sequences of human breast and colorectal cancers. Science *314*, 268-274. 10.1126/science.1133427.
Smith, D.E., Hanna, R., Della, F., Moore, H., Chen, H., Farese, A.M., MacVittie, T.J., Virca, G.D., and Sims, J.E. (2003). The soluble form of IL-1 receptor accessory protein enhances the ability of soluble type II IL-1 receptor to inhibit IL-1 action. Immunity *18*, 87-96. 10.1016/s1074-7613(02)00514-9.
Song, X., Krelin, Y., Dvorkin, T., Bjorkdahl, O., Segal, S., Dinarello, C.A., Voronov, E., and Apte, R.N. (2005). CD11b+/Gr-1+ immature myeloid cells mediate suppression of T cells in mice bearing tumors of IL-1beta-secreting cells. J Immunol *175*, 8200-8208. 10.4049/jimmunol.175.12.8200.
Sousa, C.M., Biancur, D.E., Wang, X., Halbrook, C.J., Sherman, M.H., Zhang, L., Kremer, D., Hwang, R.F., Witkiewicz, A.K., Ying, H., et al. (2016). Pancreatic stellate cells support tumour metabolism through autophagic alanine secretion. Nature *536*, 479-483. 10.1038/nature19084.
Steinkasserer, A., Spurr, N.K., Cox, S., Jeggo, P., and Sim, R.B. (1992). The human IL-1 receptor antagonist gene (IL1RN) maps to chromosome 2q14-q21, in the region of the IL-1 alpha and IL-1 beta loci. Genomics *13*, 654-657. 10.1016/0888-7543(92)90137-h.
Sterzynska, K., Klejewski, A., Wojtowicz, K., Swierczewska, M., Nowacka, M., Kazmierczak, D., Andrzejewska, M., Rusek, D., Brazert, M., Brazert, J., et al. (2018). Mutual Expression of ALDH1A1, LOX, and Collagens in Ovarian Cancer Cell Lines as Combined CSCs- and ECM-Related Models of Drug Resistance Development. Int J Mol Sci *20*. 10.3390/ijms20010054.
Stevenson, F.T., Bursten, S.L., Fanton, C., Locksley, R.M., and Lovett, D.H. (1993). The 31-kDa precursor of interleukin 1 alpha is myristoylated on specific lysines within the 16-kDa N-terminal propiece. Proc Natl Acad Sci U S A *90*, 7245-7249. 10.1073/pnas.90.15.7245.
Su, S., Chen, J., Yao, H., Liu, J., Yu, S., Lao, L., Wang, M., Luo, M., Xing, Y., Chen, F., et al. (2018). CD10(+)GPR77(+) Cancer-Associated Fibroblasts Promote Cancer Formation and Chemoresistance by Sustaining Cancer Stemness. Cell *172*, 841-856 e816. 10.1016/j.cell.2018.01.009.
Subrahmanyam, N., and Ghandehari, H. (2021). Harnessing Extracellular Matrix Biology for Tumor Drug Delivery. J Pers Med *11*. 10.3390/jpm11020088.
Sugimoto, S., Ohta, Y., Fujii, M., Matano, M., Shimokawa, M., Nanki, K., Date, S., Nishikori, S., Nakazato, Y., Nakamura, T., et al. (2018). Reconstruction of the Human Colon Epithelium In Vivo. Cell Stem Cell *22*, 171-176 e175. 10.1016/j.stem.2017.11.012.
Sun, P., Yoshizuka, N., New, L., Moser, B.A., Li, Y., Liao, R., Xie, C., Chen, J., Deng, Q., Yamout, M., et al. (2007). PRAK is essential for ras-induced senescence and tumor suppression. Cell *128*, 295-308. 10.1016/j.cell.2006.11.050.
Tandara, A.A., and Mustoe, T.A. (2011). MMP- and TIMP-secretion by human cutaneous keratinocytes and fibroblasts--impact of coculture and hydration. J Plast Reconstr Aesthet Surg *64*, 108-116. 10.1016/j.bjps.2010.03.051.
Tauriello, D.V.F., Palomo-Ponce, S., Stork, D., Berenguer-Llergo, A., Badia-Ramentol, J., Iglesias, M., Sevillano, M., Ibiza, S., Canellas, A., Hernando-Momblona, X., et al. (2018). TGFbeta drives immune evasion in genetically reconstituted colon cancer metastasis. Nature *554*, 538-543. 10.1038/nature25492.

Taylor, F.G., Quirke, P., Heald, R.J., Moran, B.J., Blomqvist, L., Swift, I.R., Sebag-Montefiore, D., Tekkis, P., Brown, G., and Magnetic Resonance Imaging in Rectal Cancer European Equivalence Study Study, G. (2014). Preoperative magnetic resonance imaging assessment of circumferential resection margin predicts disease-free survival and local recurrence: 5-year follow-up results of the MERCURY study. J Clin Oncol *32*, 34-43. 10.1200/JCO.2012.45.3258.

Thomas, N.K., and Brown, T.J. (2010). ABC transporters do not contribute to extracellular translocation of hyaluronan in human breast cancer in vitro. Exp Cell Res *316*, 1241-1253. 10.1016/j.yexcr.2010.01.004.

Tian, C., Clauser, K.R., Ohlund, D., Rickelt, S., Huang, Y., Gupta, M., Mani, D.R., Carr, S.A., Tuveson, D.A., and Hynes, R.O. (2019). Proteomic analyses of ECM during pancreatic ductal adenocarcinoma progression reveal different contributions by tumor and stromal cells. Proc Natl Acad Sci U S A *116*, 19609-19618. 10.1073/pnas.1908626116.

Tjomsland, V., Bojmar, L., Sandstrom, P., Bratthall, C., Messmer, D., Spangeus, A., and Larsson, M. (2013). IL-1alpha expression in pancreatic ductal adenocarcinoma affects the tumor cell migration and is regulated by the p38MAPK signaling pathway. PLoS One *8*, e70874. 10.1371/journal.pone.0070874.

Tomimatsu, S., Ichikura, T., and Mochizuki, H. (2001). Significant correlation between expression of interleukin-1alpha and liver metastasis in gastric carcinoma. Cancer *91*, 1272-1276. 10.1002/1097-0142(20010401)91:7<1272::aid-cncr1128>3.0.co;2-z.

Toso, A., Revandkar, A., Di Mitri, D., Guccini, I., Proietti, M., Sarti, M., Pinton, S., Zhang, J., Kalathur, M., Civenni, G., et al. (2014). Enhancing chemotherapy efficacy in Pten-deficient prostate tumors by activating the senescence-associated antitumor immunity. Cell Rep *9*, 75-89. 10.1016/j.celrep.2014.08.044.

Tountas, N.A., Casini-Raggi, V., Yang, H., Di Giovine, F.S., Vecchi, M., Kam, L., Melani, L., Pizarro, T.T., Rotter, J.I., and Cominelli, F. (1999). Functional and ethnic association of allele 2 of the interleukin-1 receptor antagonist gene in ulcerative colitis. Gastroenterology *117*, 806-813. 10.1016/s0016-5085(99)70338-0.

Traag, V.A., Waltman, L., and van Eck, N.J. (2019). From Louvain to Leiden: guaranteeing well-connected communities. Sci Rep *9*, 5233. 10.1038/s41598-019-41695-z.

Tyc-Szczepaniak, D., Wyrwicz, L., Kepka, L., Michalski, W., Olszyna-Serementa, M., Palucki, J., Pietrzak, L., Rutkowski, A., and Bujko, K. (2013). Palliative radiotherapy and chemotherapy instead of surgery in symptomatic rectal cancer with synchronous unresectable metastases: a phase II study. Ann Oncol *24*, 2829-2834. 10.1093/annonc/mdt363.

Ueno, H., Jones, A.M., Wilkinson, K.H., Jass, J.R., and Talbot, I.C. (2004). Histological categorisation of fibrotic cancer stroma in advanced rectal cancer. Gut *53*, 581-586. 10.1136/gut.2003.028365.

Valko, M., Rhodes, C.J., Moncol, J., Izakovic, M., and Mazur, M. (2006). Free radicals, metals and antioxidants in oxidative stress-induced cancer. Chem Biol Interact *160*, 1-40. 10.1016/j.cbi.2005.12.009.

van de Veerdonk, F.L., Netea, M.G., Dinarello, C.A., and Joosten, L.A. (2011). Inflammasome activation and IL-1beta and IL-18 processing during infection. Trends Immunol *32*, 110-116. 10.1016/j.it.2011.01.003.

van Gijn, W., Marijnen, C.A., Nagtegaal, I.D., Kranenbarg, E.M., Putter, H., Wiggers, T., Rutten, H.J., Pahlman, L., Glimelius, B., van de Velde, C.J., and Dutch Colorectal Cancer, G. (2011). Preoperative radiotherapy combined with total mesorectal excision for resectable rectal cancer: 12-year follow-up of the multicentre, randomised controlled TME trial. Lancet Oncol *12*, 575-582. 10.1016/S1470-2045(11)70097-3.

van Kempen, L.C., Ruiter, D.J., van Muijen, G.N., and Coussens, L.M. (2003). The tumor microenvironment: a critical determinant of neoplastic evolution. Eur J Cell Biol *82*, 539-548. 10.1078/0171-9335-00346.
Vandenbroucke, R.E., and Libert, C. (2014). Is there new hope for therapeutic matrix metalloproteinase inhibition? Nat Rev Drug Discov *13*, 904-927. 10.1038/nrd4390.
Varga, J., and Greten, F. (2017). Cell plasticity in epithelial homeostasis and tumorigenesis. Nature Cell Biology *19*. 10.1038/ncb3611.
Varga, J., Nicolas, A., Petrocelli, V., Pesic, M., Mahmoud, A., Michels, B.E., Etlioglu, E., Yepes, D., Haupl, B., Ziegler, P.K., et al. (2020). AKT-dependent NOTCH3 activation drives tumor progression in a model of mesenchymal colorectal cancer. J Exp Med *217*. 10.1084/jem.20191515.
Vaughan, D.E., Rai, R., Khan, S.S., Eren, M., and Ghosh, A.K. (2017). Plasminogen Activator Inhibitor-1 Is a Marker and a Mediator of Senescence. Arterioscler Thromb Vasc Biol *37*, 1446-1452. 10.1161/ATVBAHA.117.309451.
Ventura, A., Kirsch, D.G., McLaughlin, M.E., Tuveson, D.A., Grimm, J., Lintault, L., Newman, J., Reczek, E.E., Weissleder, R., and Jacks, T. (2007). Restoration of p53 function leads to tumour regression in vivo. Nature *445*, 661-665. 10.1038/nature05541.
Vilchez Mercedes, S.A., Bocci, F., Levine, H., Onuchic, J.N., Jolly, M.K., and Wong, P.K. (2021). Decoding leader cells in collective cancer invasion. Nat Rev Cancer *21*, 592-604. 10.1038/s41568-021-00376-8.
Vogelstein, B., Fearon, E.R., Hamilton, S.R., Kern, S.E., Preisinger, A.C., Leppert, M., Nakamura, Y., White, R., Smits, A.M., and Bos, J.L. (1988). Genetic alterations during colorectal-tumor development. N Engl J Med *319*, 525-532. 10.1056/NEJM198809013190901.
Vogelstein, B., Papadopoulos, N., Velculescu, V.E., Zhou, S., Diaz, L.A., Jr., and Kinzler, K.W. (2013). Cancer genome landscapes. Science *339*, 1546-1558. 10.1126/science.1235122.
Wan, Y.Y., and Flavell, R.A. (2007). 'Yin-Yang' functions of transforming growth factor-beta and T regulatory cells in immune regulation. Immunol Rev *220*, 199-213. 10.1111/j.1600-065X.2007.00565.x.
Wang, B., Kohli, J., and Demaria, M. (2020). Senescent Cells in Cancer Therapy: Friends or Foes? Trends Cancer *6*, 838-857. 10.1016/j.trecan.2020.05.004.
Wang, X., Wong, S.C., Pan, J., Tsao, S.W., Fung, K.H., Kwong, D.L., Sham, J.S., and Nicholls, J.M. (1998). Evidence of cisplatin-induced senescent-like growth arrest in nasopharyngeal carcinoma cells. Cancer Res *58*, 5019-5022.
Wang, Z., Tang, Y., Tan, Y., Wei, Q., and Yu, W. (2019). Cancer-associated fibroblasts in radiotherapy: challenges and new opportunities. Cell Commun Signal *17*, 47. 10.1186/s12964-019-0362-2.
Was, H., Barszcz, K., Czarnecka, J., Kowalczyk, A., Bernas, T., Uzarowska, E., Koza, P., Klejman, A., Piwocka, K., Kaminska, B., and Sikora, E. (2017). Bafilomycin A1 triggers proliferative potential of senescent cancer cells in vitro and in NOD/SCID mice. Oncotarget *8*, 9303-9322. 10.18632/oncotarget.14066.
Weber, A., Wasiliew, P., and Kracht, M. (2010). Interleukin-1 (IL-1) pathway. Sci Signal *3*, cm1. 10.1126/scisignal.3105cm1.
Wei, E.K., Giovannucci, E., Wu, K., Rosner, B., Fuchs, C.S., Willett, W.C., and Colditz, G.A. (2004). Comparison of risk factors for colon and rectal cancer. Int J Cancer *108*, 433-442. 10.1002/ijc.11540.
Wesche, H., Korherr, C., Kracht, M., Falk, W., Resch, K., and Martin, M.U. (1997). The interleukin-1 receptor accessory protein (IL-1RAcP) is essential for IL-1-induced activation of interleukin-1 receptor-associated kinase (IRAK) and stress-activated protein kinases (SAP kinases). J Biol Chem *272*, 7727-7731. 10.1074/jbc.272.12.7727.

Widodo, N., Deocaris, C.C., Kaur, K., Hasan, K., Yaguchi, T., Yamasaki, K., Sugihara, T., Ishii, T., Wadhwa, R., and Kaul, S.C. (2007). Stress chaperones, mortalin, and pex19p mediate 5-aza-2' deoxycytidine-induced senescence of cancer cells by DNA methylation-independent pathway. J Gerontol A Biol Sci Med Sci *62*, 246-255. 10.1093/gerona/62.3.246.
Wierstra, I. (2008). Sp1: emerging roles--beyond constitutive activation of TATA-less housekeeping genes. Biochem Biophys Res Commun *372*, 1-13. 10.1016/j.bbrc.2008.03.074.
Wissler Gerdes, E.O., Zhu, Y., Tchkonia, T., and Kirkland, J.L. (2020). Discovery, development, and future application of senolytics: theories and predictions. FEBS J *287*, 2418-2427. 10.1111/febs.15264.
Wolf, F.A., Angerer, P., and Theis, F.J. (2018). SCANPY: large-scale single-cell gene expression data analysis. Genome Biol *19*, 15. 10.1186/s13059-017-1382-0.
Worrall, B.B., Brott, T.G., Brown, R.D., Jr., Brown, W.M., Rich, S.S., Arepalli, S., Wavrant-De Vrieze, F., Duckworth, J., Singleton, A.B., Hardy, J., et al. (2007). IL1RN VNTR polymorphism in ischemic stroke: analysis in 3 populations. Stroke *38*, 1189-1196. 10.1161/01.STR.0000260099.42744.b0.
Wu, F., Yang, J., Liu, J., Wang, Y., Mu, J., Zeng, Q., Deng, S., and Zhou, H. (2021). Signaling pathways in cancer-associated fibroblasts and targeted therapy for cancer. Signal Transduct Target Ther *6*, 218. 10.1038/s41392-021-00641-0.
Wu, S.Z., Roden, D.L., Wang, C., Holliday, H., Harvey, K., Cazet, A.S., Murphy, K.J., Pereira, B., Al-Eryani, G., Bartonicek, N., et al. (2020). Stromal cell diversity associated with immune evasion in human triple-negative breast cancer. EMBO J *39*, e104063. 10.15252/embj.2019104063.
Wyld, L., Bellantuono, I., Tchkonia, T., Morgan, J., Turner, O., Foss, F., George, J., Danson, S., and Kirkland, J.L. (2020). Senescence and Cancer: A Review of Clinical Implications of Senescence and Senotherapies. Cancers (Basel) *12*. 10.3390/cancers12082134.
Xu, W.S., Perez, G., Ngo, L., Gui, C.Y., and Marks, P.A. (2005). Induction of polyploidy by histone deacetylase inhibitor: a pathway for antitumor effects. Cancer Res *65*, 7832-7839. 10.1158/0008-5472.CAN-04-4608.
Xue, H., Lin, B., Ni, P., Xu, H., and Huang, G. (2010). Interleukin-1B and interleukin-1 RN polymorphisms and gastric carcinoma risk: a meta-analysis. J Gastroenterol Hepatol *25*, 1604-1617. 10.1111/j.1440-1746.2010.06428.x.
Xue, W., Zender, L., Miething, C., Dickins, R.A., Hernando, E., Krizhanovsky, V., Cordon-Cardo, C., and Lowe, S.W. (2007). Senescence and tumour clearance is triggered by p53 restoration in murine liver carcinomas. Nature *445*, 656-660. 10.1038/nature05529.
Yang, F., Tuxhorn, J.A., Ressler, S.J., McAlhany, S.J., Dang, T.D., and Rowley, D.R. (2005). Stromal expression of connective tissue growth factor promotes angiogenesis and prostate cancer tumorigenesis. Cancer Res *65*, 8887-8895. 10.1158/0008-5472.CAN-05-1702.
Yao, Y., Xu, X., Yang, L., Zhu, J., Wan, J., Shen, L., Xia, F., Fu, G., Deng, Y., Pan, M., et al. (2020). Patient-Derived Organoids Predict Chemoradiation Responses of Locally Advanced Rectal Cancer. Cell Stem Cell *26*, 17-26 e16. 10.1016/j.stem.2019.10.010.
Yuhara, H., Steinmaus, C., Cohen, S.E., Corley, D.A., Tei, Y., and Buffler, P.A. (2011). Is diabetes mellitus an independent risk factor for colon cancer and rectal cancer? Am J Gastroenterol *106*, 1911-1921; quiz 1922. 10.1038/ajg.2011.301.
Yun, J., Rago, C., Cheong, I., Pagliarini, R., Angenendt, P., Rajagopalan, H., Schmidt, K., Willson, J.K., Markowitz, S., Zhou, S., et al. (2009). Glucose deprivation contributes to the development of KRAS pathway mutations in tumor cells. Science *325*, 1555-1559. 10.1126/science.1174229.
Zhang, D., Wang, Y., Shi, Z., Liu, J., Sun, P., Hou, X., Zhang, J., Zhao, S., Zhou, B.P., and Mi, J. (2015). Metabolic reprogramming of cancer-associated fibroblasts by IDH3alpha downregulation. Cell Rep *10*, 1335-1348. 10.1016/j.celrep.2015.02.006.

Zhu, Y., Tchkonia, T., Fuhrmann-Stroissnigg, H., Dai, H.M., Ling, Y.Y., Stout, M.B., Pirtskhalava, T., Giorgadze, N., Johnson, K.O., Giles, C.B., et al. (2016). Identification of a novel senolytic agent, navitoclax, targeting the Bcl-2 family of anti-apoptotic factors. Aging Cell *15*, 428-435. 10.1111/acel.12445.
Zigrino, P., Kuhn, I., Bauerle, T., Zamek, J., Fox, J.W., Neumann, S., Licht, A., Schorpp-Kistner, M., Angel, P., and Mauch, C. (2009). Stromal expression of MMP-13 is required for melanoma invasion and metastasis. J Invest Dermatol *129*, 2686-2693. 10.1038/jid.2009.130.

Copyrights

Figure 1:

BioRENDER

Confirmation of Publication and Licensing Rights

Agreement number:

MX23ETFVUL

License date:

January 7th, 2022

License Content Publisher:

BioRender

Subscription:

Individual

Journal name:

The Johann Wolfgang Goethe University Library, Frankfurt am Mai

Figure 2:

License Number:

5210180336731

License date:

Dec 15, 2021

Licensed Content Publisher:

Springer Nature

Licensed Content Publication:

Nature Reviews Gastroenterology & Hepatology

Licensed Content Title:

The multidisciplinary management of rectal cancer

Licensed Content Author:

Deborah S. Keller et al

Portions:

Figure 5

Figure 5:

License Number:

5194270249021

License date:

Nov 22, 2021

Licensed Content Publisher:

Springer Nature

Licensed Content Publication:

Nature Reviews Clinical Oncology

Licensed Content Title:

Clinical and therapeutic relevance of cancer-associated fibroblasts

Licensed Content Author:

Yang Chen et al

Licensed Content Date:

Sep 6, 2021

Portions:

Figure 1

Figure 8:

License Number:

5194270817207

License date:

Nov 22, 2021

Licensed Content Publisher:

Springer Nature

Licensed Content Publication:

Nature Reviews Cancer

Licensed Content Title:

Unmasking senescence: context-dependent effects of SASP in cancer

Licensed Content Author:

Douglas V. Faget et al

Portions:

Figure 1

Figure 9:

License Number:

5194270923517

License date:

Nov 22, 2021

Licensed Content Publisher:

Springer Nature

Licensed Content Publication:

Nature Reviews Cancer

Licensed Content Title:

Unmasking senescence: context-dependent effects of SASP in cancer

Licensed Content Author:

Douglas V. Faget et al

Portions:

Figure 2